Wheat leaf structure and function: the role of cell size, shape, and patterning across *Triticum* evolution

Emma Charlotte White

A thesis submitted to the University of Sheffield

for the degree of Doctor of Philosophy

The University of Sheffield

Faculty of Science

School of Biosciences

October 2024

Acknowledgments

I would firstly like give a huge thank you to my supervisor, Andrew Fleming. All of the guidance and support he has provided throughout the course of my PhD project has been invaluable in making it such an enjoyable experience. I would also like to thank my iCASE supervisor, Richard Summers, for injecting his enthusiasm and experience into the project.

This project was funded through a BBSRC iCASE studentship and I am grateful to both the BBSRC and RAGT Seeds for this opportunity. I want to thank George Notley and Lola Gonzáles Penadés in particular for making me feel like a valued member of the hybrid wheat team, and everyone else at RAGT for making the time I spent on my placement so special.

I would like to express my gratitude to Cristobal Uauy from the John Innes Centre for collaborating with me on this project, and to the rest of his lab for hosting me and making me feel welcome during my visits to the JIC. I also want to thank Sadiye Hayta for her help in providing the transgenic wheat lines used in this study.

Without the support of colleagues at the University of Sheffield, this project would have been impossible. I particularly want to thank Matt Wilson for helping to get the project started and teaching me many things, from how to grow wheat to using MorphographX, and just generally being my first point of call whenever I needed any help. My thanks also go to Jen Sloan for providing technical support with leaf sectioning and for helping with troubleshooting many coding issues. I want to thank Colin Osborne for his support as my academic advisor and for his suggestions and ideas for the project, in particular relating to C4 evolution in grasses. I am grateful for the assistance of Darren Robinson and Nick Van Hateren from the Wolfson Light Microscopy Facility. I would like to express my genuine gratitude to everybody in the D59 and C33 lab groups for making my time at the University of Sheffield so wonderful. Particularly, I want to say thank you to: Shauni McGregor, Tom Grand and Rob Brench for the fantastic memories made during our Dungeons & Dragons sessions; Sarah Im-Chai for our walks, coffee and chats; Eleanor Briggs in whom I have made a lifelong friend.

Finally, I would like to thank my Mum and sister, Sarah, for their constant support and encouragement throughout my PhD, and Arthur for being the best dog in the entire world.

Collaborations

The work done for Chapter 5 of this project is in collaboration with Cristobal Uauy from the John Innes Centre. Plant material for this chapter was provided by Sadiye Hayta from the Wheat Transformation platform (JIC).

Abstract

Gas flux into leaves for photosynthesis occurs through small pores on the surface called stomata. Subsequent gas movement to the photosynthetic cells relies on porous mesophyll tissue. However, maximising the density of stomata and porosity of the airspace to improve the rate of gas flow for photosynthesis increases the amount of water lost. Therefore, there is a trade-off of maximising photosynthetic rate while keeping water loss to a minimum. The effect of leaf structure in *Triticum* (wheat) species on this trade-off is the subject of this thesis, with a focus on how this has changed during the breeding of modern hexaploid wheat from lower ploidy progenitors.

At the level of whole leaf structure, the *Triticum* mesophyll has traditionally been considered to be homogenous. Here I show that in fact it comprises four distinct cell layers. This patterning is conserved across all Triticum ploidy levels and cultivation statuses, suggesting an evolutionary advantage.

Focussing on tetraploid wheat varieties, I show that that modern cultivated varieties have larger stomatal, pavement and mesophyll cells, fewer stomata and are more water-use efficient than wild, landrace varieties, suggesting that water-use efficiency has been a driver during the selection of modern tetraploid wheat.

Finally, to test the hypothesis that increased cell size is linked to improved water-use efficiency, transgenic hexaploid wheat overexpressing a construct expected to modify cell size were analysed. This resulted in improved water-use efficiency, but the underlying changes in cellular architecture were complicated, with the major influence on gas exchange probably linked to altered pavement traits rather than the mesophyll.

The work in this thesis provides insight into the impact of leaf structure on water-use efficiency during the breeding of modern wheat which has been superimposed on an ancient underlying mesophyll cellular architecture.

Table of Contents

Table of Figures

List of Tables

Chapter 1. Introduction

1.1. Wheat Evolution and Domestication

Wheat is a globally important grain crop, consisting of two main types: hexaploid bread wheat *(Triticum aestivum*) and tetraploid durum wheat (*Triticum durum*). *T aestivum* accounts for around 95% of the world's wheat production and has undergone over 8000 years of selection. The evolution of wheat is shown in Figure 1.1 and can be summarised as follows. Cultivated wheat belongs to the *Triticum L.* genus, which consists of only six species. The sub-family Pooideae that includes around 300 species (Clayton & Renvoize, 1986) including wheat and barley, diverged from the Poaceae family of grasses around 20 Mya (Inda et al. 2008). A member of this sub-family, *Triticum uratu* (wild diploid wheat, 2n = 2x = 14, genome A^uA^u), hybridized with the B genome ancestor of modern wheat (*Aegilops speltoides*, 2n = 2x = 14, genome SS) around 400,000 years ago (Dvorak *et al*,. 2012) to produce wild emmer wheat (*T. turgidum ssp. dicoccoides*, 2n = 4x = 28, genome A^uA^uBB). About 10,000 years ago, in the Fertile Crescent, wild emmer began to be cultivated (Feldman & Kislev, 2007; Kislev *et al*., 1992) without prior knowledge of selective breeding to create a cultivated emmer (*T. turgidum ssp. dicoccum*, 2n = 4x = 28, genome A^uA^uBB). After another 1000 years, the cultivated emmer spontaneously hybridized with another goat grass, similar to the B genome progenitor (*Ae. tauschii*, 2n = 2x = 14, genome DD) to produce an early spelt variety (*T. spelta*, 2n = 6x = 42, genome A^uA^uBBDD). This hybridisation event likely occurred as emmer cultivation spread eastwards into the natural habitat of *Ae. tauschii* around the Caspian Sea (Nesbitt & Samuel, 1998; Salamini *et al.*, 2002). One hypothesis is that, around 8,500 years ago, a natural mutation resulted in changes in the ears of both emmer and spelt leading to more easily threshed types that later evolved into the free-threshing durum (*T. turgidum ssp. durum*) and bread (*T. aestivum*) wheat. However, the idea that *T. spelta* is the ancestor of modern bread wheat has been disputed (Dvorak *et al.,* 2006), and instead presented the idea that cultivated wheat ancestry is more complicated, involving factors such as gene flow from wild cereals (Dvorak *et al.*, 2011).

The UK is highly reliant on wheat to feed its population. It is also the most widely cultivated crop worldwide, with 790.54 million metric tons being produced in the 2023/2024 season (USDA, 2024). Wheat provides a large proportion of the global population with around 20% of their calorific and 25% of their protein intake (FAO, 2024). It is grown in both temperate and tropical environments, many of which being water-restricted or facing increasing problems of water scarcity due to climate change.

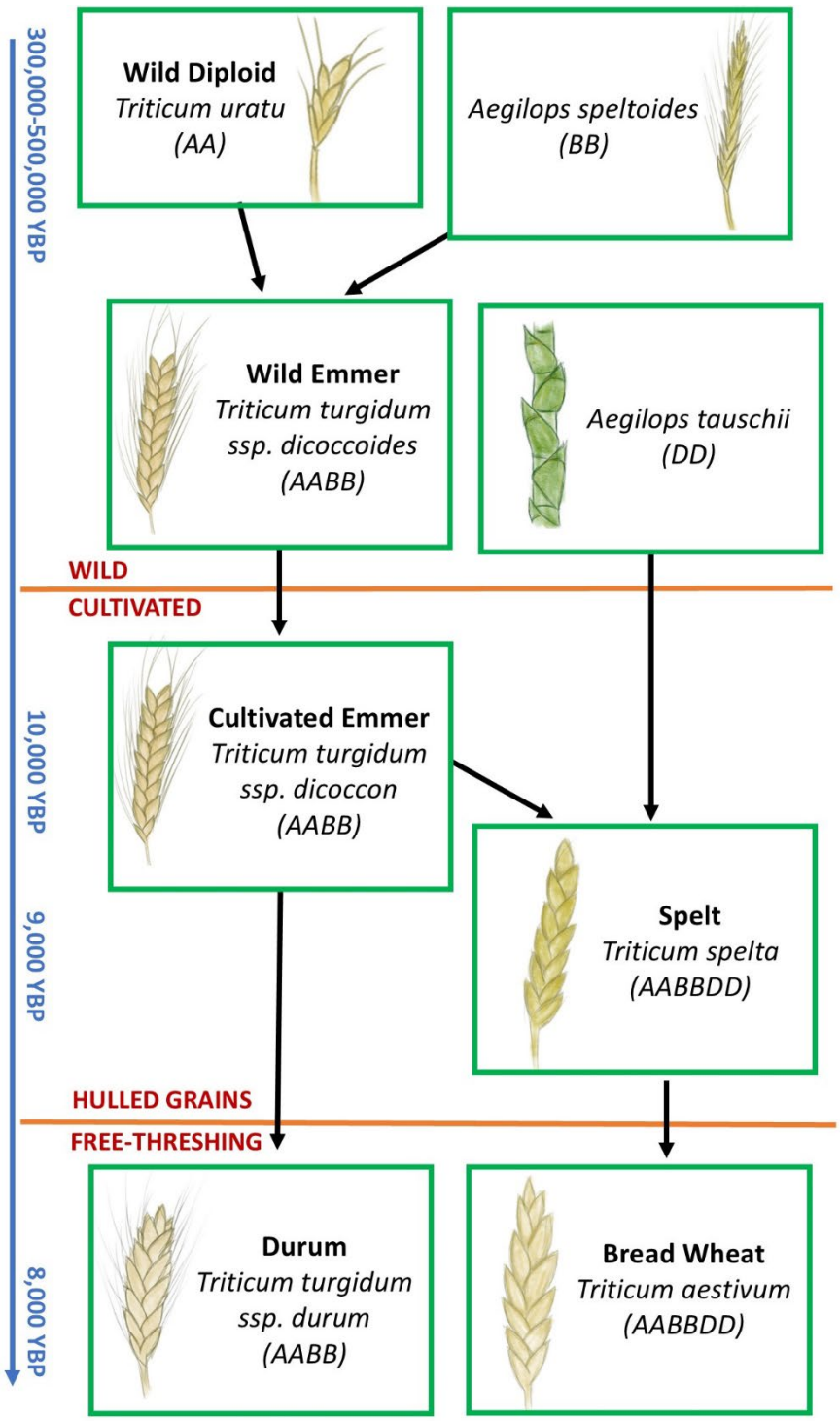

Figure 1.1. Wheat domestication and evolution. Modern hexaploid bread wheat has evolved as the result of two isolated hybridisation events. Hybridisation of the diploid species *T. uratu* (AA) with what is thought to be *A. speltoides* (BB) resulted in the generation of a tetraploid *T. turgidum* containing A and B genomes. Wild *T. turgidum* is of the sub-species *T. turgidum ssp. dicoccoides,* early cultivated Emmer (*T. turgidum ssp. dicoccon*) was selected from this and through later evolved in to a modern, free-threshing Durum (*T. turgidum ssp. durum*). A second hybridisation event occurred between cultivated tetraploid Emmer wheat (AABB) and *A. tauschii* (DD) and led to the formation of modern hexaploid wheat, *T. aestivum* (AABBDD).

1.2 Water Use Efficiency and Drought Tolerance

Water use efficiency (WUE) is a measure of the productivity of a plant per unit of water used (Hatfield & Dold, 2019). This can reflect the responsiveness of crops to water stress in relation to yield values (Richard, 2006; Zhang *et al.*, 2010). An increasing area of concern with regards to WUE is that of staple food crops, with major cereal crops such as wheat and rice accounting for 27% of global water consumption (Hoekstra & Mekonnen, 2012). Presently, one in eleven people are classed as living under food insecurity (FAO, 2024). In the near future, as water supplies become scarcer and more variable due to the impacts of climate change, worldwide crop production must be substantial to feed the growing population (SOFI, 2018). For this to happen, crops that require less water in order to produce an equal or greater amount of food must be produced, in combination with further strategies for yield improvement.

Water is used in an extensive number of processes in every plant on the planet, and plants that grow in water-restricted environments have adapted ways to deal with the stress by reducing water loss and improving water-use efficiency. There are a range of adaptations that different plant species employ to confer drought resistance (Levitt, 1980). One category is 'drought escape' in that the plant aims to complete its life cycle before experiencing the effects of the drought, as they are able to modulate their vegetative and reproductive growth depending on the availability of water (Jones, Turner & Osmond, 1981). 'Drought avoidance' applies to plants which are able to maintain a moderately high tissue water content despite reduced water availability (Levitt, 1980), and this is achieved through a variety of adaptations relating to either the minimisation of water loss (water savers) or optimisation of water uptake (water spenders). The latter tend to maintain water uptake through features such as increased rooting and hydraulic conduction, whereas water savers use water more efficiently by reducing factors like transpiration, transpiration area and radiation absorption under water-stress. The ability of plants to withstand low tissue water content is known as 'drought tolerance'. Another way in which some plants have adapted to cope with living in water-stressed environments is through carrying out the C4 pathway of carbon assimilation instead of the more widely used C3 pathway. The C4 pathway has been suggested to limit water loss, reduce photorespiration, and improve photosynthetic efficiency under drought stress (Edwards & Walker, 1983).

The loss of water vapour from the leaves of plants, transpiration, is what drives uptake of water from the soil through the roots by generating a water pressure gradient. The rate of transpiration therefore must be in balance with the supply of water to the roots, and too much water loss in water-stressed conditions can have a devastating impact on plant growth (Seleiman *et al.,* 2021). Transpiration rate can be affected by a variety of environmental factors such as light, humidity, temperature, and atmospheric CO_2 concentrations, as well as endogenous factors such as hormone production and age (Pallardy, 2008). Water loss from the leaves is largely regulated by the presence of pores called stomata, which are also vital for photosynthetic gas exchange. It is important that plants are able to optimise both the rate of gas

uptake by the leaves for photosynthetic carbon fixation, while reducing the amount of water lost by transpiration through the same pores, in order to maximise productivity. Stomata have been observed to be key players in the trade-off between these two processes (Lawson & Blatt, 2014). The path through which CO_2 enters the photosynthesising leaf cells begins at the layer of air immediately surrounding the leaf (boundary layer), and stomatal pores provide a resistance to gas flux into the leaf. For water leaving the leaf, this occurs in reverse with stomatal pores being the main resistance to water loss. The behaviour of the stomata therefore plays a key role in controlling both the volume of CO_2 entering the intercellular leaf airspace and in minimising the amount of water lost.

1.3. Measuring Leaf Gas Exchange

CO_2 and H_2O exchange between the internal leaf cells and the atmosphere is required for photosynthesis to occur. The rate of gas exchange can be quantified *in vivo* using either an infra-red gas analysis system (IRGA) (Long & Bernacchi, 2003; Johnson & Murchie, 2011) or through the use of a porometer. In an IRGA system, the leaf is clamped into an airtight cuvette whilst still attached to the plant. Indirect measurements are taken through comparing CO_2 and water vapour concentrations by detecting differences in infra-red absorbance of a sample and empty reference cell, combined with a measure of gas flow rate through the sample chamber (Figure 1.2). From this, the assimilation rate of CO_2 per unit of leaf area, A, can be calculated (Busch, 2018), along with further parameters including stomatal conductance (g_s), which gives an indication of the quantity of stomatal pore space (taking into account pore size and density) that is available for gas exchange (Johnson & Murchie, 2011; Busch, 2018). IRGA systems allow for steady state measurements to be taken in a highly controlled environment, as well as for easy manipulation of parameters that affect leaf gas exchange such as light intensity, temperature, humidity and CO_2 concentration to provide insight into how gas exchange responds to changes in environmental conditions. In addition, generating A/C_i curves in response to changing light and CO_2 concentration using IRGAs allows for more complex datasets to be extracted (Bellasio *et al.*, 2016; Sharkey, 2016). IRGAs are extremely useful tools for studying leaf function, however issues such as leaks and incorrect recording of leaf area are likely to cause errors and impact the usability of the data (Johnson & Murchie, 2011), so the correct setup programme and appropriate protocols must be followed.

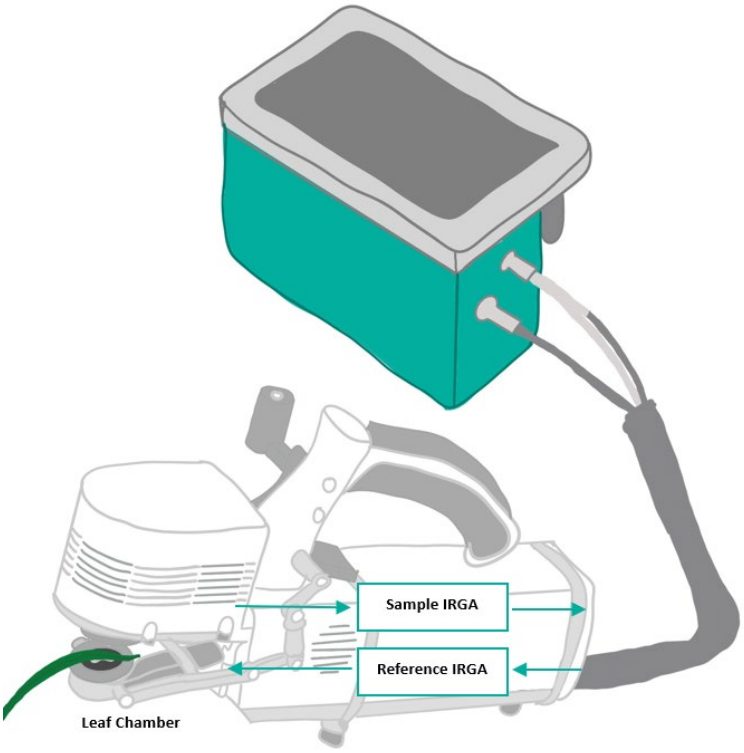

Figure 1.2. Using an IRGA to measure leaf gas exchange. A simplified diagram showing how an infra-red gas exchange analysis (IRGA) system measures gas exchange of a leaf. By measuring flow rate and comparing H_2O and CO_2 concentrations between the reference and sample IRGAs, an estimation of a leaf's photosynthetic gas exchange parameters can be measured.

Porometry, for example using the LI-600 system (LiCOR, NE, USA), captures instantaneous gas exchange information for leaf stomatal and boundary layer conductance from a leaf, allowing for much higher throughput than using an IRGA like the LI-6800. Specifically, the LI-600 quantifies transpiration, *E,* in a similar way to an IRGA: by measuring the flow rate and water vapor fraction of air that enters and leaves the chamber. Simultaneously, total conductance to water vapor (g_{tw}) is calculated using E values and vapor pressure readings in the leaf and cuvette. Stomatal conductance to water (g_{sw}) is then recorded as a function of g_{tw} and the boundary layer conductance to water vapor (g_{bw}). Despite porometers being ideal for larger scale experiments, one of the major drawbacks when compared to an IRGA system is the limited number of output parameters and the ability to only capture snapshot readings of leaf gas exchange and lack of capability to generate response curves. However, the LI-600 is able to match closely to ambient conditions and allows for much more rapid stabilisation than with an IRGA, making it better for quantifying gas exchange in the field.

Analysing gas exchange is acknowledged as an effective way to assess the physiological performance of wheat (Araus *et al.,* 1986; Yin *et al*., 2009; Driever *et al.*, 2014; Dunn *et al*., 2019). Gas exchange has also been shown to vary greatly depending on environmental conditions, however when using an IRGA to control parameters and saturate light intensity while maintaining ambient CO_2, the mean A of

modern hexaploid wheat ranges between 20 and 30 μmol $m^{-2}s^{-1}$ (Driever *et al.,* 2014), with g_s between 0.3-0.45 mol m^{-2} s^{-1} (Gaju *et al.,* 2016). Both g_s and *A* are known to be driven by a variety of anatomical factors such as the density and size of stomatal pores on the surface of the leaf, stomatal patterning, and altered pore aperture (Willmer & Fricker, 1996; Hetherington & Woodward, 2003; Casson & Hetherington, 2010; Lawson & Blatt, 2014; Matthews *et al*., 2018; Faralli *et al.,* 2020). It is during leaf development that these are determined through both environmental and genetic drivers (Hepworth *et al.,* 2018; Zoulias *et al*., 2018; Pillitteri *et al*., 2007).

1.4. Wheat Leaf Architecture and Development

1.4.1. Formation of leaf primordium

Distinct tissue layers are established very early in the developing leaf. The initiation of leaf primordia in the peripheral zone (PZ) of the shoot apical meristem (SAM) is followed by the establishment of polarity across three axes: abaxial-adaxial (front-back of leaf), proximal-distal (base-tip of leaf) and medio-lateral (main vein-edge of leaf; Conklin *et al.,* 2019; Muszynski *et al.,* 2020). It is the patterning across the abaxial-adaxial axis, regulated by a combination of genetic mechanisms and environmental factors which results in the divergence of pavement vs mesophyll cell lineages (reviewed by Wang *et al*., 2021).

1.4.2. Stomata

Cells in the outermost pavement layers of a primordium are competent to form stomata, microscopic pores on the leaf surface. Stomatal complexes in monocots such as wheat consist of a pair of dumbbell-shaped guard cells (GCs) and flanking subsidiary cells (SCs) surrounding the stomatal pore (Chen *et al.*, 2017; Raissig *et al.*, 2017; Hepworth *et al.*, 2018; Nunes *et al.,* 2019). The SCs are adapted to physically interact with the GCs and help control stomatal aperture (Hepworth *et al*., 2018; Nunes *et al.,* 2019; Wu *et al.,* 2019).

Stomatal development has been well characterised, with many of the genes and components regulating stomatal differentiation and development being understood (Hepworth *et al.,* 2018; Zoulias *et al*., 2018). In early leaf development, undifferentiated pavement cells follow a well-defined cell lineage resulting in functional guard cells (Pillitteri *et al*., 2007; Zoulias *et al*., 2018). Differentiation of monocot stomata begins from an intercalary meristem near the leaf base, and they mature as the leaf extends (Conklin *et al.*, 2019). The stomatal file is defined from the pavement cell files, outlining cells that have the capability to form stomata (Raissig *et al.,* 2016). Then, guard mother cells (GMCs) and larger sister cells are formed by asymmetric cell division within this file (Facette & Smith, 2012; Vatén & Bergmann, 2012; Raissig *et al*., 2016; Hepworth *et al*., 2018). A second asymmetric division results in formation of subsidiary mother cells (SMCs) in the pavement cells flanking the GMC (Serna, 2015; Endo & Torii, 2019), followed by an increase in cell size which results in a pair of immature SMCs flanking the GMC

(Vatén & Bergmann, 2012; Hepworth *et al*., 2018). One final symmetrical cell division splits the GMC into two immature guard cells (Hepworth *et al*., 2018; Endo & Torii, 2019). The guard cells elongate into a dumbbell shape (Liu *et al.*, 2009) and separate to form a central stomatal pore (Hepworth *et al.,* 2018). The process of monocot stomatal development is summarised in Figure 1.3.

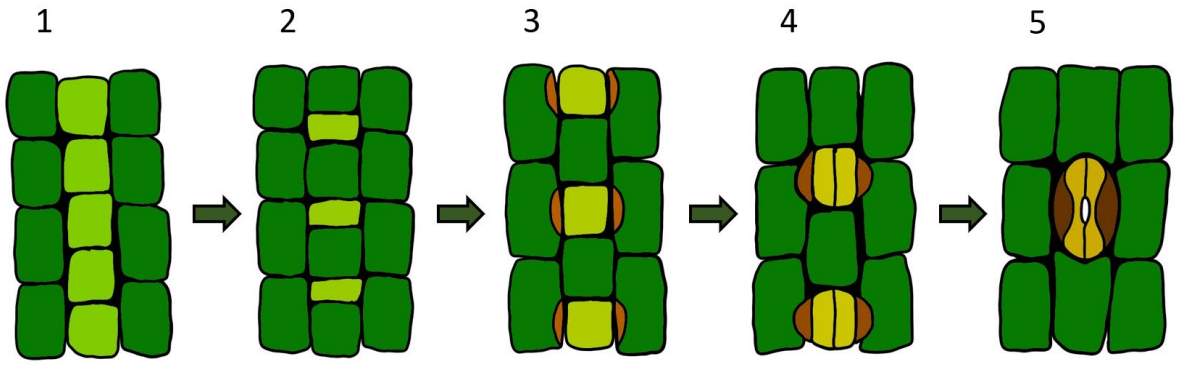

Figure 1.3. Stomatal development in grasses. Monocot stomatal development occurs in five distinct stages: 1) Determination of stomatal files. 2) Asymmetrical division results in formation of guard mother cells (GMCs). 3) A second asymmetrical division forms subsidiary mother cells (SMCs). 4) Guard cells are formed by symmetrical cell division. 5) Elongation of guard cells into a dumbbell shape and separation to form the stomatal aperture, flanked by subsidiary cells.

During pavement patterning, cells are positioned in ordered, parallel files and, from a subset of these, stomatal complexes form (Rudall *et al.*, 2017). It is functionally important that stomatal complexes are spaced at least one pavement cell apart from each other (Dow *et al.*, 2014; Bergmann & Sack, 2007; Pillitteri & Torii, 2012). Additionally, there are mechanisms in place, such as cell type determination based on proximity to the vasculature via the SHORTROOT pathway (Levesque et al., 2006; Cui et al., 2014), to ensure that stomata do not form over leaf veins. Instead, stomata are positioned over mesophyll tissue so that cell separation directly beneath the stomate leads to the formation of substomatal cavities (Bergmann, 2004; Schuler *et al.*, 2018), which help facilitate efficient diffusion of gasses in and out of the leaf. Wheat stomata are found on both the abaxial and adaxial epidermis, being slightly higher in density on the adaxial (Pemadasa, 1979; Wall *et al.*, 2022).

1.4.3. Mesophyll

While the differentiation of stomatal cells is determined by the commitment of an undifferentiated cell to the stomatal lineage (Zoulias *et al*., 2018), the development of a porous mesophyll structure is more complex. The development of mesophyll airspaces and patterning of stomata occur simultaneously and are thought to feedback on one another dynamically (Baillie & Fleming, 2020).

In young wheat leaves, there is a continuous developmental gradient of mesophyll cells with meristematic cells at the base of the leaf and differentiated cells at the tip. Mesophyll development consists of the formation lobed mesophyll cells in wheat. The mechanism behind the development of

these cell lobes was first studied in epithem cells of hydathodes (pores which let out water in the form of droplets) in *Pilea cadierei* (family Urticaceae) leaves (Galatis, 1988). Microtubules (MTs) form in ring-shaped bundles that interconnect to create a cell-wide scaffold. The cell wall is locally thickened using cellulose microfibrils (CMFs) in coordination with MT ring formation. This results in bulging of the cells where the walls have been thickened and constrictions from the MT rings, forming lobes. This mechanism, outlined in Figure 1.4, has also been shown to control lobing in *T. aestivum* mesophyll cells (Jung & Wernicke, 1990; Wernicke & Jung, 1992). The expansion phase is crucial in which the final shape of the cell is established (Jung & Wernicke 1990).

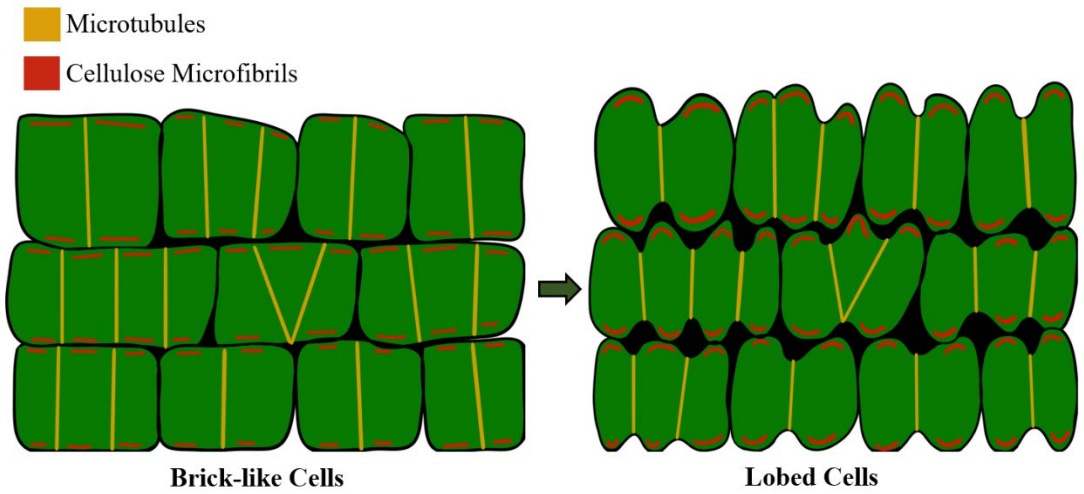

Figure 1.4. The formation of cell lobes. The combined action of constricting microtubule (MT) rings and localised thickening by cellulose microfibrils (CMFs) causes the formation of a lobed morphology as the cell expands during leaf development. Adapted from Galatis, 1988.

The controlled separation of dividing mesophyll cells caused by an array of cell wall enzymes (McCann & Carpita, 2008), followed by cell expansion to form their distinct lobed shape creates a complex pattern of airspaces, allowing for the flux of CO_2 to these cells followed by diffusion across the cell wall, plasma membrane and cytosol occurs, allowing entry of the CO_2 to the site of carboxylation in the chloroplasts (Flexas *et al.*, 2012; Lundgren & Fleming, 2020).

Across the three ploidy levels of wheat, a similar basic arrangement of mesophyll cells is observed. Unlike in eudicot species such as *Arabidopsis thaliana,* the mesophyll does not form distinct palisade and spongy mesophyll layers across the adaxial-abaxial axis. Instead, monocot mesophyll cells are patterned along the proximal-distal leaf axis, interspaced by major and minor veins (Jellings & Leech, 1984; Parker & Ford, 1982). One major difference that has been observed in wheat leaves between ploidy levels is the increase in the size of mesophyll cells from diploid to hexaploid (Jellings & Leech, 1984; Parker & Ford, 1982; Wilson *et al*., 2021), which is a general effect of polyploidy that can be seen across a range of plant species (Kondorosi *et al.,* 2000; Katagiri *et al.,* 2016). This increase in volume has been accompanied by a linear increase in cell surface area, indicating a change in shape of mesophyll cells as they increase in size, likely to maintain a high surface area to volume ratio to

maximise the cell surface available for gas exchange (Wilson *et al.,* 2021). In the same study, a decrease in overall mesophyll porosity (*i.e*. reduced airspace) in higher ploidy wheat was observed, which correlated with increased intrinsic water-use efficiency (iWUE), suggesting it may have been indirectly selected for during wheat evolution.

1.4.4. Linking stomata and mesophyll development

As well as responding to similar environmental cues, such as light intensity and CO_2 concentration (Casson & Gray, 2008; Terashima *et al.*, 2011), there is a coordination of stomatal development and mesophyll tissue formation which is not just a result of external stimuli. Some genes involved in both stomata and mesophyll development have been identified, such as ERECTA (Masle *et al.,* 2005), and STOMAGEN (Kondo *et al.*, 2010), a stomatal patterning gene that is expressed in the mesophyll. However, a full mechanistic explanation of the link between stomatal and mesophyll differentiation has yet to be discovered. Lundgren *et al.* (2019) demonstrated a possible link between the formation of substomatal cavities (which is initiated by controlled mesophyll cell separation) and the presence of functional stomata. In transgenic wheat lines overexpressing PAVEMENT PATTERINING FACTOR 1 (EPF1) in which a large proportion of stomata failed to develop, no substomatal cavities were observed beneath the arrested stomata. This phenotype suggests that the signal for the formation of sub-stomatal cavities either comes from a fully differentiated stomata or requires the flux of gas through an open stomatal pore. Combined with the existence of STOMAGEN, a mesophyll-expressed signal that has been shown to positively regulate stomatal density (Kondo *et al.,* 2010; Lee *et al.,* 2015), these findings suggest that the mechanism of mesophyll and stomatal coordination during leaf development involves signalling in both directions.

There is currently no evidence linking the development of stomata to the formation of mesophyll airspace that is not directly underneath the stomata, however as the formation of stomata and mesophyll have been shown to be linked both directly and indirectly, it is highly possible that global mesophyll cell separation is influenced by the presence of functional stomata and the gas flux through them, as well as through other unrelated developmental pathways.

Leaf development usually occurs in a constantly changing environment, where reaching the optimal structure in terms of number and size of stomata, mesophyll and cell arrangement within the leaf will involve many trade-offs linked to the life strategy and specific growth environment (Brodribb *et al*., 2013; Flexas & Carriqui, 2020; Roddy *et al*., 2020). This final structure will be to some degree adapted in terms of rate of photosynthesis and water-use efficiency for the plant to survive and grow in its local environmental conditions.

1.5. Linking Wheat Leaf Structure to Function

Understanding how the structure of leaves influences function is an important research area of plant biology (Earles *et al.*, 2018, 2019; Ren *et al*., 2019; Terashima *et al*., 2011). It is well established that stomata are key players in the trade-offs that occur between carbon fixation for photosynthesis and rate of transpiration and play a major part in controlling plant WUE through regulating CO_2 uptake and water loss (Franks and Farquhar, 1999; Xu *et al.,* 2016; Driesen *et al.,* 2020). Dumbbell-shaped guard cells belonging to grass leaves are more efficient than kidney-shaped ones, such as in Arabidopsis, as they are better at maintaining osmotic and turgor pressure between guard cells and subsidiary cells (Harrison *et al.*, 2020).

G_s is the rate at which stomata facilitate gas exchange. It is dependent on stomatal size and density at the leaf level and can also be rapidly modulated by changes in stomatal aperture (Dow & Bergmann, 2014; Dow *et al*., 2014; Lawson & Blatt, 2014; Bertolino *et al.* 2019*;* Verma *et al.* 2020). Many crop species may have been indirectly selected for increased stomatal conductance (Roche, 2015), potentially through increased stomatal density, contrasting the observation that increasing atmospheric [CO_2] causes a range of non-crop species to develop reduced stomatal densities (Hetherington & Woodward, 2003; Woodward & Kelly, 1995; Franks & Beerling, 2009). Wall *et al.* (2023) saw that diploid *Triticum* species also show this same response of reduced stomatal density under elevated atmospheric [CO_2], however no there was no significant change in that of tetraploid or hexaploid wheat. This extent of elevated CO_2 is thought unlikely to have any effect on field conditions, and it has been suggested that crop water use could be directly targeted by engineering and molecular breeding programmes through reducing stomatal density or aperture (Chaerle *et al.*, 2005; Yoo *et al.*, 2009). Contrastingly, Roche (2015) argues that high stomatal conductance is often required in the field to maximise cooling and enhance photosynthesis for increased yields. Dunn *et al*. (2019) demonstrated that overexpressing EPF1 in wheat plants (a manipulation that results in a decrease in the number of functional stomata and sub-stomatal cavities (Lundgren *et al*., 2019), has a detrimental effect on yield. However, this was only the case with lines that had >50% reduction in stomatal density. Those with a more moderate phenotype had no yield reduction but increased iWUE coupled with improved drought tolerance. These results suggest that only a large decrease in stomatal density will impact photosynthetic efficiency, and that smaller decreases could be utilised as a tool in wheat breeding to improve WUE and drought tolerance. Wheat has greater stomatal density on the adaxial surface, and Wall *et al*. (2022) found that higher photosynthetic capacity on the adaxial surface led to greater carbon assimilation which would be supported by greater adaxial g_s, which also allows for greater leaf cooling. However, in this study by Wall *et al.*, abaxial gas exchange was also seen to contribute around 50% of total leaf photosynthesis, suggesting that stomata on both pavement layers contribute roughly equally despite having significantly different densities.

It is also important to consider other stomatal traits, such as speed of stomatal movement (Lawson & Blatt, 2014*;* Chen *et al.,* 2017), when looking to enhance WUE, and to consider the effect of stomatal patterning on other plant traits such as leaf temperature and susceptibility to pathogen infection. Cowan and Farquhar (1977) proposed that stomatal aperture is regulated to reduce water loss while maintaining an optimum rate of photosynthetic carbon assimilation. Carbon gain is important to consider when thinking about water use efficiency, as iWUE is calculated as the rate of carbon assimilation (*A*) / stomatal conductance (g_s) or A / transpiration rate (*E*). Therefore, in improving WUE, the core concept is to increase *A* while only allowing for a small increase in g_s, as increased transpiration through high gs results in a significant impact on biomass production and crop yield (Urban *et al.* 2017; Guerrieri *et al.* 2019*).*

Although leaf gas exchange is regulated dynamically by the opening and closing of stomatal pores, the patterning of stomata combined with mesophyll architecture determine the maximum potential flux of gases (Momayyzi *et al*., 2022; Dow *et al*., 2017; Lundgren *et al.,* 2019; Baillie & Fleming, 2019). Mesophyll cells are important determinators in the rate of carbon assimilation and require sufficient light and CO_2 for their role in photosynthesis. However, the availability of these to the internal mesophyll cells depends greatly on the architecture of the whole leaf, which in turn is greatly influenced by the size and geometry of the mesophyll cells and their arrangement and interactions with each other and other cell types in 3D space. It is important to also consider that the arrangement, shape, and size of mesophyll cells not only has an impact on CO_2 flux, but also other photosynthetic parameters such as permeability to and scattering of light (Terashima *et al.,* 2011; Tholen *et al.,* 2012), and additional factors linked to leaf structure and function including mechanical integrity and water transport (Buckley *et al.,* 2015). Lehmeier *et al*. (2017) show that altering pattens of leaf cell division within an Arabidopsis leaf (resulting in altered airspace patterning) can lead to an increase in photosynthetic rate. This occurred both through increasing and decreasing mesophyll cell size, but likely through different mechanisms. They suggest that increasing mesophyll cell size likely increases the rate of photosynthesis through a simple increase in leaf thickness. Decreasing mesophyll cell size was suggested to improve photosynthetic rate through improving the *in vivo* activity of the enzyme Rubisco, and potentially through the structural changes linked to decreased volume and patterning of mesophyll airspace and increased CO_2 conductance in the leaf.

Throughout wheat evolution and cultivation, there have been a series of complex changes with regards to the shape and size of both the mesophyll cells and their surrounding airspace that have had important implications for leaf function. From diploid to hexaploid wheat, as the mesophyll cells have become larger there has been a reduction in mesophyll porosity, with an accompanying increase in iWUE (Wilson *et al.,* 2021). Interestingly, there has also been a transition to more water-use efficient plants in tetrapoloid wheat following domestication to *T. turgidum ssp. durum* that has not been accompanied by as significant changes to mesophyll or stomatal parameters (Wilson *et al.,* 2021).

The increase in global cell size that accompanies increases in ploidy also encompasses stomatal cells (Beaulieu *et al.,* 2008; Austin *et al*., 1982; Wang & Clarke, 1993; Maosong *et al*., 2008; Khazaei *et al*., 2010). Not only are the stomatal complexes of higher ploidy wheat larger, but the increase in pavement cell size also reduces the density of stomata that can be packed onto the surface of the leaf (Wilson *et al.,* 2021). This reduction in stomatal density is likely the greatest contributor to decreased stomatal conductance and increased iWUE observed with increasing ploidy.

It has been suggested that manipulating the existing relationship between stomatal density and mesophyll structure could prove useful in improving WUE (Dow *et al.*, 2017; Lundgren *et al.*, 2019). Mesophyll conductance (g_m; how easily CO_2 can diffuse from the leaf air space into the chloroplasts) and g_s are positively correlated, although the reason for this remains undetermined (Guiliani *et al.,* 2013; Barbour & Kaiser, 2016). G_m has been suggested to play an important role in photosynthetic efficiency, as improved CO_2 flux within the mesophyll increases the supply of CO_2 to Rubisco and hence increases the rate of carbon fixation (Flexas *et al.,* 2008; Kaldenhoff, 2012; Adachi *et al.,* 2023). Manipulating this relationship and enhancing g_m independently of g_s by breaking coordination of stomatal patterning and mesophyll architecture is one avenue for improving WUE (Flexas *et al*., 2013; Lundgren *et al.,* 2019). However, it is important to consider other traits that could be affected by altering mesophyll structure, such as light capture for photosynthesis.

Genes that alter leaf structure to influence plant WUE have been identified in different species. The first published gene identified by QTL mapping that regulates WUE was *ERECTA* in *Arabidopsis* (Masle et al., 2005). A non-functional *erecta* allele increases stomatal density, increases stomatal conductance, and reduces photosynthetic capacity by reducing rubisco carboxylation rate, resulting in decreased WUE (Masle *et al.,* 2005). Similarly, other genes that regulate stomatal function have been seen to impact WUE to different degrees (Klein *et al.,* 2003; Thompson *et al.,* 2007; Iuchi *et al.*, 2001; Zhang *et al.*, 2008), and combining loss-of-function mutations can further improve WUE (Yu *et al.*, 2008; Yoo *et al.*, 2008).

There have also been attempts to alter leaf function and improve WUE by modifying the mesophyll. In *Arabidopsis,* for example by exploiting the *HARDY (HRD)* gene which positively regulates the production of mesophyll cells (Karaba *et al.,* 2007). A gain-of-function mutation of this gene increased the number of mesophyll cell layers in *Arabidopsis,* which contributed towards increased drought and salt tolerance. Overexpression of *HRD* in rice increased both WUE and iWUE; a result of decreased transpiration and increased biomass production and carbon assimilation (Karaba *et al.,* 2007).

1.6. Genetic Techniques and Modification in Wheat

Domestication of modern wheat varieties occurred through the selection of desirable traits. One of the initial major drivers of selection in domesticated wheat is thought to have been increased yield (Peng *et al.*, 2011; Preece *et al.*, 2017), and in recent history there have been some major genes uncovered and targeted for crop improvements related to yield. During the Green Revolution of the 1950s-60s, the introduction of novel traits such as semi-dwarfing alleles of the *RHT1* (*REDUCED HEIGHT 1*) gene led to gains in wheat yield due to reduced lodging and increases in assimilate partitioning to the developing ears (Borlaug *et al*., 1968). In the past, the introduction of these traits has occurred through selective breeding and have led to many further improvements in wheat yield (Fleury *et al*., 2010; Ihsan *et al*., 2016; Richards *et al.,* 2002). However, the demand for wheat is expected to rise by 1.6% annually until 2050 and the traditional selective breeding approach is both time- and resource-consuming and unlikely to achieve the desired yield increase to 5 tonnes per ha from the current 3.3 tonnes (CGIAR, 2013). To tackle the yield gap, key genes need to be identified related to plant productivity and adaptation to environmental stresses, as well as tolerance to future climate changes. Modern genetic methods, such as gene editing (GE) and genetic modification (GM) approaches will probably be required if the yield gap is to be closed in a timely manner.

Despite over 790 million tonnes of wheat grain being harvested worldwide in 2023/2024 (USDA, 2024), wheat lags behind other key agricultural crops in terms of current yield and application of genomic tools for yield improvement (Uauy, 2017). This is likely due to its large polyploid genome, containing an estimated 107,891 genes with over 85% repetitive sequences with a three-fold redundancy reflecting its hexaploid genome (Appels *et al.,* 2018). Modern genetic tools such as molecular breeding allow for the rapid discovery of genes linked to crop improvement, as well as reduced number of generations needed for the desired phenotype to be observed. Natural variation has helped with identification of QTLs responsible for agriculturally important traits such as WUE (Mitchell-Olds & Schmitt, 2006; Shindo *et al.,* 2007; Takeda & Matsuoka, 2008), with functional annotations of a fully sequenced Chinese Spring wheat genome being a key tool (Bolser *et al.,* 2015). The sequencing of the Chinese Spring genome allowed for the application of functional genomics to wheat. Prior to this, generating ethyl methanesulfonate (EMS) mutations in a wheat panel and selecting mutants with desired phenotypes was the way in which changes could be made to a wheat plants genetics faster than via selective breeding.

Genetic transformation facilitates the introduction and alters expression of a wide range of genes, bypassing the barriers of sexual incompatibility that exist in nature. Another obstacle to the advancement of wheat genomic technologies is the relative recalcitrance to *in vitro* culture and regeneration (Shrawat & Armstrong, 2018). The first successful genetic transformation of wheat was in 1992 (Vasil *et al.,* 1992), and in 1997, there was the first report of the generation of transgenic wheat using Agrobacterium-mediated transformation (Cheng *et al*., 1997). *Agrobacterium*-mediated transformation using immature embryos and biolistics are the main methods currently used for genetic

engineering of wheat. Each technique offers advantages in different situations. For example, *Agrobacterium* transformation allows for a relatively high ratio of single copy gene inserts while having a simple transformation protocol, while biolostics are particularly good at transforming organelles and delivering RNA, proteins, dyes and complexes into cells (Borisjuk *et al*., 2019). Additionally, biolistically-delivering Minimal Expression Cassettes (MECs) facilitates easy cotransformation of several genes into the plant, as well as allowing for the transfer of larger DNA fragments than with transformation via *Agrobacterium* (Partier *et al*., 2017). There are disadvantages for both *Agrobacterium* and biolistic transformation methods in wheat, the main being that the transformation frequency (TF) is highly genome-dependent and both require long periods of tissue culture. One way to overcome this is by using *in planta* approaches as opposed to *in vitro* methods, and the direct injection of *Agrobacterium* has been shown to improve TF of wheat (Supartana *et* al., 2006; Zhao *et al.*, 2006; Razzaq *et* al., 2011; Hayta *et* al., 2019), and a biolistic *in planta* method developed by Hamada *et al.* (2017) also demonstrated improved TF. Wheat genetic manipulation efforts using transgene expression has so far targeted all major agronomic traits such as yield (Bednarek *et al*., 2012; Hu *et al*., 2012; Hong *et al*., 2014; Zhang *et al*., 2014; Qu *et al.,* 2015; Yadav *et al*., 2015; He *et al*., 2015; Qin *et al*., 2016; Peña *et al*., 2017), grain quality (Altpeter *et al.,* 1996; Barro *et al*., 1997; Rooke *et al*., 1999; Lucrecia-Alvarez *et al.,* 2001; Sherwy *et al*., 2006; Smidansky *et al*., 2007; Weichert *et al*., 2010; Li *et al*., 2012; Zhao *et al*., 2013; Bravo *et al*., 2013; Liu *et al*., 2016; Zhao *et al*., 2021) and stress tolerance (Hu *et al*., 2018; Tian *et al.,* 2018).

Another method used to alter gene expression in wheat is RNA interference (RNAi). This works by expressing antisense or hairpin RNAi constructs or other short interfering RNA molecules (siRNAs) to trigger posttranscriptional gene silencing to targeted genes. The first wheat gene to be targeted by RNAi in this way was *TaVRN2*, the vernalisation gene, which reduced flowering time (Yan *et al*., 2004). RNAi technologies have also contributed to improving wheat grain size (Uauy *et al*., 2006; Li *et al*., 2018a; Zhao *et al*., 2016) and quality (Regina *et al*., 2006; Barro *et al.* 2016; Li *et al.,* 2005; Yue *et al*., 2008). However, the most promising application has been in pathogen and pest control using virus and host-induced gene silencing (HIGS) platforms (Lee *et al*., 2012; Nowara *et al.,* 2012; Cheng *et al.,* 2015; Chen *et al.,* 2015).

More recently, targeted genome modifications have become more prevalent in wheat research. Zinc finger nucleases (ZFNs) and TAL effector nucleases (TAL-ENs) were developed at the end of the 20th century as tools to generate targeted mutations (Puchta & Fauser, 2013). Such nuclease-based mutagenesis induces site-specific double-strand breaks (DSBs) which, through either error-prone non-homologous end joining (NHEJ1) or homologous recombination (HR) results in either insertions or deletions (InDels) leading to loss-of-function knockouts, or precise genome modifications. However, in 2012 these techniques were made somewhat redundant by the introduction of CRISPR/Cas9 (bacterial Clustered Regularly Interspaced Short Palindromic Repeats) technology (Jinek *et al.,* 2012).

CRISPR/Cas9 works by conferring the targeted gene mutation via the Cas9 nuclease that is guided by small RNAs (sgRNAs) through base paring to the target gene. Due to its operational simplicity and universality compared to ZFNs and TAL-Ens, CRISPR/Cas9 is now widely used among the scientific community (Mali *et al*., 2013; Demirci *et al*., 2018). The applicability of CRISPR/Cas9 in wheat protoplasts was demonstrated in 2013 (Shan *et al.,* 2013; 2014; Upadhyay *et* al., 2013). The original methods for CRISPR-Cas9 genome editing in plants used plasmids carrying cassettes for co-expression of Cas9a and sgRNA and were transformed by either *Agrobacterium* or particle bombardment.

One of the major advantages of CRISPR/CAS9 editing is its's potential to simultaneously target several genes with a single construct. In hexaploid wheat, editing has been reported in protoplasts (Shan *et* al., 2013; 2014; Liang *et al.,* 2017; Gil-Humanes *et al.,* 2017), microspores (Bhowmik *et al*., 2018), cell suspension cultures transformed using *Agrobacterium* (Zhang *et al.,* 2017). CRISPR/Cas9 edited wheat plants have been regenerated from embryos, embryo-derived callus or shoot apical meristems transformed by *Agrobacterium* (Singh *et al.,* 2018; Howells *et al.,* 2018) or biolistics (Liang *et al.,* 2017; Gil-Humanes *et al.,* 2017; Wang *et al*., 2014; Zong *et al*., 2017; Hamada *et al.,* 2018). CRISPR/Cas9 has also been able to overcome the major issue with genetic modification - presence of transgenic DNA in transformed plants – through delivering *in-vitro* transcripts or ribonucleoprotein complexes (RNPs) of CRISPR/Cas9 (Čermák *et al.,* 2017; Gil-Humanes *et al.* 2017). Additionally, this approach has been shown to reduce off-target effects, allowing for completely transgene-free and highly precise wheat mutants. However, these transgene-protocols lack the ability to select for transformants in the transformation and regeneration process. More recently, targeted base editing using Cas9 fused with a cytidine deaminase (Zong *et al.,* 2017) or adenosine deaminase (Li *et al.,* 2018b) has been able to successfully induce specific loss-of-function mutations (Zong *et al.,* 2018).

The first successful experiment using CRISPR/Cas9 editing in wheat was on *TaMLO*, a powdery mildew-resistance gene (Shan *et al.,* 2013). Since then, CRISPR/Cas9 editing has been successful in wheat for a broad range of applications, including resistance/tolerance to abiotic (Liang *et al.,* 2018) and biotic (Wang *et al.,* 2014; Upadhyay *et al.,* 2013; Nalam *et al.,* 2015; Shan *et al.,* 2014; Zhang *et al.,* 2017) stresses, yield and grain quality (Wang *et al.,* 2018; Hamada *et al.,* 2018; Zhang *et al.,* 2016) and male sterility (Singh *et al.,* 2018). This included the editing of a wheat homolog of *TaCer9 (ECERIFERUM9)* to improve drought tolerance and water-use efficiency (Liang *et al.,* 2018). Recently, the efficiency of wheat CRISPR-Cas9 transformation has been further improved, as Debernardi *et al.* (2020) found that co-transforming wheat with a desired CRISPR-Cas9 construct alongside a chimera of *GROWTH REGULATING FACTOR 4* (*GRF4*) and its *GRF-INTERACTING FACTOR 1* (*GIF1*) cofactor produced transgenic plants with a high regeneration frequencies that could be used for future transformation experiments.

The ability to utilise modern genetic transformation and modification technologies and induce targeted changes in the wheat genome has revolutionised the potential for reducing the yield gap in polyploid crop species such as wheat and has opened up new avenues to creating future-proof wheat cultivars.

1.7. Aims

The main aim of this project was to further our understanding on the effect of wheat leaf architecture on leaf function, specifically water-use efficiency. The aims for each data chapter are listed below:

Chapter 3: Explore the variation that is present in wild, landrace, and modern domesticated tetraploid wheat varieties, observing leaf morphologies and identifying any links to iWUE.

Chapter 4: Test the hypothesis that leaves of *Triticum* species with a range of ploidy and cultivation levels show abaxial-adaxial patterning of cells within the mesophyll tissue.

Chapter 5: Use gene-edited wheat lines overexpressing a *GRF4-GIF1* construct to test the hypothesis that cell size, shape, and arrangement in wheat leaves influences iWUE.

Chapter 2: Methodology

2.1. Plant Growth

For all experiments, plants were sown in F2+S compost (F2 compost and sand; ICL, Suffolk, UK) and placed into a controlled environment growth chamber (Conviron PGR15; Conviron, Winnipeg, MB, Canada) in the Sir David Read Controlled Environment Facility (University of Sheffield, Sheffield, UK). The environmental conditions of the chamber: air temperature = 21°C:16°C, 16h light = 400 μmol m^{-2} s^{-1}, 8h dark, 60% relative humidity.

After germination and 1 week of growth, the seedlings were transplanted into larger pots (square pots, 12.75cm depth and 13cm width at top) containing 6:1 mix of F2+S compost and Perlite (Sinclair Pro, Cheshire, UK), and five grams of Osmocote Exact 5-6 slow-release fertiliser (ICL, Suffolk, UK) was added to each pot and mixed into the top layer of compost. Plants were watered and number of leaves and plant height were recorded at three times a week throughout the 40-day growth period. Leaf width was measured at the broadest part of the 5th leaf from the main tiller at 28 days after sowing of seeds (vegetative phase).

Information on plant materials used can be found in the relevant chapters.

2.2. Stomatal and Pavement Cell Measurements

2.2.1. Slide Preparation and Imaging

After 28 days post-sowing of seeds, dental putty (Coltene Whaledent, Switzerland) was painted onto both sides of the fifth leaf of each plant and left to dry for 5 minutes. The putty was then removed and painted with transparent nail polish. After the first layer of polish had dried, this was repeated. The nail varnish pavement imprints of both the adaxial and abaxial surfaces were carefully peeled off the dental putty and fixed to microscope slides by taping over a cover slip. The imprints were imaged on an Olympus BX51 microscope with an Olympus DP71 camera (Olympus, Japan) – this was done at 4x magnification for counting stomatal density and 10x for measuring stomatal and pavement cell size. Three images were taken from each plant for technical repeats (from which the mean was then used), and six biological repeats (plants) were imaged per line for a total of 18 images.

2.2.2. Stomatal size and density measurements and anatomical g_{smax} calculation

The total area of the field of view of an image taken at 4x magnification was measured using FIJI (ImageJ 5.3g; Schindelin *et al*., 2012), and the number of stomata within this area was counted. Stomatal density was calculated as: number of stomata/total area. This was done separately for Abaxial and

Adaxial epidermises, and the mean was calculated to represent the average stomatal density across both surfaces.

Stomatal cell size was measured from images taken at 10x magnification using an ImageJ macro in FIJI. At least five stomatal complexes were measured per image. Parameters measured were: guard cell length, guard cell width, pore length and stomatal complex width. These are highlighted in Figure 2.1. Stomatal area was estimated using the following equation:

$$A = \pi \frac{L \, x \, W}{4}$$

Where L is guard cell length and W is stomatal complex width.

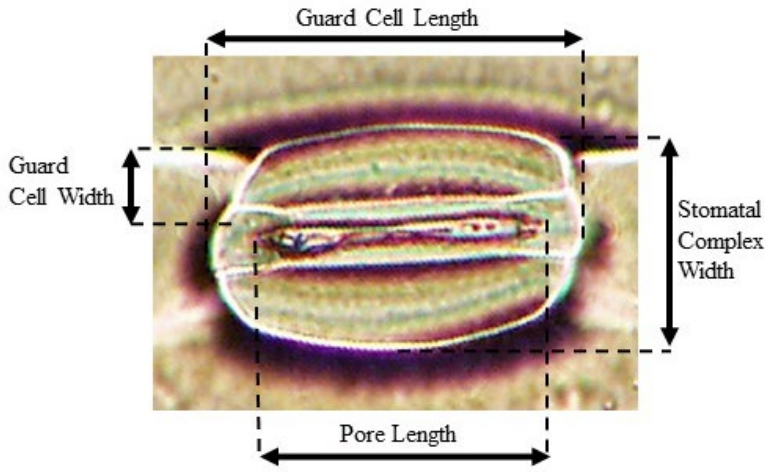

Figure 2.1. Stomatal size measurements. Stomatal cell size measurements. These measurements are used to calculated stomatal complex area and maximum anatomical stomatal conductance (g_{smax}). 'Guard cell' width includes both guard and subsidiary cells. This image is of hexaploid Fielder cells from the adaxial leaf surface.

Anatomical g_{smax} was calculated from stomatal size and density data, using the following equation from Caine *et al.* (2019):

$$Abaxial\ anatomical\ g_{smax} = (d \cdot D \cdot a_{max}) / (v \cdot (l + (\pi/2) - \sqrt{(a_{max}/\pi)}))$$

Where D is stomatal density, a_{max} (μm^2) is the maximum pore aperture calculated as an ellipse from axes equal to the measured pore length and half of the pore length, d (m^2 s^{-1}) is the diffusivity of water in air and v (m^3 mol^{-1}) is the molar volume of air, and l is pore depth (μm) estimated as being equal to guard cell width.

The abaxial:adaxial stomatal density ratio measured for each leaf (between 0.86 and 0.98) was used to calculate total anatomical g_{smax}.

2.2.3. Pavement Cell Size Measurements

Pavement cell size was measured using an ImageJ macro in FIJI using images taken at 10x magnification. Parameters measured were: pavement cell length, non-stomatal file pavement cell width and stomatal file pavement cell width. These measurements are demonstrated in Figure 2.2. Pavement cell area was calculated by multiplying the mean of both types of pavement cell widths by the mean pavement cell area of each image. A minimum of 10 cells per image were measured.

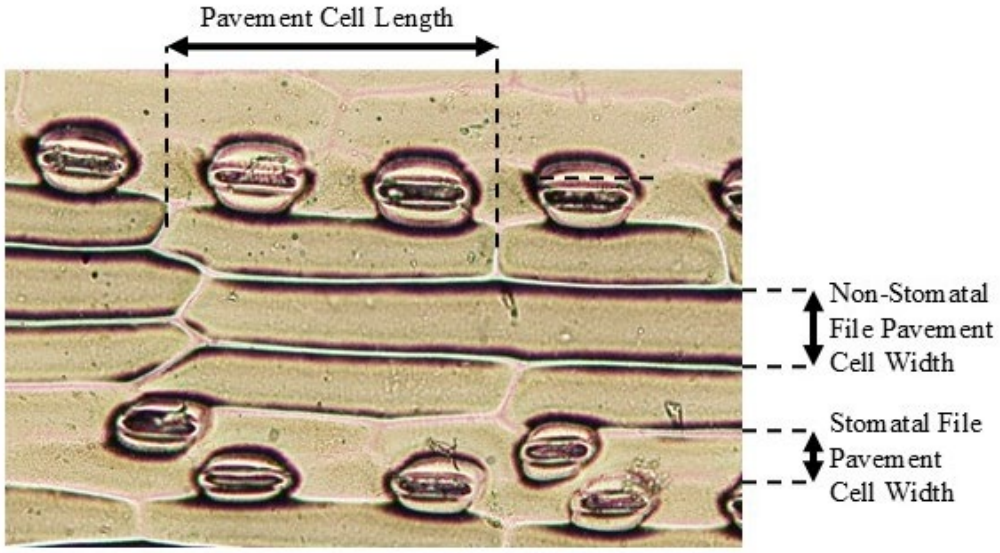

Figure 2.2. Pavement size measurements. The stomatal and non-stomatal cell file widths were measured to independently determine any cause/effect of stomatal complex width differences. This image is of hexaploid Fielder cells from the adaxial leaf surface

2.3. 2D Mesophyll Imaging and Analysis

2.3.1. Sample preparation and Imaging

Sample Collection, Fixation and Storage

After 28 days of plant growth from sowing of seeds, three sections approximately 1cm in length were taken from the fifth leaf on the main tiller of each plant and immediately placed into a fixative comprising of 3:1 ethanol (EtOH):acetic anhydride (v/v) in glass vials. The same leaf was used for imaging epidermal cells using dental putty imprints. The samples were placed into a vacuum pump for one hour to vacuum infiltrate them, before being stored room temperature for 48 hours. This fixative forms ethyl acetate, aiding permeability of the sample. After the minimum of 48 hours, samples were washed with a 50% ethanol solution for 15 minutes, before being rinsed and stored in 70% ethanol at 4°C until imaged.

Infiltration

Samples were transferred to 1:1 EtOH:Technovit® (TAAB Laboratories Equipment Ltd, UK) base liquid and vacuum infiltrated for one hour before being left for 24 hours at room temperature. The samples were then moved to 100% Technovit® base liquid and refrigerated for 48 hours. Next, samples were moved to Technovit® 1 (1g Hardener 1 per 100ml Technovit® base liquid, made fresh every time), and refrigerated for 24 hours.

Embedding and curing

In a small Petri dish, ~3ml of Technovit® 1 was mixed with a large forcep pinch of neutral red dye and mixed until a uniform colour.

Working with one unlabelled sample at a time, samples were placed in the neutral red dye for 5 minutes before blotting on tissue paper to remove excess dye. Hardener 2 liquid was added to Technovit® 1 in a 1:15 ratio (Technovit® 2). 280ul of Technovit® 2 was pipetted into each of a pair of Eppendorf lids (one positioned for transverse sectioning and one for longitudinal for one sample). Leaf sections were embedded with veins perpendicular to the base of the lid. Samples were left at room temperature for 2hrs to set then transferred to 32°C oven overnight.

Mounting onto Histoblocs

Samples were removed from Eppendorf lid by making two opposite cuts down the side of the lid, allowing the lid to be bent away like a hinge.

A ~0.75cm blob of Technovit® 3040 was poured onto the centre of the Histobloc (TAAB Laboratories Equipment Ltd, UK) and the samples were placed with the leaf tissue pointing towards one of the shorter ends of the bloc. The Histoblocs were left to set before sectioning.

Sectioning

Prior to sectioning, each resin block was cut in half with a hacksaw to remove the smooth edge and make the sectioning process easier, retaining the half containing the leaf sample on the Histobloc.

A Leica RM2245 microtome (Leica Microsystems, UK) was used to section the resin blocks into 8µm slices. Six transverse slices were taken from each line. These slices were placed in a Petri dish filled with water to lie flat, and then collected on a glass coverslip and placed on a wire mesh over a heat block at 60°C until all water had evaporated. The sections were then stained with toluidine blue dye + 0.05% Borax**,** rinsed twice with $_dH_20$ and left on the heat once more until completely dry. The samples, along with the coverslips, were mounted onto slides using Eukitt® Quick-hardening mounting medium (Sigma-Aldrich, UK).

Imaging

Images were taken on an Olympus BX51 microscope with an Olympus DP71 camera (10x and 20x objectives). Two images from each section (six transverse and six longitudinal sections per plant) were taken where possible, resulting in a maximum of 12 plant and 4-6 biological repeats for both transverse and longitudinal directions. Example images of leaf sections are shown in Figure 2.3. Transverse (Figure 2.3a) were taken between the 2nd and 3rd veins out from the midvein.

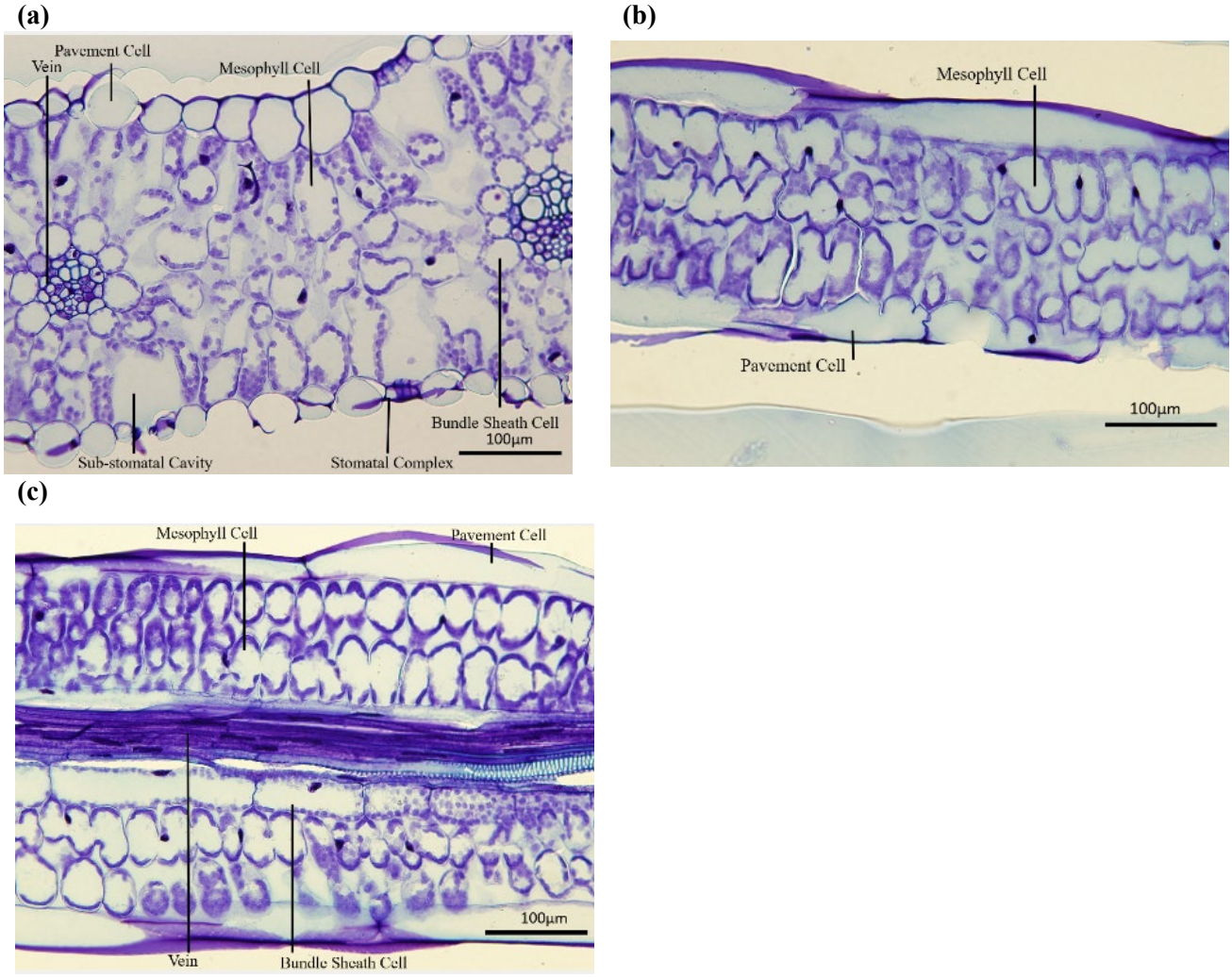

Figure 2.3. Light microscope images of 2D wheat leaf sections. a) Transverse section b) Longitudinal sections, with no vasculature present. c) longitudinal section where the vasculature is visible. Samples were stained with toluidine blue and imaged on a light microscope at 20x magnification. These are images of a tetraploid *T. turgidum ssp. durum* leaf, 5th leaf from the main tiller sampled at 28 days after planting.

2.3.2 Interveinal Distance, Mesophyll Thickness, and Leaf Thickness Measurements

Interveinal distance (IVD), leaf and mesophyll thickness were measured from transverse leaf sections (Figure 2.3a) in FIJI (ImageJ) using a custom macro (.ijm). Mesophyll thickness was measured over

and in between the 2nd and 3rd veins out from the mid vein, and leaf thickness was measured as the mean of the leaf thickness above the mesophyll in the same region and across the 3rd vein on transverse leaf sections. IVD was measured from the centremost points of the 2nd and 3rd veins from the mid vein.

2.3.3. 2D Mesophyll Cell Measurements

Mesophyll cell area and shape was measured by outlining each cell using images of both transverse and longitudinal sections in FIJI (ImageJ) using a custom macro (.ijm). Every cell within was outlined in ImageJ, and area (μm^2), perimeter (μm), circularity, cell length (Feret), cell width (MinFeret), and convex hull perimeter (μm) measurements were taken. Mesophyll cell lobing area was calculated as convex hull area minus cell area. For transverse sections, circularity was used to quantify shape and lobing area for longitudinal sections.

The data from all ImageJ macros used in this project were exported as an annotated image, a zipped folder containing ROI data and CSV files. The numerical data were then organised and analysed using RStudio (ver. 4.1.0). The script (adapted from Sloan *et al*., 2023) outputs data for variables such as cell area and circularity/lobing for each leaf.

For Chapter 4 Only: For the work done in Chapter 4, the above data for each mesophyll cell was allocated a 'layer' identity depending on its location in the mesophyll. See figure 4.2 for information on how cell layer was determined.

For Chapter 5 Only: In Chapter 5, in addition to mesophyll cell area and shape measurements as above, the number and transverse area of mesophyll and bundle sheath cells was recorded. The structure of a wheat leaf showing inner (IBSC) and outer bundle sheath cells (OBSC) is shown in Figure 2.4.

Mesophyll cells (MSC) were counted between the purple dotted lines indicated in Figure 2.4, and the IBSC and OBSC counts from surrounding the 2nd and 3rd veins out from the mid vein were recorded, the mean across the two veins was calculated and the BSC:MSC ratio calculated. The transverse area of the mesophyll and I/OBSCs were measured in FIJI (ImageJ) using a custom macro (.ijm) in which the cells were outlined by hand. From these cell area measurements, the total area in each transverse section of each cell type was calculated by multiplying the cell count by the mean cell area and this was then expressed as a ratio of I/OBSC:MSC total area to understand the proportion of the leaf in a section that is mesophyll and bundle sheath tissue.

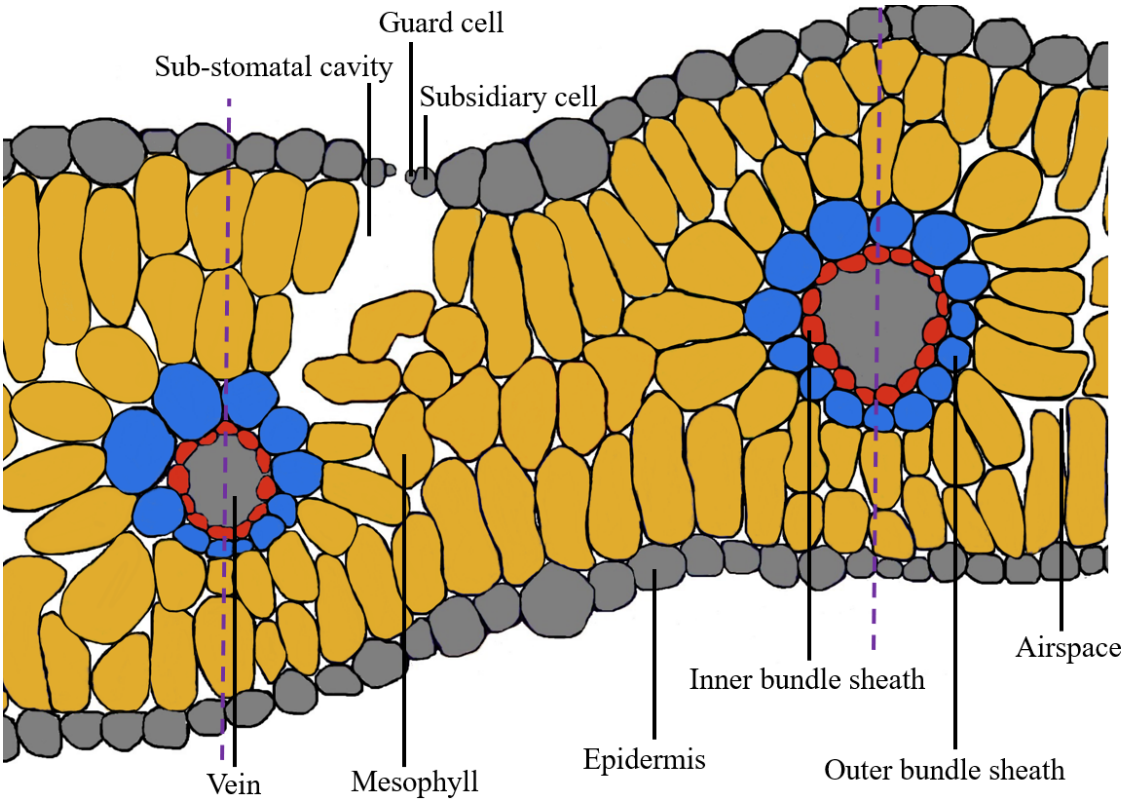

Figure 2.4. A diagram of a typical wheat leaf. This diagram was generated using a transverse cross-section of a *Triticum durum* leaf and highlights mesophyll and inner/outer bundle sheath cells.

2.4. 3D Imaging and Analysis

2.4.1. Sample Preparation and Imaging

Sample Collection, Fixation and Storage

After 28 days from sowing of seeds, three sections approximately 1cm in length were taken from the fifth leaf of each plant and immediately placed into a fixative comprising of 3:1 EtOH:acetic anhydride (v/v) in glass vials. The samples were placed into a vacuum pump for one hour to vacuum infiltrate them, before being stored at room temperature for 48 hours. This fixative forms ethyl acetate, aiding permeability of the sample. After the minimum of 48 hours, samples were washed with a 50% ethanol solution for 15 minutes, before being rinsed and stored in 70% ethanol at 4°C in the dark until imaged.

Sample preparation for confocal microscopy

When required for imaging, one leaf section was transferred into a new vial, where it was treated with chloroform for a period of 10 minutes to remove leaf cuticular waxes (Wuyts *et al.*, 2010). The chloroform was then replaced with a solution of 70% ethanol for 15 minutes to initiate a progressive rehydration. This was followed by rinsing in 50% ethanol and finally in dH_2O, leaving for 15 minutes in each solvent.

Next, the sample was suspended in 0.2 M NaOH solution containing 1% Sodium dodecyl sulphate (w/v) (SDS) for 15 minutes before rinsing three times with distilled water. The leaf tissue was then treated with a starch digester solution consisting of phosphate buffered saline (PBS), 0.1% Tween-20 and 0.01% (w/v) alpha-amylase (Sigma-Aldrich, UK) and incubated at 37°C overnight. This step removed starch grains from the sample which could potentially impact on image quality and any downstream processing required.

After incubation, samples were treated with a freshly prepared solution of 1% (v/v) periodic acid (Sigma-Aldrich, UK) for 40 minutes, before rinsing in dH_2O. Samples were then stained using the fluorescent dye propidium iodide (PI, Sigma-Aldrich, UK), which stains the cell walls. Leaf sections were treated in a Pseudo-Schiff propidium iodide (PI) solution consisting of 0.1 M $Na_2S_2O_5$, 0.15 N HCl, 0.01% PI for 4 hours. Periodic acid treatment results in the formation of aldehyde groups at cell walls, which react with the PI and strongly label the cell walls with this fluorescent dye (Truernit *et al*., 2008). This step should be carried out in the dark to avoid decay of the PI fluorophore, which is light labile.

After the staining period, samples were washed three times in water and left overnight in the third rinse at 4°C under dark conditions. A successful stain results in the leaf sections becoming pink in colour, with more intense staining along leaf vasculature and at the edges of the sample.

After staining, the next step in the sample preparation was clearing. A few drops of a clearing solution consisting of 200 g chloral hydrate (Sigma-Aldrich, UK), 20 ml glycerol and 30 ml dH_2O were added to the vials containing the leaf sections and left for 6 hours. Once cleared, the leaf sections were blotted using a tissue to remove excess liquid. Each section was then dissected along the midrib to allow for the preparation of flatter samples. One piece of the dissected sample was flipped so that the adaxial side was facing up and was placed directly onto coverslip using a few drops of mountant consisting of: 3 g 20% (v/v) Arabic gum, 10 g chloral hydrate and 1 g glycerol and mounted onto microscope slides. This reduced the distance between the sample and the coverslip. Coverslips were then secured using clear nail varnish. The other half of each sample was left with the abaxial side upwards and was mounted in the same manner. Once mounted on slides, samples were kept in dark conditions at 4°C to prevent the sample bleaching and imaged within one week of mounting.

Imaging leaf sections using confocal microscopy

The leaf sections were imaged using a ZEISS (Oberkochen, Germany) Airyscan confocal microscope. The PI stain was excited using the 561nm DPSS Diode laser. Scans were performed at a resolution of 1024 x 1024 pixels, with a pixel dwell of 1.06 µs/pixel and with a z-step interval of 0.3µm per slice. The 20x dry objective was used. Once an appropriate area was chosen based on sufficient absence of noise, vasculature and significant substomatal cavities, the capture area was zoomed to 2x before beginning the experiment. Correction was used to increase the laser power to manually inputted values

at regular intervals throughout the z-stack, between a laser power of roughly 3-18%. Piezo (Piezoelectric actuator) was used to capture z-stacks to increase resolution. An example z-stack can be seen in Figure 2.5a.

2.4.2. 3D Image Processing and Segmentation using MorphographX

3D reconstruction and segmentation of the leaf mesophyll cells was carried out using MorphographX software (Barbier de Reuille et al., 2015). Stacks were initially converted into TIFF format using FIJI/ImageJ. The TIFF image files were loaded into the MGX user interface to open the stack. Stacks were loaded in MorphoGraphX and the built-in, pre-trained CNN for cell boundary prediction using the process "Stack/CNN/UNet3D" (Vijayan *et al.,* 2021) was used prior to segmentation. The correct voxel size was inputted, and Gaussian blur was added to the stack at a value of between 0.3 and 0.7 in all directions, optimised for each individual sample.

Segmentation of the sample was carried out using the ITK Threshold Autoseeded Watershed function, set to a threshold of 1000-1500, manually optimised for each sample (Figure 2.5b). This value was altered appropriately depending on whether the stack was over- or under-segmented. The seeding was examined, and labels were fused and reseeded where necessary. Any under-segmented regions and intercellular airspaces were removed at this stage.

The mesh was generated using a 3D marching cubes algorithm, with a cube spacing of 1µm and three smooth passes (Figure 2.5c). Once this mesh was created, final cleaning up of the sample was carried out so that all incomplete cells touching the edges of the z-stack were removed. Any remaining artefacts were also removed along with other any non-mesophyll cells remaining. Data relating to cell volume and surface area were exported as spreadsheets and heat-maps (Figure 2.5d), and the number of 'lobes' per each cell was manually documented.

Prior to generation of heat-maps, the mesh was rescaled by 1.55x in the z-direction due to issues with spherical aberration and axial distortion experienced during imaging due to differences in refractive index, as described by Diel *et al*., (2020).

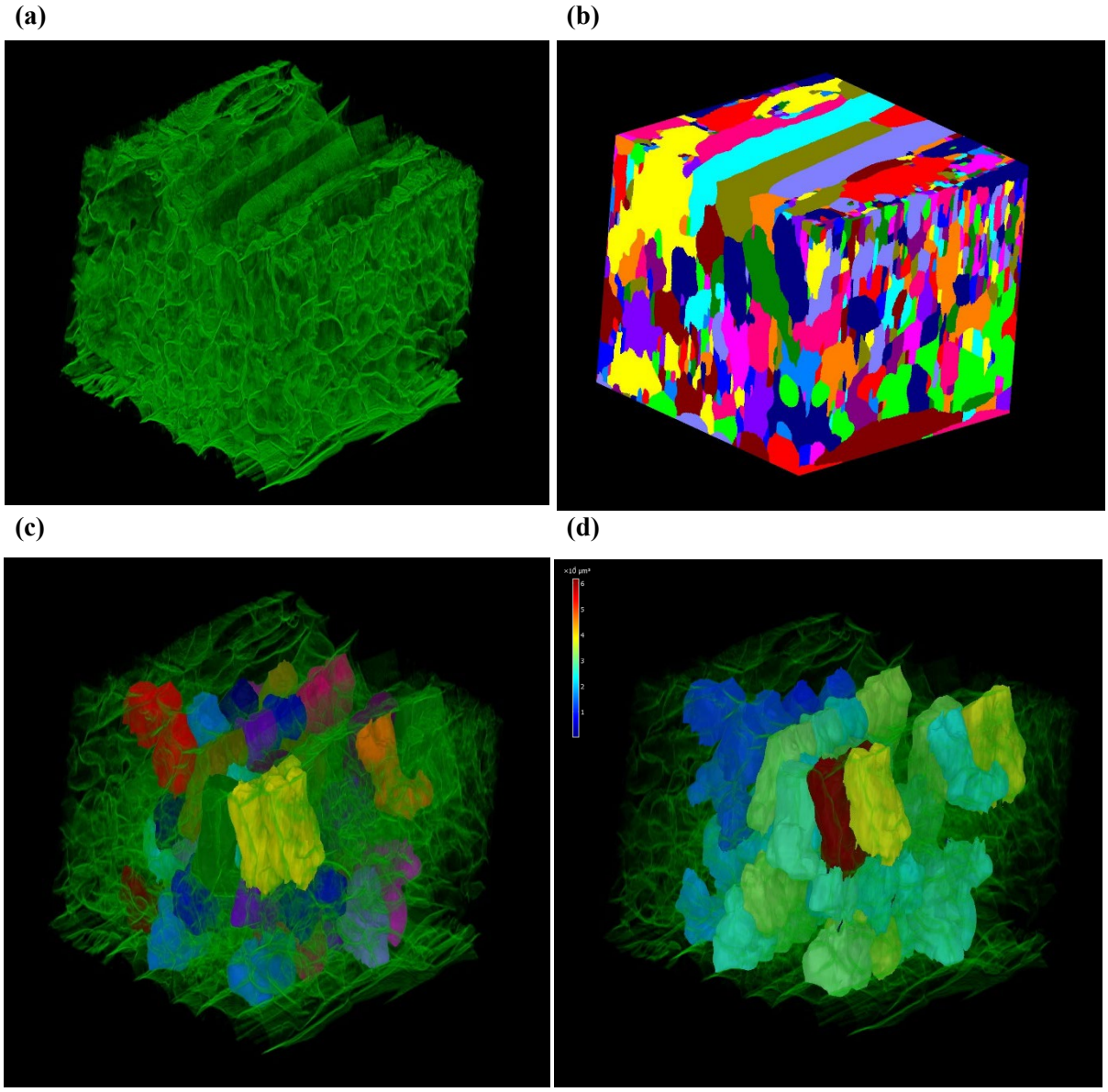

Figure 2.5. Processing confocal z-stacks in MorphographX. a) a confocal z-stack of a *Triticum turgidum ssp.durum* leaf with reduced opacity b) a segmented 'stack' created using the ITK Threshold Autoseeded Watershed function of MorphoGraphX. c) A 3D mesh of mesophyll cells displayed over the original z-stack with reduced opacity d) a heat map of cell volume of Figure (c), displayed over (a).

2.5. Gas Exchange Measurements and iWUE Calculation

2.5.1. Infrared Gas Analyser (IRGA) Measurements

Steady state IRGA measurements were carried out using a LI-COR 6800 (LI-6800; Evans & Santiago, 2014) portable photosynthesis system (LI-COR Biosciences, Lincoln, NE, USA) with the Multiphase Flash Fluorometer (6800-01A) used as a light source and the 6cm chamber attachment. The temperature exchanger was set at 21°C and chamber light intensity was set at 425 µmol m^{-2} s^{-1} (90% red, 10% blue). Relative humidity was set at 60% and maintained using DrieriteTM (Drierite, OH, USA) as a self-indicating desiccant and Stuttgarter masse (Pall, NY, USA) as a humidifying agent. The reference CO_2 concentration was set at 400 µmol mol^{-1} using 8g CO_2 cartridges (LISS, Hungary), and wet soda lime

(LI-COR Biosciences, Lincoln, NE, USA) was used to scrub CO_2 as required. Chamber fan speed was set at 10,000 rpm and the flow rate was set at 300 μmol s^{-1}.

Gas exchange measurements were carried out on the newest fully expanded leaf of each well-watered plant. The samples were randomised, and two technical repeats taken using two different IRGAs, the mean of which was then calculated. The leaf blade was clamped into the IRGA chamber for 20-30 minutes to allow for both *A* and g_s values to stabilise. The leaf width was measured and inputted to allow for the calculation of the correct leaf area within the cuvette. Before running each program, the reference and sample IRGA chambers were matched. The AutoLog program was used to log data every 30 seconds for 15 minutes. From the exported datasets, the mean *A* and g_s were calculated from the 15-minute logging period.

Intrinsic water-use efficiency (iWUE) was estimated as assimilation rate divided by stomatal conductance (A/g_s).

2.5.2. Porometer Measurements

In Chapter 3, gas exchange analysis using both an Infrared Gas Analyser (LI-6800, LiCOR, NE, USA) and handheld porometer (LI-600, LiCOR, NE, USA) was carried out to assess the accuracy and reliability of both machines. The differences in these pieces of equipment have been highlighted in the Chapter 1, Section 1.3. Instantaneous measurements of stomatal conductance were taken at chamber conditions using a LI-COR porometer on randomised samples. Three technical repeat measurements were taken at 28, 29 and 30 days after planting, 5-7 hours into the photoperiod. Due to loss of plants during growth, Emmer line TRI28049 was not included in this porometer experiment.

2.6. Data Analysis

Data was statistically analysed and graphed primarily using GraphPad Prism 9 (ver. 9.3.1; Graphpad Software Inc.) unless otherwise stated. Datasets were first assessed for normality, and for data of the discreet variable 'Number of Lobes' in all experimental chapters, a non-parametric Kruskal-Wallis test was carried out followed by a Dunn's multiple comparisons test to test for significant interactions (95% confidence). For all tests, significance was determined if p=<0.05. All error bars on graphs indicate +/- one standard deviation of the mean (SD).

Chapter 3: Significant differences between species (*T. araraticum., T. turgidum ssp. dicoccoides, T. turgidum ssp. dicoccon* and *T. turgidum ssp. durum*) were identified using one-way analysis of variance (ANOVA). Where significance was detected, Tukey's HSD was used as a multiple comparisons test to determine significance in the differences in means between lines to 95% confidence. Significant differences between individual lines were also assessed in the same way in this chapter, and tables

showing the results of these tests can be found in the Appendices. Figure 3.10 is a correlation plot, generated in RStudio (www.r-project.org; ver 4.1.0) using the corrplot package.

Chapter 4: Significant differences between mesophyll 'layers' within species were identified using one-way ANOVA and Tukey's HSD (95% confidence). For ranked analysis of 2D mesophyll layer cell size and shape, the frequency that the mean of cells in each layer were of a particular rank (e.g. largest, second largest, third largest or fourth largest across all four transverse leaf layers) per biological replicate was recorded. Friedman multiple comparison test weas carried out, followed by a Dunn's post-hoc test to check for significant interactions between ranked data. Data was plotted as a multiple variables frequency plot in GraphPad Prism.

Chapter 5: Comparisons between the tetraploid Fielder and hexaploid Kronos GRF4-GIF1 lines and corresponding controls were carried out using unpaired, two-tailed t-tests ($p=<0.05$). Covariance between mesophyll cell surface area and volume in Figure 5.8 was analysed and plotted in RStudio using linear regression.

Chapter 3. Linking Leaf Morphology and Water Use Efficiency in Tetraploid Wheat

3.1. Introduction

3.1.1. Evolution of tetraploid wheat

Tetraploid wheat, *Triticum turgidum (AABB)*, is not only a precursor of modern hexaploid bread wheat but is also a crop itself (*T. turgidum ssp. Durum*), with Durum wheat being an important crop primarily in mediterranean regions, North Africa and West Asia. Durum wheat is the 10th most cultivated cereal worldwide and makes up 5% of global wheat crop, with 38.1 million tonnes produced in 2019 (Xynias *et al.,* 2020). Early wild Emmer wheat (*T. turgidum ssp. dicoccoides*), formed by hybridisation of diploid *Triticum uratu* and *Aegilops speltoides* in the wild around 400,000 years ago (Dvorak *et al*., 2012), was cultivated around 10,000 years ago in modern-day Turkey (Shewry 2009; Feldman and Kislev, 2007; Kislev *et al*., 1992). The cultivated Emmer (*T. turgidum ssp. dicoccum*) plants were likely selected from the wild Emmer due to desirable traits such as high grain yield and grown for thousands of years without prior knowledge of selective breeding. One hypothesis is that, around 8,500 years ago, a natural mutation resulted in changes in the ears of both emmer and spelt leading to more easily threshed types that later evolved into the free-threshing durum (*T. turgidum ssp. durum)*. Another mutation evident in cultivated *T. turgidum* is the absence of shattering of the spike at maturity (Nalam *et al*., 2006), which prevents seed loss at harvesting and is important in wild populations but disadvantageous in crops. The Durum wheat that is grown today has undergone many improvements as a result of the Green Revolution of the 1960s. In addition to the discovery of the dwarfing gene *RHT1* (Borlaug 1968), these include: reduced time between sowing and anthesis which resulted in the grain filling period being under more optimal conditions; increased number of grains per spike; reduction in floral abortion; increased grain setting (Isidro *et al*., 2011).

3.1.2 Water-use efficiency: an Important Breeding Target

Water use efficiency (WUE) refers to the productivity of a plant per unit of water used (Hatfield & Dold, 2019). This reflects the responsiveness of crops to water stress in relation to yield values (Richard, 2006; Zhang *et al*., 2010). An increasing area of concern with regards to WUE is that of food crops, with major cereal crops such as wheat accounting for 27% of global water consumption (Hoekstra & Mekonnen, 2012). As future climate change is predicted to increase the frequency of droughts (Lobell *et al.,* 2011; Wheeler & Von Braun, 2013), and global population is continuing to increase exponentially to reach an estimated 9-10 billion by 2050, improving water-use efficiency of crops is an important breeding target to ensure we are able to obtain high enough yields while keeping water use to a minimum (Bertolino *et al.*, 2019; Leakey *et al.,* 2019). This has proven to be a challenge as the exchange of gases within the leaf which determine the rate of transpiration and photosynthesis are linked, and it is the rate

of carbon assimilation (*A*) and stomatal conductance (g_s; the degree of pore aperture for gas flux into the leaf) that are used to quantify intrinsic water-use efficiency (iWUE). Trade-offs occur during leaf development to optimise the rates of carbon fixation for photosynthesis and rate of transpiration, and this plays a major part in controlling plant WUE through regulating CO_2 uptake and water loss (Franks and Farquhar, 1999; Xu *et al.,* 2016; Driesen *et al.,* 2020). Since the Green Revolution of the 1960s, the initial yield increases achieved are beginning to stall, and a need to identify methods to improve wheat yield, especially under the threat of climate change, has arisen (Ray et al., 2012; 2013). For this reason, research has turned to improving crop water-use efficiency as an agronomic trait to help make our crops more future-proof through reducing yield losses due to drought (Bertolino et al., 2019; Leakey et al., 2019). It is therefore important that our understanding of the mechanisms that underlie plant water-use regulation is revised and used to influence future wheat breeding programmes.

Previous research by Wilson *et al.* (2021) has explored the effect of changes in wheat ploidy on WUE. For example, it is known that hexaploid bread wheat has greater iWUE than diploid and tetraploid wheat, and that this is likely due to factors related to leaf structure, such as stomatal density, size and mesophyll cell size and shape, as well as additional factors which vary with ploidy. However, Wilson *et al*. also observed that domesticated tetraploid wheat (*T. turgidum ssp. dicoccum* and *T. turgidum ssp. durum*) had a significantly greater iWUE than wild *T. turgidum* varieties, with no such differences in cell size. Due to its complicated evolution and cultivation, tetraploid wheat demonstrates great phenotypic and genetic variability across the subspecies, with Durum wheat being the most optimised for productivity and stress tolerance in today's environment. This makes them an interesting tool for studying wheat as it negates the effect of having lines with different numbers of genomes while still demonstrating such a large variation. Understanding the contributing factors of the improved iWUE in Durum wheat will not only elucidate physiologies that have been subconsciously selected for across thousands of years of tetraploid wheat evolution, but also give a broader insight into the mechanisms behind reducing water loss from wheat leaves.

3.1.3. Factors that control water-use efficiency in wheat leaves

Stomata are thought to be major players in leaf gas exchange, as they form the direct interface between the leaf and surrounding environment (Heatherington & Woodward, 2003). Grass stomata are formed of a central pore flanked by two dumbbell-shaped guard cells and subsidiary cells (Raissig *et al*., 2016; Endo & Torii, 2019). In addition to CO_2 passing through the stomatal pores and into the leaf, loss of water vapour through transpiration occurs simultaneously (Farquhar & Sharkey, 1982; Miner *et al.,* 2017). This can be quantified as stomatal conductance (g_s; the rate of gas diffusion across the pore) and represents both the rate of CO_2 influx available for carbon fixation via photosynthesis as well as water use (Vialet-Chabrand *et al*., 2017; Lawson & Vialet-Chabrand, 2019). High g_s is linked to greater rates

of CO_2 assimilation (A) but also with an increase in the loss of water vapour and hence reduced WUE. At the leaf level, the ratio of photosynthesis and water vapour loss through the stomata (A/g_s) is referred to as intrinsic water-use efficiency (iWUE) (Flexas *et al*., 2016; Lawson & Vialet-Chabrand, 2019) and gives an idea of the amount of 'crop per drop' in terms of plant productivity relative to water input. In practice, variation in stomatal conductance is associated with variation in iWUE (Gilbert *et al*., 2011; Hubbart et al., 2007) and crops with greater WUE/iWUE are more resilient to drought stress and require less water to reach the same yield (Condon *et al*., 2004; Faralli *et al.,* 2019a).

The size, density, and pore area of the stomata are important determiners of resistance to gas diffusion and therefore have a large impact on g_s (Dow *et al*., 2014; Vialet-Chabrand *et al*., 2017; Faralli *et al*., 2019a) (Franks & Beerling, 2009; Harrison *et al*., 2020; Hetherington & Woodward, 2003; Lehmann & Or, 2015). Franks & Beerling observed that leaves with a higher g_s normally have greater stomatal density (s_{dens}) and smaller stomatal size (2009a, b). With respect to wheat, diploid species have increased stomatal density when compared hexaploid wheat, with tetraploid acting as an intermediate, in part due to increased s_{dens} (Austin, 1982; Wilson *et al.,* 2021). The relationship between s_{dens} and g_s has been further investigated though the generation of mutant plants with altered stomatal density. Efforts to reduce s_{dens} by manipulating stomatal development have resulted in reduced g_s and increased iWUE in Arabidopsis (Doheny-Adams *et al*., 2012; Franks *et al*., 2015; Hepworth *et al*., 2015), barley (Hughes *et al*., 2017), rice (Caine *et al*., 2019; Mohammed *et al*., 2019) and wheat (Dunn *et al*., 2019). Increasing s_{dens} through genetic manipulation had the opposite effect, leading to increase in g_s in Arabidopsis (Doheny-Adams *et al.,* 2012; Tanaka *et al*., 2013). Stomatal size is also known to impact gas exchange, with larger stomata having greater pore size being slower to open and close (Drake *et al*., 2013; Lawson & Blatt, 2014). Each individual smaller stomatal complex also occupies less space on the epidermis and reduces the distance for gas molecules to travel across the pore (Franks & Beerling, 2009; Franks & Farquhar, 2007). As stomatal size and density are thought to cumulatively determine stomatal conductance, they can be used to estimate the potential maximum rate of g_s in the form of anatomical g_{smax} (Dow *et al.,* 2014; McElwain *et al.,* 2015; de Boer *et al.,* 2016)

In previous research on wheat, domesticated lines have a relatively large variation in g_s (Rebetzke *et al*., 2001; Condon *et al.,* 2007; Sadras *et al.,* 2012) and high g_s has been shown to correlate with improved yield under well-watered conditions (Fischer *et al*., 1998). There has been an abundance of research exploring the relationships between stomatal parameters, g_s and iWUE (Farquhar & Richards, 1984; Jahan *et al*., 2014; Barbour *et al*., 2016; Wang *et al.,* 2015; Ouyang *et al*., 2017; Faralli *et al*., 2019b). Ouyang *et al.* (2017) observed that the rates of stomatal conductance of two different wheat lines are associated with changes in s_{dens}. Faralli *et al*., (2019b) found that s_{dens} was positively correlated with the speed of stomatal opening and had a negative effect on iWUE in eight hexaploid winter wheat varieties. The speed of stomatal opening and closing in response to environmental stimuli can also affect iWUE as slower stomata demonstrate a disconnect between *A* and g_s which has been suggested to limit

photosynthesis in C3 and C4 crops by up to 15% (McAusland *et al*., 2016). There has been discussion as to what extent the size of the stomata affects the speed of response (Hetherington and Woodward, 2003; Franks & Beerling, 2009; Lawson & Blatt, 2014; Drake *et al*., 2013, McAusland *et al*., 2016, Kardiman and Ræbild, 2018; Zhang *et al*., 2019; Ozeki *et al*., 2022; Elliott-Kingston *et al*., 2016; Deans *et al*., 2019). However, the morphology of the grass dumbbell-shaped guard cells is thought to increase the speed of stomatal opening and closing in response to environmental stimuli (Franks & Farquhar, 2007; Lawson & Blatt, 2014; Raissig *et al*., 2016; Durney *et al*., 2023) and is therefore beneficial for crop species such as wheat as it allows them to quickly optimise the rate of gas flux.

In addition to the role that stomata play in leaf gas exchange, the size, shape and packing of mesophyll cells is also thought to have some influence over determining rates of photosynthesis and WUE. The effects of the two cell types are likely intrinsically linked, as the development of the mesophyll is thought to rely upon the presence of functional stomata (Lundgren *et al*., 2019). Wilson *et al.* (2021) observed that increases in stomatal size and decreases in density that occur with the increase in wheat ploidy results in a decrease in the surface area to volume ratio (SA/Vol) of the mesophyll cells, and therefore less exposed surface area for water-loss, without any reductions in photosynthetic rate. Wilson *et al*. suggest that changes in mesophyll SA/Vol can reduce g_s without limiting photosynthesis, improving iWUE.

3.1.4 Aims

The aim of this chapter is to explore the variation that is present in wild, landrace, and modern domesticated tetraploid wheat varieties, observing leaf morphologies using 2D and 3D microscopy techniques and identifying any links to iWUE. By choosing to study just tetraploid varieties, any effect of changing ploidy level has been avoided.

3.2. Plant Materials

Table 3.1. Tetraploid lines used in this study. Lines are referred to by the 'Line Code' and simplified 'Name' throughout this chapter, and colour coded by status (Wild *T. turgidum* = Black, Wild *T. araraticum* = Grey, Emmer = Blue, Durum = Red).

Species	Line Code	Status	Name
Triticum turgidum (subsp. dicoccoides)	TRI18505	Wild	*T. dicoccoides*
Triticum turgidum (subsp. dicoccoides)	TRI18530	Wild	*T. dicoccoides*
Triticum araraticum	TRI16599	Wild	*T. araraticum*
Triticum araraticum	TRI18513	Wild	*T. araraticum*
Triticum turgidum (subsp. dicoccon)	TRI16877	Domesticated (Landrace)	Emmer
Triticum turgidum (subsp. dicoccon)	TRI28049	Domesticated (Landrace)	Emmer
Triticum turgidum (subsp. dicoccon)	TRI14734	Domesticated (Landrace)	Emmer
Triticum durum (subsp. durum)	VOILUR	Domesticated (Modern)	Durum
Triticum durum (subsp. durum)	AVENTADUR	Domesticated (Modern)	Durum
Triticum durum (subsp. durum)	ANVERGUR	Domesticated (Modern)	Durum

3.3. Results

3.3.1. Plant Growth

There is great variation in the physical characteristics of different tetraploid *Triticum* species and crop lines (Figure 3.1). There were significant differences in leaf width (ANOVA: p<0.0001****, f=72.76), length (ANOVA: p<0.0001****, f=16.25), plant height (ANOVA: p<0.0001****, f=40.45) and number of leaves (Kruskall-Wallis: p<0.0001****, Kruskall-Wallis Statistic = 30.26) at 21 days after planting across the species/subspecies (Figure 3.2).

The wild *T. dicoccoides* and *T. araraticum* had narrower leaves compared with Emmer (Tukey: p<0.0001**** for both species, df=36) and Durum (Tukey: p<0.0001**** for both species, df=36) lines (Figure 3.2a). Emmer leaf width was intermediate, being significantly narrower than Durum (Tukey: p=0.0015**, df=36). The Emmer varieties stood out in terms of leaf length (Figure 3.2b), having significantly longer leaves than both wild *T. araraticum* and Durum varieties (Tukey: p<0.0001**** and p=0.0001*** respectfully, df=36).

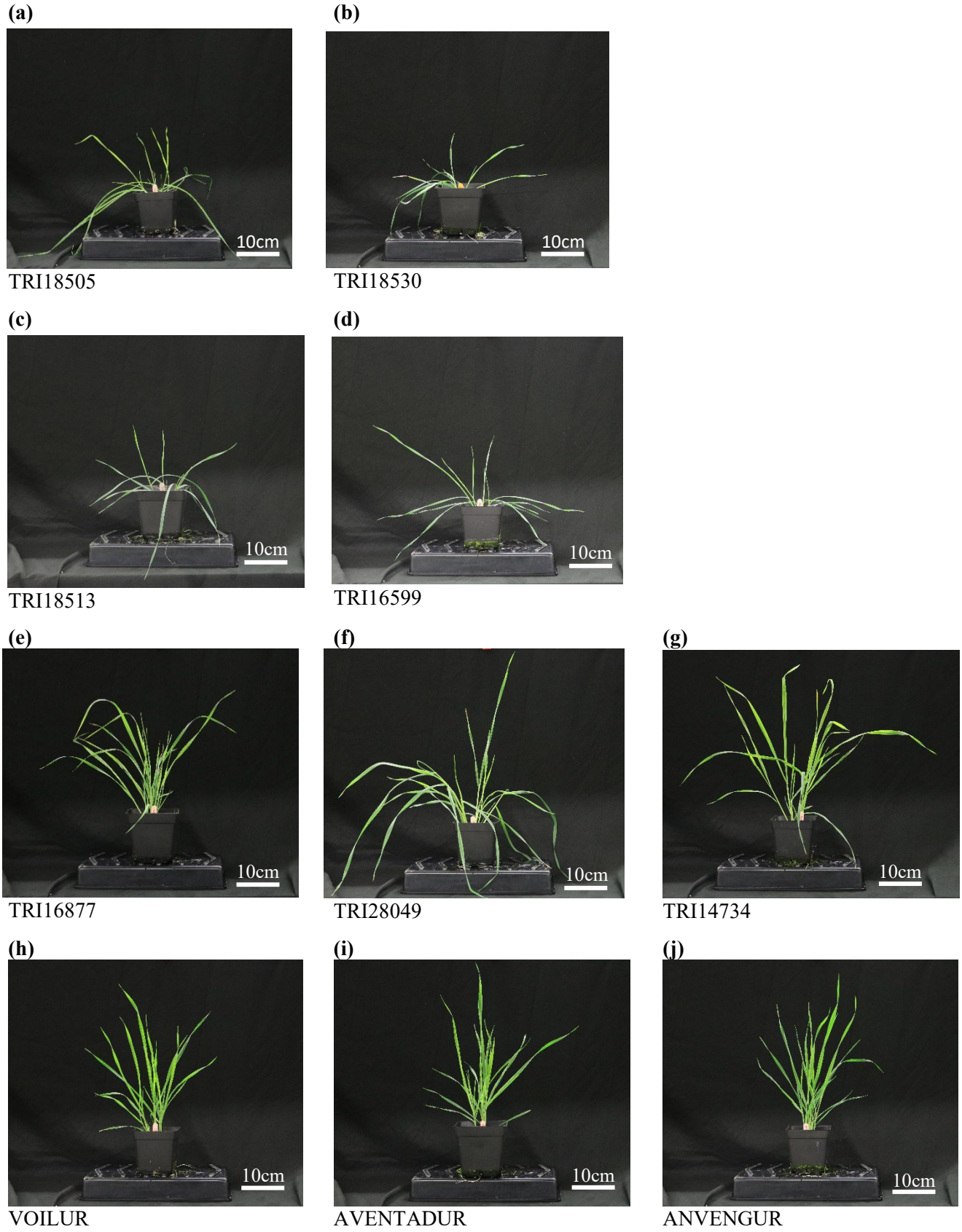

Figure 3.1. Images of tetraploid wheat lines at 28 days after germination. a-b) Wild *T. turgidum ssp. dicoccoides*. c-d) Wild *T. araraticum*. e-g) Domesticated *T. turgidum ssp. dicoccon* (Emmer). h-j) Domesticated *T. turgidum ssp. durum* (Durum).

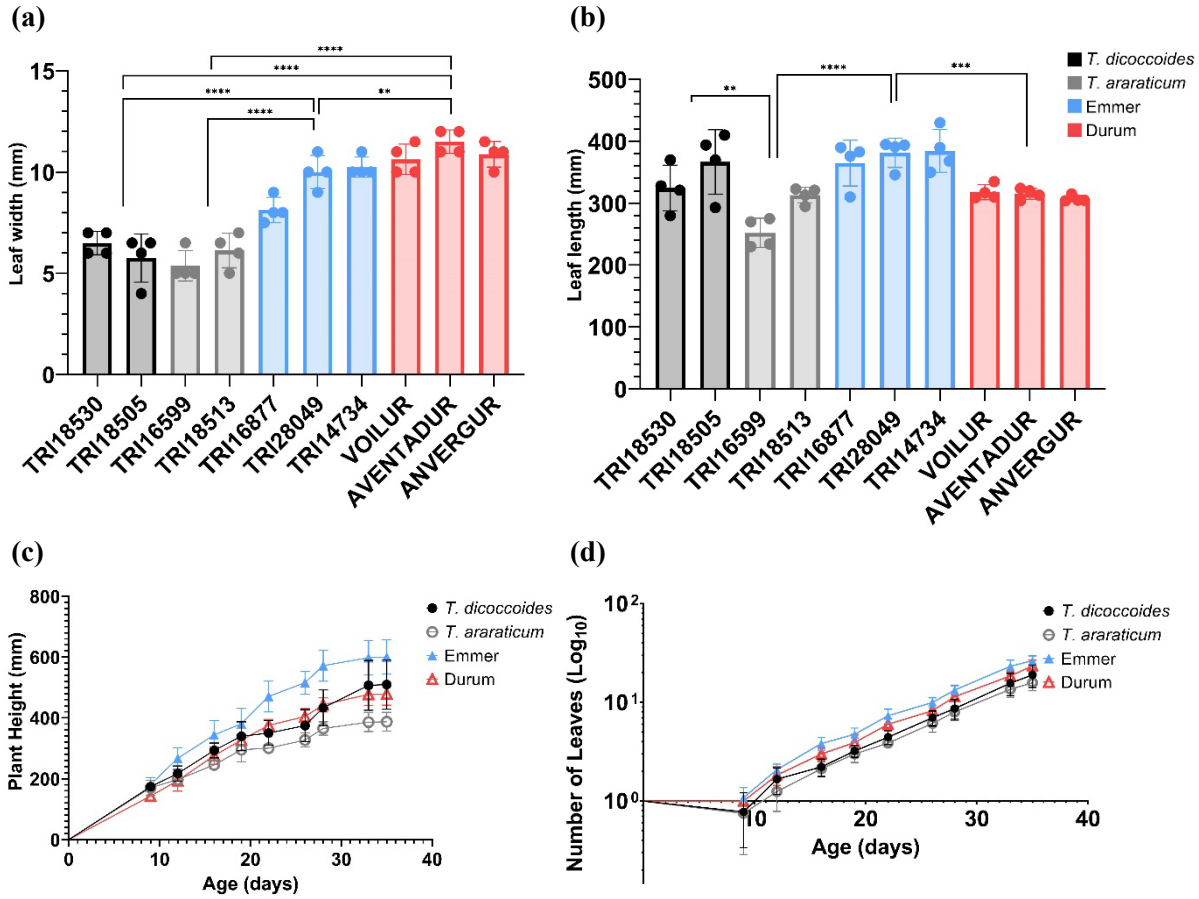

Figure 3.2. Tetraploid wheat lines have different growth phenotypes. a) Leaf width of the 5th leaf on the main tiller at 4 weeks (28 days). b) Length from base to tip of the 5th leaf on the main tiller at 4 weeks. Each data point represents one plant. c) Plant height from 0 to 35 days after germination. d) Log_{10} of the number of leaves on each plant from 0 to 35 days after germination. Black = wild *T. turgidum ssp. dicoccoides*, grey = wild *T. araraticum*, blue = Emmer (*T. turgidum sbsp. dicoccon*), red = Durum (*T. turgidum sbsp. durum*). For (a) and (b), each datapoint represents a single plant. Error bars represent standard deviation from the mean. ANOVA and post-hoc Tukey tests were carried out in (a) and (b) to test for significant interactions between the four species/subspecies: p<0.005**, p<0.0005***. For (a) and (b), n=4. For (c) and (d) when the data was grouped into species/subspecies, n=8 for *T. dicoccoides* (black) and *T. araraticum* (grey) and n=12 for Emmer (blue) and Durum (red). For full details on statistical significances between each line, see supplementary statistics tables.

In the case of plant height and number of leaves (Figure 3.2c, d), Durum (red) varieties appear to be intermediate to Wild (black) and Emmer (blue). Emmer varieties grew significantly taller at 28 days after planting than the wild *T. dicoccoides* and *T. araraticum* varieties (Tukey: P<0.0001***, p=0.0003*** respectively, df=37), and Durum (Tukey: p<0.0001****, df=37). Emmer varieties also had significantly more leaves at 28 days after planting than both *T. dicoccoides* (Dunn's: p=0.0003***, z=4.021) and *T. araraticum* (Dunn's: p<0.0001****, z=4.831), but not than Durum varieties. Durum varieties were significantly taller than wild *T. araraticum* (Dunn's: p=0.0048**, z=3.354).

3.3.2. Domesticated Tetraploid Wheat Lines Have a Greater Intrinsic WUE than Wild Varieties

To confirm and expand upon previous observations (Wilson *et al.,* 2021). An analysis of stomatal conductance (g_s) was carried out in a range of wild and domesticated tetraploid wheat lines. These data are shown in Figure 3.3. When measuring g_s using a porometer (Figure 3.3a), the wild varieties (black) had greater g_s than the Durum varieties (red). Statistically comparing the data grouped by species/subspecies showed that there was a difference in g_s (ANOVA: p=0.0029**, f=5.726), with Durum being lower than both wild *T. dicoccoides* and *T. araraticum* (Tukey: p=0.0211* and p=0.0033** respectfully, df=33). This was also the case with g_{sw} data measured using an IRGA (Figure 3.3b) (ANOVA: p<0.0001****, f=13.2), with Durum g_s again being reduced compared to *T. dicoccoides* (Tukey: p<0.0001****, df=49) and *T. araraticum* (Tukey: p=0.0048**, df=49). In both instances, Emmer (blue) appears to fall intermediate to Durum and the wild varieties, and the lines of this species are the most variable. Emmer is a landrace of tetraploid wheat that was cultivated ~10,000 years ago and is not currently used today, as Durum wheat is. Emmer g_s was neither significantly greater than that of Durum or reduced compared to the wild varieties when measured using a porometer (Figure 3.3a). However, when measured using an IRGA (Figure 3.3b), Emmer g_s was significantly lower than *T. dicoccoides* (Tukey: p= 0.0373*, df=49) and greater than Durum (Tukey: p= 0.0036**, df=49). The stomatal conductance values measured using a porometer (Figure 3.3a) were much greater than those measured using an IRGA (Figure 3.3b).

A, carbon assimilation rate, followed a similar trend as was seen with g_s: wild varieties had the highest *A* and Durum the lowest, with Emmer acting as an intermediate (Figure 3.3c). This interaction was statistically significant (ANOVA: p<0.0001****, f= 11.28), with *T. dicoccoides* and *T. araraticum* having significantly higher *A* than the Durum varieties (Tukey: p<0.0001* and p=0.0091* respectively, df=49). Of the wild species, only Emmer had significantly reduced A compared to *T. dicoccoides* (Tukey: p=0.0006**, df=49), and there was no significant difference compared with Durum.

Intrinsic water-use efficiency, iWUE, is calculated as A/g_s, and differences in the measured values of gas exchange parameters measured using an IRGA (Figure 3.3b, c) resulted in significant variation in iWUE between tetraploid wheat species/subspecies (ANOVA: p=0.0029**, f=5.334) (Figure 3.3d). The only significant difference in iWUE however was between Durum and wild/Emmer varieties, with Durum having improved iWUE compared with *T. dicoccoides* and Emmer varieties (Tukey: p=0.0091* and p=0.0057* respectfully, df=49). Interestingly, Emmer iWUE did not sit as an intermediate, instead was similar to that of the wild *T. dicoccoides* and *T. araraticum* varieties.

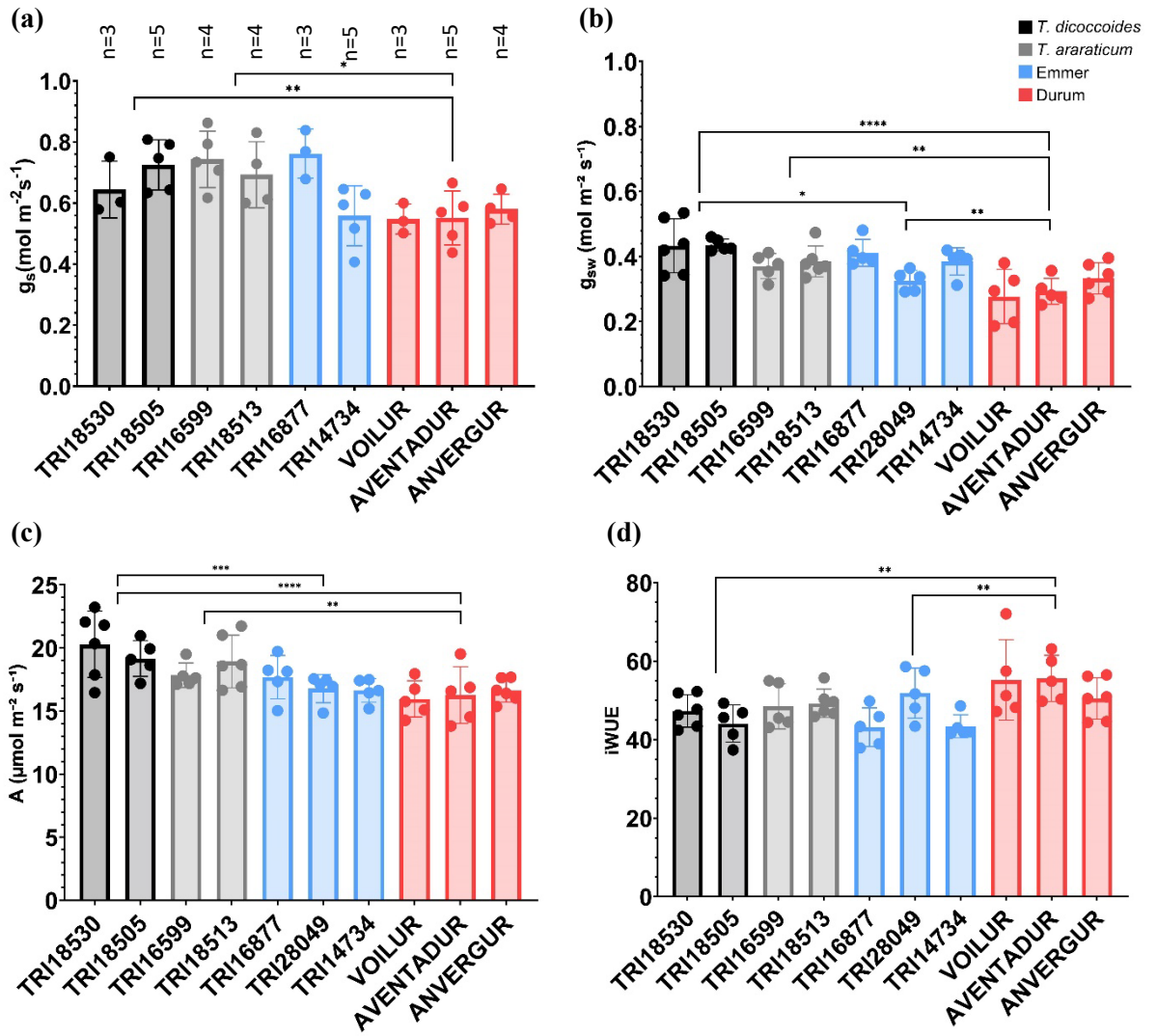

Figure 3.3. Gas exchange varies between wild and domesticated tetraploid wheat. a) Instantaneous stomatal conductance (g_s), measured using a LI-600 LI-COR Porometer. B) Steady-state g_{sw} measured using LI-6800 LI-COR IRGA. C) Steady-state carbon fixation (A) measured using LI-6800 LI-COR IRGA. D) Instantaneous water-use efficiency (iWUE) calculates as A/g_{sw}, using IRGA measurements. For all graphs: Black = wild *T. turgidum ssp. dicoccoides*, grey = wild *T. araraticum*, blue = Emmer (*T. turgidum ssp. dicoccon*), red = Durum (*T. turgidum ssp. durum*). Each datapoint represents a single plant. Error bars represent standard deviation from the mean. ANOVA and post-hoc Tukey tests were carried out to test for significant interactions between the four species/subspecies: p<0.05*, p<0.005**, p<0.0005***, P<0.0001****. n=5 for all IRGA data (b-d). For figure (a), n=3-5. For statistical significance p-values between each line, see supplementary statistics tables.

3.3.3. Domesticated Tetraploid Wheat Lines Have Fewer, Larger Stomata than Wild Varieties

Differences in g_s might reflect differences in stomatal size and density, therefore I measured these parameters in the wild and domesticated tetraploid lines (Figure 3.4). There was significant variation in stomatal density (ANOVA: p<0.0001****, f=17.27), with Durum lines demonstrating a significantly lower total stomatal density than wild *T. dicoccoides* and *T. araraticum* (Tukey: p<0.0001**** for both, df=44) (Figure 3.4a). Once again, Emmer acted as an intermediate, having significantly reduced stomatal density compared to *T. dicoccoides* and *T. araraticum* (Tukey: p=0.0224* and p=0.0114* respectively, df=44) and greater stomatal density than Durum varieties (Tukey: p=0.0226*, df=44).

There was also a difference in the width (ANOVA: p<0.0001****, f=32.49) and area (ANOVA: p<0.0001****, f=18.89) of the stomatal complexes between the species, with Durum varieties having wider stomatal complexes than *T. dicoccoides*, *T. araraticum* and Emmer varieties (Tukey: p<0.0001**** for all, df=46) (Figure 3.4c) with a greater overall complex area than *T. dicoccoides*, *T. araraticum* and Emmer (Tukey: p<0.0001**** for all, df=46) (Figure 3.4d). There was no significant difference in stomatal complex length (Figure 3.4b) between the species/subspecies.

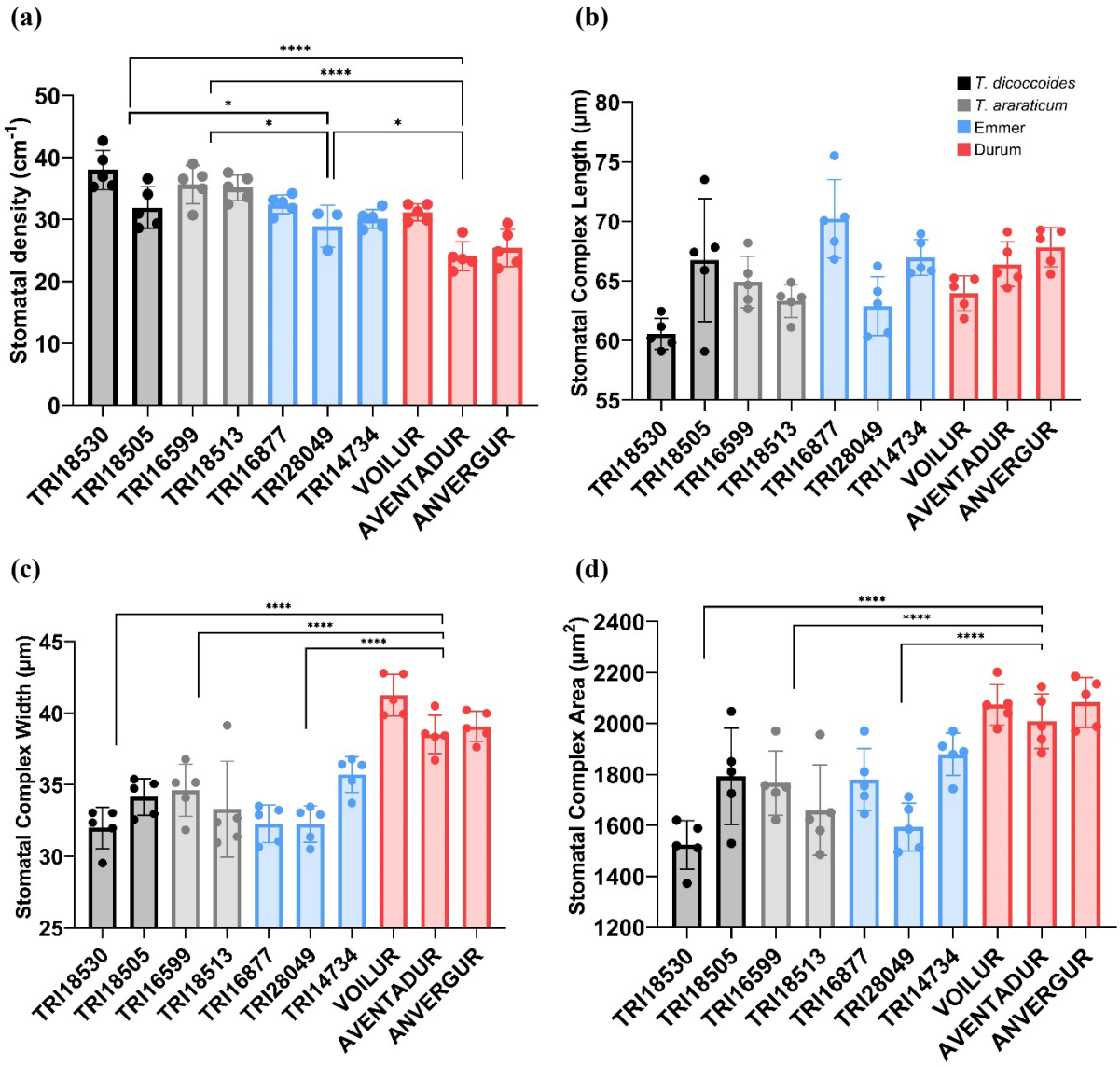

Figure 3.4. Stomatal density and size varies between wild and domesticated tetraploid wheat. a) Total stomatal density of each species. b) Stomatal complex length. c) Stomatal complex width d) Stomatal complex area, calculated using the following equation: area = πab, where a = stomatal complex length / 2, and b = stomatal complex width / 2. Black = wild *T. turgidum ssp. dicoccoides*, grey = wild *T. araraticum*, blue = Emmer (*T. turgidum ssp. dicoccon*), red = Durum (*T. turgidum ssp. durum)*. Each datapoint represents a single plant. Error bars represent standard deviation from the mean. ANOVA and post-hoc Tukey tests were carried out to test for significant interactions between species/subspecies: p<0.005*, p<0.0001****. n=5 (for all except TRI28049 stomatal density, where n=3). For statistical significance between each line, see supplementary statistics tables.

To assess whether the increase observed in Durum stomatal complex size was linked to pavement cell size, the length width and area of pavement cells of the tetraploid varieties were measured (Figure 3.5).

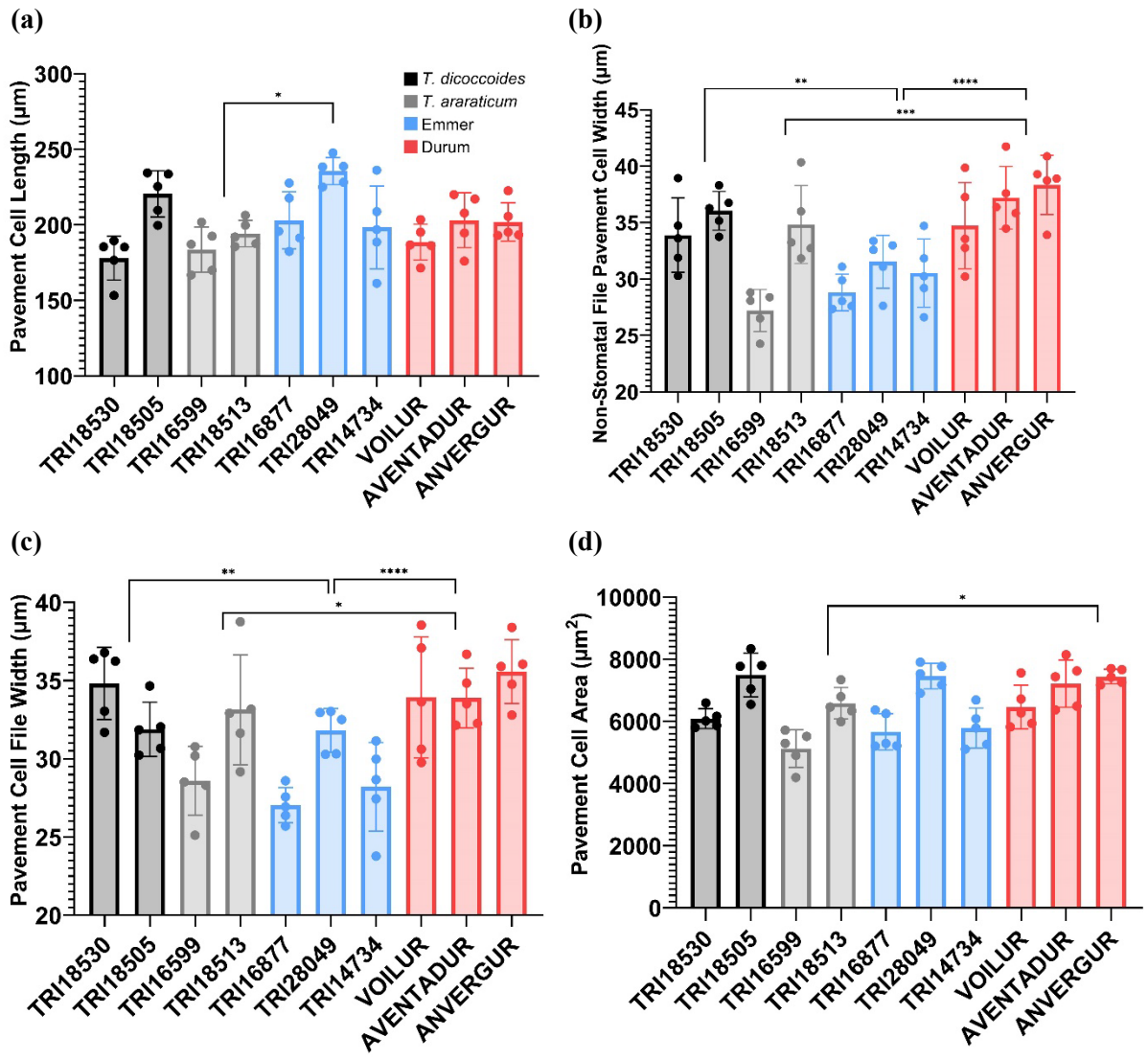

Figure 3.5. Pavement cell size varies between wild and domesticated tetraploid wheat. a) Pavement cell length. b) Non-stomatal file width. c) Stomatal file width. d) Pavement cell area Black = wild *T. turgidum ssp. dicoccoides*, grey = wild *T. araraticum*, blue = Emmer (*T. turgidum ssp. dicoccon*), red = Durum (*T. turgidum ssp. durum)*. Each datapoint represents a single plant. Error bars represent standard deviation from the mean. ANOVA and post-hoc Tukey tests were carried out to test for significant interactions between species/subspecies: p<0.005*, p<0.005**, p<0.0005***, p<0.0001****. n=5 (for all except TRI28049 stomatal density, where n=3). For statistical significance between each line, see supplementary statistics tables.

In addition to measuring physiological gs in growing plants, it is possible to estimate the maximal g_s of a leaf based on the anatomical parameters of stomatal size and density. Anatomical g_{smax} calculated using stomatal size, density and pore size measurements as described in Chapter 2 Section 2.2.3 varied significantly across species/subspecies (ANOVA: p<0.0001****, f=17.79; Figure 3.6a). g_{smax} was lower in the Durum lines compared to wild *T. dicoccoides* and *T. araraticum,* and Emmer (Tukey: p<0.0001**** for all, df=46). The g_{smax} of Emmer was more similar the wild varieties than to Durum.

When iWUE was re-calculated using anatomical g_{smax} (Fig. 3.6b) and measured *A* values (Figure 3.3c), this also showed significant variation across species/subspecies (ANOVA: p=0.0059*, f=4.718), with

the Durum varieties having higher theoretical maximum iWUE values than *T. araraticum* (Tukey: p=0.0207, df=46) and Emmer (Tukey: p=0.0086*, df=46). This difference is comparable to that seen when iWUE is calculated using measured g_s (Figure 3.3d), although the values calculated here on the basis of anatomical g_{smax} are smaller.

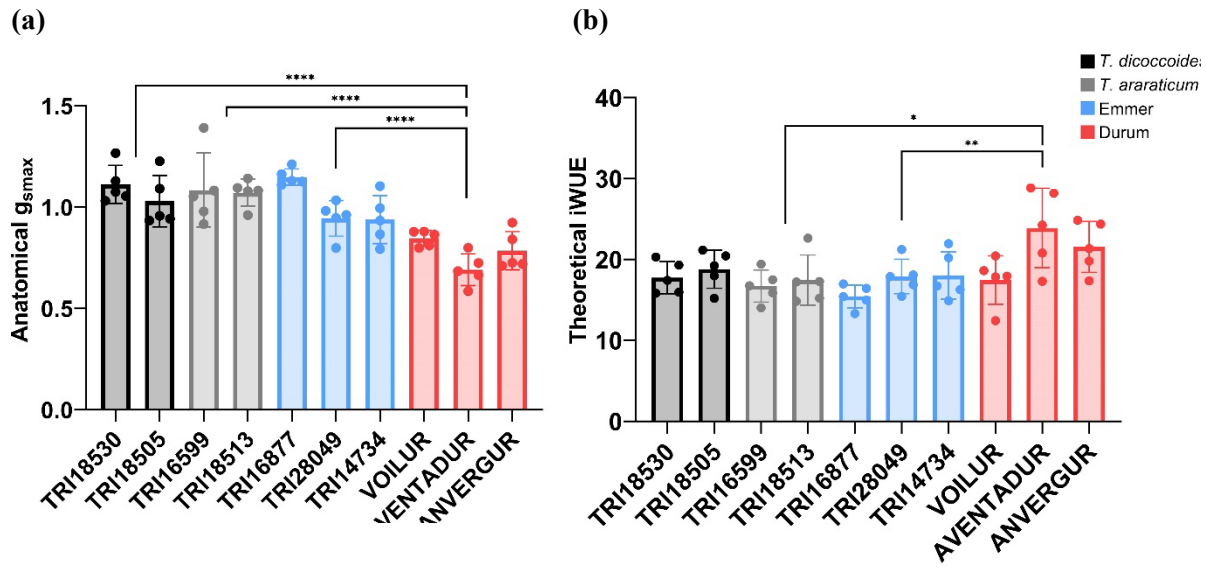

Figure 3.6. Anatomical g_{smax} and theoretical iWUE vary between wild and domesticated tetraploid wheat. a) Anatomical g_{smax} by species. b) iWUE wild and domesticated tetraploid wheat based on g_{smax}, calculated using the measured *A* values for each line. Black = wild *T. turgidum ssp. dicoccoides*, grey = wild *T. araraticum*, blue = Emmer (*T. turgidum ssp. dicoccon*), red = Durum (*T. turgidum ssp. durum*). Each datapoint represents a single plant. Error bars represent standard deviation from the mean. ANOVA and post-hoc Tukey tests were carried out to test for significant interactions between species/subspecies: p<0.05*, p<0.005**, p<0.0001****. n=5. For statistical significance between each line, see supplementary statistics tables.

3.3.4. Quantitative Analysis of Internal Leaf Structure in Wild and Domesticated Tetraploid Lines.

Previous work has linked stomatal development with the development of the mesophyll tissue (Lundgren *et al.* 2019) and has shown that differences in mesophyll structure can be linked to g_s between diploid, tetraploid and hexaploid varieties (Wilson *et al.* 2021). I explored whether differences in mesophyll structure were linked to differences in gas conductance within the range of tetraploid leaves.

To do this, I performed a quantitative analysis of leaf cellular architecture of the lines described in the previous section (Table 3.1). The initial analysis was performed on 2D sections of tissue, in both transverse and longitudinal sections, providing an overview which was then followed up by more time-intensive 3D imaging to provide an in-depth analysis of selected lead lines. Example images of transverse and longitudinal sections of leaves used to collect data for Figure 3.7 are shown in Figure 2.3.

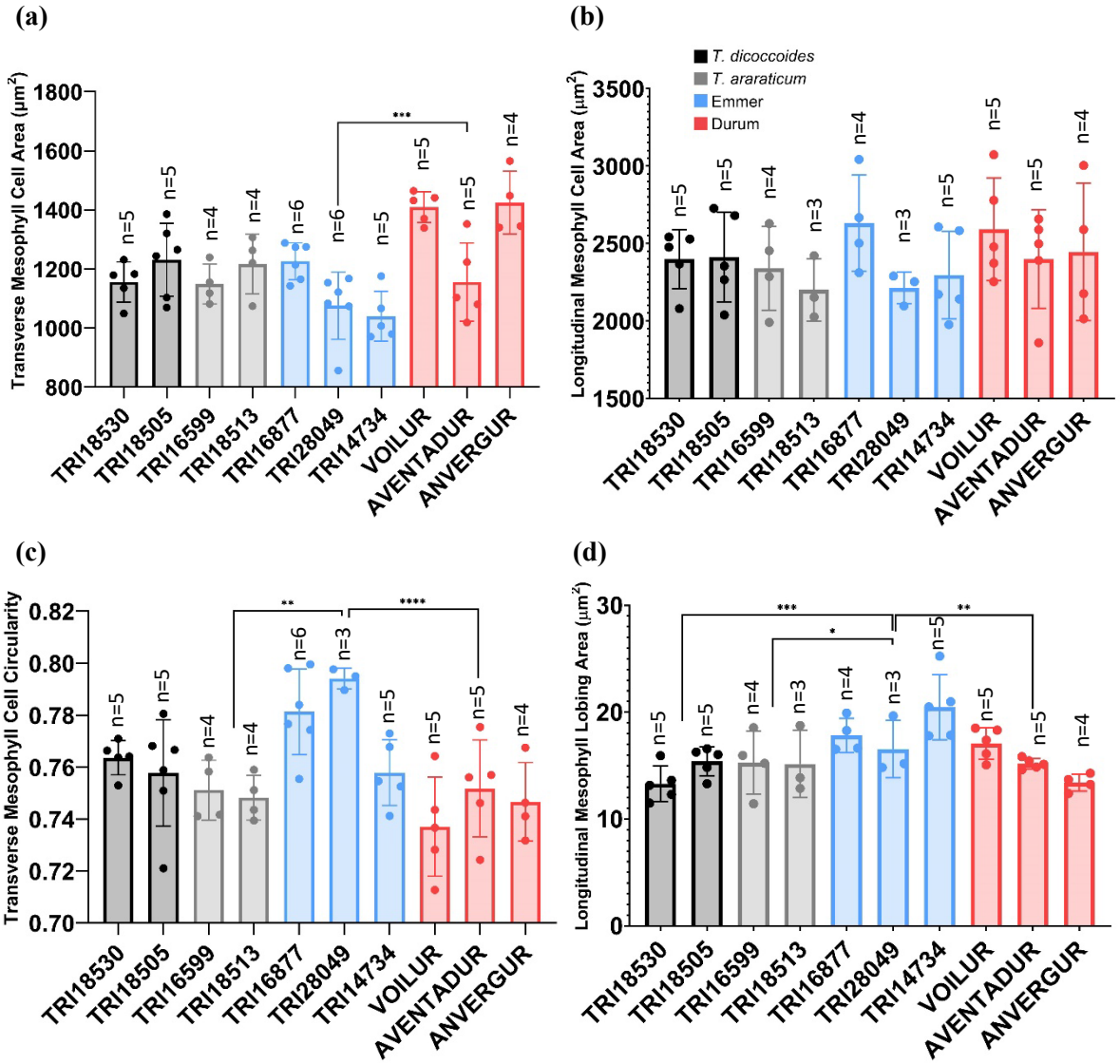

Figure 3.7. 2D mesophyll cell area and shape vary by cultivation status in tetraploid wheat. a) transverse and b) longitudinal. c) transverse cell circularity and d) longitudinal cell lobing area. Black = wild *T. turgidum ssp. dicoccoides* (TRI18530, TRI18505), grey = wild *T. araraticum* (TRI16599, TRI18513), blue = Emmer (*T. turgidum ssp. dicoccon*), red = Durum (*T. turgidum ssp. durum*). Each datapoint represents a single plant. Error bars represent standard deviation from the mean. ANOVA and post-hoc Tukey tests were carried out to test for significant interactions between species/subspecies: p<0.05*, p<0.005**, p<0.0005***. For statistical significance between each line, see supplementary statistics tables. For example images of 2D transverse and longitudinal leaf sections, see Figure 2.3.

For the 2D analysis, mesophyll cell size was measured, and mean values compared. There was significant variation in the transverse cell area between lines (ANOVA: p=0.0006***, f=6.949) (Figure 3.7a). Although it appears that Durum varieties had a larger mean transverse mesophyll cell area compared to both Emmer and wild varieties, this was only significantly greater than Emmer when grouped by species/subspecies (Tukey: p=0.0002***, df=46). There was no significant variation in the longitudinal mesophyll cell areas between species/subspecies (Figure 3.7b).

Analysis revealed a range of transverse mesophyll cell size from 970.8057 µm^2 to 1565.38 µm^2, and longitudinal mesophyll cell (MSC) size from 1883.381 µm^2 to 3379.8 µm^2. Domesticated Emmer and

Durum lines included both the smallest and largest mean MSC size, with the wild lines showing an overall smaller range of MSC size. Mesophyll cell size is an important parameter that impacts on mesophyll packing within the leaf, as is the shape of the mesophyll cells.

As wheat mesophyll cells form lobes only in the longitudinal direction (i.e. parallel to the veins) and mesophyll cells viewed on transverse sections appear oblong (see Figure 2.3), transverse mesophyll cell shape was quantified as 'circularity'. Circularity represents the deviation of a shape from a perfect circle, with a perfectly circular object having a value of 1. There was significant variation in species/subspecies in terms of transverse mesophyll cell circularity (ANOVA: p=0.0001***, f=8.782) (Figure 3.7c), with the mesophyll cells of Emmer varieties being more circular on average than those of *T. araraticum* (Tukey: p=0.0056*, df=43) and Durum (Tukey: p<0.0001****, df=43).

As the lobes of wheat mesophyll cells are visible in longitudinal sections, longitudinal cell shape was quantified as 'lobing area'. Lobing area is calculated as per Chapter 2, Section 2.2.3, and represents the cumulative degree of cell lobing and not just the number of lobes. There also was significant variation in the species/subspecies in terms of longitudinal mesophyll cell lobing area (ANOVA: p=0.0005***, f=7.421) (Figure 3.7d), with the mesophyll cells of Emmer varieties having a greater lobing area than those of *T. dicoccoides* (Tukey: p=0.0006, df=39), *T. araraticum* (Tukey: p=0.0194*, df=39) and Durum (Tukey: p=0.0049*, df=39).

Interestingly, Emmer varieties stand out in terms of 2D cell shape, being more rounded in transverse sections and having a higher degree of lobing in longitudinal sections than other varieties, while Durum mesophyll cells stand out in terms of increased transverse cell area. Looking at cells in 2D allows us to gain understanding into how cells behave in distinct transverse and longitudinal sections. In reality, a cell exists in 3D and not two intersecting 2D planes, and information is lost in the parts of the cells that get excluded from 2D image analysis. Therefore, I took 3D confocal stacks of a subset of the same lines and acquired data on cell volume and surface area, using cell volume to surface area ratio as an indicator of shape of the 3D objects (Figure 3.8).

Due to time constraints, one line per cultivation status/subspecies was studied. For wild, this was TRI18505 (*T. dicoccoides*), for Emmer TRI16877 and for Durum this was VOILUR. Mesophyll cells of wild tetraploid and Emmer leaves appeared similar in terms of 3D size and shape and were smaller by volume compared with Durum mesophyll cells, although this was not statistically significant (Figure 3.8c). Despite also having a slightly lower surface area (Figure 3.8d), the mesophyll cells of the wild line had greater surface area to volume ratio than those of the Durum line studied (Figure 3.8e). There was also a significant difference in lobe counts between lines (Figure 3.8f; Kruskal-Wallis, p=0.05*, Kruskal-Wallis statistic: 5.6) with Durum mesophyll cells being more lobed than *T. dicoccoides* (wild) and Emmer, but these individual interactions were not statistically significant.

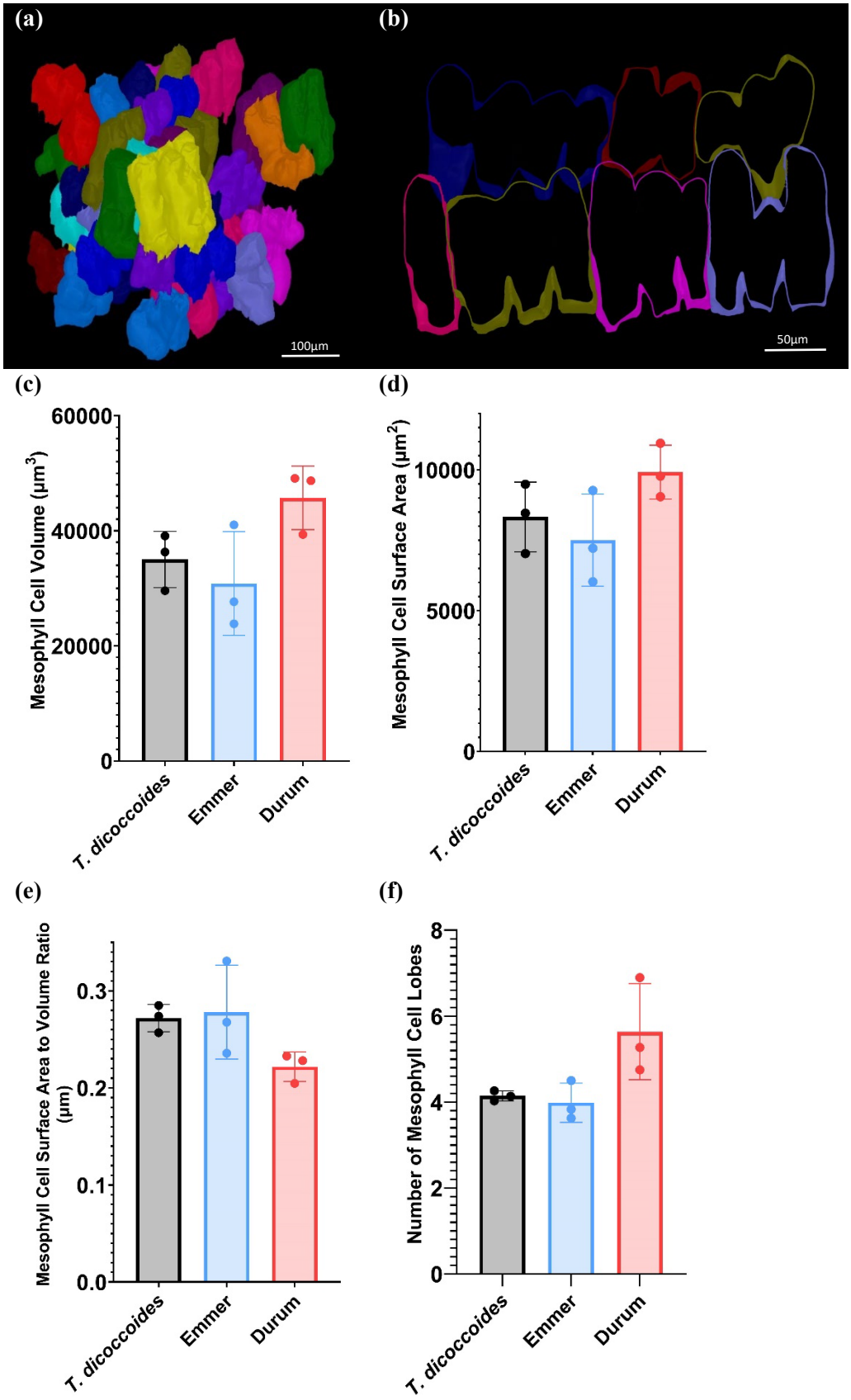

Figure 3.8. 3D cell volume and shape do not vary significantly between wild and domesticated tetraploid wheat. (a) 3D snapshot of *T. turgidum ssp. durum* mesophyll cells segmented from a confocal z-stack using MorphographX (b) 2D clipped mesophyll cells from a *T turgidum ssp. durum* leaf, generated from 3D segmented cells in MorphographX (c) Mean cell volume (d) Mean Cell Surface Area (e) Mean Cell Surface Area to Volume

Ratio (f) Mean cell lobe number. Each datapoint represents a single plant. Error bars represent standard deviation from the mean. ANOVA and post-hoc Tukey tests were carried out for (c)-(e) and Kruskal-Wallis and post-hoc Dunn's test for (f) to test for significant interactions between species/subspecies. n=3.

As previously stated, the size and shape of mesophyll cells affects how they are packaged within the leaf. Another influencing factor is the volume of space that the cells have to be packed in to, and this is defined by the leaf thickness, considering the volume of space taken up by the pavement cells, and the distance between the leaf veins. I measured interveinal distance (IVD), mesophyll thickness and leaf thickness from 2D transverse leaf sections (Figure 3.9).

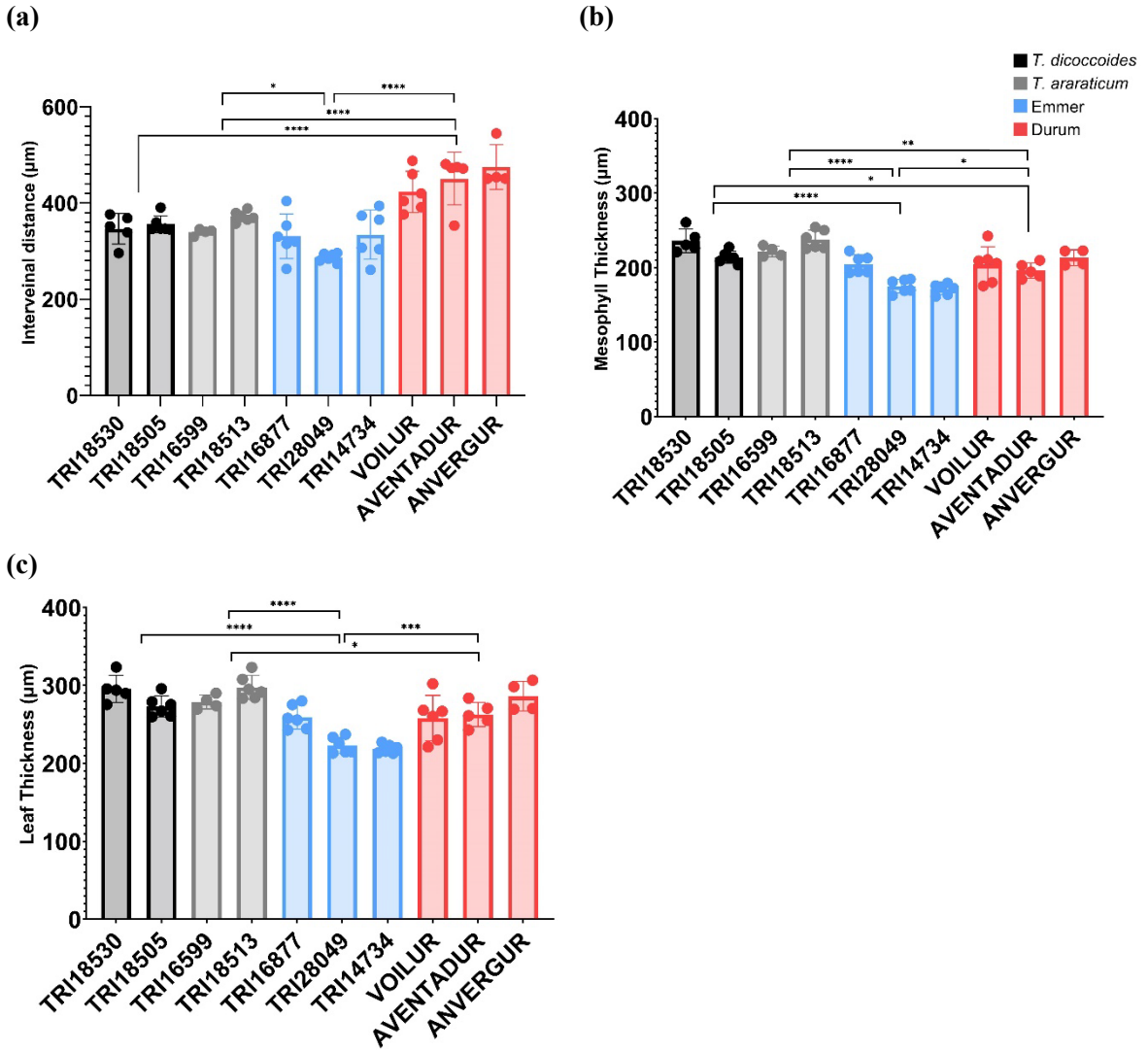

Figure 3.9. Leaf structure varies between tetraploid wheat species of different cultivation status. (a) Interveinal Distance, measured between the 2nd and 3rd veins from the central major vein. (b) Mesophyll Thickness, value presented as a mean calculated from thicknesses measured over and between the 2nd and 3rd veins from the central major vein. (c) Leaf Thickness, value presented as a mean calculated from thicknesses measured over the 2nd and 3rd veins from the central major vein and across the bulliform cells between the same veins. Black = wild *T. turgidum ssp. dicoccoides*, grey = wild *T. araraticum*, blue = Emmer (*T. turgidum ssp. dicoccon)*, red = Durum (*T. turgidum ssp. durum)*. Each datapoint represents a single plant. Error bars represent standard deviation from the mean. ANOVA and post-hoc Tukey tests were carried out to test for significant interactions between species/subspecies: $p<0.05$*, $p<0.005$**, $p<0.0005$***, $p<0.0001$****. n=6 for all lines except: TRI18530 and

AVENTADUR (n=5), and TRI16599 and ANVERGUR (n=4). For statistical significance between each line, see supplementary statistics tables.

There was significant variation between the species/subspecies in terms of IVD (ANOVA: p<0.0001****, f=31.07) (Figure 3.9a). The IVD of Durum varieties was higher than that of *T. dicoccoides*, *T. araraticum* and Emmer varieties (Tukey: p<0.0001****, df=50 for all three interactions). Interestingly, the IVD of the Emmer varieties was significantly smaller than *T. araraticum* (Tukey: p=0.0436, df=50). There was also significant variation between species/subspecies when comparing mesophyll (ANOVA: p<0.0001****, f=22.43; Figure 3.9b) and leaf (ANOVA: p<0.0001****, f=20.74; Figure 3.9c) thickness.

The greatest mesophyll thickness was observed in the wild varieties in this study, with both wild species having significantly greater leaf mesophyll thickness than Emmer (Tukey: p<0.0001****, df=50 for both interactions). The mesophyll thickness of the Durum lines analysed was also significantly smaller than that of *T. dicoccoides* (Tukey: p=0.0197*, df=50) and *T. araraticum* (Tukey: p=0.0012**, df=50), but greater than Emmer (Tukey: p=0.0064*, df=50). The wild varieties also had the greatest total leaf thickness, with both wild species having thicker leaves than Emmer (Tukey: p<0.0001****, df=50 for both interactions). Of the two wild species, only *T. araraticum* had significantly greater leaf thickness than the Durum varieties studied (Tukey: P=0.0482*, df=50), while the Durum varieties had greater leaf thickness than the Emmer (Tukey: p=0.0002***).

A summary plot showing the correlation of leaf traits in Figures 3.2-3.7 and Figure 3.9 is shown in Figure 3.10. The strongest positive correlations were seen between: g_{smax} and stomatal density; interveinal distance and stomatal complex width; leaf count and plant height; leaf length and plant height; mesophyll thickness and leaf thickness. The strongest negative correlations were seen between: leaf width and stomatal density (and subsequently g_{smax}); mesophyll thickness and plant height; leaf thickness and plant height. Interveinal distance was also positively correlated with increased pavement cell width and transverse mesophyll cell area, and longitudinal mesophyll cell lobing area was negatively correlated with leaf (and mesophyll) thickness.

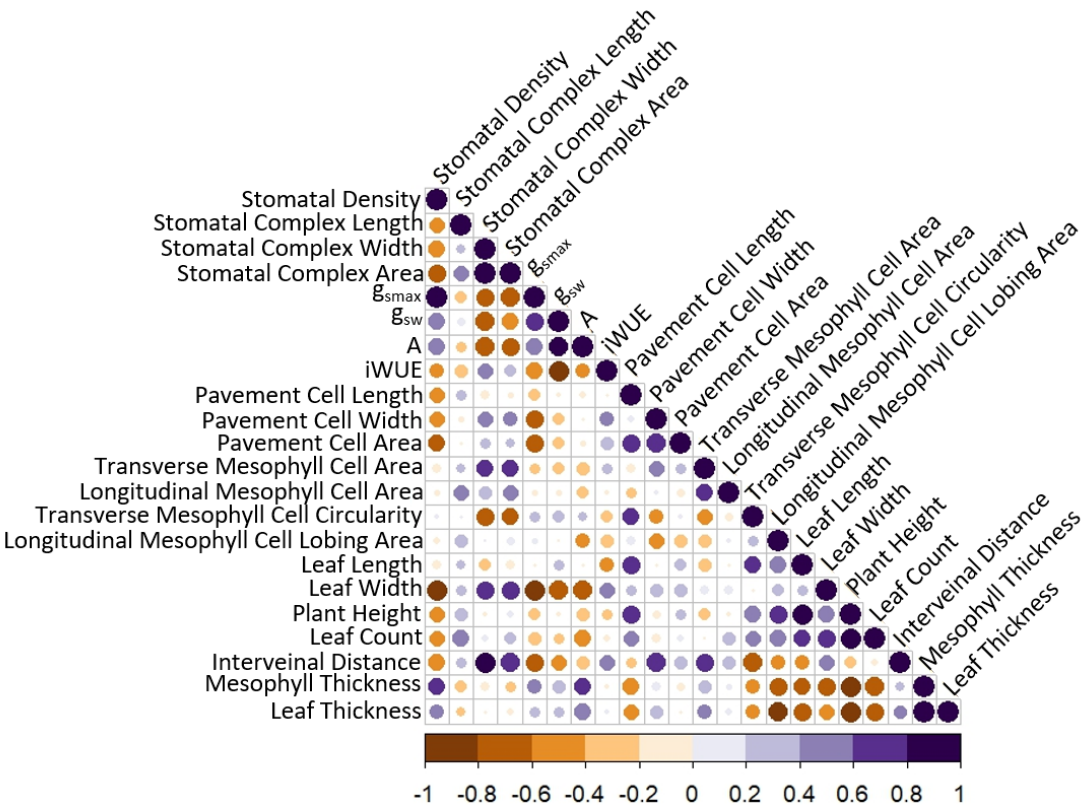

Figure 3.10. Wheat leaf traits show different degrees of correlation. A correlation plot of all data from Figures 3.2-3.7 and Figure 3.9. The mean value for each line was used for this correlation analysis, with blue dots indicating a positive correlation and red indicating a negative correlation. The size and shade of the dot show the strength of the correlation, with larger, darker dots representing a stronger correlation.

3.4. Discussion

3.4.1. Selection of Cultivated Tetraploid Wheat has Mirrored Diploid to Hexaploid Evolution.

Durum varieties were observed in this study to have increased stomatal size and decreased density (Figure 3.4), likely contributing to the reduced g_s compared with wild and Emmer varieties (Figure 3.3a, b). This very closely mirrors changes observed in the evolution and cultivation of hexaploid *T. aestivum* from diploid *Triticum*. Wilson *et al*. (2021) observed that hexaploid wheat has greater stomatal length, width and area than tetraploid. In this study, we saw no difference in stomatal complex length between Durum wheat and the wild/Emmer varieties, instead the increased area observed was driven by Durum varieties having significantly greater stomatal complex width (Figure 3.4c, d). Changes in density also reflect the evolution and selection of hexaploid bread wheat as Durum varieties showed the lowest stomatal density (Figure 3.4a) similar to hexaploid wheat (Wilson *et al*. 2021). The increase in cell size with polyploidy is a general effect which is observed across plant species due to changes in genome size (Jellings & Leech, 1984; Parker & Ford, 1982; Wilson *et al*., 2021). However, in this study the increase in stomatal cell size is seen to occur independent of polyploidy or genome size as there are no real differences in genome size of any of the varieties used in this study (Zhu *et al*., 2019; Avni *et al*., 2017; Maccaferri *et al*., 2019; Özkan *et al*., 2010), and are solely as a result of selection and cultivation.

This suggests that stomatal density was an important trait in the cultivation of Durum wheat. Anatomical g_{smax} calculated using stomatal traits reflected the measured g_s (Figure 3.3a, b; Figure 3.6a), suggesting that stomatal traits are contributing greatly to gas exchange. Interestingly, while this decreased stomatal density has likely resulted in decreased g_s, there is no evidence for selection for improved photosynthesis (*A*) (Figure 3.3), suggesting that water-use efficiency was the key element for selection. This contradicts previous studies which have shown that g_s and A in wheat are positively correlated (McAusland *et al*., 2021; Hu *et al*., 2023a), but could be due to there being smaller variation in g_s in this study.

The stomatal cells are not the only cell type observed to increase in size as a result of selection in this study. The pavement cell width and area are also larger in Durum varieties than wild tetraploid (Figure 3.5) and, although not statistically significant, there is also a trend for Durum mesophyll cells to be larger in terms of volume (Figure 3.8a) and transverse area (Figure 3.7c). This once again mirrors the evolution and selection from diploid to hexaploid wheat leaves as Wilson *et al.* (2021) saw increases in mesophyll cell volume and pavement cell area. The occurrence of slightly larger mesophyll cells with reduced SA/Vol concurrent with reduced stomatal density supports Lundgren *et al.*'s (2019) hypothesis that mesophyll cell separation and development is reliant upon the presence of functional stomata. The slight observed reduction in SA/Vol of the mesophyll cells of Durum wheat in this study (Figure 3.8c), and therefore proportionally less exposed surface area for water-loss, has been suggested to contribute to improved iWUE (Wilson *et al.* 2021). As the shape of the mesophyll cells changes with an increase in size from wild to Durum tetraploid lines, it is somewhat similar to that which occurs in the evolution of hexaploid wheat. Wilson *et al.* observed that hexaploid varieties had slightly decreased SA/Vol compared with diploid and tetraploid. The Durum varieties in this study also demonstrated slightly decreased SA/Vol relative to wild and Emmer varieties. More interestingly, the increase in overall cell volume with increasing ploidy level was accompanied by a greater number of lobes on each cell across ploidy level. This was also the case with Durum mesophyll cells in this study, although not statistically significant with three biological replicates. This suggests that the mechanism behind 'adding lobes' when increasing mesophyll cell volume is not just an effect of polyploidy, but can occur rather by either indirect selection or a merely a consequence of wheat mesophyll cell volume increase. Further exploration into increasing mesophyll cell size even more in hexaploid wheat (hence once more negating any possible effect of ploidy) could further elucidate the relationship of mesophyll cell size with shape, lobing and g_s.

When looking at the overall leaf architecture, the differences between wild and Durum tetraploid wheat reflect changes in the evolution of hexaploid wheat. For example, the leaves of diploid wheat are a lot narrower than hexaploid (Austin *et al.,* 1982; Wilson *et al.,* 2021), and this has been suggested to likely result in the generation of alternative arrangements of leaf vasculature, such as differing vein densities and interveinal distance. Similarly, Durum varieties have wider leaves than wild varieties (Figure 3.2a)

and also have increased IVD (Figure 3.9a). In combination with reduced stomatal density, this increased IVD increases the pathway distance of water from the xylem to the nearest stomata, potentially acting to reduce water loss.

3.4.2 Emmer wheat sometimes appears as an intermediate between wild and cultivated Durum

As previously mentioned, many differences observed in terms of leaf form and function of wild and Durum tetraploid leaves reflect those that occur during the evolution from diploid to hexaploid *Triticum*. Similar to the role of tetraploid wheat in the study by Wilson *et al.* (2021), Emmer varieties sometimes appear to act as an intermediate stage. Measured g_s, *A,* and iWUE (A/g_s) all lie between the values for wild and Durum tetraploid varieties (Figure 3.3), as is stomatal density (Figure 3.4a), reflecting the behaviour of tetraploid *Triticum* varieties relative to diploid and hexaploid (Wilson *et al.,* 2021). Reduced stomatal density has therefore been inadvertently selected for thousands of years as a determiner of drought stress tolerance without yield reductions and is present in landrace Emmer varieties.

In other cell types, Emmer varieties are indistinguishable from wild tetraploids. This is the case in terms of stomatal (Figure 3.4b-d) and mesophyll cell size (Figure 3.7a, b; Figure 3.8). Variables falling under this category underwent drastic changes during selective breeding of Durum varieties after Emmer varieties had stopped being cultivated.

There are some traits that stood out in Emmer varieties which were different to both wild and Durum. For example, Emmer varieties had reduced pavement cell width in this study (Figure 3.5b, c), in addition to having mesophyll cells that were more circular in the transverse direction (Figure 3.7c) and had a greater lobing area (Figure 3.7d) than both wild and Durum tetraploid varieties. This lobing area increase was due to an increase in the degree of lobing rather than absolute lobe number (Figure 3.8d). Changes to pavement and mesophyll cells in this way occurred in landrace varieties but were lost during the more intensive selective breeding undergone by the Durum varieties, suggesting that they were not overly beneficial to leaf function in terms of yield or stress tolerance. Emmer varieties also demonstrated reduced mesophyll and leaf thickness compared to wild and Durum varieties in this study, a factor which can likely be attributed to differences in mesophyll cell shape and packing. Despite not distinguishing between Emmer and Durum cultivated wheat, Wilson *et al.* (2021) observed that the one Emmer line (TRI16877) had slightly greater mesophyll porosity (i.e. the percentage of the mesophyll that consists of airspace) than the Durum lines. It would be interesting to explore further whether the changes observed in mesophyll cell shape in this study have any implications on packing of the mesophyll cells within the leaf that may have resulted in the reduced mesophyll/leaf thickness. The variation in cell size was unrelated to genome size, as wild and cultivated Emmer and Durum wheat

have similar genome sizes of around 10-11Gb (Zhu *et al*., 2019; Avni *et al*., 2017; Maccaferri *et al*., 2019; Özkan *et al*., 2010).

The most dramatic differences between Emmer and the other varieties studied were in terms of the height of the plants and leaf length. In this study, Emmer varieties grew the tallest and with the greatest number of leaves over the 40-day growth period, while also having the longest leaf length (Figure 3.2). A milestone of the Green Revolution was the discovery of the *REDUCED HEIGHT1* (RHT1) gene and its role in reducing plant height and potential for yield loss due to lodging (Borlaug, 1968): a discovery which contributed to earning Borlaug the Nobel Peace Prize in 1970. For this reason, it is understandable that Durum varieties have reduced leaf length and plant height compared with landrace, pre-Green Revolution Emmer varieties.

3.5. Conclusion

In summary, cultivated Durum varieties have larger stomatal and pavement cells compared with wild tetraploid and landrace varieties, contributing to an improved iWUE which has been selected for throughout cultivation. Durum varieties also had the shortest, widest leaves of the tetraploid varieties studied, suggesting other benefits such as reduced lodging and increased leaf area for light absorption have also been beneficial during selective breeding. Landrace Emmer varieties that represent ancient, cultivated wheat have not undergone the intensive selection associated with modern breeding techniques. Stomatal size and density are examples of characteristics that were selected for during the domestication of Emmer and which have been further selected for during Durum cultivation, again linked to improved iWUE. However, some traits such as plant height and leaf length are distinct in Emmer varieties, suggesting possible initial advantages during ancient cultivation relating to plant productivity, followed by selection-driven reduction in plant height in modern Durum varieties, possibly related to lodging.

Chapter 4. Mesophyll Patterning in *Triticum*

4.1. Introduction

4.1.1. Wheat Mesophyll Development and Structure

Leaf development is complex and dynamic and occurs in five main steps: leaf primordium initiation, establishment of polarity, control of blade size, regulation of leaf shape (Yan *et al*., 2008; Xiong and Jiao, 2019; Wang *et al*., 2021), and leaf senescence (Tian *et al.*, 2020). These have been reviewed recently by Zhuo *et al*. (2023). Briefly, leaf primordium initiation begins in the peripheral zone (PZ) of the shoot apical meristem (SAM), where auxin acts as a growth regulator of organ initiation. Polarity establishment is a vital process that affects leaf morphology, and the emerging leaf primordium is determined by polar growth on three axes: adaxial-abaxial (front-back of leaf), proximal-distal (base-tip of leaf) and medio-lateral (main vein-edge of leaf). (Conklin *et al.,* 2019; Muszynski *et al.,* 2020). Leaf morphogenesis along these three axes is regulated by a combination of genetic mechanisms and environmental factors (Wang *et al*., 2021). Patterning across the abaxial-adaxial axis involves the divergence of pavement vs mesophyll cell lineages. In dicots, palisade mesophyll tissue develops on the adaxial plane, while spongy tissue on the abaxial. This adaxial-abaxial patterning is influenced by a combination of transcription factors, small RNAs and auxin (Barkoulas *et al*., 2007; Kalve *et al*., 2014; Wang *et al*., 2021; Burian *et al.,* 2022). However, monocot mesophyll appears more homogenous and does not form such distinct palisade and spongy layers (Parker & Ford, 1982; Jellings & Leech, 1984). For example, across the three ploidy levels of the *Triticum* genus, a similar basic arrangement of leaf cells is observed, with the mesophyll not forming distinct palisade and spongy mesophyll layers across the adaxial/abaxial axis. Instead, the monocot mesophyll is most commonly reported to be patterned along the proximal-distal leaf axis with small meristematic cells from the SAM at the base of the leaf and larger, differentiated cells towards the tip, with longitudinal veins (major and minor) interspaced across the leaf width (Jellings & Leech, 1984; Parker & Ford, 1982). However, a recent paper by Sloan *et al.,* (2023) observed that the mesophyll of rice (*Oryza sativa*) forms in distinct ‘layers’ across the abaxial-adaxial axis, distinguished by variation in mesophyll cell size and shape.

The final lobed morphology of individual *Triticum* mesophyll cells reflects the outcome of cell wall shaping combined with cell expansion, with by cytoskeletal organisation being a key driver and co-ordinator of these events (Galatis, 1988). Cortical microtubules (MTs) form in ring-shaped bundles that interconnect to create a cell-wide scaffold, while the cell wall is locally thickened using cellulose microfibrils (CMFs). This results in bulging of the cells where the walls have been thickened and constrictions from the MT rings, forming lobes (Reviewed by Panteris & Galatis, 2005). This shaping occurs across the developing leaves, resulting in a gradient from the brick-like cells adjacent to the meristem to the fully lobed cells towards the leaf tip. The process of *Triticum* mesophyll development is summarised in Figure 4.1.

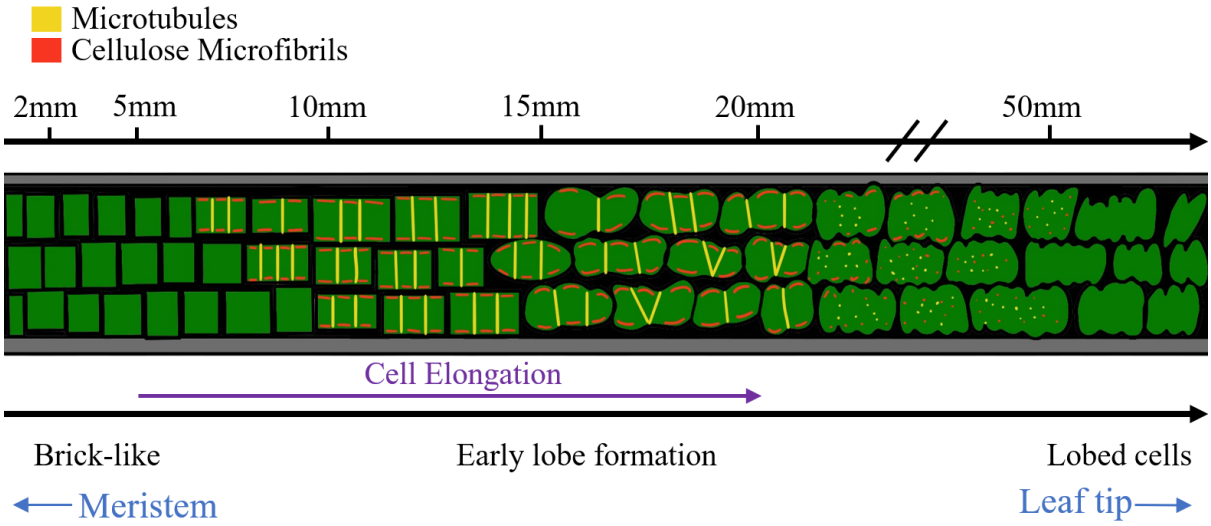

Figure 4.1. Formation of the *Triticum* mesophyll, initiating at the leaf base. Mesophyll development across the proximal-distal axis at 7 days after planting, adapted from Jung & Wernicke (1990; 1992). Mesophyll development initiates at SAM, where the cells undergo elongation followed by cytoskeleton restructuring to form a lobed structure. At 50mm from the leaf base, the mesophyll cells are fully developed, and the leaf begins to unroll.

4.1.2. The Role of the Mesophyll

The controlled separation of dividing mesophyll cells followed by cell expansion to form their distinct lobed shape creates a complex pattern of intercellular airspaces (IAS), allowing for the flux of CO_2 to these cells followed by diffusion across the cell wall, plasma membrane and cytosol, allowing entry of the CO_2 to the site of carboxylation in the chloroplasts (Flexas *et al.,* 2012; Lundgren & Fleming, 2020). Mesophyll cells are therefore important in determining the rate of carbon assimilation and require sufficient light and CO_2 for their role in photosynthesis. However, the availability of these to the mesophyll cells depends greatly on the architecture of the whole leaf, which in turn is greatly influenced by the size and geometry of the mesophyll cells and their arrangement and interactions with each other and other cell types in 3D space.

Mesophyll porosity (i.e. the percentage of mesophyll tissue that is not solid cells), is determined by the lobing and separation of the mesophyll cells during development. In wheat, an increase in mesophyll porosity is accompanied by an increase in stomatal conductance (g_s; gas flux across stomatal pores; Wilson *et al.* 2021), theoretically increasing the rate of photosynthesis but reducing water-use efficiency (WUE; defined as rate of photosynthesis vs transpiration). Leaves with more densely packed mesophyll tissue, such as those that undergo crassulacean acid metabolism (CAM), have lower mesophyll porosity (Nelson *et al.*, 2005) making them optimised for growing in water-limited environments (Males, 2016; Griffiths and Males, 2017). However, understanding the impact of mesophyll cell size, shape and arrangement is more complex than simply increasing/decreasing leaf porosity and must be thought of in terms of the pathway that CO_2 travels between the stomatal pores to the site of photosynthesis within the mesophyll chloroplasts.

The diffusive path length through the IAS can be thought of in terms of tortuosity: the ratio of actual travelled path length (i.e. the geodesic distance) to the direct, unobstructed path length (i.e. the Euclidean distance; Gommes *et al*., 2009). The diffusion pathway is increased by the complexity of the mesophyll and cellular interconnectivity, as well as the distance from the site of CO_2 entry through the closest stomata (Parkhurst, 1994; Morison *et al*., 2007; Pieruschka *et al.,* 2005, 2006, 2008; Morison and Lawson, 2007). In a study on C3 and CAM bromeliads, Earles *et al*., (2018) found that leaves with larger mesophyll cells and lower porosity had lower mesophyll surface area exposed to the IAS and were associated with high tortuosity and long lateral paths that increased the average diffusive plant length, reducing g_s and improving water-use efficiency (WUE). Reducing mesophyll porosity can lead to improved water-use efficiency, but if mesophyll cells were to become too closely packed, plants are at risk of disconnecting the IAS diffusion pathways completely, leading to areas of isolated airspace that are only linked to the atmosphere and other airspace pockets by a liquid pathway through the cell. This would reduce the CO_2 supply rate to the mesophyll cells and subsequently leaf-level photosynthetic capacity, as CO_2 diffuses ~10,000 slower in water than in air, meaning that diffusion in the liquid phase through the cytosol is often considered the rate-limiting step (Evans *et al*., 2009). It is important to also consider that the size, shape and arrangement of mesophyll cells not only has an impact on CO_2 flux, but also other photosynthetic parameters (Terashima *et al.,* 2011; Tholen *et al.,* 2012), and additional factors linked to leaf structure and function including mechanical integrity and water transport (Buckley *et al.,* 2015).

The conductance of the IAS (g_{IAS}) to CO_2 plays a part in determining mesophyll conductance. Mesophyll conductance (g_m) is the conductance of the diffusion pathway of gaseous CO_2 from the substomatal cavity to the site of photosynthesis, encompassing movement across the mesophyll tissue and into the cells and then chloroplasts (Flexas *et al*., 2012). Other contributors include conductance of cell walls (g_{cw}) and chloroplast outer membrane (g_{chl}). G_m is known to impact on both CO_2 and H_2O transport within the leaf due to opposite but overlapping transport pathways (Evans *et al*., 2009; Terashima *et al*., 2011), to an extent coregulating gas flux with g_s. This co-regulation (i.e. linking gas flux across the mesophyll with that across the stomatal pores) is thought to optimise photosynthesis, but uncoupling may be advantageous to increase leaf water-use efficiency (the ratio between photosynthesis and transpiration rate; Flexas *et al*., 2016). Through comparison of closely related species that demonstrated variation in g_m independently of g_s, Peguero-Pina *et al.* (2012) saw increased WUE through larger g_m that was wholly due to differences in leaf anatomy. Masle *et al.* (2005) similarly saw that altering mesophyll anatomy, this time by genetic manipulation in *Arabidopsis*, can lead to improved WUE. Additionally, g_m has been observed to be positively correlated with whole leaf hydraulic conductance (K_{leaf}) (Flexas *et al.,* 2012), further highlighting the importance of the mesophyll in determining overall leaf function relating to photosynthesis and water-use efficiency.

4.1.3. Wheat Evolution and Domestication

Globally grown, our staple cultivated bread wheat belongs to the *Triticum L.* genus, which consists of six species. *Triticum uratu* (wild diploid wheat, 2n = 2x = 14, genome A^uA^u), hybridized with the B genome ancestor of modern wheat (*Aegilops speltoides*, 2n = 2x = 14, genome SS) around 400,000 years ago (Dvorak *et al.,* 2012) to produce wild emmer wheat (*T. dicoccoides*, 2n = 4x = 28, genome A^uA^uBB). About 10,000 years ago, wild emmer began being cultivated (Feldman and Kislev, 2007; Kislev *et al*., 1992) to create a cultivated emmer (*T. turgidum ssp. dicoccon*, 2n = 4x = 28, genome A^uA^uBB). After another 1000 years, the cultivated emmer spontaneously hybridized with another goat grass, similar to the B genome progenitor (*Ae. tauschii*, 2n = 2x = 14, genome DD), to produce an early spelt variety (*T. spelta*, 2n = 6x = 42, genome A^uA^uBBDD). One hypothesis is that, around 8,500 years ago, a natural mutation resulted in changes in the ears of both emmer and spelt leading to more easily threshed types that later evolved into the free-threshing durum (*T. turgidum ssp. durum*) and bread (*T. aestivum*) wheat.

Alongside *T. uratu*, the A^u genome progenitor of all tetraploid and hexaploid wheats, there is another wild diploid *Triticum* species: *T. boeotium* (A^bA^b). These two differ morphologically (Dorofeev *et al*., 1979) and biochemically (Dvorak *et al.,* 1998, 2011; Kilian *et al.,* 2007) and therefore find it difficult to cross-pollinate. Additionally, not all tetraploid wheat has been cultivated, with both *T. dicoccoides* (A^uA^uBB - later cultivated to emmer) and *T. araraticum* (A^uA^uGG) existing as wild tetraploid species. The existence of wild, landrace and cultivated varieties of *Triticum* makes it an experimentally attractive family.

Throughout wheat evolution and cultivation, there have been a series of complex changes with regards to the shape and size of both the mesophyll cells and their surrounding airspace that have had important implications for leaf function. From diploid to hexaploid *Triticum*, the mesophyll cells have become larger and there has been a reduction in mesophyll porosity, with an accompanying increase in iWUE (Wilson *et al.,* 2021).

4.1.4. Imaging the Wheat Mesophyll in 3D

Techniques for imaging leaves to observe mesophyll characteristics are constantly improving with the advancement of 3D microscopes and analysis software. With the ability to now combine this high-quality image data with modern technologies which measure parameters relating to photosynthesis and water-use, it allows us to gain a deeper understanding of how whole leaf architecture is related to its function.

In traditional studies from the 1980s, the limited technology available meant that conclusions of how the mesophyll cells behave in 3D space, i.e. their arrangement and volume, were drawn from the analysis of 2D images and approaches that involved separating mesophyll cells from the rest of the leaf

tissue (Parker & Ford, 1982; Jellings & Leech, 1984). While these studies were able to yield key findings, such as how mesophyll cell size increases as a result of polyploidy, the lack of true 3D image data led to inaccuracies in cell and tissue parameter estimates (Théroux-Rancourt *et al*., 2017; Earles *et al*., 2018; Mathers *et al.,* 2018; Harwood *et al*., 2020) meaning that further conclusions drawn from early data can give little reliable insight into leaf form and function.

A better way to image wheat leaves is using X-ray μCT, building up 2D projections to construct a 3D image. The major advantage compared with older imaging techniques is that it is non-invasive and allows for a data on mesophyll tissue to be collected without the need to separate it from the rest of the leaf. However, there are limitations when approaching questions of mesophyll structure when trying to observe individual cell shape and size, as discerning the boundaries between mesophyll cells from cell lobing is impossible, and obtaining higher resolution images requires long scanning and processing time (Pajor *et al*., 2013). X-ray CT is more useful when looking at the patterning of mesophyll airspace and overall leaf porosity, as the low-density airspace can easily be separated from the higher density mesophyll cells (Dhondt *et al.,* 2010; Pajor *et al.,* 2013; Mathers *et al*., 2018).

Confocal laser scanning microscopy (CLSM) allows for the generation of super high-resolution images of the mesophyll for extraction of quantitative data on the shape and size of individual mesophyll cells (Wuyts *et al*., 2010). Confocal microscopy works by focusing a laser on the sample, which passes through a pinhole and is reflected by a dichroic mirror and scanned across the desired focal plane. The fluorescence emitted from the stained sample passes back through the mirror and a second pinhole that is confocal with the first, before hitting a detector. Light that is not from the plane of focus is prevented from being detected due to the presence of the second pinhole, reducing flare (Paddock, 2000). These confocal pinholes are a major advantage comparted to conventional widefield fluorescence for imaging thick samples such as wheat leaves; they allow for the capture of high-quality images throughout the sample (Paddock, 2000; Hepler & Gunning, 1998; Amos & White, 2003). The 2D scans (or slices) can be built up into a z-stack for rendering of a 3D image (Truernit *et al.,* 2008; Buda *et al*., 2009; Wuyts *et al.,* 2010) and from these reconstructions, it is possible to segment the tissue into individual cells and acquire measures of cell geometry. Unlike μCT and other 3D imaging techniques, confocal microscopy allows for imaging of individual cells, and has been frequently used on a range of plant tissues (Hutzler, 1998; Truernit *et al.,* 2008; Omasa *et al*., 2009; Buda *et al*., 2009; Yoshida *et al.*, 2014) including Arabidopsis (Wuyts *et al.,* 2010; Dow *et al*., 2017) and wheat (Wilson *et al.,* 2021) mesophyll cells.

4.1.5. Aims

As indicated above, the traditional view of the monocot mesophyll, including wheat, is that it is uniform, distinguishing it from the eudicot leaf which shows clear separation into palisade and spongy mesophyll

layers. Recent data has shown that cells in the mesophyll of rice leaves can be assigned to layers based on cell size and shape (Sloan *et al.,* 2023).

The main aim of the experiments described in this chapter was to test the hypothesis that leaves of *Triticum* species of a range of ploidy and cultivation levels showed a similar mesophyll patterning. This was done using a combination of 2D and 3D imaging techniques and analytical approaches.

4.2. Plant Materials

The plant materials used in this chapter can be found in Table 4.1.

Table 4.1 *Triticum* lines used in this study. Lines are referred to by the simplified 'Name' throughout this chapter, and colour coded by ploidy and cultivation status status. The lines used for confocal imaging were a subset of the total panel: 2n – 6735; 4nW – TRI18505; Emmer – TRI16877; Durum – VOILUR; 6n – Fielder.

Ploidy	Species	Line Code	Status	Name
Diploid	*Triticum baeoticum*	TRI 18344	Wild	*T. baeoticum*
Diploid	*Triticum uratu*	TRI 6735	Wild	*T. uratu*
Tetraploid	*Triticum turgidum (subsp. dicoccoides)*	TRI18505	Wild	*T. turgidum*
Tetraploid	*Triticum turgidum (subsp. dicoccoides)*	TRI18530	Wild	*T. turgidum*
Tetraploid	*Triticum araraticum*	TRI16599	Wild	*T. araraticum*
Tetraploid	*Triticum araraticum*	TRI18513	Wild	*T. araraticum*
Tetraploid	*Triticum turgidum (subsp. dicoccon)*	TRI16877	Domesticated (Landrace)	Emmer
Tetraploid	*Triticum turgidum (subsp. dicoccon)*	TRI28049	Domesticated (Landrace)	Emmer
Tetraploid	*Triticum turgidum (subsp. dicoccon)*	TRI14734	Domesticated (Landrace)	Emmer
Tetraploid	*Triticum durum (subsp. durum)*	VOILUR	Domesticated (Modern)	Durum
Tetraploid	*Triticum durum (subsp. durum)*	AVENTADUR	Domesticated (Modern)	Durum
Tetraploid	*Triticum durum (subsp. durum)*	ANVERGUR	Domesticated (Modern)	Durum
Hexaploid	*Triticum aestivum*	COUGAR	Domesticated (Modern)	*T. aestivum*
Hexaploid	*Triticum aestivum*	FIELDER	Domesticated (Modern)	*T. aestivum*

4.2.1. The Wheat Mesophyll is Not Homogenous

Although grass leaves are generally perceived as having a uniform cellular architecture (not clearly being divided into a palisade and spongy layer characteristic of many eudicot leaves), recent analysis in rice has indicated that there is celular patterning within the leaf reflecting distribution of cell size and shape (Sloan *et al*., 2023). This allows for the rice leaf to be divided into a series of cell layers, with each layer being distinguished by relative size and shape. An exploration of g_s and leaf cellular structure based simply on mean cell size (as performed in Chapter 3) might, therefore, miss potential links of domains of cellular architecture with physiological performance.

To explore this possibility, mesophyll cells (MSCs) in each cross-section to were assigned to a layer based on the following rules. Sub-adjacent to upper epidermis (Upper); sub-adjacent to lower epidermis (Lower); Adjacent to vascular bundle (Radial); Not adjacent to epidermis or vascular bundle (Middle). This is shown in Figure 4.2. In longitudinal sections, the Upper and Lower cells could not be

differentiated, and radial/middle cells were only present under the presence/absence of vascular tissue in the section (Figure 4.2b, c).

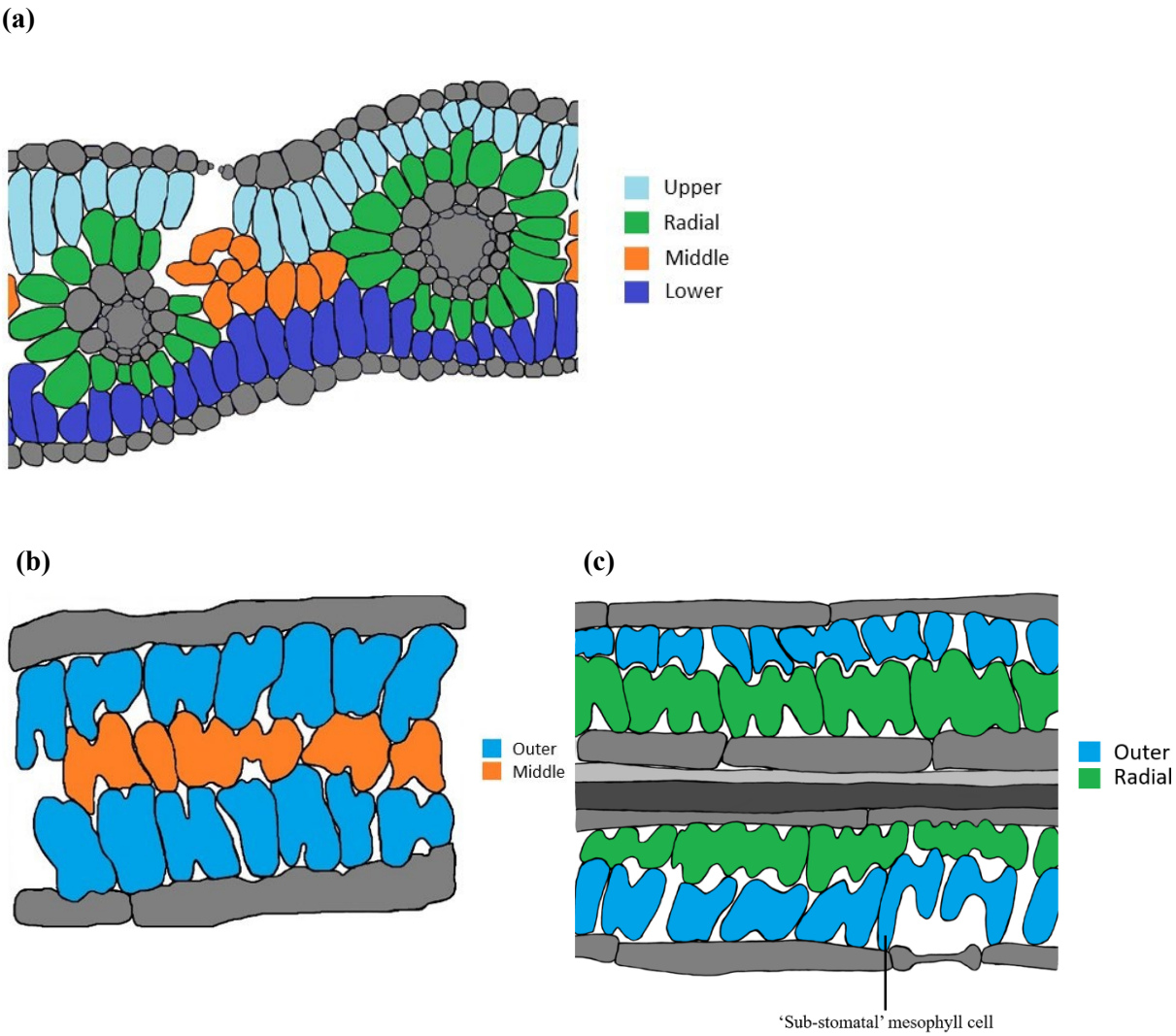

Figure 4.2. The assignation of mesophyll cells to layers in a typical wheat leaf. a) Transverse leaf cross-section b) longitudinal cross-section, where radial cells are not visible c) longitudinal cross-section, where radial cells are visible. Diagrams are based on cross sectional images of a Durum leaf, 5th leaf at 28 days after planting.

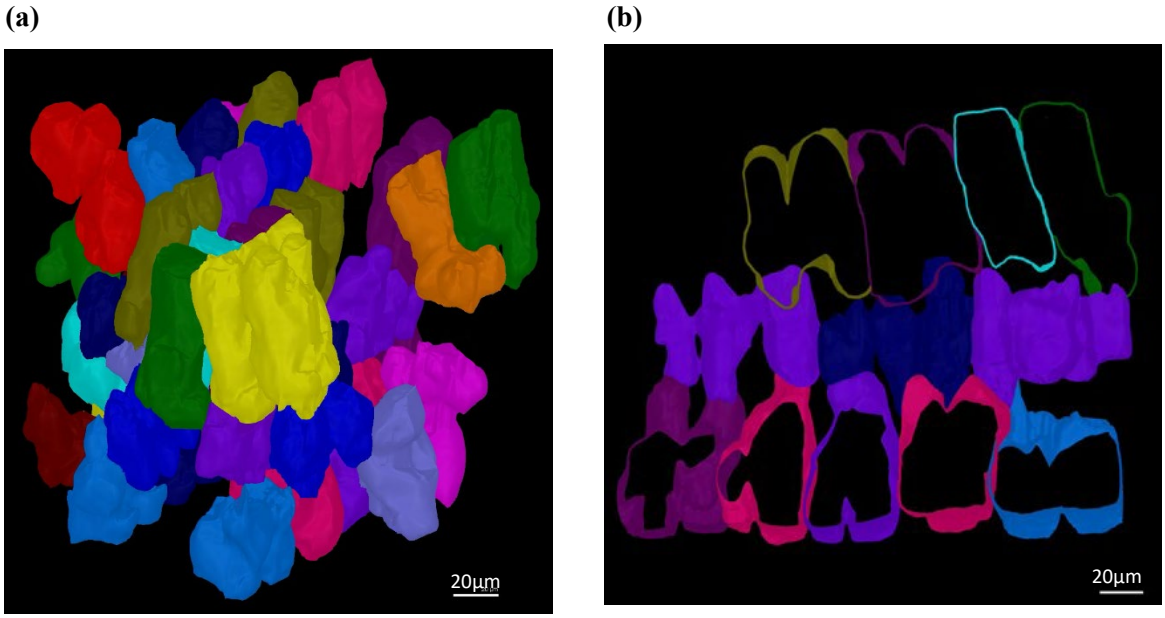

Figure 4.3. 3D imaging of wheat mesophyll cells. a) Snapshot of mesophyll segmented using MorphographX b) Image showing clipped 3D cell objects generated from confocal stacks in MorphographX. (b) has undergone minor editing to make image neater so that cell boundaries are clearer. From each 3D stack, 'Outer' and 'Middle' cells can be observed. All images are from a Durum 'VOILUR' leaf.

The image datasets for wild and domesticated wheat lines were analysed so that MSCs in each section were allocated to one of four groups for transverse sections (Upper, Lower, Middle, Radial) and three for longitudinal (Outer, Middle and Radial). The Upper layer consists of cells in direct contact with the adaxial epidermis, the Lower layer of cells in direct contact with the abaxial epidermis, the Radial layer of cells in direct contact with the bundle sheath tissue and the Middle layer of cells only in direct contact with other mesophyll cells. Due to the inability to distinguish the abaxial and adaxial epidermis in longitudinal sections, the Upper and Lower layers are both included in the Outer longitudinal layer, and the Radial cells have been omitted from this analysis due to their absence in slices containing Outer and Middle cells.

Alongside 2D data for mesophyll cell morphology, 3D data were collected using confocal imaging of fixed leaf samples and processing in MorphoGraphX (Barbier de Reuille *et al*., 2015) to generate mesh reconstructions and quantitative cell volume and surface area data (Figure 4.3). Z-stacks were acquired between the vasculature (i.e., omitting cells in the Radial layer) and allowed for cell data to be assigned to either Outer or Middle layers, as the abaxial and adaxial epidermis are indistinguishable in these z-stacks.

4.3. Results

4.3.1. The Mesophyll Cell Layers can be Defined by Size

Analysis of 2D MSC area data across all ploidy levels and cultivation statuses showed significant differences between cells in assigned layers (Figure 4.4). Broadly, our data showed that all cell types

studied are larger in higher ploidy species, which is consistent with the literature (Jellings & Leech, 1984; Parker & Ford, 1982; Wilson *et al*., 2021; Kondorosi *et al*., 2000; Katagiri *et al*., 2016). Consistently across all *Triticum* lines studied, cells in the Middle and Radial layers had significantly lower transverse MSC area than those in the Upper and Lower layers. The p values for ANOVA tests conducted to test for significant interactions of transverse MSC area between layers within each Triticum species/subspecies were <0.0001**** for all. Values for the transverse cell area of cells in the Middle and Radial layers were indistinguishable from each other, as were cells in the Upper and Lower layers.

This was strongly supported by a ranked data analysis (Figure 4.4h). In each leaf, the layers were assigned a rank of 1 to 4 based on mean transverse mesophyll cell area. All plants from each ploidy level and cultivation status were grouped together and plotted using a heat map and circle size to represent frequency of each layer having a specific rank. As demonstrated in figure 4h, the largest circles in the 1st and 2nd rank are always the upper and lower layers, showing that the cells in upper and lower layers were always the largest in terms of area, and the middle and radial cells the smallest (Friedman: p<0.0001****, Friedman statistic= 112.0). Statistically, the upper and lower layers both ranked lower than radial and middle cells at a 0.01% confidence interval (Dunn's: p<0.0001**** for all interactions except Middle-Radial and Upper-Lower). The most common order from largest to smallest cells was Upper; Lower; Radial; Middle.

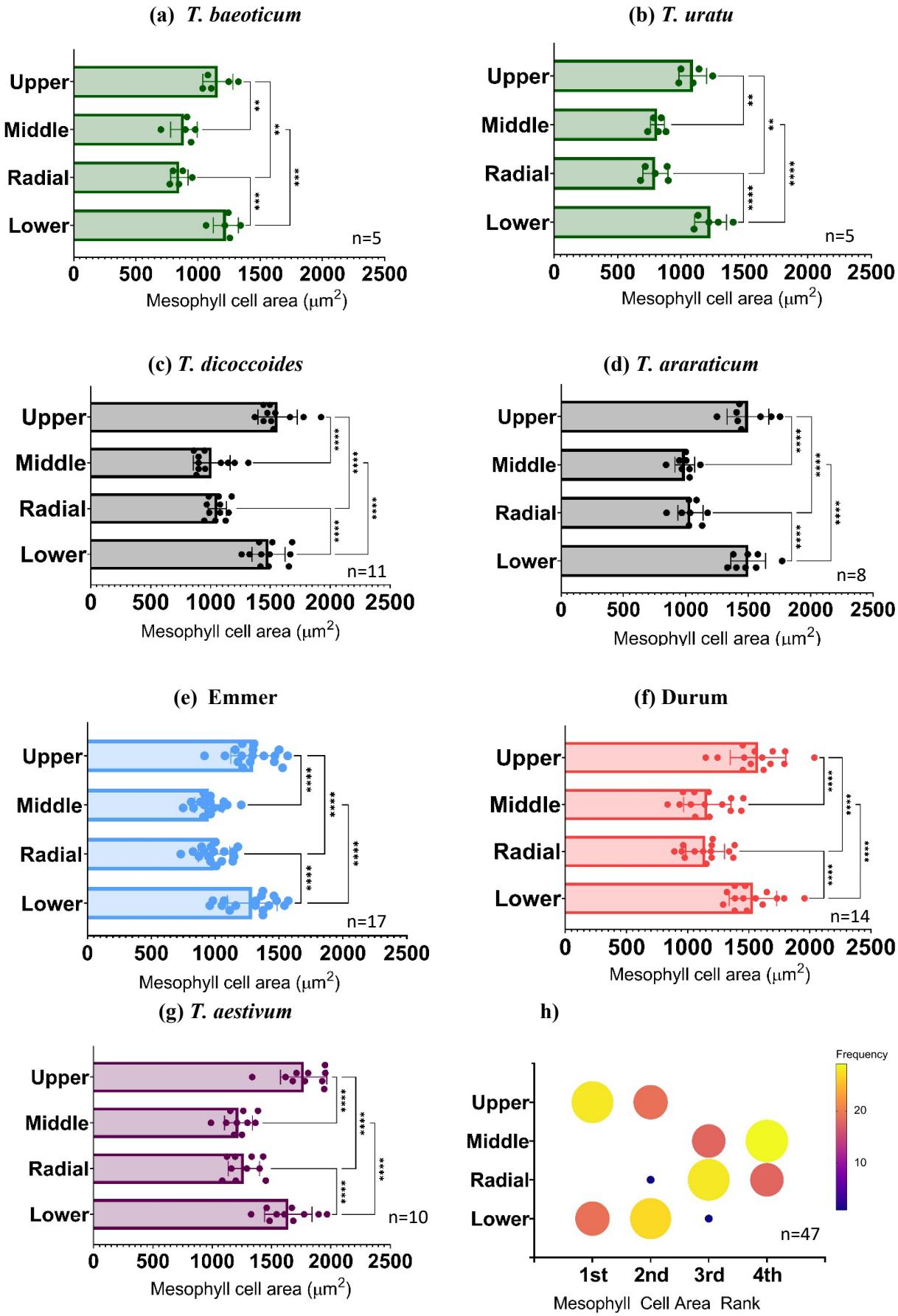

Figure 4.4. Analysis of transverse mesophyll cell area shows distinct layering of cells by size in diploid, tetraploid and hexaploid *Triticum* lines. a-b) Transverse area of diploid cells in designated mesophyll layers. c-

d) Transverse area of wild tetraploid cells in designated mesophyll layers. e-f) Transverse area of cultivated tetraploid wheat cells in designated mesophyll layers. g) Transverse area of hexaploid *T. aestivum* cells in designated mesophyll layers. h) Ranked data of transverse mesophyll cell area from all lines, separated by layer. Frequency of rank is indicated by colour and size of circle. Ranking is determined based on the frequency that cells in a particular layer rank 1st (largest) –4th (smallest) in terms of cell area. In this case, Upper and Lower cells are consistently the largest in terms of transverse cell area (ranked 1st and 2nd), and Radial and Middle cells consistently the smallest (ranked 3rd and 4th). Error bars represent standard deviation from the mean. ANOVA and post-hoc Tukey tests were carried out to test for significant interactions between cell layers within each species/subspecies: p<0.005**, p<0.0005***, p<0.0001****. Statistical significance for ranked data in (h) was assessed using a Friedman test.

In contrast, the area of MCs in longitudinal sections was found to be a feature that could not be used as strongly as the transverse data to distinguish mesophyll layers, as the majority of lines studied showed no significant differences between the layers (Figure 4.5a-e). The only wheat varieties that significantly varied in terms of longitudinal MSC area the two modern cultivated species: tetraploid Durum (ANOVA: p=0.0083*, f=5.413) and hexaploid *T. aestivum* (ANOVA: p=0.0011**, f=8.598) (Figure 4.5f, g). The Middle cells demonstrated decreased longitudinal area compared to the Outer cells in both Durum (Tukey: p=0.0153*, df=40) and *T. aestivum* (Tukey: p=0.0118*, df=30). In Durum leaves, Radial mesophyll cells also had increased longitudinal area compared with the Middle cells (Tukey: p=0.0216*, df=40). This was not the case with *T. aestivum* however, as the Radial cells were indistinguishable from the Middle in terms of area but were instead significantly smaller than cells in the Outer layers (Tukey: p=0.001**, df=30).

Although in most cases longitudinal cell area was not statistically different between mesophyll layers, when cells in each layer were assigned a rank for each leaf and all data was grouped together (Figure 4.5h), the trend for defined layers by longitudinal area was significant (Friedman: p<0.0001****, Friedman statistic: 23.82). Cells in the Middle layer were often ranked highest, therefore having consistently smaller longitudinal cell area than cells in both the Outer (Dunn's: p<0.0001****) and Radial layers (Dunn's: p=0.0002***).

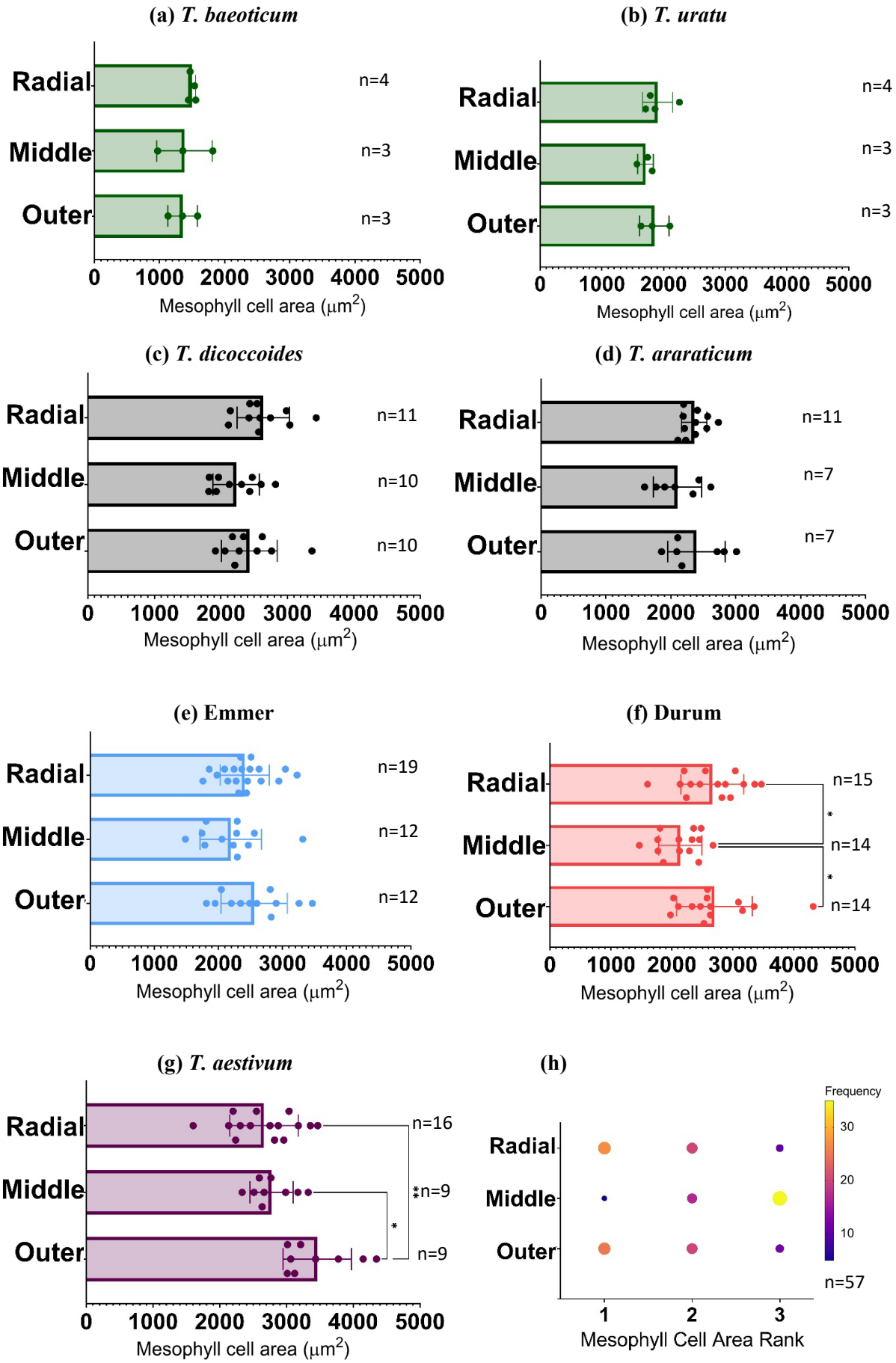
(a) T. baeoticum
Radial
Middle
Outer
n=4
n=3
n=3
0 1000 2000 3000 4000 5000
Mesophyll cell area (μm2)
(b) T. uratu
Radial
Middle
Outer
n=4
n=3
n=3
0 1000 2000 3000 4000 5000
Mesophyll cell area (μm2)
(c) T. dicoccoides
Radial
Middle
Outer
n=11
n=10
n=10
0 1000 2000 3000 4000 5000
Mesophyll cell area (μm2)
(d) T. araraticum
Radial
Middle
Outer
n=11
n=7
n=7
0 1000 2000 3000 4000 5000
Mesophyll cell area (μm2)
(e) Emmer
Radial
Middle
Outer
n=19
n=12
n=12
0 1000 2000 3000 4000 5000
Mesophyll cell area (μm2)
(f) Durum
Radial
Middle
Outer
n=15
n=14
n=14
*
*
0 1000 2000 3000 4000 5000
Mesophyll cell area (μm2)
(g) T. aestivum
Radial
Middle
Outer
n=16
n=9
n=9
*
*
0 1000 2000 3000 4000 5000
Mesophyll cell area (μm2)
(h)
Radial
Middle
Outer
Frequency
30
20
10
n=57
1 2 3
Mesophyll Cell Area Rank

Figure 4.5. Analysis of longitudinal cell area shows distinct layering of cells by size in tetraploid Durum and hexaploid *T. aestivum*. a-b) Longitudinal area of diploid cells in designated mesophyll layers. c-d) Longitudinal area of wild tetraploid cells in designated mesophyll layers. e-f) Longitudinal area of cultivated tetraploid cells in designated mesophyll layers. g) Longitudinal area of hexaploid *T. aestivum* cells in designated mesophyll layers. h) Ranked data analysis of longitudinal mesophyll cell area from all lines, separated by layer. Frequency of rank is indicated by colour and size of circle. Ranking is determined based on the frequency that cells in a particular layer rank 1st (largest) –3rd (smallest) in terms of cell area. In this case, Middle cells were most frequently the smallest in terms of longitudinal cell area (ranked 3rd). Error bars represent standard deviation from the mean. ANOVA and post-hoc Tukey tests were carried out to test for significant interactions between cell layers within each species/subspecies: $p<0.05$*, $p<0.005$**. Statistical significance for ranked data in (h) was assessed using a Friedman test.

Despite being able to acquire cell data from both longitudinal and transverse sections, information on whole cell morphology is lost by limiting imaging to 2D. Therefore, 3D imaging of a subset of lines was carried out using confocal microscopy to further explore mesophyll cell size and shape, with the z-stacks segmented using MorphographX to generate quantitative cell data. This data is presented in Figure 6. Mesophyll cell volume can generally be seen to increase from diploid to tetraploid to hexaploid plants regardless of the layer (ANOVA: p=0.0009***, f=13.15). There was also a trend for outer layer mesophyll cells in Durum and hexaploid lines to have a greater volume, however this was not statistically significant (Figure 4.6a). The only statistically significant difference between cell size of mesophyll cells was in the surface area of Outer and Middle layers was in tetraploid Durum where the surface area of the outer layer cells was greater than the middle cells (t-test: p=0.0318*, t=3.237, df=4) (Figure 4.6b).

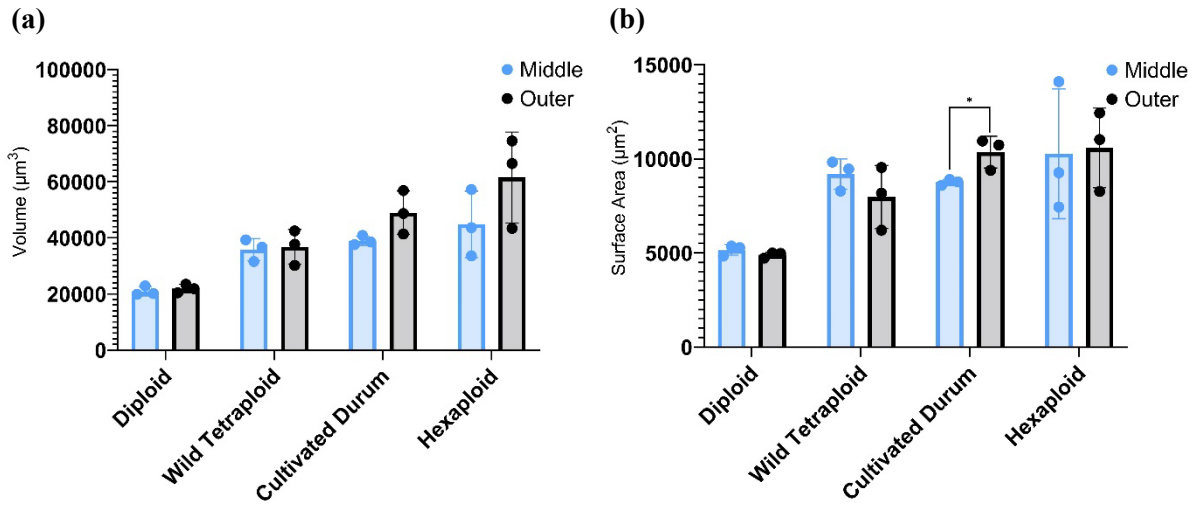

Figure 4.6. 3D analysis of mesophyll cell volume and surface area in diploid, tetraploid and hexaploid *Triticum* based on cell layer designation shows some distinction between layers. (a) Mesophyll cell volume of diploid, tetraploid and hexaploid lines. (b) 3D mesophyll cell surface area of diploid, tetraploid and hexaploid lines. Error bars represent standard deviation from the mean. T-tests were carried out to test for significant interactions between cell layers within each species/subspecies: $p<0.05$*. n=3.

The cell volume data in figure 4.6b supports the observations of 2D cell area that only the cultivated varieties (tetraploid Durum and hexaploid) had larger Outer layer mesophyll cells compared with Middle cells (Figure 4.5f, g).

4.3.2. The Mesophyll Cell Layers can be Defined by Shape

In addition to size, Sloan *et al.,* (2023) reported that the cells in different layers of the rice leaf can be distinguished by shape, notably their degree of circularity and lobing. To investigate whether the layers of wheat mesophyll distinguished by cell size could also be distinguished by shape, I performed an analysis of shape in both 2D transverse (Circularity; Figure 4.7) and 2D longitudinal sections (Lobing Area; Figure 4.8), as well in 3D by calculating the surface area to volume ratios and counting love number (Figure 4.9).

In transverse sections, mesophyll cell layers differed significantly from each other in terms of cell circularity across all ploidy levels and cultivation statuses (Figure 4.7).

Circularity is used in this case to quantify 2D shape where cell lobing is not visible, and is a FIGI/ImageJ output that can briefly be described as a shape's deviation from a perfect circle, with a circle given a value of 1. Statistical tests using ANOVA supported the existance of transverse mesophyll layers that are distinct by cell circularity at a <0.01% confidence interval (ANOVA: $p<0.0001$**** for all species/subspecies; Figure 4.6). The number of significant differences across the layers varied, with wild tetraploid *T. araraticum* being the only species for which cells in every layer had significantly different circularity than every other (Figure 4.7d). In this case, Upper cells were the least circular, followed by Lower cells then Radial, with MCs in the Middle layer being the most circular. This trend was observed across most of the other varieties studied, although with some of the layers being statistically indistinguishable – in particular the Upper-Lower, Lower-Radial and Radial-Middle interactions. In all cases, cells in the Upper and Lower layers were statistically less circular than those in the Middle, and the Radial cells also significantly more circular than those in the Upper layer.

From the combined ranked analysis, the largest circle in the 1st rank was for middle cells, in 2nd rank were radial cells, 3rd rank were lower cells and 4th were upper cells, demonstrating that the average leaf had its most circular cells in the middle layer, followed by radial, lower and upper respectively (Figure 4.7h). This ranking was less well defined than for analysis based on transverse area (Figure 4.5h) but was still statistically significant (Friedman: $p<0.0001$****, Friedman statistic = 70.4), with the most consistent observation being that cells in the Upper layer are most commonly the least circular. The Upper-Middle, Upper-Radial and Upper-Lower rank differences were all statistically significant (Dunn's: $p<0.0001$****, $p<0.0001$****, $p=0.0026$ respectfully). Cells in the Middle mesophyll layer were also consistently ranked higher (aka more circular) than both the Radial (Dunn's: $p=0.0396$*) and Lower (Dunn's: $p<0.0001$****), and cells in the Radial layer were indistinguishable from Lower cells in terms of transverse circularity.

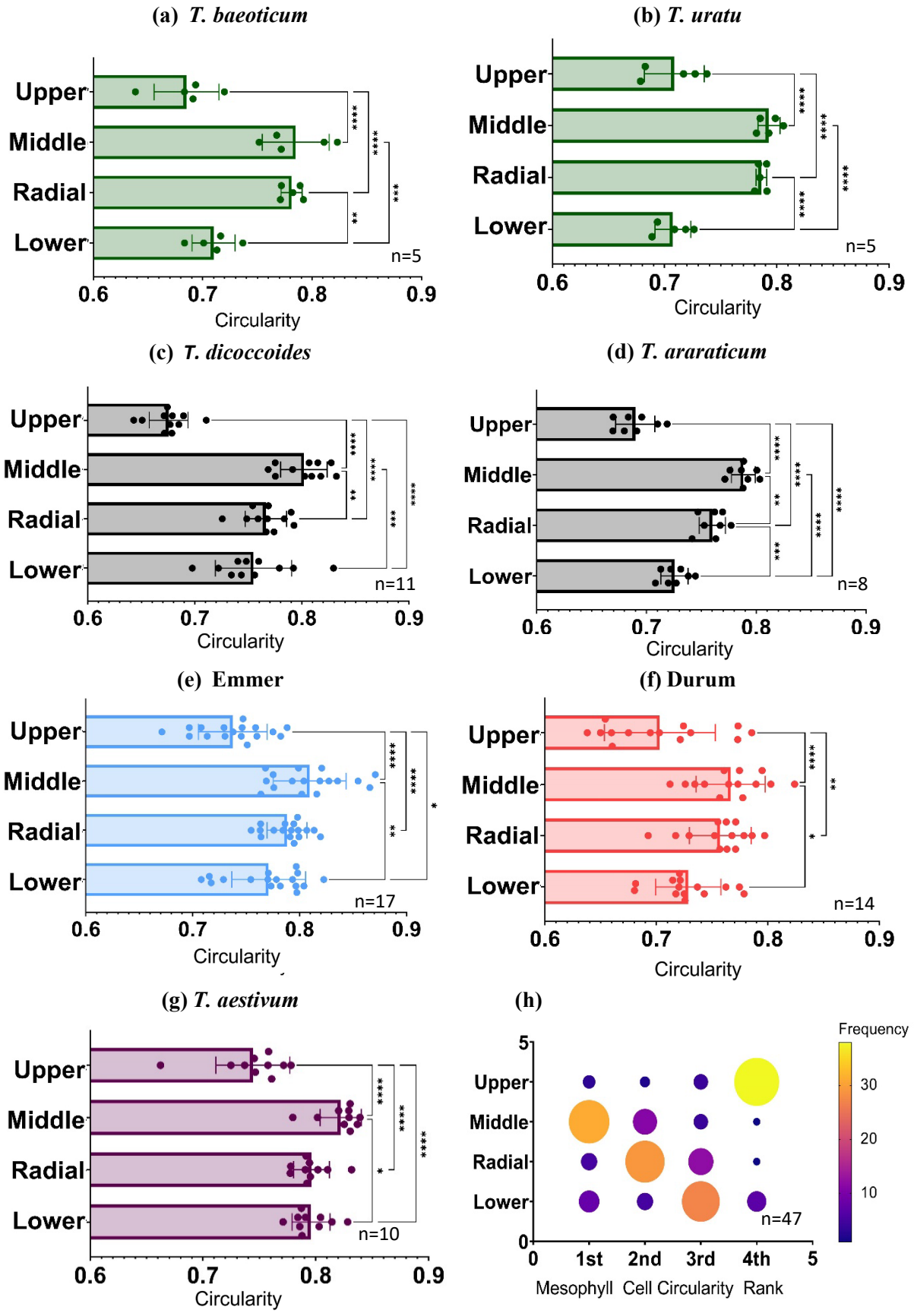

Figure 4.7. Analysis of transverse mesophyll cell circularity shows distinct layering of cells by shape in diploid, tetraploid and hexaploid *Triticum* lines. Circularity represents a shape's deviation from a perfect circle

which has a value of 1. a-b) Transverse circularity of diploid cells in designated mesophyll layers. c-d) Transverse circularity of wild tetraploid cells in designated mesophyll layers. e-f) Transverse circularity of cultivated tetraploid wheat cells in designated mesophyll layers. g) Transverse circularity of hexaploid *T. aestivum* cells in designated mesophyll layers. h) Ranked data analysis of mesophyll cell circularity from all lines, separated by layer. Frequency of rank is indicated by colour and size of circle. Ranking is determined based on the frequency that cells in a particular layer rank 1st (most circular) –4th (least circular) in terms of cell circularity. Error bars represent standard deviation from the mean. ANOVA and post-hoc Tukey tests were carried out to test for significant interactions between cell layers within each species/subspecies: $p<0.05$*, $p<0.005$**, $p<0.0005$***, $p<0.0001$****. Statistical significance for ranked data in (h) was assessed using a Friedman test.

For longitudinal sections which demonstrate lobing of the cells (Figure 4.2b, c), shape was quantified using lobing area. Briefly, lobing area is defined as the difference between the convex hull area and area of the object and can be thought of in this case as the 'degree of lobing'. More information on the calculation of lobing area can be found in Section 2.3.3 of Chapter 2. Differences in lobing area between cells assigned to different layers were significant for all lines studied (Figure 4.8): *T. baeoticum* (ANOVA: p= 0.0048**, f=12.81), *T. uratu* (ANOVA: p=0.0006**, f=25.22), *T. dicoccoides* (ANOVA: p= 0.0069*, f=6.646), *T. araraticum* (ANOVA: p=0.0005***, f=10.94), Emmer (ANOVA: p<0.0001****, f= 14.66), Durum (ANOVA: p<0.0001****, f= 18.07) and *T. aestivum* (ANOVA: p<0.0001****, f= 18.42). Across all ploidy levels and cultivation statuses, Radial cells had significantly greater lobing area than Outer cells. For all except for *T. baeoticum* (Figure 4.8a) and *T. dicoccoides* (Figure 4.8c), the Outer cells also had decreased lobing area compared to cells in the Middle layers. Cells in Middle and Radial layers were indistinguishable in terms of lobing area.

When the data was combined and each layer ranked by longitudinal lobing area, this supported the observation of distinct layers by longitudinal shape (Friedman: p<0.0001****, Friedman statistic: 54.94; Figure 4.8h). Cells in the Outer layer were ranked as consistently having the lowest lobing area compared to both Middle and Radial cells (Dunn's: p<0.0001**** for both), and ranking of lobing area of the cells in the Middle and Radial layers was not significantly different.

(a) *T. baeoticum*

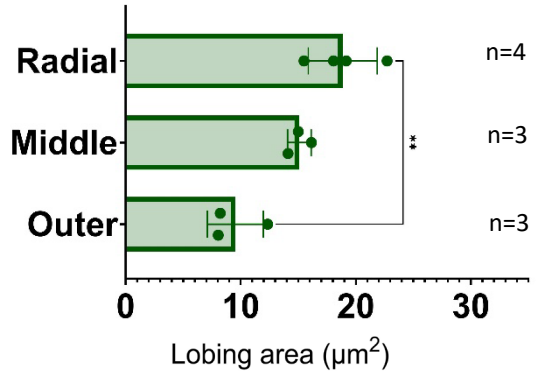

(b) *T. uratu*

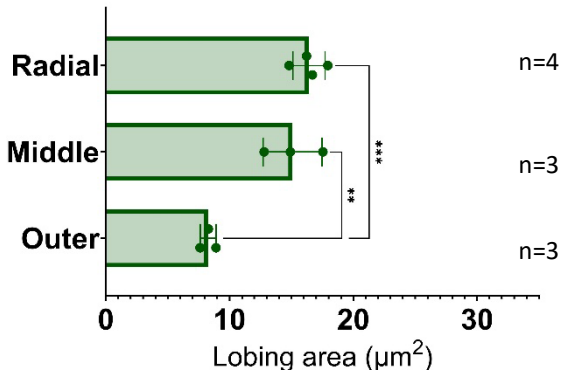

(c) *T. dicoccoides*

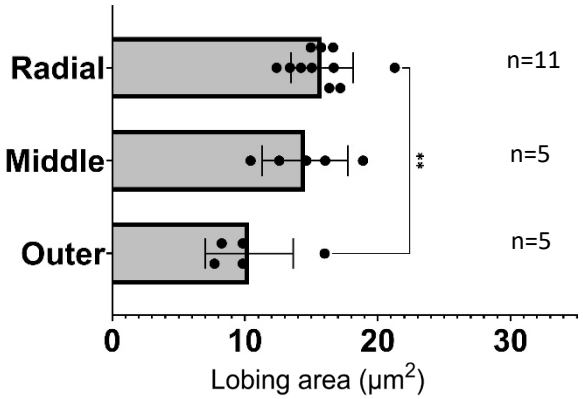

(d) *T. araraticum*

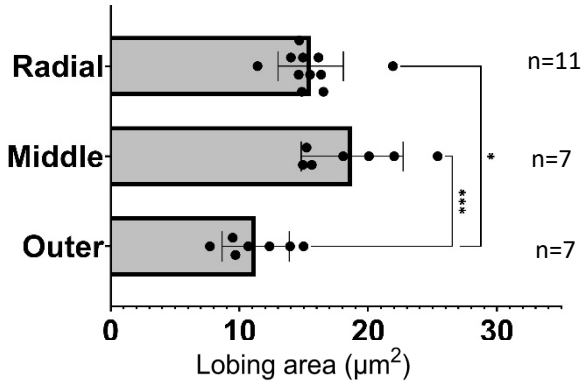

(e) Emmer

(f) Durum

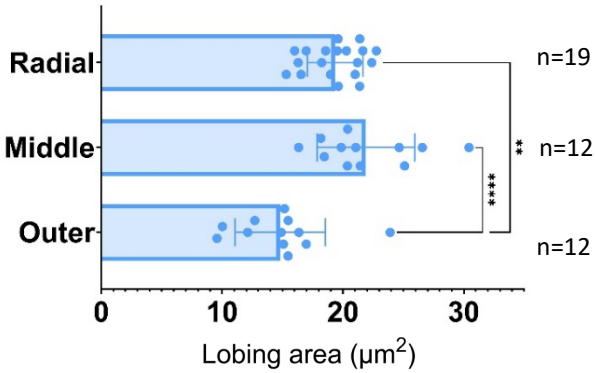

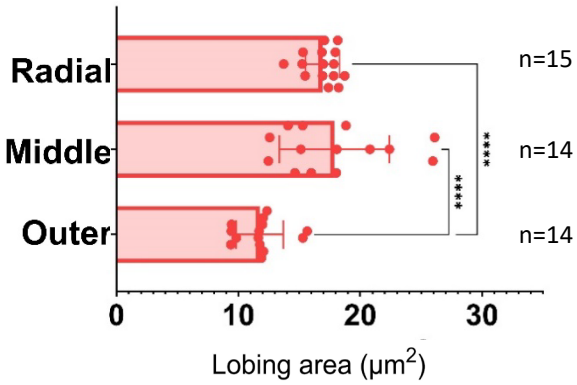

(g) *T. aestivum*

(h)

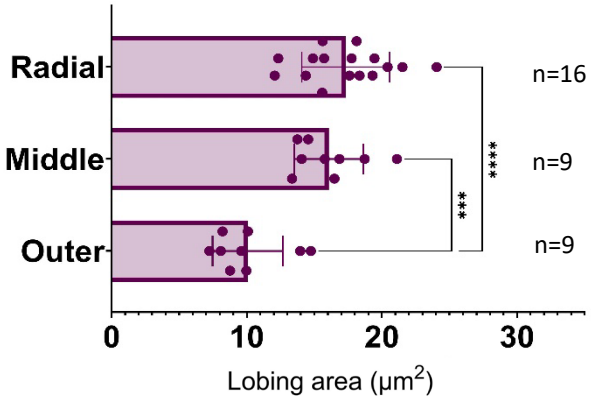

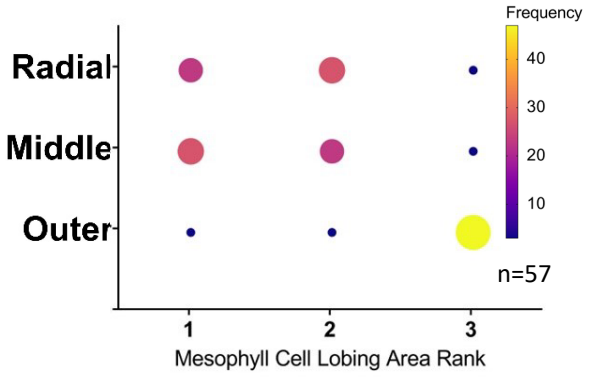

Figure 4.8. Analysis of longitudinal cell lobing area shows distinct layering of cells by shape in diploid, tetraploid and hexaploid *Triticum* lines. a-b) Longitudinal cell lobing area of diploid cells in designated mesophyll layers. c-d) Longitudinal cell lobing area of wild tetraploid cells in designated mesophyll layers. e-f) Longitudinal cell lobing area of cultivated tetraploid cells in designated mesophyll layers. g) Longitudinal cell lobing area of hexaploid *T. aestivum* cells in designated mesophyll layers. h) Ranked data analysis of longitudinal mesophyll cell lobing area from all lines, separated by layer. Frequency of rank is indicated by colour and size of circle. Ranking is determined based on the frequency that cells in a particular layer rank 1st (most circular) –3rd (least circular) in terms of cell circularity. Error bars represent standard deviation from the mean. ANOVA and post-hoc Tukey tests were carried out to test for significant interactions between cell layers within each species/subspecies: $p<0.05$*, $p<0.005$**, $p<0.0005$***, $p<0.0001$****. Statistical significance for ranked data in (h) was assessed using a Friedman test.

As previously stated, information is at risk of being lost when only looking at cell morphology in 2D. When trying to quantify shape in 3D, two approaches were used. The first was to calculate surface area to volume ratio, which can be used to approximate the simplicity/complexity of the shape (Figure 4.9a). The second was to count the number of lobes, with a basic oblong-shaped cell being counted as two lobes and each additional lobe at either pole added to the total (Figure 4.9b). Cells in the Middle layers had greater surface area to volume ratio, which was statistically significant compared to Outer cells for the wild tetraploid (t-test: p=0.022*, t=3.640, df=4) and hexaploid lines (t-test: p=0.025*, t=3.495, df=4) (Figure 4.9a). A likely contributor to this is the increased number of lobes observed in middle layer cells, although none of the differences were significant across the lines studied (Mann-Whitney: $p>0.05$) (Figure 4.9b)

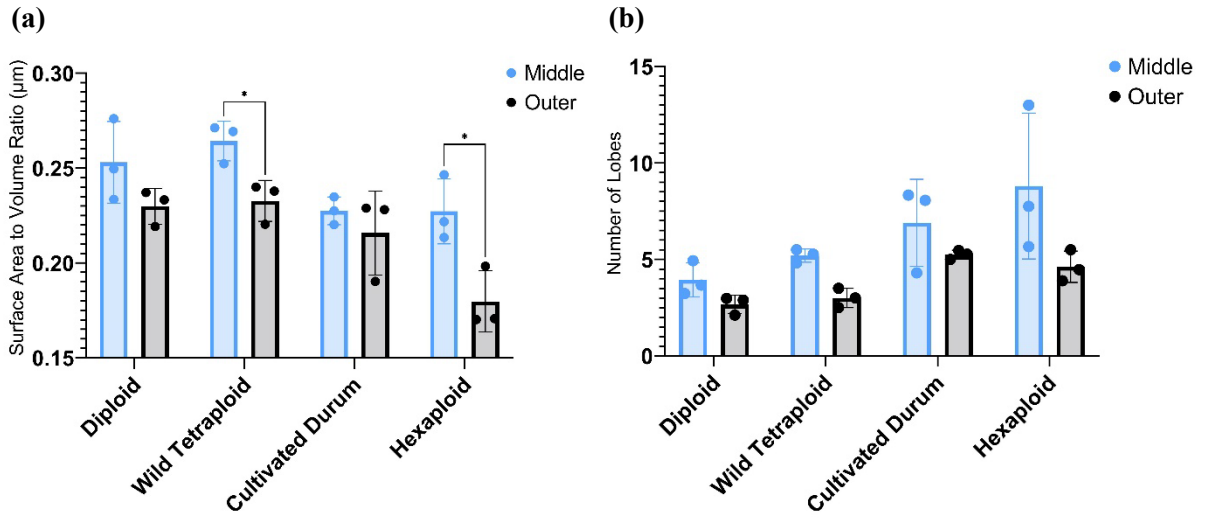

Figure 4.9. Analysis of 3D mesophyll cell shape shows distinct layering of cells by shape in diploid, tetraploid and hexaploid *Triticum* lines. a) Surface area to volume ratio of cells assigned to layers in 2n, 4n and 6n lines. b) Number of lobes of cells assigned to layers in 2n, 4n and 6n lines. Error bars represent standard deviation from the mean. T-tests (a) and Mann-Whitney (b) tests were carried out to test for significant interactions between cell layers within each species/subspecies: $p<0.05$*. n=3.

The data described above suggests that there are differences in cell size and shape between different mesophyll layers to varying degrees in all diploid, tetraploid and hexaploid lines studied.

4.3.3. Sub-Stomatal Mesophyll Cells are Distinct from Other 'Outer' Layer Mesophyll Cells

While assessing morphological differences in cells assigned to mesophyll layers, it became obvious that cells directly adjacent to sub-stomatal cavities looked different compared to other Outer layer cells (Figure 4.10a, b). I separated data for Outer cells in one line of Durum (VOILUR) into 'sub-stomatal' and other 'Outer' cells and the assessed differences in 3D size and shape (Figure 4.10c-f).

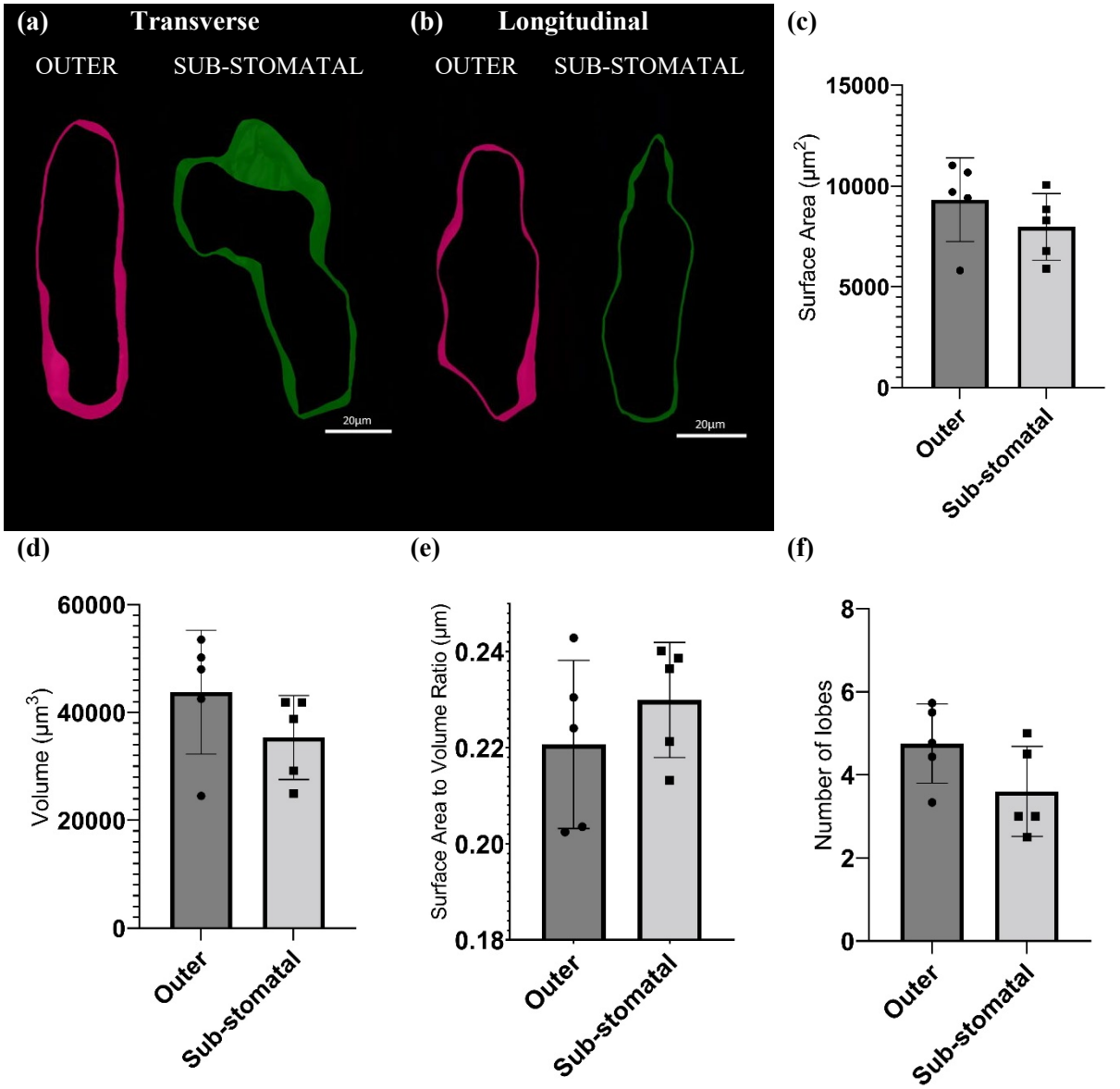

Figure 4.10. Mesophyll cells around sub-stomatal cavities have distinct morphologies compared with other Outer layer cells. (a) Clipped image from a 3D mesh showing the transverse plane of an Outer layer (left) and sub-stomatal (right) mesophyll cell. (b) Clipped image from a 3D mesh showing the longitudinal plane of an Outer layer (left) and sub-stomatal (right) mesophyll cell. (c) 3D surface area of mesophyll cells the outer layer and those surrounding sub-stomatal cavities. (d) Volume of mesophyll cells the outer layer and those surrounding sub-stomatal cavities. (e) 3D surface area to volume ratio of mesophyll cells the outer layer and those surrounding sub-stomatal cavities. Number of lobes of mesophyll cells the outer layer and those surrounding sub-stomatal cavities. n=5, and error bars represent standard deviation from the mean. To test for statistical significance between cell types, t-tests were carried out for all graphs. All images and data are from the Durum line 'Voilur'.

Despite absence of statistical significance, there appears to be a trend of mesophyll cells surrounding the sub-stomatal cavity having a greater surface area to volume ratio and fewer lobes than other outer layer mesophyll cells, suggesting that they have a slightly different morphology that has led to increased surface area relative to volume concurrent to a decrease in lobe count.

4.4. Discussion

4.4.1. Wheat Mesophyll Cells Form in Layers that are Distinct by Size and Shape

The results presented in this chapter support the hypothesis that the wheat mesophyll is not homogenous and that cells can be assigned to distinct layers based on size and shape, as highlighted in Figures 2 and 3. Moreover these overall patterns were found to be conserved across all seven *Triticum* species studied. Taken in combination with evidence of mesophyll patterning in rice (Sloan *et al.* 2023) my data suggest that the monocot mesophyll should not be considered homogenous and that the patterns reported might be evolutionary ancient within the monocots.

Triticum cell layers can be discerned by the size of the cells, particularly when looking at transverse 2D sections. As demonstrated in Figure 4.4, cells in direct contact with the epidermis (i.e., in Upper and Lower layers) were observed to have a significantly greater transverse cell area compared with those only in direct contact with other mesophyll cells or bundle sheath tissue (i.e., in Middle and Radial layers, respectfully) across all of the diploid, tetraploid and hexaploid lines studied. The most common order of layers in terms of transverse cell area was: Upper, Lower, Radial, Middle, demonstrated by a ranked analysis (Figure 4.4f). While cells in the Middle layer of the longitudinal leaf sections were most frequently the smallest, (Figure 4.5h), only the cultivated Durum and hexaploid lines had significantly smaller Middle layer mesophyll cells compared to Outer layer cells (Figure 4.5f, g). When looking at the 3D volume of these cells, which is essentially the product of 2D transverse and longitudinal areas, there was no significant difference observed (Figure 4.6), with a trend for larger mesophyll cells being located in Outer layers compared with Middle layer cells only being present in the cultivated tetraploid Durum and hexaploid *T. aestivum* leaves. This suggests that the mesophyll cells rely equally on changing size in both the 'transverse' and 'longitudinal' directions, as both are required to bring about the difference in volume in the two cultivated wheats. Unfortunately, due to time constraints, 3D Radial cell morphology was unable to be assessed in this project.

The cell layers of *Triticum* leaves can also be separated by the shape of the cells in both 2D transverse and longitudinal sections and, to some extent, in 3D confocal stacks. We observed across all species and ploidy studied that in transverse sections (the direction where no cell lobing is visible; Figure 4.2a), cells in Upper and Lower layers were significantly less circular than those in the Middle layers, where the cells are only in direct contact with other mesophyll cells (Figure 4.7). In wild tetraploid lines *T. dicoccoides* and *T. araraticum*, and hexaploid *T. aestivum*, cells adjacent to the adaxial epidermis (Upper)

were less circular (and more elongated) than those adjacent to the abaxial epidermis (Lower). The ranked analysis gave the most common order of least to most circular as: Upper, Lower, Radial, Middle, which is interestingly the same order as the transverse cell area rankings of largest to smallest by area. When taking into account the lobing that occurs parallel to the vasculature in the wheat mesophyll, cells surrounding the bundle sheath tissue in the Radial layer had a consistently greater lobing area than those in the Outer layers (Figure 4.8). Cells in the Middle layers also had a greater lobing area than Outer layer cells in most lines across all ploidy levels. Translated to the actual 3D morphology of the cells, cells in Middle layers across all species and subspecies studied had a slightly higher number of lobes on average than those in outer layers (Figure 4.9b; although not statistically significant), which likely contributes to the increased lobing area observed in 2D sections combined with increased lobing 'intensity' (i.e., more extreme indentations created by lobing). This increased lobe count and lobing area combined with slightly reduced overall cell size in the Middle layer cells compared with Outer cells has underpinned an increase in surface area to volume ratio in these cells, although this was only significant for the wild tetraploid and hexaploid lines (Figure 4.9a).

The data in this chapter also suggests that the mesophyll cells which are directly adjacent to the sub-stomatal cavities could be considered separately from the rest of the cells in the Outer (i.e. Upper and Lower) layers, despite no statistically significant differences in morphology. As demonstrated in Figure 4.10, these cells have a hook-like shape (that can also be observed in transverse 2D sections) compared to the oblong shape of normal cells adjacent to the pavement cells. Although not statistically significant, these 'sub-stomatal cells' had decreased volume and increased surface area to volume ratio, as well as a decrease in number of lobes per cell compared with typical Outer layer cells. In typical mesophyll cells, we observed that an increased surface area to volume ratio was usually concurrent with an increased number of lobes per cell (as was the case in cells in the Middle layer compared with Outer layer cells). However, this slight decrease in lobe number alongside an increase in surface area to volume ratio supports the observation of a different cell shape that is not solely related to lobing.

To summarise, cells adjacent to the epidermis are larger in the transverse plane, more elongated and less circular than those which only have direct contact with other mesophyll cells and bundle sheath tissue, while having fewer lobes and a reduced lobing area on the longitudinal plane. This is summarised in the form of a graphical model in Figure 4.11.

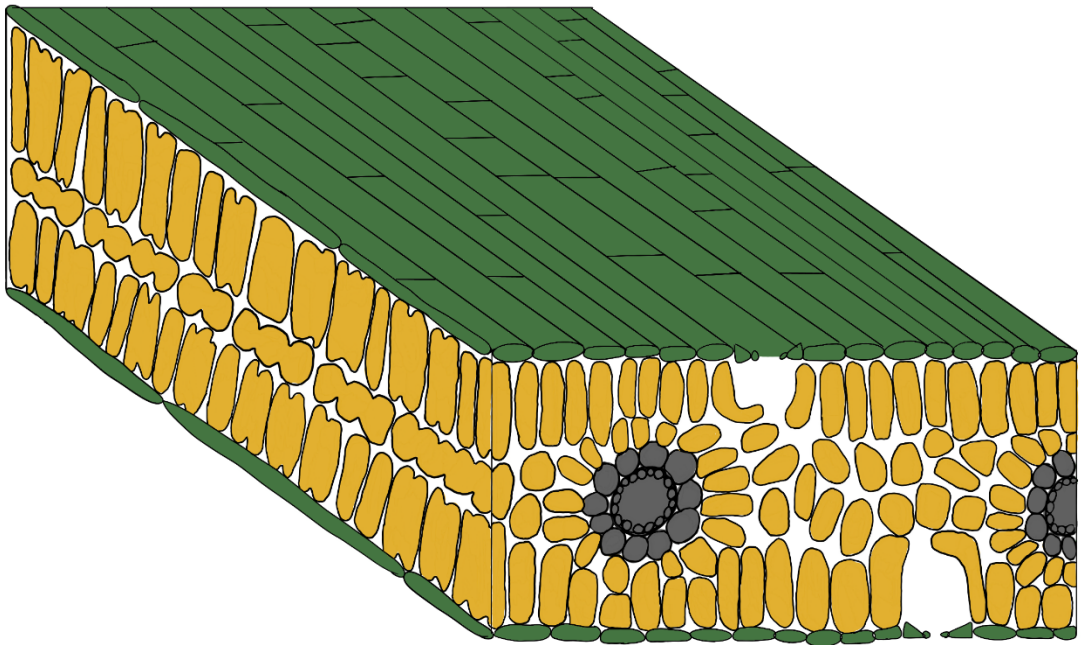

Figure 4.11. Model of a typical wheat leaf, highlighting how the location of a mesophyll cell along the abaxial-adaxial axis determines its size and shape. Mesophyll cells are yellow, vascular tissue in grey, pavement cells in dark green. Stomatal complexes have been omitted for simplicity.

When comparing the data observed in this project to that available for the rice mesophyll, both similarities and differences can be seen. One point to note is that lobing of the mesophyll cells in rice occurs perpendicular to the vasculature and not parallel as in wheat and can therefore be observed in 2D transverse leaf sections. Sloan *et al*. (2023) observed that the rice mesophyll forms in 5 distinct layers, and no such 'Radial' patterning is observed as has been observed in wheat in this project. The main conserved feature of wheat and rice mesophyll architecture is that, in both cases, cells adjacent to the epidermis have the lowest cell lobing area. In rice, this is most striking on cells adjacent to the adaxial epidermis which, in wheat, were more elongated than those adjacent to the abaxial epidermis. Unfortunately, as lobing in wheat can only be viewed in longitudinal leaf sections and 3D z-stacks, it was impossible to discern the adaxial from abaxial pavement tissue so whether the uppermost cells also have decreased lobing in wheat remains unknown. In direct contrast to wheat, Sloan *et al.* (2023) observed that cells in the Middle layers had the greatest transverse cross sectional surface area when compared to the outermost cells. The patterns of cell circularity observed in transverse leaf sections was also inverse, with outermost rice mesophyll cells being the most circular, however this was likely due to the fact that cells in rice form lobes in this direction while wheat mesophyll cells form simple shapes. In most wheat lines there was no difference in the longitudinal 'lobed' 2D area, but in the cultivated varieties this was once again in opposition to rice mesophyll patterning, with cells in the Outer layer of *Triticum* leaves having the greatest cell area.

4.4.2. Cells in Different Mesophyll Layers may have Different Roles

It is known that in eudicots and most plants with laminar leaves, the mesophyll tissue differentiates across the abaxial-adaxial axis during development, resulting in two distinct cell layers: the palisade and spongy mesophyll (Nicotra *et al*., 2011). While grass mesophyll does not form spongy and palisade mesophyll layers and has been previously considered homogenous, in this project we have demonstrated that wheat mesophyll forms in layers distinct in shape and size in such a way that is conserved across *Triticum* species, ploidy and cultivation status. Similarly to eudicot and other laminar leaves, the cells directly adjacent to the adaxial epidermis (Upper/palisade) were the most elongated. The palisade layer is optimised for high rates of photosynthesis and is typically characterised by a high surface area to volume ratio for improved CO_2 absorption, while being rich in chloroplasts and abundant in light (Parkhurst & Mott, 1990; Ho *et al.,* 2016; Théroux-Rancourt *et al*., 2017, 2021; Borsuk & Brodersen, 2019). Although when looking at wheat mesophyll cells in 3D, the cells adjacent to the epidermis (in the Outer layer) actually had slightly reduced surface area to volume ratio compared with cells in the Middle layers (Figure 4.9a), the 2D transverse sections demonstrated a cylindrical shape perpendicular to the leaf surface that is not dissimilar from eudicot palisade mesophyll cells (Figure 4.2, 4.7). This shape is known to give palisade cells the function of directing light down from the epidermis deeper into the leaf (Vogelmann & Martin, 1993), suggesting that these Upper layer cells could have taken on a palisade-like role within the wheat leaf in terms of light direction and potential increased rates of photosynthesis. However, the chlorophyll content and photosynthetic activity of cells in the wheat Upper layers was not measured in this study.

Below the palisade is the spongy mesophyll: a more irregular (Govaerts *et al*., 1996; Ivanova & P'yankov, 2002; Morison & Lawson, 2007; Terashima *et al*., 2011) and loosely packed (Nobel, 1999; Chatelet et al., 2013; Ho *et al.,* 2016) layer of cells that are roughly spherical (Smith et al., 1997; Nobel, 1999) or of an undefined shape (Govaerts *et al*., 1996; Aalto & Juurola, 2002; Chatelet *et al*., 2013). This is somewhat reminiscent of characteristics observed of cells in the Middle layer of the wheat mesophyll in this project, appearing significantly more circular in the transverse leaf sections (Figure 4.7). The spongy mesophyll layer has a variety of functions, including promoting CO_2 diffusion between the stomata and palisade and light scattering/absorption (Smith *et al.*, 1997; Terashima *et al*., 2011). Borsuk *et al.* (2022) observed that the spongy mesophyll forms in a honeycomb-like topology, where the cells join to form a lattice surrounding interconnected voids of IAS. Visualising the IAS structure of the layers of wheat leaves was not something that was within the scope of this project, but it would be interesting to see if this honeycomb-like pattern is also present within this spongy-like Middle layer of mesophyll cells.

When comparing patterning of the wheat mesophyll to what we know of cell specialisation of cells in spongy and palisade mesophyll layers, a major complication is the presence of cell lobes in grasses compared with the more simplistic morphology of eudicot mesophyll cells. In transverse leaf sections,

the Upper and Middle cells appear to be somewhat comparable to the palisade and spongy mesophyll layers respectively. However, when taking into account mesophyll cell morphology observed in 2D longitudinal leaf sections and in 3D, the lobing of cells, combined with less clear differentiation between layers in terms of cell size, does not support the hypothesis of the wheat mesophyll having palisade- and spongy-like layers. Cells in the Middle layers of the wheat mesophyll demonstrated an increased surface area to volume ratio due to increased complexity of their shape through lobing (Figure 4.8, 4.9), suggesting they are more optimised for increased rates of CO_2 and H_2O diffusion into the cell: the direct opposite of palisade/spongy function. However, this is also reliant on factors such as g_m and the amount of mesophyll surface area that is exposed to the IAS (S_{mes}), neither of which were measured in this study.

There are a few other physiological processes that may be improved through wheat having non-homogenous mesophyll. For example, there is a humidity gradient that exists from the boundary layer through to the centre of the mesophyll, and Wong *et al.* (2022) suggest that this gradient shifts when the plant is experiencing drought and high external humidity to maintain cytosolic water potential. This shift occurs across the mesophyll airspace, and a change in mesophyll airspace patterning could affect the plant's ability to respond to changes in atmospheric water vapour content. Visualising leaf porosity could help to explore this in the future.

When treating cells directly surrounding the sub-stomatal cavities as separate from the rest of the cells in the Outer layers, it is perhaps the easiest to infer their role. The formation of sub-stomatal cavities is triggered by the presence of functional stomata, either through direct stomata-mesophyll signalling or more likely by CO_2 flux into the leaf (Lundgren *et al*., 2019). The cells that form around this cavity have slightly greater surface area to volume ratio than other cells that are in contact with the epidermis (Figure 4.10; which is not caused by changes to lobing), suggesting that they likely form this hook-like shape to increase their surface area for CO_2 absorption, with a varying effect depending on how far the cuticle extends into the cavity. This would suggest that, despite being present adjacent to both the abaxial and adaxial epidermis, they may be optimised for slightly higher rates of photosynthesis than other cells in the same layers.

As the development of the leaf structure occurs as part of a trade-off between maximising the rate of photosynthesis while reducing water loss through the stomatal pores, Figure 4.12 represents the shape and size of the mesophyll cells on the theoretical path of H_2O from the xylem, through the IAS in gaseous form and/or the mesophyll cells in liquid form (where they may be used in photosynthesis), to the sub-stomatal cavities. It is important to note that this schematic is greatly simplified representation of the transpiration pathway.

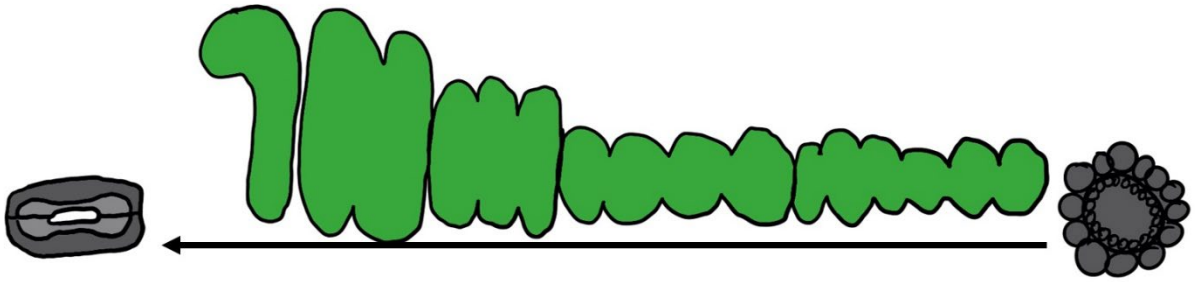

Figure 4.12. An illustration of wheat mesophyll cell morphology along the theoretical transpiration pathway. Water travels from the vasculature (right) in liquid form, through the mesophyll cells via the apoplastic pathway (where it is potentially used in photosynthesis) and the intercellular airspace to reach the sub-stomatal airspace in gaseous form, where it exits through the stomata (right). Mesophyll cell morphology becomes more elongated and less lobed across this transpiration pathway, ending with the hook-like sub-stomatal cells.

The most significant observation is the decrease in number of lobes (and lobing area) of mesophyll from the vascular tissue to the stomata. A higher number and severity of lobes increases the complexity of the cell morphology and subsequently the mesophyll cell surface area to volume ratio with no change to total cell volume. In terms of reducing water loss, this could be to ensure that most of the H_2O transported to the leaf via the xylem is moved into the cells before reaching the stomata and less is being lost from the leaf. Conversely, the increase in cell lobing may lead to increased pockets of airspace, allowing for gaseous H_2O to be diffused more rapidly away from the centre of the leaf and to mesophyll cells with higher rates of photosynthesis, such as those in Upper layers that receive the most sunlight. The difference in leaf lobing may also affect the uptake and availability of CO_2 for photosynthesis in different cell layers. As information on airspace patterning in these *Triticum* lines is unknown, these are, at present, just a few working hypotheses.

4.4.3. Mesophyll Patterning May Lead to Altered Overall Leaf Function

There was little evidence in this study for variation between wheat lines in terms of mesophyll patterning in cell size, aside from data of longitudinal cell area (Figure 4.5) and 3D cell volume (Figure 4.6). In both cases, cells in the Outer layers (i.e., adjacent to the epidermis) of both the tetraploid Durum wheat and hexaploid *T. aestivum* were larger than the Middle layer cells, although this was only statistically significant for the 2D longitudinal cell area data in Figure 4.5. Durum is a cultivated tetraploid wheat that is grown as a crop in present day and, unlike Emmer, has undergone the intensive selection and breeding brought about by the Green Revolution of the 1960s alongside hexaploid *T. aestivum*. The fact that both of these lines have layers that are more distinct by 2D longitudinal and 3D cell size suggests that this may have been as a result of indirect selection for improved leaf function, such as increased water-use efficiency or photosynthetic rate. Both tetraploid Durum and hexaploid wheat are known to have overall larger mesophyll cells by volume than Emmer, wild tetraploid and diploid wheat (Chapter 4.2; Wilson *et al.* 2021), and perhaps this distinction between layers by volume

is possible due to an increase in the 'upper cell size' limit defined during development. These differences correlate with improved intrinsic water-use efficiency (iWUE), however these changes are also accompanied by decreased stomatal density so the mesophyll patterning may in fact have no direct affect.

Alternatively, as Lundgren *et al.* (2019) suggest that mesophyll development is linked to the presence of functional stomata, reduced stomatal density, and subsequently stomatal conductance (g_s), in these lines has perhaps led to the differences observed in mesophyll cell size patterning. In rice, reducing stomatal conductance by overexpressing *OsEPF1* led to the overall reduction in transverse cell area, while increasing circularity and lobing (Sloan *et al*., 2023). This change in rice mesophyll cell area did not occur uniformly across the whole leaf, being significant in some layers of some lines and not others, but the changes in cell shape were universal. It would be interesting to see the effect of overexpressing *AtEPF1* in wheat to see how the shape and size of mesophyll cells in different layers changes, and if it reflects any of the differences seen in the transition from diploid and wild tetraploid/Emmer to Durum and hexaploid varieties in this project.

As stomatal and mesophyll development is linked, it is hard to separate the impact of g_s and g_m on iWUE and photosynthetic gas exchange, and g_s is often most attributed to impacting iWUE. This study is unable to provide further insight into the effects of the mesophyll on iWUE directly as any differences between lines known to differ in iWUE in terms of mesophyll patterning occur simultaneously with changes in g_s (Chapter 3, Figure 3.3). Aside from the basic volume size and shape cells in each mesophyll layer, it is important to consider how the mesophyll cells interact with the airspace. Key areas to next investigate would be mesophyll conductance, g_m, the mesophyll surface area that is exposed to the IAS, s_{mes}, and mesophyll porosity. It is known that there is no difference in total S_{mes} across these *Triticum* lines and that total mesophyll porosity decreases from diploid to hexaploid (Wilson *et al.,* 2021), however this data is averaged across the whole leaf and is not separated into the layers which are now known to exist. It has been shown that altering the structure of the lattice formed by the spongy mesophyll and surrounding airspace of laminar leaves altered s_{mes} and photosynthetic carbon fixation (*A*) (Borsjuk *et al.,* 2022). Changes in total values, patterning or distribution caused by the presence of these distinct layers could therefore have an impact on iWUE. Non-homogenous mesophyll airspace patterning across the adaxial-abaxial axis may also have an effect on the gaseous movement of CO_2 and lead to a differential intercellular concentration of CO_2 (c_i) across the leaf, potentially availability of CO_2 for photosynthesis in different cell layers.

4.5. Conclusion

In contrast to the widely held view that the wheat mesophyll structure is homogenous, there is a clear patterning of cells across the adaxial-abaxial plane of the leaf in all ploidy levels analysed. Cells in the

outer layers (Upper and Lower; i.e. adjacent to the epidermis) are more elongated and less lobed, resulting in a reduced surface area to volume ratio when compared with cells in the Middle and Radial layers (i.e. cells only in contact with mesophyll and/or vascular cells). This consistency in pattern suggests an evolutionary advantage, with one possibility being that layering of the wheat mesophyll might mimic the spongy and palisade mesophyll layers of eudicot leaves, with the Outer cells directing light into the leaf for photosynthesis and the Middle layer mesophyll cells being more optimised for gas exchange and water transport. Mesophyll cells that line the sub-stomatal cavities also have a shape that is distinct from other Outer layer mesophyll cells, forming a curved structure to form the distinct air pockets, potentially increasing surface area to volume ratio for the efficient exchange of gases.

Chapter 5. Altering Wheat Leaf Structure to Improve Water Use Efficiency

5.1. Introduction

5.1.1. Water-Use efficiency

Water-use efficiency (WUE) of staple crops is an area of increasing concern, with major cereal crops such as wheat and rice accounting for 27% of global water consumption (Hoekstra & Mekonnen, 2012). The net efflux of water vapour from the leaf into the surrounding atmosphere, transpiration rate, can be influenced by the boundary layer conductance as well as stomatal and mesophyll conductances. Gas exchange through stomatal pores makes them also vital for photosynthetic activity. It is important that plants are able to optimise both the rate of gas uptake by the leaves for photosynthetic carbon fixation, while reducing the amount of water lost by transpiration, in order to maximise productivity. Intrinsic water-use efficiency (iWUE) is typically used to experimentally quantify WUE and is described as the ratio of net photosynthetic rate (A_n) to stomatal conductance for water vapor (g_{sw}). Recent research in wheat identified an unexpected strong correlation between the size and arrangement of mesophyll cells and WUE, raising the question of whether this reflects a casual relationship and, if so, whether it might represent a novel trait for breeding improved crop WUE (Wilson *et al.,* 2021).

5.1.2. Wheat Leaf Structure and Development

Wheat leaves initiate as small groups of cells on the flanks of the shoot apical meristem. At this stage, the meristem-derived cells are approximately uniform in size and shape, but as the leaf develops cells take on specific shapes and sizes which define the leaf anatomy. With respect to mesophyll cell differentiation, a similar basic arrangement is observed in wheat which is typical of grass leaves. Unlike in eudicot species such as *Arabidopsis thaliana,* the mesophyll does not form distinct palisade and spongy mesophyll layers across the adaxial/abaxial axis. Instead, mesophyll cells are patterned across the proximal-distal leaf axis, interspaced by major and minor veins (Jellings & Leech, 1984; Parker & Ford, 1982).

With respect to shape, wheat mesophyll cells develop distinct lobes (a characteristic of many other plants) which is thought to help define the mesophyll cell surface area/volume ratio, an important parameter for gas exchange linked to photosynthetic CO_2 diffusion. A potential mechanism behind the development of cell lobes is highlighted in Chapter 1 but can be briefly described as follows: microtubules (MTs) form in interconnected, ring-shaped bundles, while the cell wall is locally thickened using cellulose microfibrils. This results in bulging of the cells where the walls have been thickened and constrictions from the MT rings, forming lobes. It is known that the phase of cell expansion growth crucial in defining the final shape of the cell (Jung & Wernicke 1990), however, our understanding of the molecular machinery involved in directing changes in cell lobing is very limited and remains elusive in wheat.

With respect to cell size, one major characteristic that has been observed in wheat leaves between ploidy levels is a significant increase in mesophyll cell sized from diploid to hexaploid (Jellings & Leech, 1984; Parker & Ford, 1982; Wilson *et al*., 2021). Increasing size with ploidy is a common observation in plants (Kondorosi *et al.,* 2000; Katagiri *et al.,* 2016). Advances in our understanding of the relevant cell cycle machinery underpinning cell expansion have generally been made in model eudicots (such as Arabidopsis) but given the highly conserved nature of the eukaryotic cell cycle, they open the door to application in wheat to manipulate cell size.

This increase in wheat mesophyll cell volume with ploidy has been accompanied by a linear increase in cell surface area, indicating a change in shape of mesophyll cells as they increase in size, likely to maintain a high surface area to volume ratio to maximise the cell surface available for gas exchange (Wilson *et al.,* 2021). Interestingly, in the same study, a decrease in overall mesophyll porosity (i.e. reduced airspace) in higher ploidy wheat was observed which correlated with increased iWUE, suggesting that it may have been indirectly selected for during wheat evolution.

The increased mesophyll cell size observed on the transition from diploid to hexaploid wheat and the accompanying improvement in iWUE raises the question of whether there is a casual relationship. Extending these observations using genetic manipulation to increase mesophyll cell size could provide valuable insight into this hypothesis.

5.1.3. Genetic manipulation of wheat

Domestication of modern wheat varieties occurred through the selection of desirable traits, including increased yield (Peng *et al*., 2011; Preece *et al.,* 2017), which have been further advanced since the Green Revolution of the 1950s-60s. In the past, the introduction of these traits occurred through selective breeding which has led to many further improvements in wheat yield (Fleury *et al*., 2010; Ihsan *et al*., 2016; Richards *et al*., 2002). However, the urgency for genetic improvement to be implemented in wheat indicates that conventional breeding methods are too time-consuming to tackle the expected yield gap (CGIAR Research Program Wheat Annual Report, 2013). Consequently, modern genetic methods, including CRISPR-Cas9 editing, are used more frequently in wheat research with the aim of implementation in the field. This has been a challenge and wheat has historically lagged behind other key agricultural crops in terms of application of genomic tools (Uauy, 2017), likely due to its large polyploid genome and highly repetitive sequences with three-fold redundancy (Appels *et al*., 2018).

Genetic transformation has allowed for the introduction and altered expression of a range of genes, with the first report of successful generation of transgenic wheat using *Agrobacterium*-mediated transformation in 1997 (Cheng *et al*., 1997). Wheat genetic manipulation efforts using transgene expression has so far targeted all major agronomic traits such as yield (Bednarek *et al*., 2012; Hu *et al*., 2012; Hong *et al*., 2014; Zhang *et al*., 2014; Qu *et al.,* 2015; Yadav *et al*., 2015; He *et al*., 2015; Qin *et al*., 2016; Peña *et al*., 2017), grain quality (Altpeter *et al.,* 1996; Barro *et al*., 1997; Rooke *et al*., 1999;

Lucrecia-Alvarez *et al.,* 2001; Sherwy *et al*., 2006; Smidansky *et al*., 2007; Weichert *et al*., 2010; Li *et al*., 2012; Zhao *et al*., 2013; Bravo *et al*., 2013; Liu *et al*., 2016; Zhao *et al*., 2021) and stress tolerance (Hu *et al*., 2018; Tian *et al.,* 2018). However, attempts directed at improving wheat leaf WUE in the field have been reported, notably in the development of Rees and Drysdale varieties (Condon *et al*., 2004).

In model plants, there have been a number of investigations using transgenic approaches to alter mesophyll structure and improve WUE. Lehmeier *et al.* (2017) found that modulating the expression of cell cycle genes in *Arabidopsis* leads to altered leaf cellular architecture in terms of tissue density and pattern airspace distribution. Also in *Arabidopsis,* exploiting the *HARDY (HRD)* gene which positively regulates the production of mesophyll cells (Karaba *et al.,* 2007) was investigated. A gain-of-function mutation increased the number of mesophyll cell layers in *Arabidopsis,* which contributed towards increased drought and salt tolerance. Overexpression of *HRD* in rice increased water-use efficiency (WUE) as a result of decreased transpiration and increased biomass production and carbon assimilation (Karaba *et al.,* 2007). These results suggest that there is a pool of genes outside of wheat that can be potentially exploited to alter leaf structure for improved WUE. One such family are the GROWTH REGULATION FACTORs: highly conserved transcription factors (Omidbakhshfard *et al*., 2015) that act as activators of transcription. GRF proteins are known to work together in complexes with GRF-INTERACTING FACTOR (GIF) cofactors (Debernardi *et al*., 2012; 2014) to regulate cell proliferation and leaf size (Wang *et al* 2020; Wu *et al.,* 2021; Horiguchi *et al*., 2005; Kim & Lee, 2006).

5.1.4. GRF Family and GIF Cofactors

The *GROWTH REGULATION FACTOR* (*GRF*) family are highly conserved transcription factors (Omidbakhshfard *et al*., 2015) which regulate patterns of plant growth and development though encoding proteins with conserved WRC and QLQ domains which mediate protein-DNA and protein-protein interactions respectively (Kim *et al.,* 2003; Kim & Kende, 2004; Horiguchi *et al., 2005*). GRF proteins form complexes with GIF cofactors (Kim & Kende, 2004) that interact *in vivo* with chromatin remodelling complexes to regulate leaf and shoot development and architecture (Zhang *et al.,* 2018; Debernardi *et al.,* 2014; Vercruyssen *et al.,* 2014).

GRF genes are positive regulators of cell proliferation in leaf primordia, and are known to regulate leaf growth and development in a range of plant species (Wang *et al.,* 2020; Wu *et al.,* 2021; Lee *et al.,* 2022; Zhang *et al*., 2021a; Shimano *et al*., 2018), with loss-of-function *Arabidopsis* mutants having smaller, narrower leaves, cotyledons and petals (Kim *et al*., 2003; Kim & Kende, 2004; Shimano *et al*., 2018), whereas overexpressors have larger leaves and cotyledons (Kim *et al*., 2003; Horiguchi *et al*., 2005; Kim & Lee, 2006**;** Zhou *et al*., 2019; Lee *et al*., 2009). Unlike other GRF genes, GRF9 was actually

shown to negatively regulate leaf growth and restrict cell proliferation in Arabidopsis (Omidbakhshfard *et al*., 2018**)**.

GRF transcription factors work together with GRF-INTERACTING FACTOR (GIF) cofactors to positively regulate leaf development (Kim & Kende, 2004; Lee *et al.*, 2009; Debernardi *et al.*, 2014; Lee & Kim, 2014). *Arabidopsis* loss-of function GIF mutants are similar to GRF loss-of-function plants in terms of reduced organ size (Kim *et al.,* 2003; Kim & Kende, 2004; Horiguchi *et al., 2005*; Rodriguez *et al.,* 2010) including narrower leaves (Kende & Kim, 2004), and GIF overexpression promotes organ growth and increases the activity of GRFs (Kim & Kende, 2004; Horiguchi *et al., 2005*; Debernardi *et al.,* 2014; Shimano *et al.,* 2018; Zhang *et al*., 2018; He *et al*., 2017). Simultaneous overexpression of both *Arabidopsis* GRF and GIF leads to further increased leaf size compared to when only one of the genes has increased expression (Debernardi *et al*., 2014). GRF-GIF complexes have also been demonstrated to regulate their own transcription through a positive feedback loop in Arabidopsis, maize and rice (Kim & Tsukaya, 2015; Zhang *et al*., 2018)**.**

Interestingly, based on the evidence of the interaction between GRF and GIFs, Debernardi *et al.* (2020) assessed the effect of GRF-GIF chimeric proteins and found that it also substantially increases regeneration efficiency of both monocots and dicots, increasing the number of transformable cultivars and resulting in more fertile transgenic plants, making it an important tool in the field of CRISPR-Cas9 gene editing, particularly extending genome editing to crops which have naturally low regeneration efficiencies.

GRF genes have been demonstrated to be involved in many other plant processes, including drought tolerance (Liu *et al*., 2017; Hu *et al*., 2023b), leaf longevity (Debernardi *et al*., 2014) and nitrogen use (Zhang *et al*., 2021; Wu *et al.,* 2020). A summary of known biological functions of the GRF-GIF complexes is illustrated in Figure 5.1.

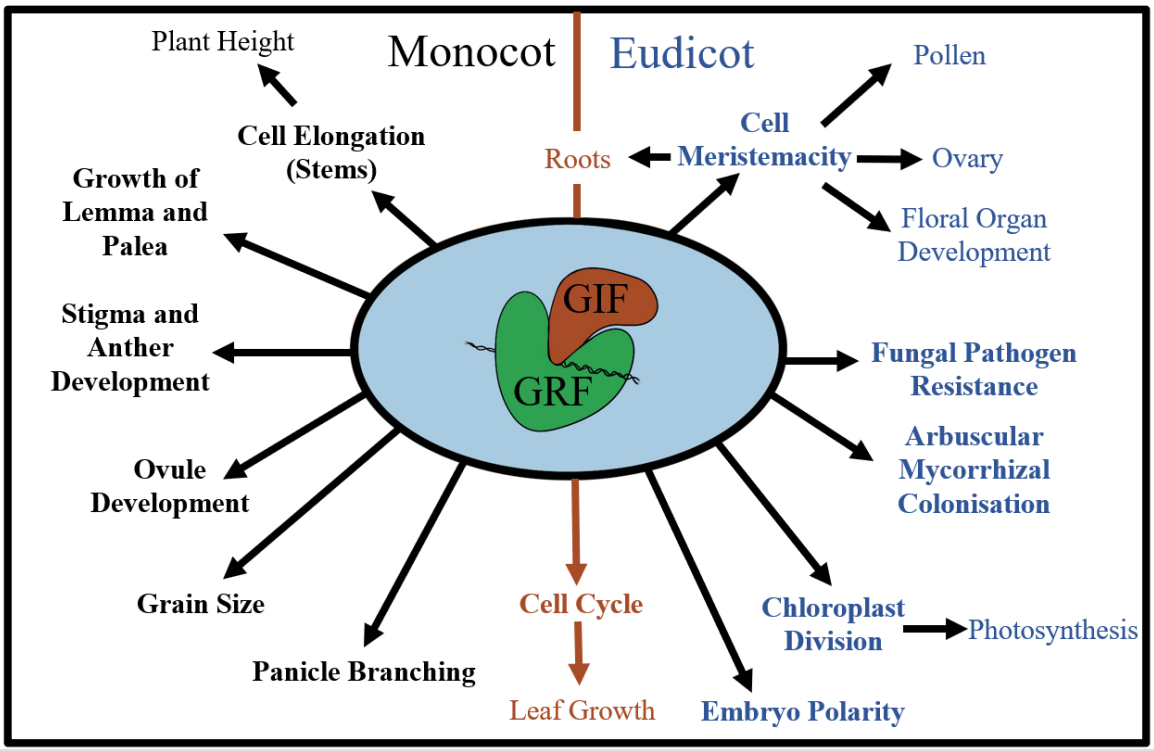

Figure 5.1. A summary of the main known functions of GRF-GIF complexes in plants. Shows only biological functions that have been confirmed in monocots (black), eudicots (blue) or both (orange). Adapted from Kim (2019).

5.1.5. Aims

The aim of the experiments described in this chapter was to test the hypothesis that cell size and shape in wheat leaves influences WUE. The first hypothesis to test was that overexpressing a *GRF4-GIF1* construct in wheat leaves lead to increased leaf and mesophyll cell size. The second hypothesis was that the *GRF4-GIF1*-overexpressing leaf phenotype results in increased iWUE.

We first identified the GRF family of transcription factors as candidates for genetic engineering through bioinformatic and literature-based approach with the purpose of identifying genes whose misexpression might lead to increased mesophyll cell size. GRFs emerged as a prime candidate from this approach. Subsequently, wheat mutants were generated in which these target genes were misexpressed, then investigated the outcome on leaf structure and WUE.

5.2. Plant Materials

Kronos (tetraploid) and Fielder (hexaploid) wheat lines overexpressing *GRF4-GIF1* were provided by the John Innes Centre (Norwich, UK), which has been used in CRISPR-Cas9 transformation of other gene targets due to their increased regeneration efficiency (Debernardi *et al.* 2020). Of the potential *GRF* and *GIF* genes in the wheat genome, Debernardi *et al.* (2020) chose *GRF4* based on its homology to rice *OsGRF4* which has been shown to promote grain and plant growth when exogenously expressed in wheat (Hu *et al.*, 2015; Duan *et al.,* 2015; Che *et al.,* 2015; Sun *et al.*, 2016). *GIF1* was selected as a

cofactor for the chimera due to it being the closest homologue of *Arabidopsis* and rice *GIF1* which have been shown to control growth in *Arabidopsis*, rice and maize (Kim & Kende, 2004; Horiguchi *et al*., 2005; Shimano *et al*., 2018; Zhang *et al*., 2018). *GRF4* and *GIF1* were combined into a *GRF4-GIF1* chimera which includes a short intergenic spacer and is under the control of a maize UBIQUITIN promoter (Ubi::GRF4-GIF1; Figure 5.2). Information on the methods of generation of the ubiquitously *GRF4-GIF1*-overexpressing lines used in this study can be found in Debernardi *et al.* (2020). Lines were checked using herbicide resistance selection at the John Innes Centre, and successfully transformed lines of different copy numbers (i.e. numbers of insertions) were genotyped by PCR prior to the experiments carried out in this study. After an initial growth period, seeds were collected from the healthiest parent plant of the Kronos GRF4-GIF1 and Fielder GRF4-GIF1 plants (selected by eye based on parameters such as plant height, lack of disease yellowing), as no significant phenotypic differences were observed between lines of different copy numbers (Kronos used = x4, Fielder used = x7). The seeds from these individual lines were used for the remainder of the study. The Kronos and Fielder lines used as controls in the study were acquired from the John Innes Centre and were the untransformed lines used for the original transformations.

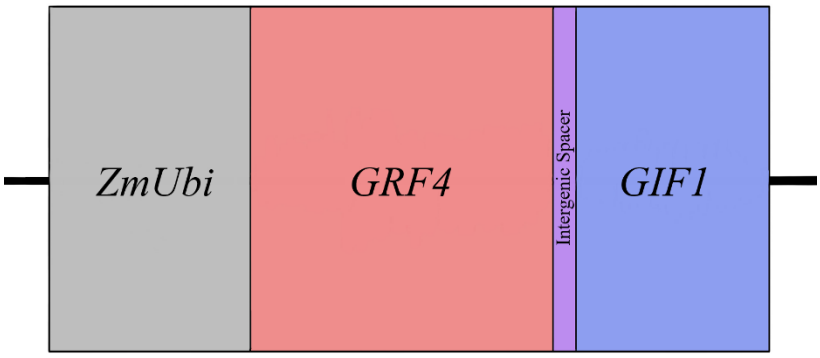

Figure 5.2. The GRF4-GIF1 chimeric construct. A diagram of the construct used in the generation of the overexpressing Kronos and Fielder lines, containing a maize ubiquitin promoter upstream of wheat *GRF4* and *GIF1* genes, separated by a four-amino-acid spacer (adapted from Debernardi *et al.,* 2019)

Seeds of each Kronos, Kronos GRF4-GIF1, Fielder and Fielder GRF4-GIF1 lines were sown and grown according to the Section 2.1 of Methodology Chapter (Chapter 2), with 5-6 biological replicates per line/control.

5.3. Results

5.3.1. Bioinformatics Screen to Identify Lead Genes for Manipulating Cell Size in Wheat

To identify lead genes in wheat that might be the focus for manipulation to increase mesophyll cell size, I performed a combined bioinformatic/literature search. Potential gene candidates for altered mesophyll

cell size were identified computationally, facilitated by the KnetMiner gene discovery platform (https://knetminer.com/). Gene trees of these candidate genes were assessed using Ensembl Plants (http://plants_ensembl.org) for identities of and relationships between *Arabidopsis thaliana*, *Triticum aestivum* (wheat), and *Oryza sativa* (rice) orthologs. This was done to decrease the need for the generation of potential knockout/down mutants in large gene families with high potential of functional redundancy. Expression data from RNA-Seq and eFP databases of candidate genes was assessed using two different online resources (http://wheat-expression.com; https://bar.utoronto.ca/eft_wheat/cgi-bin/efpWeb.cgi). For knockout mutants of these genes to influence the leaf mesophyll cells, it is important to ensure they are expressed in the leaves during development. In addition to this, research on the rice orthologs of these candidate genes was explored (https://funricegenes.github.io/) to better predict the function of generating mutants in wheat. The shortlist generated by this search has been summarised in Table 5.1.

Table 5.1. Identified *T. aestivum* genes related to cell expansion and division that are expressed in the developing mesophyll. These genes were first identified from publications found during a literature search ('Reference'), and gene trees generated to show the relatedness of Arabidopsis and Wheat Genes, as well as the number of copies within the wheat genome. The expression of these genes in wheat ('Wheat Expression') was also investigated, and those with expression in the developing leaves were selected.

Name	Arabidopsis Gene	Wheat Genes	Wheat Expression	Reference
GRF1	AT4G09000	TraesCS7B02G183800; TraesCS7A02G295500; TraesCS7D02G292400	Everywhere except grain, high absolute levels	Omidbakhshfard *et al.* (2015)
OLI2	AT5G55920	TraesCS6A02G286600; TraesCS6D02G267300; TraesCS6B02G315600	Root/shoot meristem and leaves in first leaf stage	Kojima *et al.* (2018)
GDP1/GLDP1	AT4G33010	TraesCS3A02G250200; TraesCS3D02G250600; TraesCS3B02G279700	Leaves of all stages, high absolute levels	Kojima *et al.* (2018)
GPS/NAL1	AT2G35155	TraesCS2D02G417900; TraesCS2B02G440000; TraesCS2A02G420900;	Shoot and meristem and leaves in first leaf stage	Takai et al. (2013)
RBR1	AT3G12280	TraesCS7D02G265600; TraesCS7B02G162700; TraesCS7A02G264800;	High in meristem shoot and root and slightly in developing leaf	Gutierrez *et al.* (1998)

One of the top lead genes was from the *GROWTH REGULATION FACTOR (GRF)* family of transcription factors. GRF proteins form complexes with GIF cofactors that interact *in vivo* with chromatin remodelling complexes (Debernardi *et al*., 2014; Vercruyssen *et al*., 2014) to modulate target gene expression (Kim & Kende, 2004). GRFs have been frequently associated with altered cell size and, interestingly, have also been linked to improving the efficiency of regeneration of transgenic wheat. Coincidently, lines of transgenic hexaploid wheat overexpressing a *GRF4-GIF1* transcription module were already available via collaborators at the John Innes Centre, Norwich. Although these plants had been widely used as a platform for transgenic wheat regeneration, their cellular phenotype, including leaf development, had not been reported. GRF1 was identified during the bioinformatic screen as it is expressed highly across most organs, but particularly during leaf development (Omidbakhshfard *et al*., 2015), and GRF1 knockouts have been demonstrated show development of smaller leaf cells (Kim *et*

al., 2003; Kim & Kende, 2004; Shimano *et al*., 2018). Bearing in mind the occurrence of GRF1 (and GRF2) in our list of top genes, I focussed my initial investigation on the *GRF4-GIF1* overexpressing plants.

5.3.2. Plants Overexpressing GRF4-GIF1 Show a Growth Phenotype

Both hexaploid and tetraploid plants overexpressing *GRF4-GIF1* showed a clear phenotype, both at whole plant level (Figure 5.3; Figure 5.4a, b) and when leaf traits were measured (Figures 5.4c, d). For example, the hexaploid Fielder GRF4-GIF1 plants were significantly taller (t-test: P=0.0105*, t=3.138, df=10) and had fewer leaves (t-test: P=0.0001***, t=6.272, df=10) than the control plants at the end of the growth period of 40 days (Figure 5.4b).

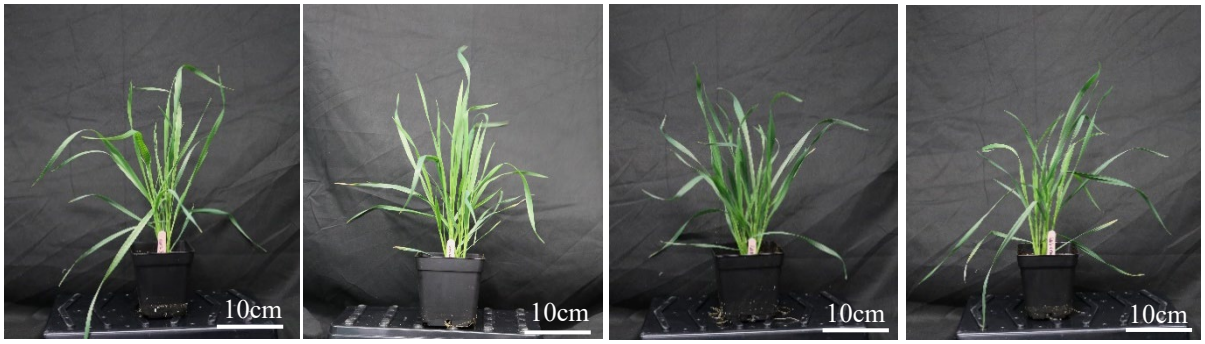

Figure 5.3. Images of Kronos, Kronos GRF4-GIF1, Fielder and Fielder GRF4-GIF1 plants. Images were taken at 4 weeks (28 days) after planting.

Both the tetraploid Kronos GRF4-GIF1 (t-test: p=0.0028**, t=4.082, df=9) and hexaploid Fielder GRF4-GIF1 (t-test: p=0.459*, t=2.279, df=10) lines had decreased leaf width compared to the untransformed controls (Figure 5.4c), but no difference was observed in the length of the 5th leaf at 4 weeks (Figure 5.4d).

In addition to plant biomass growth, ears and seeds were counted and harvested to give an estimation of variation in yield and grain weight in the GRF4-GIF1 lines (Figure 5.4e-h). The yield data showed no significant difference in the mean number of ears per plant at time of harvesting despite a trend for Fielder GRF4-GIF having a greater number of ears (Figure 5.4e), and a reduction in the number of seeds per ear (Figure 5.4f; t-test: p<0.0001****, t=8.114, df=8) resulting in a reduced total seed yield per plant (Figure 5.4g; t-test: 0.0243*, t=2.770, df=8). Although the grains of the Fielder GRF4-GIF1 lines appeared to have slightly greater weight, this was not statistically significant (Figure 5.4h).

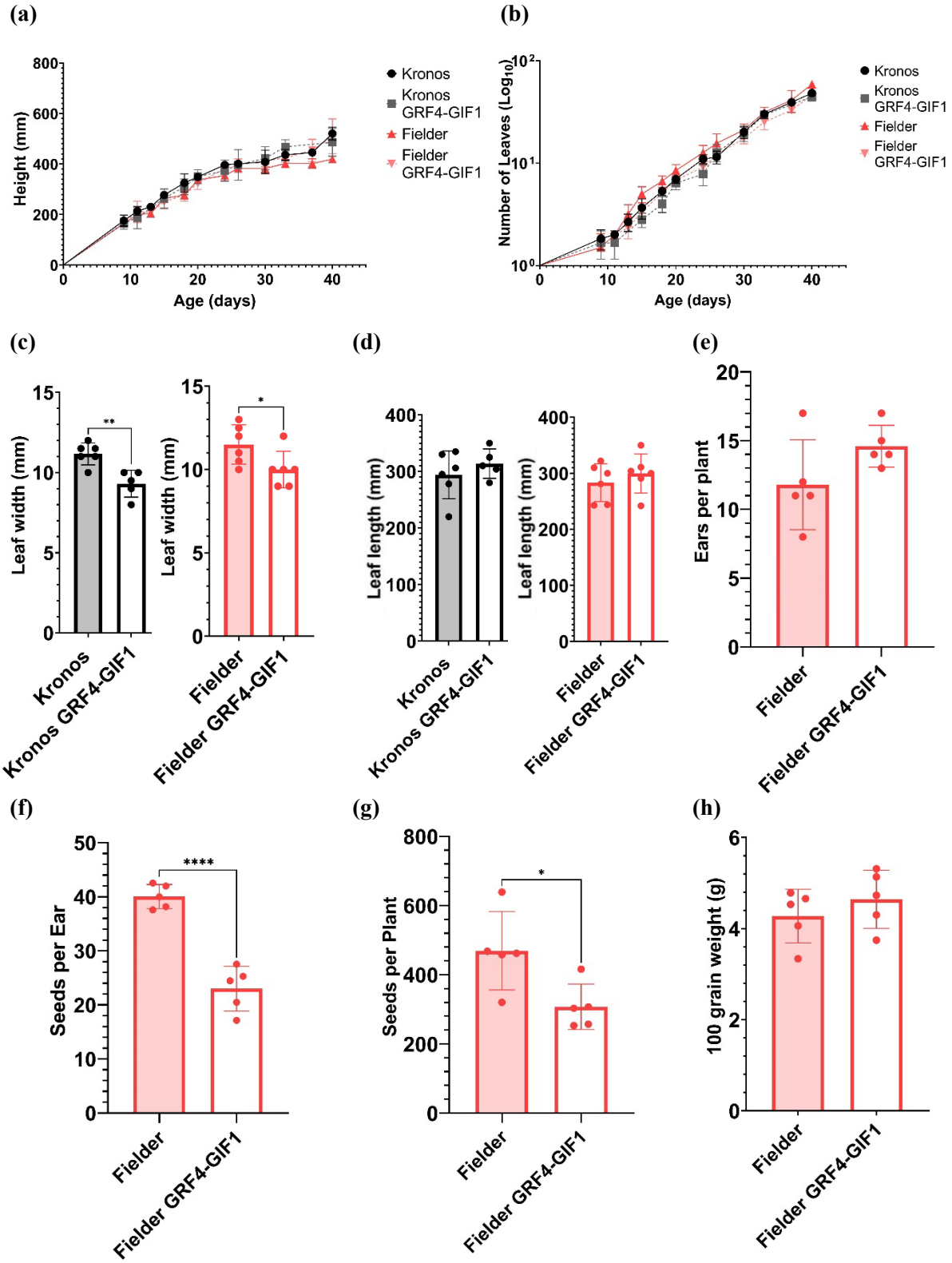

Figure 5.4. *GRF4-GIF1* overexpressing plants have distinct phenotypes relating to growth and seed yield. (a) plant height and (b) number of leaves from 9 to 40 days after planting for tetraploid (Kronos) and hexaploid (Fielder) lines overexpressing a *GRF4-GIF1* construct. (c) Leaf width of the 5th leaf on the main tiller at 4 weeks (28 days) after planting. (d) Leaf length of the 5th leaf on the main tiller at 4 weeks (28 days) after planting (e) Number of ears per plant at time of harvesting (f) Number of seeds per ear of each line (c) Total number of seeds per plant of each line (d) 100 grain weight. Black/grey = tetraploid, red/peach = hexaploid with grey/peach symbols indicting *GRF4-GIF1* overexpression. Error bars represent one standard deviation from the mean. For

(a)-(d), n=6 for each line. For (e)-(h), n=5 for each line. T-tests were carried out to test for significant differences between GRF4-GIF1 lines and relevant controls: $p<0.05$*, $p<0.005$**, $p<0.0001$****.

5.3.3. Altered Stomatal and Pavement Cell Features After Overexpressing GRF4-GIF1

Stomatal size and density of the *GRF4-GIF1* overexpressing lines and their controls was measured (Figure 5.5). When looking at stomatal density, both the Kronos GRF4-GIF1 (t-test: p=0.0319*, t=2.537, df=9) and Fielder GRF4-GIF1 (t-test: 0.0045**, t=3.649, df=10) had significantly fewer stomata per area (Figure 5.5a). This was coupled with increased stomatal length (t-test: p=0.0009***, t=4.692, df=10) (Figure 5.5b) and width (p=0.0256*,t=2.619, df=10) (Figure 5.5c) in the Fielder mutants only, resulting in greater stomatal complex area in the Fielder GRF4-GIF1 leaves (t-test: p=0.0018**, t=4.205, df=10) (Figure 5.5d).

Pavement cell characteristics of the *GRF4-GIF1* overexpressing mutants were also analysed (Figure 5.6). The lengths of the pavement cells were measured, as were the widths of cells not in the stomatal cell files and the widths of the cells in the stomatal cell files. There was a significant increase in the pavement cell length in the Fielder GRF4-GIF1 line (t-test: p=0.0236*, t=2.667, df=10) (Figure 5.6a), which , combined with the increased cell width in both stomatal (Figure 5.6c) and non-stomatal cell files (t-test: p<0.0001****, t=7.097, df=10) (Figure 5.6b), resulted in significantly greater pavement cell area in Fielder GRF4-GIF1 leaves (t-test: p=0.0005***, t=5.110, df=10) (Figure 5.6d).

The trend of increased stomatal complex width in Fielder *GRF4-GIF1* mutants seen in Figure 5.5d can likely be explained by the statistically significant increase in the width of pavement cells in the stomatal files in this line (t-test: 0.0008***, t=0.4729, df=10) (Figure 5.6c). Despite Kronos GRF4-GIF1 pavement cells being wider in both the stomatal files (t-test: p=0.0028**, t=4.079, df=9) (Figure 5.6c) and non-stomatal files (t-test: P=0.0005***, t=5.269, df=9) (Figure 5.6b), there was no significant difference in pavement cell length (Figure 5.6a) or area (Figure 5.6d) when compared to controls for the tetraploid Kronos transgenics.

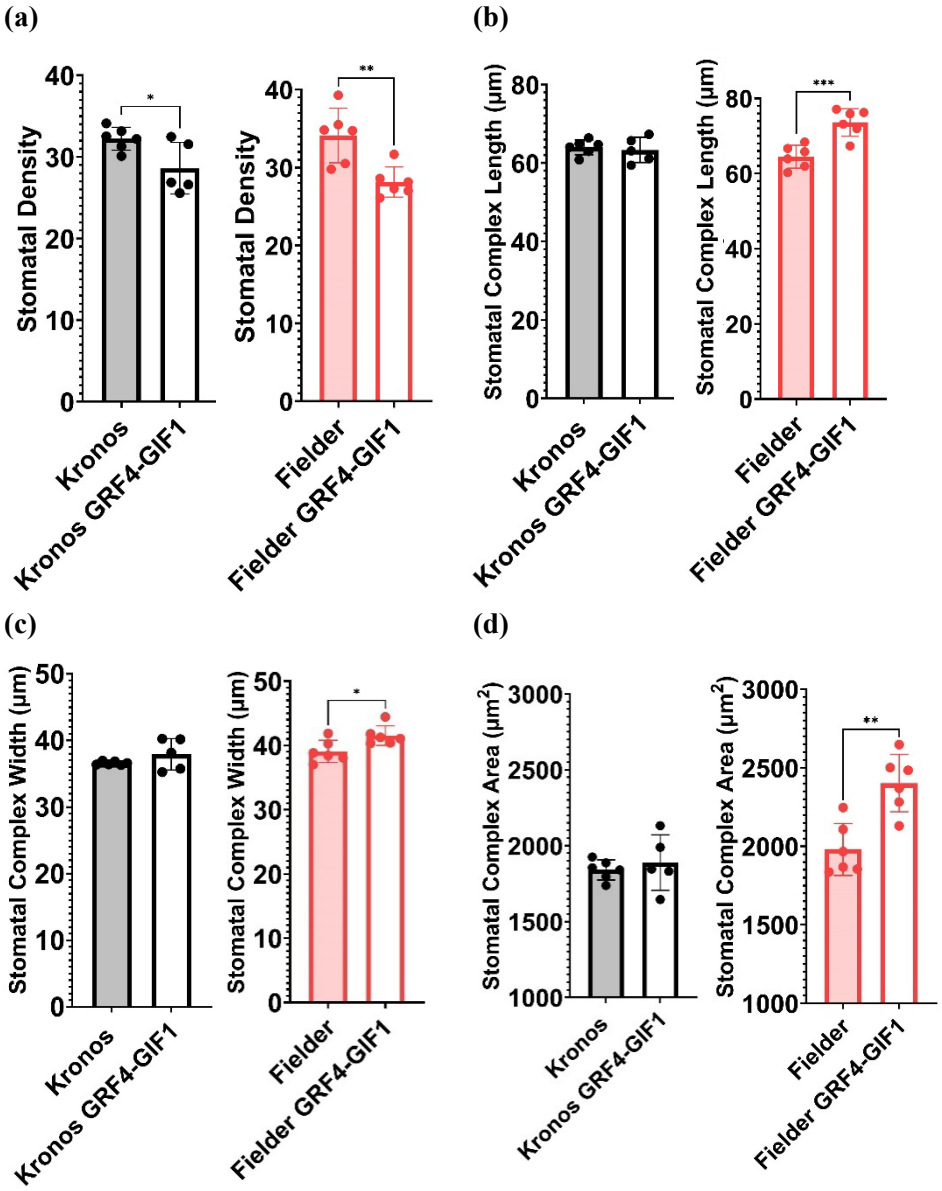

Figure 5.5. Hexaploid *GRF4-GIF1* overexpressing leaves have fewer, larger stomata. (a) Stomatal Density, expressed as number of stomata per mm^2 (b) Stomatal length (guard cell length) (c) Stomatal Width (stomatal complex width), (d) Stomatal Complex Area, calculated as: area = π x (complex length/2) x (complex width/2). Each data point represents one plant, and error bars show standard deviation from the mean. Black = tetraploid (Kronos), red = hexaploid (Fielder). All data is the mean of a combination of the abaxial and adaxial surfaces. For information on how each measurement was taken, see Figure 1a. n = 6 (for Kronos GRF4-GIF1, n = 5). T-tests were carried out to test for significant differences between GRF4-GIF1 lines and relevant controls: $p<0.05$*, $p<0.005$**, $p<0.0005$***.

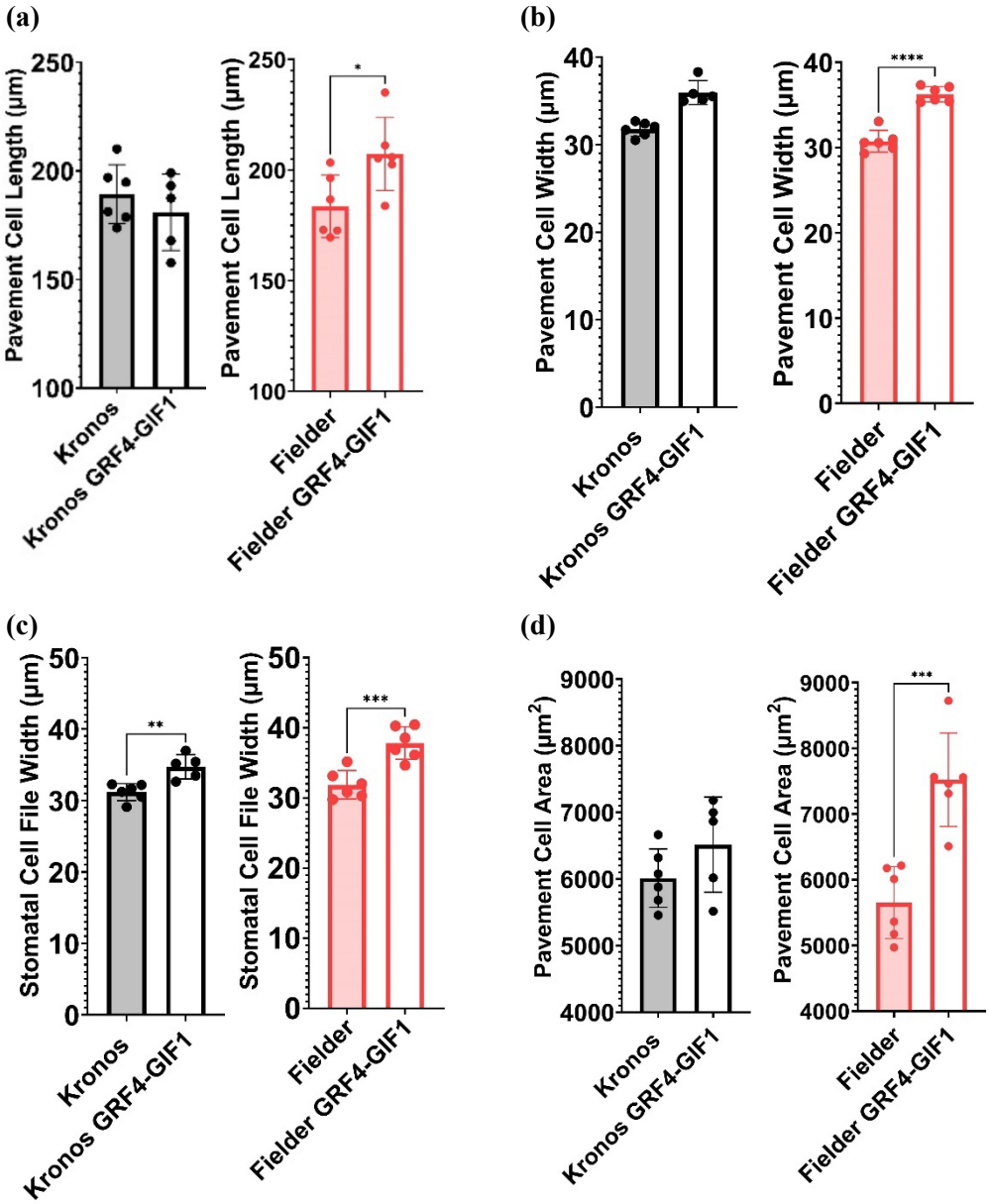

Figure 5.4. Overexpressing *GRF4-GIF1* in hexaploid wheat results in increased pavement cell size. (a) Pavement cell length. (b) Non-stomatal file pavement cell width. (c) Stomatal file pavement cell width. (d) Pavement cell area. Each data point represents one plant, and error bars show standard deviation from the mean. Black = tetraploid (Kronos), red = hexaploid (Fielder). All data is the mean of a combination of the abaxial and adaxial surfaces. . n = 6 (for Kronos GRF4-GIF1, n = 5). T-tests were carried out to test for significant differences between GRF4-GIF1 lines and relevant controls: $p<0.05$*, $p<0.005$**, $p<0.0005$***, $p<0.0001$****.

5.3.4. Mesophyll Cells in Leaves Overexpressing GRF4-GIF1

Segmentation of 3D confocal stacks of wheat leaves allowed the quantitative analysis of mesophyll cell size and shape.

Although visual inspection revealed the presence of some very large cells in the GRF4-GIF1 lines, my analysis indicated that the *GRF4-GIF1* overexpressing lines could not be distinguished from the controls based on cell volume (Figure 5.7a). This was true for both tetraploid and hexaploid lines. Similarly, analysis of mesophyll cell surface area (Figure 5.7b), surface area to volume ratio (Figure 5.7c) and the number of lobes per mesophyll cell (Figure 5.7d) did not allow the control and transgenic lines to be distinguished from each other. Mesophyll cells of Kronos *GRF4-GIF1* overexpressors tended to have a reduced number of lobes, although this was not significant (Figure 5.7d).

However, there did appear to be a greater range and different distribution of mesophyll cell volume in Fielder GRF4-GIF1 compared with the Fielder controls, with a greater number of both larger and smaller cells observed (Figure 5.8b). This was not the case in Kronos GRF4-GIF1, with the distribution of mesophyll cell sizes indistinguishable from the control cells (Figure 5.8a).

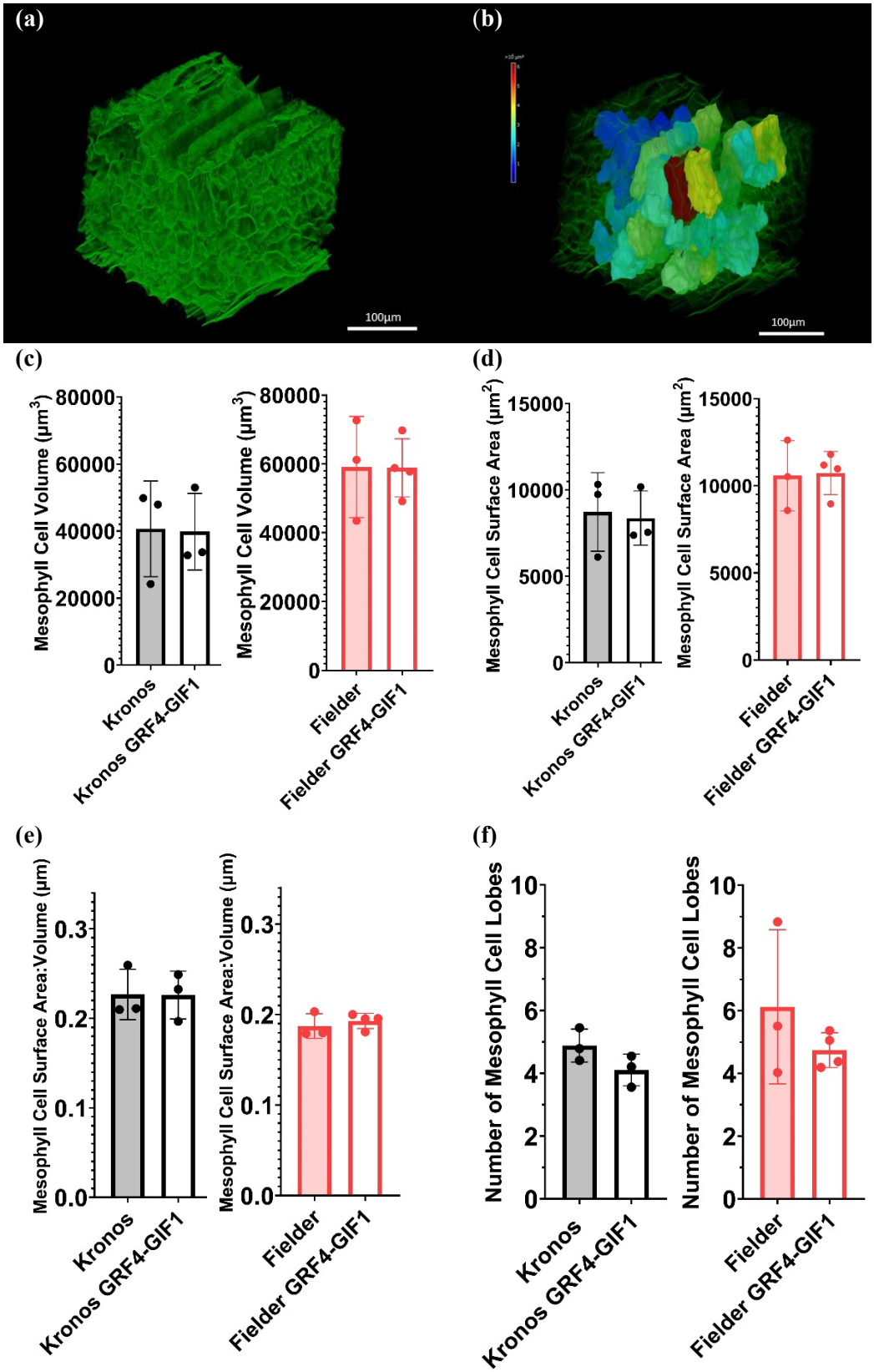

Figure 5.7. Overexpressing *GRF4-GIF1* did not result in changes to mean 3D mesophyll cell size or shape. (a) 3D confocal z-stack (b) Snapshot of mesophyll cells segmented using MorphoGraphX overlayed on a projection of the same confocal z-stack, heat map for cell volume applied. Confocal stacks is of a tetraploid Kronos leaf. (c) Mesophyll cell surface area of *GRF4-GIF1* overexpressing lines. (d) Volume of *GRF4-GIF1* overexpressing lines, (e) Surface area to volume ratio (SA/Vol) of mesophyll cells of *GRF4-GIF1* overexpressing lines. (f) Number of lobes of mesophyll cells of *GRF4-GIF1* overexpressing lines. Each data point represents one

plant, and error bars show standard deviation from the mean. Black = tetraploid (Kronos), red = hexaploid (Fielder). n=3 (for Fielder GRF4-GIF1, n=4). T-tests were carried out to test for significant differences between GRF4-GIF1 lines and relevant controls.

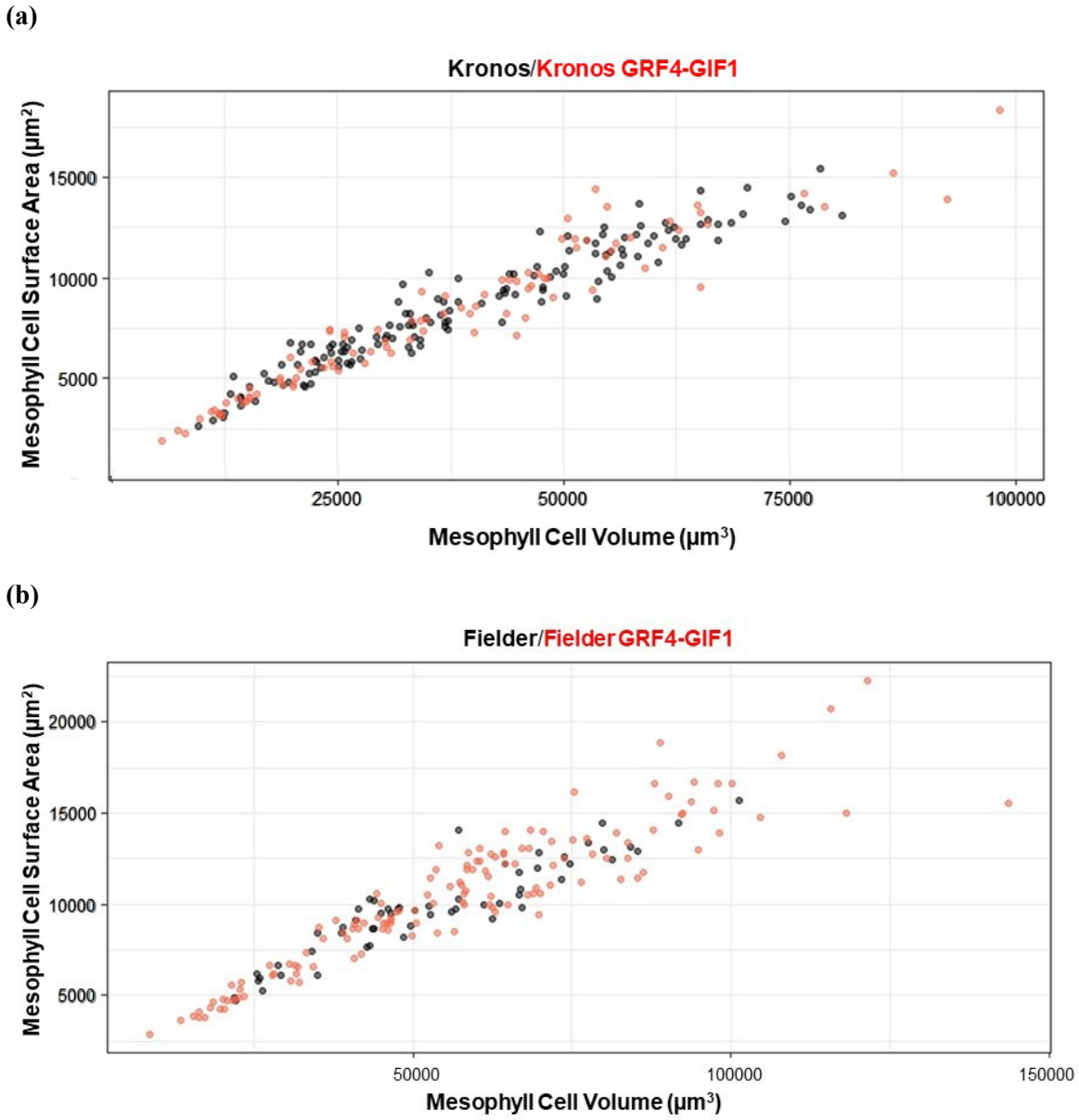

Figure 5.8. Hexaploid *GRF4-GIF1* overexpressors had an increased range of 3D mesophyll cell size. (a) Volume and Surface area of Kronos and Kronos GRF4-GIF1 mesophyll cells. (b) Volume and surface area of Fielder and Fielder GRF4-GIF1 mesophyll cells. Each datapoint represents an individual cell.

In addition to looking at cell size and morphology in 3D, I also used 2D imaging of leaf sections to quantify cell size and shape (Figure 5.9). Although there were no significant differences between *GRF4-GIF1* overexpressors and relevant controls, there was a trend of GRF4-GIF1 lines having slightly greater transverse mesophyll cell area (Figure 5.9a) and reduced longitudinal lobing area (Figure 5.9d). Lobing area is calculated as described in Section 2.3.3 of the Methodology Chapter (Chapter 2) and

quantifies the degree of 'lobing' of a cell in the longitudinal direction. For an example of cells demonstrating this lobing, see Figure 2.2 in Chapter 2.

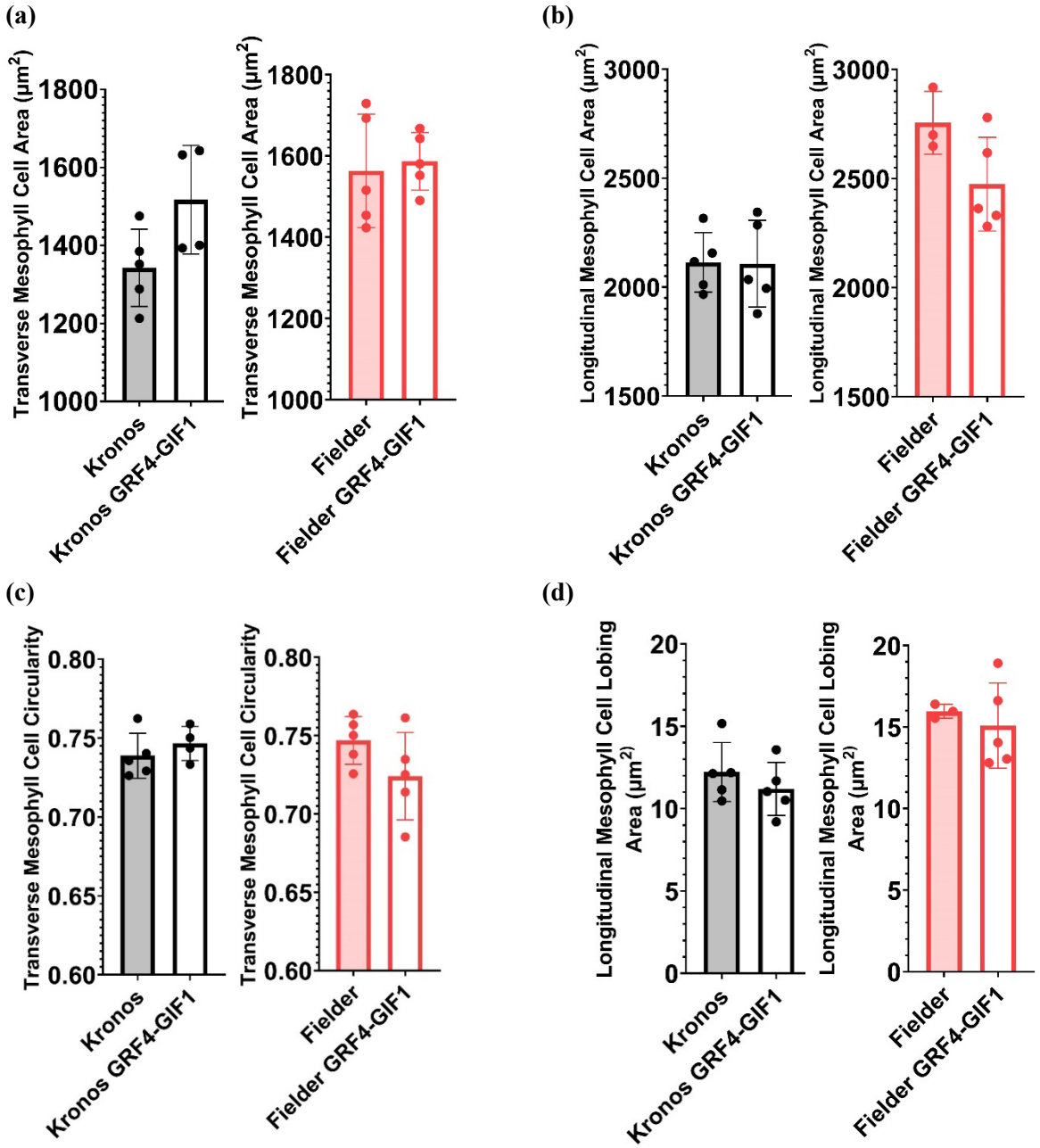

Figure 5.9. No significant changes observed in 2D mesophyll cell size and shape of *GRF4-GIF1* overexpressing lines. (a) Transverse mesophyll cell area (b) Longitudinal mesophyll cell area. (c) Transverse mesophyll cell circularity. (d) Longitudinal mesophyll cell lobing area, calculated according to section 2.3.3 of Chapter 2. Each data point represents one plant, n=5 (n=4 for Kronos GRF4-GIF1 in (a) and (c), n=3 for Fielder in (b) and (d)). T-tests were carried out to test for significant differences between GRF4-GIF1 lines and relevant controls.

5.3.5. Elements of Leaf Architecture are Altered in Hexaploid Leaves Overexpressing GRF4-GIF1

Considering more broadly the arrangement of different cell types within the leaf, several different variables were measured from 2D leaf sections. These were: Inner and Outer Bundle Sheath Cell to Mesophyll Cell Count Ratio (Figure 5.10a, b); the Number of Mesophyll Cells between Veins (Figure 5.10c); Counts of Bundle Sheath Cells surrounding a single leaf vein (Figure 5.10d, e) Proportion by total area of leaf tissue that is Inner and Outer Bundle Sheath relative to Mesophyll (Figure 5.10f, e); Mean Bundle Sheath Cell Area (Figure 5.10h, i); the Interveinal Distance (Figure 5.11a); Leaf Thickness (Figure 5.11b) and Mesophyll Thickness (Figure 5.11c).

Fielder GRF4-GIF1 leaves were observed to have a greater Inner Bundle Sheath Cell (IBSC) to Mesophyll Cell (MSC) ratio (t-test: P=0.0012**, t=4.867, df=8) (Figure 5.10a) and a greater Outer Bundle Sheath Cell to MSC ratio (t-test: p=0.0001***, t=7.039, df=8) (Figure 5.10b) in terms of cell counts, and fewer mesophyll cells between the veins (t-test: P<0.0001****, t=8.927, df=8) (Figure 5.10c). When the number of IBSCs and OBSCs were counted, there was no significant difference between *GRF4-GIF1* overexpressing lines and the relevant controls (Figure 5.10d, e). When looking at the ratio between mesophyll and bundle sheath cells in terms of total cell area per leaf section – calculated as mean cell area multiplied by cell count – differences were seen in both IBSC:MSC and OBSC:MSC (Figure 5.10f, g). The area of the leaf section occupied by IBSCs relative to MSCs was greater in Fielder GRF4-GIF1 leaves than in the controls (Figure 5.10f; t-test: p=0.0009***, t=5.13, df=8). This was also the same with regards to total OBSC area (Figure 5.10g; t-test: p=0.001***, t=5.075, df=8). This was likely due to the increased number of IBSCs and OBSCs relative to MSCs (Figures 5.10a, b), combined with increases in mean BSC area shown in Figures 5.10h and 5.10i. However, the difference in mean cell area was only significant for IBSCs (t-test: p=0.0116*, t=3.255, df=8).

The Kronos GRF4-GIF1 line also showed significantly increased BSC total area relative to MSC total area (Figures 5.10f, g), but this was only significant for OBSC:MSC ratio (t-test: p=0.0240*, t=2.869, df=7). As Kronos GRF4-GIF1 lines didn't show a significant difference in BSC:MSC counts (Figure 5.10a, b), this can be attributed to Kronos GRF4-GIF1 OBSCs having a greater cell area than those of the controls (Figure 5.10i). The difference was not statistically significant for the IBSCs (Figure 5.10h).

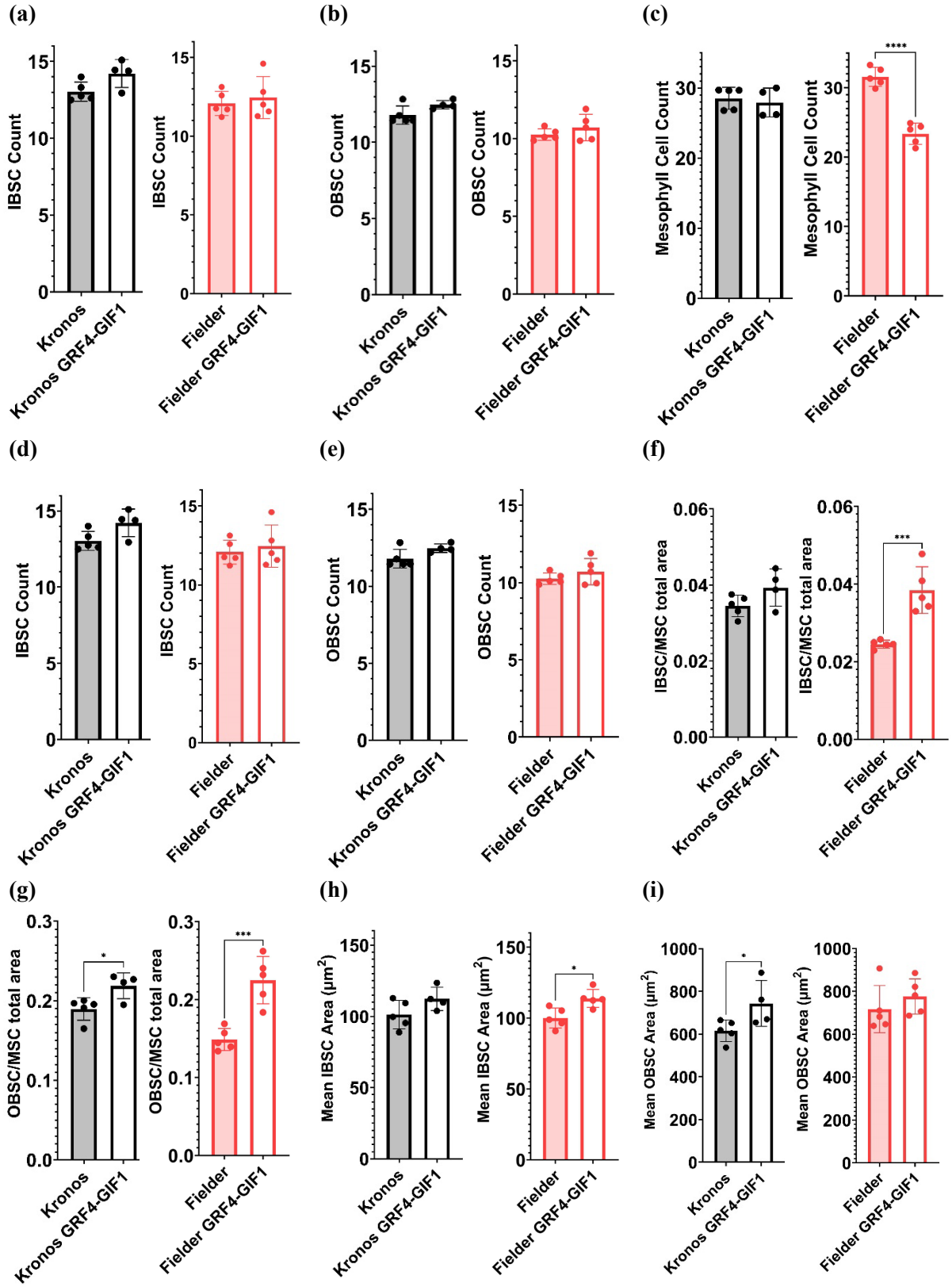

Figure 5.10. Overexpressing *GRF4-GIF1* in hexaploid wheat leaves alters the bundle sheath to mesophyll cell ratio. (a) Inner Bundle Sheath Cell (IBSC):Mesophyll Cell (MSC) Number Ratio. (b) Outer Bundle Sheath Cell (OBSC):Mesophyll Cell (MSC) Number Ratio. (c) Number of mesophyll cells between veins (d) Mean Number of Inner Bundle Sheath Cells around a single vein (e) Mean Number of Outer Bundle Sheath Cells around a single vein. (f) IBSC:MSC Ratio of total area of leaf section that is made up of each cell type, calculated as mean cell area multiplied by cell count. (g) OBSC:MSC Ratio of total area of leaf section that is made up of each

cell type, calculated as mean cell area multiplied by cell count. (h) Mean IBSC cell area. (i) Mean OBSC area. Each data point represents one plant (n=5, n=4 for Kronos GRF4-GIF1), and error bars show standard deviation from the mean. Black = tetraploid (Kronos), red = hexaploid (Fielder). T-tests were carried out to test for significant differences between GRF4-GIF1 lines and relevant controls: p<0.05*, p<0.005**, p<0.0005***, p<0.0001****.

Although the mean interveinal distance in the Fielder GRF4-GIF1 lines was lower than controls, this difference was not significant (Figure 5.11a). These differences in architecture were not seen in Kronos GRF4-GIF1 leaves. Interestingly, the only significant difference observed in the tetraploid mutants was an increase in interveinal distance (t-test: p=0.0196, t=3.012, df=7 (Figure 5.11a). Finally, no differences in leaf or mesophyll thickness were seen in either the Kronos GRF4-GIF1 or Fielder GRF4-GIF1 overexpressing mutants compared to non-transgenic controls (Figure 5.11b, c).

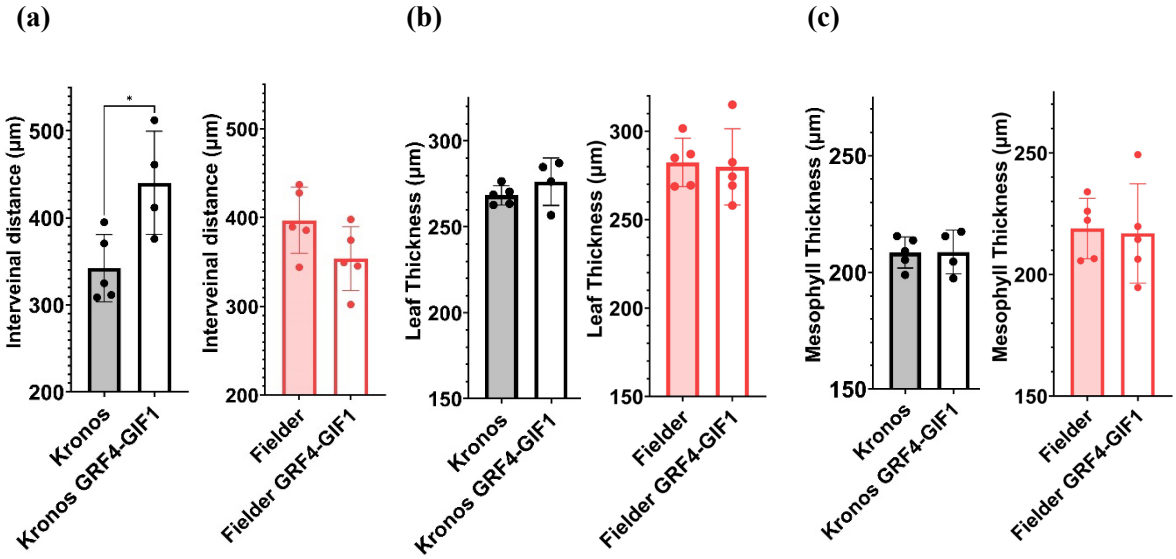

Figure 5.11. Overexpressing *GRF4-GIF1* does not have major effects on interveinal distance, mesophyll thickness or leaf thickness. (a) Interveinal distance, measured between the 2nd and 3rd veins from the central major vein (b) Leaf Thickness. Equal measurements across the veins and bulliform cells were taken and the mean calculated and plotted. (c) Mesophyll thickness**.** Each data point represents one plant, and error bars show standard deviation from the mean. Black = tetraploid, red = hexaploid. n = 5 (for Kronos GRF4-GIF1, n = 4) Stats: t-test between GRF4-GIF1 lines and relevant controls: p<0.05*.

5.3.6. Hexaploid Plants Overexpressing GRF4-GIF1 have Increased iWUE

To investigate whether *GRF4-GIF1* overexpressing lines showed any difference in physiology from control lines, I performed gas exchange analysis using IRGAs. These data showed a small but statistically insignificant in stomatal conductance (g_s; Figure 5.12a) and increase in carbon assimilation rate (*A*; Figure 5.12b) in the *GRF4-GIF1* overexpressing lines. Although neither value independently indicated as significantly different from controls for Fielder GRF4-GIF1, calculation of iWUE (which involves dividing *A* by g_s) indicated a significant increase for the *GRF4-GIF1* overexpressing Fielder line (t-test: P=0.0089*, t=3.586, df=7; Figure 5.12c). Although the assimilation rate in the tetraploid

Kronos overexpressing *GRF4-GIF1* was increased relative to control (t-test: P=0.0459, t=2.315, df=9; Figure 5.12b), iWUE could not be distinguished from controls (Figure 5.12c).

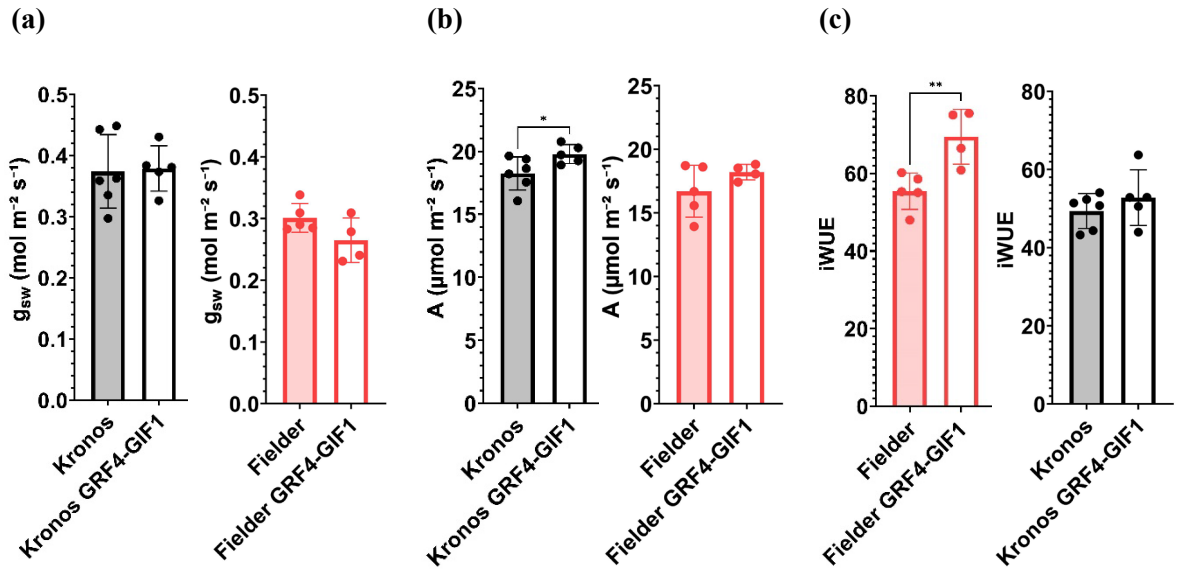

Figure 5.12. Overexpressing *GRF4-GIF1* in wheat alters leaf gas exchange. (a) Steady-state stomatal conductance (g_{sw}) of tetraploid (Kronos) and hexaploid (Fielder) *GRF4-GIF1* overexpressing lines. (b) Carbon assimilation (A) of tetraploid and hexaploid GRF4-GIF1 lines. (c) Intrinsic water-use efficiency (iWUE) of tetraploid and hexaploid GRF4-GIF1 lines, calculated using the equation: iWUE = A/gsw. Each data point represents one plant (n = 6, for Kronos GRF4-GIF1 n = 5), and error bars show standard deviation from the mean. Black = tetraploid (Kronos), red = hexaploid (Fielder). T-tests were carried out to test for significant differences between GRF4-GIF1 lines and relevant controls: $p<0.05$*, $p<0.005$**.

In addition to measured g_s, I also calculated the anatomical maximum stomatal conductance of each line (g_{smax}) using measured stomatal size and density parameters, then used this to calculate theoretical anatomical iWUE (Figure 5.13). These data showed a decrease in the anatomical g_{smax} of the *GRF4-GIF1* overexpressing lines (Figure 5.13a) resulting in them being having a higher anatomical iWUE (Figure 5.13b). However, these were both statistically significant only in the tetraploid Kronos GRF4-GIF1 plants (g_{smax} - t-test: p=0.0074*,t=3.438, df=9; anatomical iWUE - t-test: 0.0038**, t=3.867, df=9).

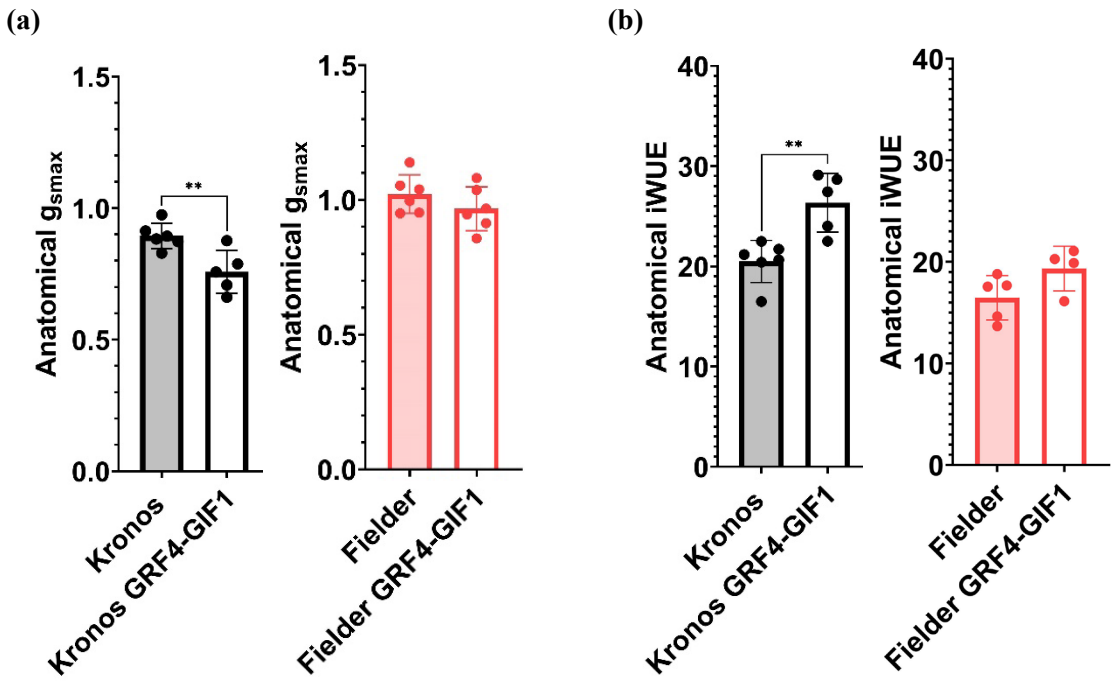

Figure 5.13. Anatomical calculated g_{smax} and iWUE from stomatal traits are altered by the overexpression of *GRF4-GIF1*. (a) Anatomical maximum stomatal conductance (g_{smax}) calculated using measurements of stomatal size and density. (b) Theoretical maximum iWUE, calculated using measured A and anatomical g_{smax}: iWUE = A/g_{smax}. Each data point represents one plant (n = 6, for Kronos GRF4-GIF1 n = 5), and error bars show standard deviation from the mean. Black = tetraploid (Kronos), red = hexaploid (Fielder). T-tests were carried out to test for significant differences between GRF4-GIF1 lines and relevant controls: $p<0.05$*, $p<0.005$**.

5.4. Discussion

5.4.1. GRF4-GIF1 Overexpression Changes Multiple Factors of Leaf Morphology in Hexaploid Fielder Background, Leading to Improved iWUE

Several observations from this project support previous evidence of the role of GRF-GIF complexes in leaf expansion and development. *GRF4-GIF1* overexpressors with both tetraploid and hexaploid wheat backgrounds demonstrated decreased leaf width (Figure 5.4c). *GRF4-GIF1* overexpression also showed an increase in cell size in some cell types, such as stomatal (Figure 5.5) and pavement cells (Figure 5.6). This contradicts previous studies which suggest that overexpressing *GRF-GIF* complexes results in larger leaves (Kim & Lee, 2006; Horiguchi *et al.* 2005; Zhou *et al*., 2019; Lee *et al.,* 2009) and loss-of-function mutations result in narrower leaves (Kim & Kende, 2004; Kim *et al.,* 2003; Shimano *et al*., 2018). In terms of leaf size *GRF4-GIF1* overexpression in wheat appears to be more similar to GRF9, where overexpression results in decreased leaf width (Omidbakhshfard *et al*. 2018).

Major differences were observed in the leaf anatomy of *GRF4-GIF1* overexpressing Fielder plants in this study. Firstly, reduced stomatal density (Figure 5.5a) likely contributed to a decrease in stomatal conductance and improved intrinsic water-use efficiency (Figure 5.12). However, as g_{smax}, a predictor of theoretical maximum stomatal conductance calculated using stomatal anatomical parameters, did not show a significant decrease in GRF4-GIF1 Fielder lines (Figure 5.13), this observed improvement in

iWUE is likely caused by a combination of a variety of anatomical and biochemical traits. GRF4-GIF1 stomatal complexes were also larger than in Fielder controls, in terms of length, width and area (Figure 5.5). This was likely a result of a general increase in size of pavement cells, as a similar increase in pavement cell size was seen in the transgenics in both the files containing stomata (Figure 5.6c) and those without stomata (Figure 5.6b). Stomatal cell size does not appear to have a large effect on g_s, instead larger cells have been shown to influence the patterning of the epidermis resulting in reduced stomatal density (Rudall *et al*., 2013). The increased size of stomatal complexes and pavement cells in the *GRF4-GIF1* overexpressing Fielder transgenics was accompanied by a decreased stomatal density which contributed to reduced stomatal conductance and improved water-use efficiency. This phenotype of increased pavement/stomatal cell size was similar to that of overexpressing the *KRP1* gene (another cell cycle gene) on the Arabidopsis epidermis (Lehmeier *et al.,* 2017).

Interestingly, and unlike the decreased mesophyll cell size observed by Lehmeier *et al.* (2017) when overexpressing *KRP1*, there was no difference in mean mesophyll cell size in either transgenic line (Figure 5.7, 5.9). As discussed in Chapter 4, the wheat mesophyll is patterned in an adaxial-abaxial direction and therefore by taking mean values for the mesophyll cells across the whole leaf, there is a risk of losing information. This could be incorporated into future studies using these lines but was not within the scope of this project. When looking at the volume data for individual cells, there appears to be a different distribution in Fielder GRF4-GIF1 lines with a greater number of larger and smaller cells in this line (Figure 5.8b). However, this was not observed in the tetraploid Kronos transgenics. Why overexpression of *GRF4-GIF1* led to a predominantly epidermal phenotype (i.e. increased cell size) is unclear. Previous work comparing mesophyll size in different ploidy level clearly showed that wheat mesophyll cells have the capacity to massively increase in volume (Wilson *et al.,* 2021). Presumably there is some control on mesophyll cell size which GRF4-GIF1 alone cannot break, but this is absent (or less powerful) in the epidermis. The nature of this has yet to be elucidated.

My analysis revealed an unexpected increase in the ratio of bundle sheath to mesophyll cells (counts) with *GRF4-GIF1* overexpression, as well as area of the bundle sheath relative to mesophyll tissue (Figure 5.10). The bundle sheath is a distinct group of cells arranged radially around the vascular bundle. Although their precise function in open to discussion, a role in facilitating transport to/from the vascular tissue seems clear. There has also been significant interest in the bundle sheath due to its role in C4 photosynthesis where the Calvin-Benson cycle becomes localised to this tissue. This is normally accompanied by a decreased number of mesophyll cells between veins, hence an increase in bundle sheath/mesophyll cell ratio (Brown 1975; Hatch, 1987; Lundgren *et al*., 2014), a phenotype reminiscent to that observed in the *GRF4-GIF1* overexpressing lines. Interestingly, GRF1, a member of the GRF family, was identified by Alenazi *et al.* (2024) in a genome wide association study (GWAS) investigating the development of C4 leaf anatomy in the model grass *Alloterposis semialata*. In this

study, GRF1 was one of the genes seen to be associated with an increasing proportion of bundle sheath tissue within the leaf for C4 photosynthesis in *A. semialata*.

A main characteristic linked with the switch from C3 to C4 anatomy is the development of minor veins and, thus, increase in vein density (Lundgren *et al*., 2019). This was not observed in *GRF4-GIF1* overexpressing lines in this study, and neither were other key characteristic changes associated with C3-C4 transition, such as decreased distance between bundle sheath cells (Alenazi *et al*., 2023). However, an increase in the proportion of both inner and outer bundle sheath tissue relative to mesophyll tissue (Figure 5.10f, g) observed in the Fielder *GRF4-GIF1* overexpressors, and for the OBSCs only in the Kronos GRF4-GIF1 lines, mirrors the phenotypes of the C4-like leaves reported by Alenazi *et al*. (2023).

It is also interesting to note that stomata become fewer but larger across the C3-C4 gradient (Zhao *et al.*, 2022) and the Fielder *GRF4-GIF1* overexpressors have larger stomata and reduced stomatal density (Figure 5.5). However, this may have been a consequence of an increase in pavement width in the *GRF4-GIF1* overexpressors, as pavement cells showed an increase in width in both Kronos and Fielder mutants (Figure 5.6b, c). Interestingly, increased pavement cell width in Kronos GRF4-GIF1 lines did not translate to larger stomata, as was the case with Fielder, but they did also demonstrate reduced stomatal density that did not correlate with increased stomatal size.

Overall, it seems that the outcome of *GRF4-GIF1* overexpression has a level of cell/tissue specificity, with, e.g., pavement cells showing the most dramatic changes. The altered bundle sheath/mesophyll cell proportions support the hypothesis that GRF family genes are involved in the transition to a more C4-like leaf architecture in grasses. A model summarising the observed and hypothesised phenotypes that result from overexpressing *GRF4-GIF1* in hexaploid wheat leaves can be found in Figure 5.14.

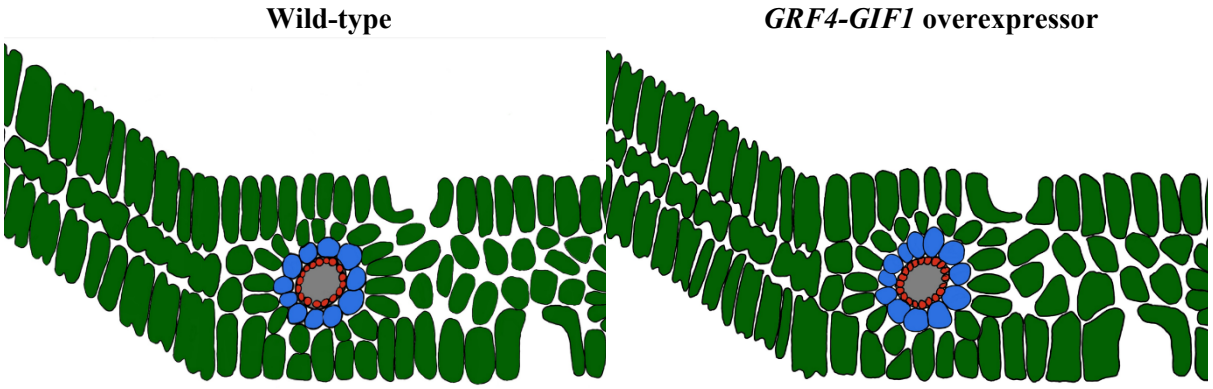

Figure 5.14. Model mesophyll and bundle sheath cells in wild-type hexaploid and *GRF4-GIF1* overexpressors. *GRF4-GIF1* overexpressors have both larger and a greater number of inner and outer bundle sheath cells. The mesophyll cells of *GRF4-GIF1* overexpressors are hypothesised to have mesophyll cells that are larger in the transverse (medio-lateral) direction and smaller in the longitudinal (proximal distal) direction, with no change in longitudinal cell lobing area or total mesophyll cell volume. Green = mesophyll, blue = outer bundle sheath, red = inner bundle sheath.

5.4.2. GRF4-GIF1 Overexpression has a Different Phenotype in Fielder (Hexaploid) than in Kronos (Tetraploid)

There were many differences associated with the overexpression of the *GRF4-GIF1* construct that were present in the Kronos background and not Fielder, and vice versa. For example, Fielder GRF4-GIF1 demonstrated larger stomatal constructs (Figure 5.5c-e) and pavement cell area (Figure 5.6e), but for Kronos GRF4-GIF1 these were indistinguishable from the controls. It is important to note that the pavement cell length and area may have been subjected to slight bias during recording of the data as any cells longer than the width of the image were unable to be recorded, meaning that the largest cells in each case were unintentionally excluded from the dataset.

An interesting phenotype seen in Fielder GRF4-GIF1 was the increase in the range of mesophyll cell size with more extreme large and small cells (Figure 5.8b), but this was also not observed in Kronos GRF4-GIF1 (Figure 5.8a). From these observations, it appears that most phenotypes relating to leaf cell size and proliferation were not present in the Kronos *GRF4-GIF1* mutants. This is supported by the reduced number of mesophyll cells between the veins, despite no differences in average cell volume, and subsequent increased bundle sheath cell: mesophyll cell ratio in Fielder GRF4-GIF1 which is not observed in the Kronos mutants. However, the Kronos GRF4-GIF1 showed a substantial increase in interveinal distance (Figure 5.11a) and, combined with similar mesophyll cell counts between these veins and no change in mean cell volume, this suggests that the cells could be packaged between these veins in a similar way to the hexaploid mutants. With regards to how fewer mesophyll cells are packaged across the same distance in *GRF4-GIF1* overexpressing leaves, it is important to consider the size of these mesophyll cells in 3-dimensional space and across both the transverse and longitudinal planes. Although not statistically significant, there is a trend towards both the Fielder and Kronos GRF4-GIF1 lines having increased transverse mesophyll cell area (Figure 5.9a) and the Fielder GRF4-GIF1 lines also having reduced longitudinal cell area (Figure 5.9b). This increase in transverse cell area could explain the reduction in number of mesophyll cells found across the same 2-dimensional space (Figure 5.10c and Figure 5.11a), while the maintenance or subtle decrease in longitudinal cell area explains the lack of difference in overall 3D mesophyll cell volume (Figure 5.7d). As the mesophyll cells may have undergone subtle, contrasting size changes across the transverse vs longitudinal planes, the shape of the cells in terms of circularity and with regards to cell lobing did not change (Figure 5.9c, d).

One or a combination of changes that were observed in Fielder GRF4-GIF1 but not in the Kronos mutants, such as increased BSC:MSC and range of mesophyll cell size, have resulted in improved iWUE (Figure 5.12c). The different phenotypes caused by the overexpression of the GRF4-GIF1 complex could be a result of the preexisting differences in the background lines. As Kronos is tetraploid and Fielder hexaploid, Kronos has generally smaller cells within the leaf in terms of stomata (Figure 5.5d) and mesophyll (Figures 5.7-5.9).

Both Kronos and Fielder are spring wheat varieties of USA origin. Buffagni *et al*. (2020) observed that Kronos is a drought-adapted variety through increased expression of the *TdDHN15.3* gene. There is no evidence that Fielder has any such tolerance to drought, and this could be contributing to the lack of statistically significant improvement in Kronos GRF4-GIF1 g_s and iWUE, despite the reduction in stomatal density, that is observed in the Fielder background.

5.4.3. Stomatal Conductance and iWUE Cannot be Predicted Using Stomatal Traits Alone

G_{smax} , i.e. maximum theoretical stomatal conductance, is calculated using stomatal density and size measurements such as pore length and guard cell width. When calculating g_{smax} in this study based on these characteristics, a statistically significant decrease was seen only in Kronos GRF4-GIF1 and mutants in the Fielder background did not show the same improved theoretical iWUE (Figure 5.13). This was unexpected as both transgenic lines showed reduced stomatal density: the main driver in both g_{smax} calculation and (is hypothesised to be) for measured g_s, and subsequently for iWUE calculation. The likely cause is that stomatal complex and guard cell size, which are used to estimate the maximum pore size in the g_{smax} calculation, are larger in the Fielder *GRF4-GIF1* overexpressors and not in the Kronos mutants, offsetting the predicted effect of decreased stomatal conductance and resulting in reduced g_{smax} in the Kronos mutant but not the Fielder.

However, the measured g_s and iWUE showed the opposite of the anatomically calculated values: improved iWUE was only observed in Fielder GRF4-GIF1 (Figure 5.12c). This raises questions as to whether stomatal traits have as much of an impact on iWUE as previously thought, and whether characteristics observed in the Fielder mutants, for example relating to increased BSC:MSC (Figure 5.10), are more important in determining the rate of gas flux than stomatal guard cell and pore size. iWUE is calculated as A/g_s, where A is carbon assimilation rate. There are many resistances to CO_2 movement to the site of photosynthesis. The ease of CO_2 diffusion from the leaf airspace into the chloroplasts is termed mesophyll conductance (g_m), with g_m influenced by both anatomical and biochemical factors, as well as being affected by changes in the local environment (Heckwolf *et al*., 2011; Terashima *et al*., 2011; Flexas *et al.,* 2012). A major influence on g_m is S_{mes}: the mesophyll surface area exposed to intracellular airspace (IAS) per unit of leaf area, as high S_{mes} results in increased cell surface area in contact with gas phase H_2O and CO_2. IAS depends on several factors, including the number of cells per tissue volume, the size and shape of those cells and the degree of cell separation (i.e. the extent of the separation that occurs along adjoining cell edges). Investigation into how altering mesophyll structure, in such a way as has been achieved with overexpressing *GRF4-GIF1* in this study, effects measured g_m could further elucidate links between S_{mes} and leaf gas exchange, expanding on the current physiological toolbox for improving iWUE.

5.5. Conclusion

The *GRF4-GIF1* overexpressing tetraploid and hexaploid wheat varieties used in this study demonstrated changes in leaf morphology that was, to some extent, ploidy-dependent. In particular, there was a reduced stomatal density compared with controls, which likely contributed towards the improved iWUE observed in hexaploid Fielder GRF4-GIF1 lines. The hexaploid transgenics also demonstrated increased stomatal and pavement cell size. A greater range of mesophyll cell sizes, with no change in mean size, was observed in the Fielder *GRF4-GIF1* overexpressor but not in the tetraploid Kronos lines. It is important to consider that another factor which may contribute to this change in leaf cell size could be related to nitrogen nutrition, as *GRF4* is known to play a role in activating plant nitrogen metabolic processes (Wu *et al*., 2020; Zhang *et al*., 2021b), and it is well established that increased nitrogen availability is linked to development of larger cells and leaves (Morton & Watson, 1948).

The internal leaf structure was altered in the transgenics, leading to an increase in the ratio of bundle sheath to mesophyll cells in terms of both count and cell area, and a decrease in the total count of mesophyll cells between the vasculature in the Fielder GRF4-GIF1 leaves. This effect was mimicked in the Kronos GRF4-GIF1 leaves as there was an accompanying increase in IVD and no change in the total mesophyll cell count. This decrease in mesophyll cell count in the same volume of space was observed in both Fielder and Kronos *GRF4-GIF1* overexpressing lines, with no change in cell volume. This was achieved by a decrease in mesophyll cell area in the longitudinal direction and an increase in mesophyll cell area in the transverse direction. To what extent these changes in the internal leaf structure contributed to the increased iWUE observed in the Fielder GRF4-GIF1 plants is open to discussion.

Chapter 6. Discussion

6.1. General Discussion

During leaf development, trade-offs occur between rates of carbon fixation for photosynthesis and rate of transpiration, which are largely determined by the final leaf architecture. Stomata are well known to be key players in this trade off (Franks and Farquhar, 1999; Xu *et al.,* 2016; Driesen *et al.,* 2020), however it is also thought that mesophyll cells are important in determinators the rate of carbon assimilation and water-use efficiency (Wilson *et al*., 2021; Earles *et al*., 2018; Evans *et al*., 2009; Terashima *et al*., 2011). Improving the water-use efficiency and drought tolerance of crops such as wheat in order to achieve 'more crop per drop' is an important area of study as major cereal crops currently account for 27% of global water consumption (Hoekstra & Mekonnen, 2012). This will become an even greater issue in the future under the threat of climate change.

Throughout the domestication and selection of wheat to modern cultivars, there have been many changes in leaf morphology that have resulted in an improved iWUE (Chapter 3; Wilson *et al*., 2021). The work done in Chapter 3 of this project supports the hypothesis that domestication and selection of modern wheat cultivars has led to improved iWUE, in part due to a decrease in stomatal density parallel to an increase in stomatal complex size. This mirrors the observation of Wilson *et al.* (2021) that domesticated hexaploid wheat has the lowest stomatal conductance (g_s; and subsequently highest iWUE), lowest stomatal density and largest stomatal complexes of the diploid, tetraploid and hexaploid varieties used in the study. However, the increased size and subsequent reduced density linked to stomatal patterning can also likely be attributed to a general increase in cell size as an effect of polyploidy (Jellings & Leech, 1984; Parker & Ford, 1982). By studying only the leaves of tetraploid *Triticum* in this study, any effect of polyploidy was negated and I have shown that having fewer, larger stomata is a trait that has been selected for during the evolution of these modern cultivated tetraploid wheat varieties.

Similar to Wilson *et al.* (2021), I saw that tetraploid *Triticum* varieties fall intermediate of diploid and hexaploid in terms of stomatal density and iWUE, and landrace Emmer varieties were seen to behave similarly to wild and Durum tetraploid varieties in this study. This intermediate behaviour of Emmer varieties was also observed in leaf, carbon assimilation for photosynthesis (A) and g_s. This suggests that these are traits which had a selective advantage in early wheat cultivation that have been further selected for and improved upon over thousands of years. In these traits, the wild-Emmer-Durum trend mirrored that of the diploid-tetraploid-hetraploid trend previously observed (Austin *et al.,* 1982, Wilson *et al.,* 2021).

Interestingly, some traits were observed in which Emmer varieties did not act as an intermediate between wild tetraploid and Durum lines, including plant height, pavement cell size and mesophyll cell shape. One explanation for this could be that having taller plants with narrower pavement cell files and

more rounded mesophyll cells gave the early cultivated Emmer varieties an advantage in the climate in which they grew that was no longer needed once wheat cultivation spread away from the Nile Delta (Kilian *et al.,* 2009). An alternative theory is that traits which were neutral in ancient crop plants became unfavourable when the need for higher-yielding, more stress-tolerant wheat arose. Plant height was shorter in Durum lines than Emmer, most likely due to the improvement of Durum varieties during the Green Revolution and the introduction of the *RHT1* gene (Borlaug *et al*., 1968).

In the tetraploid lines studied, there was no link between g_s and A, with the observed increases in g_s suggesting that iWUE was most likely the driver of selection and not rate of photosynthesis, however this contradicts previous studies which show g_s and A are positively correlated (McAusland *et al*., 2021; Hu *et al.,* 2023a). This could be due to there being less variation in g_s in this study. Another general trend across the tetraploid lines in Chapter 3 was that mesophyll cell size was negatively correlated with both mesophyll cell surface area to volume ratio and also with stomatal density. This supports the hypothesis of Lundgren *et al.* (2019) that mesophyll cell separation relies on the presence of functional stomata, either occurring through cell-cell signalling or CO_2 flux. Reduced mesophyll cell surface area to volume ratio was observed in Durum lines which had the highest iWUE, and this could be linked to the idea that less exposed mesophyll cell surface area results in improved iWUE (Wilson *et al*, 2021).

When looking at mesophyll cells traits in Chapter 3, data was averaged over the entire tissue as the wheat mesophyll is often thought to be homogenous across the abaxial-adaxial axis (Parker & Ford, 1982; Jellings & Leech, 1984). This is widely accepted, and in many studies, the wheat mesophyll is often treated as a whole, unlike Arabidopsis studies which focus on the palisade and spongy mesophyll layers separately. In Chapter 4 of this project, clear evidence is provided that the wheat mesophyll actually consists of four distinct 'layers' of cells which behave differently in terms of cell size and shape, and may in fact perform slightly different roles. In the wheat mesophyll, 'Outer' (Upper/Lower) cells which are in direct contact with the abaxial and adaxial epidermis are larger and more elongated than those cells which are not adjacent to pavement tissue. One hypothesis is that these cells may have a similar function to eudicot palisade mesophyll cells, with the cells adjacent to the adaxial epidermis directing light deeper into the leaf (Vogelmann & Martin, 1993). In the centre of the leaf, 'Middle' layer cells are more rounded and appear to mimic the spongy mesophyll layer of eudicots, facilitating CO_2 diffusion through the leaf and scattering light (Smith *et al.,* 1997; Terashima *et al.,* 2011). However, there are multiple ways in which the wheat mesophyll abaxial-adaxial patterning differs from that of eudicots. For example, 'Lower' layer cells adjacent to the abaxial epidermis are more palisade-like for reasons which must be unrelated to light direction, and that the palisade-like cells actually have slightly reduced 3D surface area to volume ratio compared to the 'Middle' spongy-like cells due to increased cell lobing along the proximal-distal axis. Additionally, 'hook-like' mesophyll cells lining the substomatal cavities appear to be distinct from other 'Outer' (Upper/Lower) layer cells. It is likely that their distinct form is linked to their role in gas exchange, being the first mesophyll cell encountered by

CO_2 entering the leaf via the stomata. These cells are likely formed in response to CO_2 flux into the leaf (Lundgren *et al.,* 2019).

This patterning of the mesophyll into 'Upper', 'Lower', 'Middle', and 'Radial' layers which are distinct in terms of cell size and shape was conserved across all fourteen varieties and seven species/sub-species of diploid, tetraploid and hexaploid *Triticum* used in this study, suggesting that there are advantages to this mesophyll layering. Similar layering has also been observed in rice (*Oryza sativa;* Sloan *et al*., 2022), but with key differences as to the location-based characteristics of the cells. One major difference is that there was no obvious distinction of morphology of the mesophyll cells surrounding the bundle sheath in rice as there was in *Triticum*, in which they appear to form in a wheel shape surrounding the vasculature. Additionally, in complete opposition with the *Triticum* mesophyll, rice mesophyll cells in the most central layer were observed to be the largest in terms of transverse cell area. The presence of significant mesophyll patterning of both monocot species however raises the question as to whether monocot mesophyll should be treated as homogenous going forward, or whether important information could be being excluded by averaging mesophyll cell data across the whole abaxial-adaxial axis.

The work done in Chapter 5 on this study builds upon the observation by Wilson *et al.* (2021) that iWUE in cultivated hexaploid bread wheat is greater than that of diploid and tetraploid varieties. With the use of gene editing, it aims to answer the question of whether the traits that are thought to have caused this increase in iWUE, such as cell size with ploidy, can be further increased without the use of polyploidisation. The GRF family of transcription factors, along with their GIF co-factors, were chosen as target genes for this study due to their role in cell proliferation (Debernardi *et al*., 2012; 2014; Wang *et al*., 2020; Wu *et al.,* 2021; Horiguchi *et al*., 2005; Kim & Lee, 2006). There was a clear reduction in stomatal density in each of the independent lines of both tetraploid and hexaploid *GRF4-GIF1* overexpressors used in this study, with hexaploid Fielder GRF4-GIF1 stomatal complexes being significantly larger than the controls, and a subsequent improvement in Fielder GRF4-GIF1 iWUE. This was also accompanied by an increase in pavement cell size. Interestingly, a decrease in leaf width in both tetraploid and hexaploid *GRF4-GIF1* overexpressing lines, which is contradictory to previous studies that suggest overexpressing *GRF-GIF* complexes results in larger leaves (Kim & Lee, 2006; Horiguchi *et al.* 2005; Zhou *et al*., 2019; Lee *et al.,* 2009) and it is loss-of-function mutations which result in narrower leaves (Kim & Kende, 2004; Kim *et al.,* 2003; Shimano *et al*., 2018). *GRF4-GIF1* overexpression in wheat appears to be more similar to GRF9, where overexpression results in decreased leaf width (Omidbakhshfard *et al*. 2018).

There was also an increase in the range of mesophyll cell volume observed in the Fielder transgenic lines, although this was not observed in the tetraploid Kronos background and resulted in no mean difference in overall mesophyll cell volume. When looking at the photosynthetic rate of these lines (with relation to A), Kronos *GRF4-GIF1* overexpressing plants had improved photosynthetic rate, supporting

the outcome of Lehmeier *et al.*'s 2017 study that modulating cell cycle gene expression leads to altered leaf cellular architecture. Overexpression of the *KRP1* and *RBR1* genes do this through increasing mesophyll cell and tissue density, decreasing the volume of the airspace and altering its patterning, assessed through the use of microCT (Lehmeier *et al.,* 2017). Future research into the effect of *GRF4-GIF1* overexpression on mesophyll airspace patterning using microCT could be used to assess the mechanism behind the increased A observed in the Kronos GRF1-GIF1 lines, and potentially elucidate a potential cause of the increased iWUE in the Fielder GRF4-GIF1 lines in this chapter.

One interesting observation seen in the *GRF4-GIF1* overexpressors, particularly in the hexaploid Fielder background, was the increase in ratio of bundle sheath tissue to mesophyll tissue and a potential shift to a more C4-like phenotype (Brown, 1975; Hatch, 1987; Lundgren *et al*., 2014; Alenazi *et al*., 2023). The GRF family gene *GRF1* was identified by Alenazi *et al*. (2024) in a genome-wide association study (GWAS) to play a part in C4 evolution in the model grass *Alloteropsis semialata*, and it is possible that ubiquitous overexpression of the GRF4-GIF1 complex in this study has resulted in the emergence of similar characteristics. Another piece of evidence which supports the idea of Fielder GRF4-GIF1 being more C4-like is the presence of fewer, larger stomata, which is a trait seen across the C3-C4 gradient (Zhao *et al*., 2022). As an increase in iWUE was observed in Fielder GRF4-GIF1 and not Kronos GRF4-GIF1, the absence of this C4-like morphology in the Kronos transgenic line supports the hypothesis that this change in bundle sheath to mesophyll cell ratio caused by *GRF4-GIF1* overexpression has a functional benefit in further improving hexaploid wheat iWUE.

6.2 Future Work

From the work done in this project, potential avenues for future research have been uncovered.

What is the evolutionary advantage of mesophyll patterning?

This study showed that the presence of cell layers distinct by size and shape within the mesophyll is conserved across a broad range of *Triticum* species/sub-species. Such mesophyll patterning may influence traits such as mesophyll porosity at different leaf depths, mesophyll conductance (g_m) and the amount of mesophyll cell surface area that is exposed to the intracellular airspace (s_{mes}). Additionally, Wong *et al.* (2022) observed that the presence of humidity gradients through the leaf are vital to buffer against external humidity changes and maintenance of the cytosolic water potential, a system which may be benefited by the presence of mesophyll layers. All of these traits will impact leaf function, and further exploration may provide insight into the evolutionary advantage for the presence of distinct mesophyll layers across the *Triticum* genus.

To further explore whether the cells in the Upper and Middle *Triticum* mesophyll layers mimic the eudicot palisade and spongy mesophyll cells respectively in terms of function as well as morphology, chlorophyl and Rubisco content and the photosynthetic activity of these different cells could be

measured. In addition, changing this patterning of layers may affect leaf function in terms of photosynthesis and water-use efficiency. This could be done practically through genetic engineering methods, or through a 3D modelling approach similar to how Xiao *et al*. (2022) generated *eLeaf* to assess the effect of altering rice leaf morphological and biochemical properties on photosynthesis.

How does the overexpression of GRF4-GIF1 lead to the increase in cell size of specific cell types and not others?

In this study, we saw that the overexpression of *GRF4-GIF1* in hexaploid wheat increased the size of stomatal, pavement and inner/outer bundle sheath cells, but had no effect on the mean mesophyll cell size. Further investigation into the mechanism behind this will enhance our understanding of the roles of GRF family genes in cell proliferation and expansion and may provide more candidate gene targets for improving crop water-use efficiency.

Although there was no difference in mean mesophyll cell size, there were a greater range of mesophyll cell volumes observed in the GFR4-GIF1 overexpressing hexaploid lines and potentially a change in morphology through slightly increasing in size across the medio-lateral axis and slightly shrinking in the direction of cell lobing across the proximal-distal axis, resulting in fewer mesophyll cells between veins. Assessing the mesophyll porosity, g_m and s_{mes} of these leaves will provide insight into any affect that these minor changes have on other mesophyll characteristics and if this contributes in any way to the improved iWUE.

Are GRF genes potential molecular breeding targets to improve water-use efficiency in the field?

The measure of water-use efficiency used in this study, iWUE, was calculated as the relationship between g_s and A under controlled conditions under no abiotic or biotic stress. The next step would be to subject *GRF4-GIF1* overexpressing hexaploid lines to a drought experiment to assess drought resistance, and/or quantify water-use efficiency through alternative methods such as stable carbon isotope (δ13C) composition. Additionally, it is important to understand whether the phenotype observed are a direct consequence of *GRF4-GIF1* overexpression, or whether it are caused by improved nitrogen-use efficiency in these lines (as has been observed in *GRF4*-overexpressing Arabidopsis lines).

Although *GRF4-GIF1* overexpressing Fielder plants in this study had improved iWUE, there was also a reduction in number of seeds yielded from each plant. It is important to assess whether this yield reduction translates to the field and if that would reduce its viability as a breeding target, and also whether overexpressing *GRF4-GIF1* in high-yielding, agriculturally relevant wheat varieties would result in the same phenotype.

Bibliography

Aalto, T., & Juurola, E. (2002). A three-dimensional model of CO_2 transport in airspaces and mesophyll cells of a silver birch leaf. *Plant, Cell & Environment*, *25*(11), 1399–1409.

Adachi, S., Nakae, T., Uchida, M., Soda, K., Takai, T., Oi, T., Yamamoto, T., Ookawa, T., Miyake, H., Yano, M., & Hirasawa, T. (2013). The mesophyll anatomy enhancing CO_2 diffusion is a key trait for improving rice photosynthesis. *Journal of Experimental Botany*, *64*(4), 1061–1072.

Altpeter, F., Vasil, V., Srivastava, V., & Vasil, I. K. (1996). Integration and expression of the high-molecular-weight glutenin subunit 1Ax1 gene into wheat. *Nature Biotechnology*, *14*(9), 1155–1159.

Alenazi, A. S., Bianconi, M. E., Middlemiss, E., Milenkovic, V., Curran, E. v, Sotelo, G., Lundgren, M. R., Nyirenda, F., Pereira, L., Christin, P.-A., Dunning, L. T., & Osborne, C. P. (2023). Leaf anatomy explains the strength of C4 activity within the grass species *Alloteropsis semialata. Plant, Cell & Environment, 46*(8), 2310–2322.

Alenazi, A. S., Pereira, L., Christin, P.A., Osborne, C. P., & Dunning, L. T. (2024). Identifying genomic regions associated with C photosynthetic activity and leaf anatomy *in Alloteropsis semialata*. *New Phytologist, 243*(5), 1698–1710.

Amos, W. B., & White, J. G. (2003). How the Confocal Laser Scanning Microscope entered Biological Research. *Biology of the Cell*, *95*(6), 335–342.

Apostolakos, P., Galatis, B., & Panteris, E. (1991). Microtubules in Cell Morphogenesis and Intercellular Space Formation in *Zea mays* Leaf Mesophyll and *Pilea cadiere*i Epithem. *Journal of Plant Physiology, 137*(5), 591–601.

Appels, R., Eversole, K., Stein, N., Feuillet, C., Keller, B., Rogers, J., Pozniak, C. J., Choulet, F., Distelfeld, A., Poland, J., Ronen, G., Sharpe, A. G., Barad, O., Baruch, K., Keeble-Gagnère, G., Mascher, M., Ben-Zvi, G., Josselin, A.-A., Himmelbach, A., …, The International Wheat Genome Consortium. (2018). Shifting the limits in wheat research and breeding using a fully annotated reference genome. *Science*, *361*(6403), eaar7191.

Araus, J. L., Alegre, L., Tapia, L., & Calafell, R. (1986). Relationship between Leaf Structure and Gas Exchange in Wheat Leaves at Different Insertion Levels. *Journal of Experimental Botany*, *37*(182), 1323–1333.

Austin, R. B., Morgan, C. L., Ford, M. A., & Bhagwat, S. G. (1982). Flag Leaf Photosynthesis of Triticum aestivum and Related Diploid and Tetraploid Species. *Annals of Botany*, *49*(2), 177–189.

Avni, R., Nave, M., Barad, O., Baruch, K., Twardziok, S. O., Gundlach, H., Hale, I., Mascher, M., Spannagl, M., Wiebe, K., Jordan, K. W., Golan, G., Deek, J., Ben-Zvi, B., Ben-Zvi, G., Himmelbach, A., MacLachlan, R. P., Sharpe, A. G., Fritz, A., … Distelfeld, A. (2017). Wild emmer genome architecture and diversity elucidate wheat evolution and domestication. *Science*, *357*(6346), 93–97.

Baillie, A. L., & Fleming, A. J. (2020). The developmental relationship between stomata and mesophyll airspace. *New Phytologist*, *225*(3), 1120–1126.

Barbier de Reuille, P., Routier-Kierzkowska, A. L., Kierzkowski, D., Bassel, G. W., Schüpbach, T., Tauriello, G., Bajpai, N., Strauss, S., Weber, A., Kiss, A., Burian, A., Hofhuis, H., Sapala, A., Lipowczan, M., Heimlicher, M. B., Robinson, S., Bayer, E. M., Basler, K., Koumoutsakos, P., … Smith, R. S. (2015). MorphoGraphX: A platform for quantifying morphogenesis in 4D. *ELife*, *4*(MAY), 1–20.

Barbour, M. M., Bachmann, S., Bansal, U., Bariana, H., & Sharp, P. (2016). Genetic control of mesophyll conductance in common wheat. *New Phytologist*, *209*(2), 461–465.

Barbour, M. M., & Kaiser, B. N. (2016). The response of mesophyll conductance to nitrogen and water availability differs between wheat genotypes. *Plant Science*, *251*, 119–127.

Barkoulas, M., Galinha, C., Grigg, S. P., & Tsiantis, M. (2007). From genes to shape: regulatory interactions in leaf development. *Current Opinion in Plant Biology*, *10*(6), 660–666.

Barro, F., Iehisa, J. C. M., Giménez, M. J., García-Molina, M. D., Ozuna, C. v, Comino, I., Sousa, C., & Gil-Humanes, J. (2016). Targeting of prolamins by RNAi in bread wheat: effectiveness of seven silencing-fragment combinations for obtaining lines devoid of coeliac disease epitopes from highly immunogenic gliadins. *Plant Biotechnology Journal*, *14*(3), 986–996.

Barro, F., Rooke, L., Békés, F., Gras, P., Tatham, A. S., Fido, R., Lazzeri, P. A., Shewry, P. R., & Barceló, P. (1997). Transformation of wheat with high molecular weight subunit genes results in improved functional properties. *Nature Biotechnology*, *15*(12), 1295–1299.

Beaulieu, J. M., Leitch, I. J., Patel, S., Pendharkar, A., & Knight, C. A. (2008). Genome size is a strong predictor of cell size and stomatal density in angiosperms. *New Phytologist*, *179*(4), 975–986.

Bednarek, J., Boulaflous, A., Girousse, C., Ravel, C., Tassy, C., Barret, P., Bouzidi, M. F., & Mouzeyar, S. (2012). Down-regulation of the TaGW2 gene by RNA interference results in decreased grain size and weight in wheat. *Journal of Experimental Botany*, *63*(16), 5945–5955.

Bellasio, C., Beerling, D. J., & Griffiths, H. (2016). An Excel tool for deriving key photosynthetic parameters from combined gas exchange and chlorophyll fluorescence: theory and practice. *Plant, Cell & Environment*, *39*(6), 1180–1197.

Bergmann, D. C. (2004). Integrating signals in stomatal development. In *Current Opinion in Plant Biology* (Vol. 7, Issue 1, pp. 26–32). Elsevier Ltd.

Bergmann, D. C., & Sack, F. D. (2007). Stomatal Development. *Annual Review of Plant Biology*, *58*(Volume 58, 2007), 163–181.

Bertolino, L. T., Caine, R. S., & Gray, J. E. (2019). Impact of Stomatal Density and Morphology on Water-Use Efficiency in a Changing World. *Frontiers in Plant Science*, *10*, 225.

Bolser, D. M., Kerhornou, A., Walts, B., & Kersey, P. (2015). Triticeae Resources in Ensembl Plants. *Plant and Cell Physiology*, *56*(1), e3–e3.

Bhowmik, P., Ellison, E., Polley, B., Bollina, V., Kulkarni, M., Ghanbarnia, K., Song, H., Gao, C., Voytas, D. F., & Kagale, S. (2018). Targeted mutagenesis in wheat microspores using *CRISPR/Cas9. Scientific Reports, 8(1),* 6502.

Borisjuk, N., Kishchenko, O., Eliby, S., Schramm, C., Anderson, P., Jatayev, S., Kurishbayev, A., & Shavrukov, Y. (2019). Genetic Modification for Wheat Improvement: From Transgenesis to Genome Editing. *BioMed Research International*, *2019*, 1–18.

Borlaug, N. (1968). Wheat breeding and its impact on world food supply. In: Finlay KW, Shepherd KW, editors. *Proceedings of the 3rd International Wheat Genetics Symposium.*, *Canberra.*, 1-36.

Borsuk, A. M., & Brodersen, C. R. (2019). The Spatial Distribution of Chlorophyll in Leaves. *Plant Physiology*, *180*(3), 1406–1417.

Borsuk, A. M., Roddy, A. B., Théroux-Rancourt, G., & Brodersen, C. R. (2022). Structural organization of the spongy mesophyll. *New Phytologist*, *234*(3), 946–960.

Bravo, A., Ponce, L., Párraga, P., Oliva, R. F., & Proaño, K. (2013). Expression of High Molecular Weight Glutenin Subunit Genes Correlated with Gluten Content in Common Wheat Varieties from the Highland of Ecuador. *Cereal Research Communications*, *41*(4), 593–600.

Brodribb, T., Jordan, G., & Carpenter, R. (2013). Unified changes in cell size permit coordinated leaf evolution. *New Phytologist*, *199*, 559–570.

Brown, W. V. (1975). Variations in Anatomy, Associations, and Origins of Kranz Tissue. *American Journal of Botany, 62*(4), 395–402.

Buckley, T., John, G., Scoffoni, C., & Sack, L. (2015). How does leaf anatomy influence water transport outside the xylem? *Plant Physiology*, *168*(1616–1635).

Buda, G. J., Isaacson, T., Matas, A. J., Paolillo, D. J., & Rose, J. K. C. (2009). Three-dimensional imaging of plant cuticle architecture using confocal scanning laser microscopy. *The Plant Journal*, *60*(2), 378–385.

Buffagni, V., Vurro, F., Janni, M., Gullì, M., Keller, A. A., & Marmiroli, N. (2020). Shaping Durum Wheat for the Future: Gene Expression Analyses and Metabolites Profiling Support the Contribution of BCAT Genes to Drought Stress Response. *Frontiers in Plant Science, 11*.

Burian, A., Paszkiewicz, G., Nguyen, K. T., Meda, S., Raczyńska-Szajgin, M., & Timmermans, M. C. P. (2022). Specification of leaf dorsiventrality via a prepatterned binary readout of a uniform auxin input. *Nature Plants*, *8*(3), 269–280.

Busch, F. A. (2018). Photosynthetic Gas Exchange in Land Plants at the Leaf Level. In S. Covshoff (Ed.), *Photosynthesis: Methods and Protocols* (pp. 25–44). Springer New York.

Caine, R. S., Yin, X., Sloan, J., Harrison, E. L., Mohammed, U., Fulton, T., Biswal, A. K., Dionora, J., Chater, C. C., Coe, R. A., Bandyopadhyay, A., Murchie, E. H., Swarup, R., Quick, W. P., & Gray, J. E. (2019). Rice with reduced stomatal density conserves water and has improved drought tolerance under future climate conditions. *New Phytologist*, *221*(1), 371–384.

Casson, S., & Gray, J. E. (2008). Influence of environmental factors on stomatal development. *New Phytologist*, *178*(1), 9–23.

Casson, S. A., & Hetherington, A. M. (2010). Environmental regulation of stomatal development. *Current Opinion in Plant Biology*, *13*(1), 90–95.

Čermák, T., Curtin, S. J., Gil-Humanes, J., Čegan, R., Kono, T. J. Y., Konečná, E., Belanto, J. J., Starker, C. G., Mathre, J. W., Greenstein, R. L., & Voytas, D. F. (2017). A Multipurpose Toolkit to Enable Advanced Genome Engineering in Plants. *The Plant Cell, 29(6),* 1196–1217.

CGIAR (2013) "Wheat: vital grain of civilization and food security," *CGIAR Research Program Wheat Annual Report*, CGIAR, Mexico, D.F.

Chaerle, L., Saibo, N., & van der Straeten, D. (2005). Tuning the pores: towards engineering plants for improved water use efficiency. *Trends in Biotechnology*, *23*, 308–315.

Chatelet, D. S., Clement, W. L., Sack, L., Donoghue, M. J., & Edwards, E. J. (2013). The Evolution of Photosynthetic Anatomy in Viburnum (Adoxaceae). *International Journal of Plant Sciences*, *174*(9), 1277–1291.

Che, R., Tong, H., Shi, B., Liu, Y., Fang, S., Liu, D., Xiao, Y., Hu, B., Liu, L., Wang, H., Zhao, M., & Chu, C. (2015). Control of grain size and rice yield by GL2-mediated brassinosteroid responses. *Nature Plants, 2*(1), 15195.

Chen, Y., Gao, Q., Huang, M., Liu, Y., Liu, Z., Liu, X., & Ma, Z. (2015). Characterization of RNA silencing components in the plant pathogenic fungus Fusarium graminearum. *Scientific Reports*, *5*(1), 12500.

Chen, Z.H., Chen, G., Dai, F., Wang, Y., Hills, A., Ruan, Y.-L., Zhang, G., Franks, P., Nevo, E., & Blatt, M. (2017). Molecular evolution of grass stomata. *Trends in Plant Science*, *22*, 124–139.

Cheng, M., Fry, J. E., Pang, S., Zhou, H., Hironaka, C. M., Duncan, D. R., Conner, T. W., & Wan, Y. (1997). Genetic Transformation of Wheat Mediated by Agrobacterium tumefaciens. *Plant Physiology*, *115*(3), 971–980.

Cheng, W., Song, X.-S., Li, H.-P., Cao, L.-H., Sun, K., Qiu, X.-L., Xu, Y.-B., Yang, P., Huang, T., Zhang, J. B., Qu, B., & Liao, Y.-C. (2015). Host-induced gene silencing of an essential chitin synthase gene confers durable resistance to Fusarium head blight and seedling blight in wheat. *Plant Biotechnology Journal*, *13*(9), 1335–1345.

Clayton, W. D., & Renvoize, S. A. (1986). Genera graminum. Grasses of the world. *Kew Bulletin, Additional Series*, *13*, 1–389.

Cleary, A. L., & Hardham, A. R. (1989). Microtubule organization during development of stomatal complexes in *Lolium rigidum*. *Protoplasma, 149*(2), 67–81.

Condon, A. G., Reynolds, M. P., Rebetzke, G. J., Ginkel, M. van, Richards, R. A., & Farquhar, G. D. (2007). Using Stomatal Aperture-Related Traits to Select for High Yield Potential in Bread Wheat. In H. T. Buck, J. E. Nisi, & N. Salomón (Eds.), *Wheat Production in Stressed Environments* (pp. 617–624). Springer Netherlands.

Condon, A. G., Richards, R. A., Rebetzke, G. J., & Farquhar, G. D. (2004). Breeding for high water-use efficiency. *Journal of Experimental Botany*, *55*(407), 2447–2460.

Conklin, P. A., Strable, J., Li, S., & Scanlon, M. J. (2019). On the mechanisms of development in monocot and eudicot leaves. *New Phytologist*, *221*(2), 706–724.

Cowan, I., & Farquhar, G. (1977). Stomatal function in relation to leaf metabolism and environment. *Symp. Soc. Exp. Biol.*, *31*, 471–505.

Cui, H., Kong, D., Liu, X., & Hao, Y. (2014). SCARECROW, SCR-LIKE 23 and SHORT-ROOT control bundle sheath cell fate and function in rabidopsis thaliana. *The Plant Journal*, *78*(2), 319–327.

de Boer, H. J., Price, C. A., Wagner-Cremer, F., Dekker, S. C., Franks, P. J., & Veneklaas, E. J. (2016). Optimal allocation of leaf pavement area for gas exchange. *New Phytologist*, *210*(4), 1219–1228.

Deans, R. M., Brodribb, T. J., Busch, F. A., & Farquhar, G. D. (2019). Plant water-use strategy mediates stomatal effects on the light induction of photosynthesis. *New Phytologist*, *222*(1), 382–395.

Debernardi, J. M., Mecchia, M. A., Vercruyssen, L., Smaczniak, C., Kaufmann, K., Inze, D., Rodriguez, R. E., & Palatnik, J. F. (2014). Post-transcriptional control of GRF transcription factors by microRNA miR396 and GIF co-activator affects leaf size and longevity. *Plant Journal, 79*(3), 413–426.

Debernardi, J. M., Rodriguez, R. E., Mecchia, M. A., & Palatnik, J. F. (2012). Functional specialization of the plant miR396 regulatory network through distinct microRNA-target interactions. *PLoS Genetics, 8*(1).

Debernardi, J. M., Tricoli, D. M., Ercoli, M. F., Hayta, S., Ronald, P., Palatnik, J. F., & Dubcovsky, J. (2020). A GRF–GIF chimeric protein improves the regeneration efficiency of transgenic plants. *Nature Biotechnology*, *38*(11), 1274–1279.

Demirci, Y., Zhang, B., & Unver, T. (2018). CRISPR/Cas9: An RNA-guided highly precise synthetic tool for plant genome editing. *Journal of Cellular Physiology, 233(3),* 1844–1859.

Dhondt, S., Vanhaeren, H., van Loo, D., Cnudde, V., & Inzé, D. (2010). Plant structure visualization by high-resolution X-ray computed tomography. *Trends in Plant Science*, *15*(8), 419–422.

Diel, E. E., Lichtman, J. W., & Richardson, D. S. (2020). Tutorial: avoiding and correcting sample-induced spherical aberration artifacts in 3D fluorescence microscopy. *Nature Protocols*, *15*(9), 2773–2784.

Doheny-Adams, T., Hunt, L., Franks, P. J., Beerling, D. J., & Gray, J. E. (2012). Genetic manipulation of stomatal density influences stomatal size, plant growth and tolerance to restricted water supply across a growth carbon dioxide gradient. *Philosophical Transactions of the Royal Society B: Biological Sciences*, *367*(1588), 547–555.

Dorofeev V. F., Filatenko A. A., Migushova E. F., Udaczin R. A., and Jakubziner M. M. (1979). Wheat. vol. 1. In: Flora of Cultivated Plants (Dorofeev VF and Korovina ON, Eds.) Leningrad (St. Petersburg), Russia. Kolos (in Russian). 346 pp.

Dow, G. A., & Bergmann, D. (2014). Patterning and processes: how stomatal development defines physiological potential. *Current Opinion in Plant Biology*, *21*, 67–74.

Dow, G. J. B., Bergmann, D. C., & Berry, J. A. (2014). An integrated model of stomatal development and leaf physiology. *The New Phytologist*, *201*(4), 1218–1226.

Dow, G. J., Berry, J. A., & Bergmann, D. C. (2017). Disruption of stomatal lineage signalling or transcriptional regulators has differential effects on mesophyll development, but maintains coordination of gas exchange. *The New Phytologist*, *216*(1), 69–75.

Drake, P. L., Froend, R. H., & Franks, P. J. (2013). Smaller, faster stomata: scaling of stomatal size, rate of response, and stomatal conductance. *Journal of Experimental Botany*, *64*(2), 495–505.

Driesen, E., van den Ende, W., de Proft, M., & Saeys, W. (2020). Influence of Environmental Factors Light, CO_2, Temperature, and Relative Humidity on Stomatal Opening and Development: A Review. *Agronomy*, *10*(12), 1975.

Driever, S. M., Lawson, T., Andralojc, P. J., Raines, C. A., & Parry, M. A. J. (2014). Natural variation in photosynthetic capacity, growth, and yield in 64 field-grown wheat genotypes. *Journal of Experimental Botany*, *65*(17), 4959–4973.

Duan, P., Ni, S., Wang, J., Zhang, B., Xu, R., Wang, Y., Chen, H., Zhu, X., & Li, Y. (2015). Regulation of OsGRF4 by OsmiR396 controls grain size and yield in rice. *Nature Plants, 2*(1), 1–5.

Dunn, J., Hunt, L., Afsharinafar, M., Meselmani, M. al, Mitchell, A., Howells, R., Wallington, E., Fleming, A. J., & Gray, J. E. (2019). Reduced stomatal density in bread wheat leads to increased water-use efficiency. Journal of Experimental Botany, 70(18), 4737–4747.

Durney, C. H., Wilson, M. J., McGregor, S., Armand, J., Smith, R. S., Gray, J. E., Morris, R. J., & Fleming, A. J. (2023). Grasses exploit geometry to achieve improved guard cell dynamics. *Current Biology*.

Dvorak, J., Akhunov, E. D., Akhunov, A. R., Deal, K. R., & Luo, M.-C. (2006). Molecular Characterization of a Diagnostic DNA Marker for Domesticated Tetraploid Wheat Provides Evidence for Gene Flow from Wild Tetraploid Wheat to Hexaploid Wheat. *Molecular Biology and Evolution*, *23*(7), 1386–1396.

Dvorak, J., Deal, K. R., Luo, M.-C., You, F. M., von Borstel, K., & Dehghani, H. (2012). The Origin of Spelt and Free-Threshing Hexaploid Wheat. *Journal of Heredity*, *103*(3), 426–441.

Dvorak, J., Luo, M. C., & Akhunov, E. D. (2011). NI Vavilov's theory of centres of diversity in the light of current understanding of wheat diversity, domestication and evolution. . *Czech Journal of Genetics and Plant Breeding, 47*(Special), S20-S27.

Dvorak, J., Luo, M.-C., & Yang, Z.-L. (1998). Restriction Fragment Length Polymorphism and Divergence in the Genomic Regions of High and Low Recombination in Self-Fertilizing and Cross-Fertilizing Aegilops Species. *Genetics*, *148*(1), 423–434.

Earles, J. M., Buckley, T. N., Brodersen, C. R., Busch, F. A., Cano, F. J., Choat, B., Evans, J. R., Farquhar, G. D., Harwood, R., Huynh, M., John, G. P., Miller, M. L., Rockwell, F. E., Sack, L., Scoffoni, C., Struik, P. C., Wu, A., Yin, X., & Barbour, M. M. (2019). Embracing 3D Complexity in Leaf Carbon–Water Exchange. *Trends in Plant Science*, *24*(1), 15–24.

Earles, J. M., Theroux-Rancourt, G., Roddy, A. B., Gilbert, M. E., McElrone, A. J., & Brodersen, C. R. (2018). Beyond Porosity: 3D Leaf Intercellular Airspace Traits That Impact Mesophyll Conductance. *Plant Physiology*, *178*(1), 148–162.

Edwards, G., & Walker, D. (1983). C3, C4: mechanisms, and cellular and environmental regulation, of photosynthesis. Univ of California Press.

Elliott-Kingston, C., Haworth, M., Yearsley, J. M., Batke, S. P., Lawson, T., & McElwain, J. C. (2016). Does Size Matter? Atmospheric CO_2 May Be a Stronger Driver of Stomatal Closing Rate Than Stomatal Size in Taxa That Diversified under Low CO_2. *Frontiers in Plant Science*, *7*.

Endo, H., & Torii, K. U. (2019). Stomatal Development and Perspectives toward Agricultural Improvement. *Cold Spring Harbor Perspectives in Biology, 11*(5), a034660.

Evans, J. R., Kaldenhoff, R., Genty, B., & Terashima, I. (2009). Resistances along the CO_2 diffusion pathway inside leaves. *Journal of Experimental Botany*, *60*(8), 2235–2248.

Evans, J., & Santiago, L. (2014). PrometheusWiki Gold Leaf Protocol: gas exchange using LI-COR 6800. *Functional Plant Biology*, *41*, 223–226.

Facette, M. R., & Smith, L. G. (2012). Division polarity in developing stomata. *Current Opinion in Plant Biology*, *15*(6), 585–592.

FAO (2024) *The State of Food Security and Nutrition in the World 2024*. FAO; IFAD; UNICEF; WFP; WHO.

Faralli, M., Cockram, J., Ober, E., Wall, S., Galle, A., van Rie, J., Raines, C., Lawson, T., & A. (2019a). Genotypic, Developmental and Environmental Effects on the Rapidity of gs in Wheat: Impacts on Carbon Gain and Water-Use Efficiency. *Frontiers in Plant Science*, *10*.

Faralli, M., Matthews, J., Lawson, T., & B. (2019b). Exploiting natural variation and genetic manipulation of stomatal conductance for crop improvement. *Current Opinion in Plant Biology*, *49*, 1–7.

Farquhar, G. D., & Sharkey, T. D. (1982). Stomatal Conductance and Photosynthesis. *Review of Plant Physiology*, *33*(1), 317–345.

Farquhar, G., & Richards, R. (1984). Isotopic Composition of Plant Carbon Correlates With Water-Use Efficiency of Wheat Genotypes. *Functional Plant Biology*, *11*(6), 539.

Feldman, M., & Kislev, M. E. (2007). Domestication of emmer wheat and evolution of free-threshing tetraploid wheat. *Israel Journal of Plant Sciences*, *55*(3–4), 207–221.

Feldman, L. A., Segarra-Moragues, J. G., Müller, J., Peterson, P. M., & Catalán, P. (2008). Dated historical biogeography of the temperate Loliinae (Poaceae, Pooideae) grasses in the northern and southern hemispheres. *Molecular Phylogenetics and Evolution*, *46*(3), 932–957.

Fischer, R. A., Rees, D., Sayre, K. D., Lu, Z. M., Condon, A. G., & Larque Saavedra, A. (1998). Wheat yield progress associated with higher stomatal conductance and photosynthetic rate, and cooler canopies. *Crop Science*, *38*(6), 1467–1475.

Fleury, D., Jefferies, S., Kuchel, H., & Langridge, P. (2010). Genetic and genomic tools to improve drought tolerance in wheat. *J. Exp. Bot*, *61*(12), 3211–3222.

Flexas, J., Ribas-Carbó M., Diaz-Espejo, A., Galmés, J. & Medrano, H. (2008). Mesophyll conductance to CO_2: current knowledge and future prospects. *Plant, Cell & Environment*, *31*(5), 602–621.

Flexas, J., Barbour, M. M., Brendel, O., Cabrera, H. M., Carriquí, M., Diaz-Espejo, A., Douthe, C., Dreyer, E., Ferrio, J. P., Gago, J., Gallé, A., Galmes, J., Kodama, N., Medrano, H., Niinemets, U., Peguero-Pina, J. J., Pou, P., Ribas- Carbo, M., Tomas, M., … Warren, C. R. (2012). Mesophyll diffusion conductance to CO_2: an unappreciated central player in photosynthesis. *Plant Science*, *193–194*, 70–84.

Flexas, J., & Carriquí, M. (2020). Photosynthesis and photosynthetic efficiencies along the terrestrial plant's phylogeny: lessons for improving crop photosynthesis. *The Plant Journal*, *101*(4), 964–978.

Flexas, J., Díaz-Espejo, A., Conesa, M. A., Coopman, R. E., Douthe, C., Gago, J., Gallé, A., Galmés, J., Medrano, H., Ribas-Carbo, M., Tomàs, M., & Niinemets, Ü. (2016). Mesophyll conductance to CO $_2$ and Rubisco as targets for improving intrinsic water use efficiency in C $_3$ plants. *Plant, Cell & Environment*, *39*(5), 965–982.

Flexas, J., Scoffoni, C., Gago, J., & Sack, L. (2013). Leaf mesophyll conductance and leaf hydraulic conductance: an introduction to their measurement and coordination. *Journal of Experimental Botany*, *64*(13), 3965–3981.

Franks, P., & Farquhar, G. (1999). A relationship between humidity response, growth form and photosynthetic operating point in C3 plants. *Plant, Cell & Environment*, *22*, 1337–13149.

Franks, P. J., & Beerling, D. J. (2009). Maximum leaf conductance driven by CO_2 effects on stomatal size and density over geologic time. *Proceedings of the National Academy of Sciences*, *106*(25), 10343–10347.

Franks, P. J., & Farquhar, G. D. (2007). The Mechanical Diversity of Stomata and Its Significance in Gas-Exchange Control. *Plant Physiology*, *143*(1), 78–87.

Franks, P. J., W. Doheny-Adams, T., Britton-Harper, Z. J., & Gray, J. E. (2015). Increasing water-use efficiency directly through genetic manipulation of stomatal density. *New Phytologist*, *207*(1), 188–195.

Gaju, O., DeSilva, J., Carvalho, P., Hawkesford, M. J., Griffiths, S., Greenland, A., & Foulkes, M. J. (2016). Leaf photosynthesis and associations with grain yield, biomass and nitrogen-use efficiency in landraces, synthetic-derived lines and cultivars in wheat. *Field Crops Research*, *193*, 1–15.

Galatis, B. (1988). Microtubules and epithem-cell morphogenesis in hydathodes of Pilea cadierei. *Planta*, *176*(3), 287–297.

Gil-Humanes, J., Wang, Y., Liang, Z., Shan, Q., Ozuna, C. v, Sánchez-León, S., Baltes, N. J., Starker, C., Barro, F., Gao, C., & Voytas, D. F. (2017). High-efficiency gene targeting in hexaploid wheat using DNA replicons and CRISPR/Cas9. *The Plant Journal, 89(6),* 1251–1262.

Gilbert, M. E., Zwieniecki, M. A., & Holbrook, N. M. (2011). Independent variation in photosynthetic capacity and stomatal conductance leads to differences in intrinsic water use efficiency in 11 soybean genotypes before and during mild drought. *Journal of Experimental Botany*, *62*(8), 2875–2887.

Gommes, C. J., Bons, A.-J., Blacher, S., Dunsmuir, J. H., & Tsou, A. H. (2009). Practical methods for measuring the tortuosity of porous materials from binary or gray-tone tomographic reconstructions. *AIChE Journal*, *55*(8), 2000–2012.

Govaerts, Y. M., Jacquemoud, S., Verstraete, M. M., & Ustin, S. L. (1996). Three-dimensional radiation transfer modeling in a dicotyledon leaf. *Applied Optics*, *35*(33), 6585–6598.

Griffiths, H., & Males, J. (2017). Succulent plants. *Current Biology*, *27*(17), R890–R896.

Guerrieri, R., Belmecheri, S., Ollinger, S. v., Asbjornsen, H., Jennings, K., Xiao, J., Stocker, B. D., Martin, M., Hollinger, D. Y., Bracho-Garrillo, R., Clark, K., Dore, S., Kolb, T., Munger, J. W., Novick, K., & Richardson, A. D. (2019). Disentangling the role of photosynthesis and stomatal conductance on rising forest water-use efficiency. *Proceedings of the National Academy of Sciences*, *116*(34), 16909–16914.

Giuliani, R., Koteyeva, N., Voznesenskaya, E., Evans, M. A., Cousins, A. B., & Edwards, G. E. (2013). Coordination of Leaf Photosynthesis, Transpiration, and Structural Traits in Rice and Wild Relatives (Genus Oryza) . *Plant Physiology*, *162*(3), 1632–1651.

Hamada, H., Linghu, Q., Nagira, Y., Miki, R., Taoka, N., & Imai, R. (2017). An in planta biolistic method for stable wheat transformation. *Scientific Reports*, *7*(1), 11443.

Hamada, H., Liu, Y., Nagira, Y., Miki, R., Taoka, N., & Imai, R. (2018). Biolistic-delivery-based transient CRISPR/Cas9 expression enables in planta genome editing in wheat. *Scientific Reports*, *8*(1), 14422.

Harrison, E. L., Arce Cubas, L., Gray, J. E., & Hepworth, C. (2020). The influence of stomatal morphology and distribution on photosynthetic gas exchange. *The Plant Journal*, *101*(4), 768–779.

Harwood, R., Goodman, E., Gudmundsdottir, M., Huynh, M., Musulin, Q., Song, M., & Barbour, M. M. (2020). Cell and chloroplast anatomical features are poorly estimated from 2D cross-sections. *New Phytologist*, *225*(6), 2567–2578.

Hatch, M. D. (1987). C4 photosynthesis: a unique elend of modified biochemistry, anatomy and ultrastructure. *Biochimica et Biophysica Acta (BBA) - Reviews on Bioenergetics, 895*(2), 81–106.

Hatfield, J. L., & Dold, C. (2019). Water-use efficiency: advances and challenges in a changing climate. *Frontiers in Plant Science*, *10*, 103.

Hayta, S., Smedley, M. A., Demir, S. U., Blundell, R., Hinchliffe, A., Atkinson, N., & Harwood, W. A. (2019). An efficient and reproducible Agrobacterium-mediated transformation method for hexaploid wheat (Triticum aestivum L.). *Plant Methods*, *15*(1), 121.

He, X., Qu, B., Li, W., Zhao, X., Teng, W., Ma, W., Ren, Y., Li, B., Li, Z., & Tong, Y. (2015). The Nitrate-Inducible NAC Transcription Factor TaNAC2-5A Controls Nitrate Response and Increases Wheat Yield, *Plant Physiology*, *169*(3), 1991–2005.

He, Z., Zeng, J., Ren, Y., Chen, D., Li, W., Gao, F., Cao, Y., Luo, T., Yuan, G., Wu, X., Liang, Y., Deng, Q., Wang, S., Zheng, A., Zhu, J., Liu, H., Wang, L., Li, P., & Li, S. (2017). OsGIF1 Positively Regulates the Sizes of Stems, Leaves, and Grains in Rice. *Frontiers in Plant Science*, *8*.

Heckwolf, M., Pater, D., Hanson, D. T., & Kaldenhoff, R. (2011). The *Arabidopsis thaliana* aquaporin AtPIP1;2 is a physiologically relevant CO_2 transport facilitator. *The Plant Journal, 67*(5), 795–804.

Hepler, P. K., & Gunning, B. E. S. (1998). Confocal fluorescence microscopy of plant cells. *Protoplasma*, *201*(3), 121–157.

Hepworth, C., Caine, R. S., Harrison, E. L., Sloan, J., & Gray, J. E. (2018). Stomatal development: focusing on the grasses. *Current Opinion in Plant Biology*, 41(1), 1–7

Hepworth, C., Doheny-Adams, T., Hunt, L., Cameron, D. D., & Gray, J. E. (2015). Manipulating stomatal density enhances drought tolerance without deleterious effect on nutrient uptake. *New Phytologist*, *208*(2), 336–341.

Hetherington, A. M., & Woodward, F. I. (2003). The role of stomata in sensing and driving environmental change. *Nature*, *424*, 901–908.

Heun, M., Schäfer-Pregl, R., Klawan, D., Castagna, R., Accerbi, M., Borghi, B., & Salamini, F. (1997). Site of Einkorn Wheat Domestication Identified by DNA Fingerprinting. *Science*, *278*(5341), 1312–1314.

Ho, Q. T., Berghuijs, H. N. C., Watté, R., Verboven, P., Herremans, E., Yin, X., Retta, M. A., Aernouts, B., Saeys, W., Helfen, L., Farquhar, G. D., Struik, P. C., & Nicolaï, B. M. (2016). Three-dimensional microscale modelling of CO_2 transport and light propagation in tomato leaves enlightens photosynthesis. *Plant, Cell & Environment*, *39*(1), 50–61.

Hoekstra, A., & Mekonnen, M. (2012). The water footprint of humanity. *Proceedings of the National Academy of Sciences*, *109*, 3232–3237.

Hong, Y., Chen, L., Du, L., Su, Z., Wang, J., Ye, X., Qi, L., & Zhang, Z. (2014). Transcript suppression of TaGW2 increased grain width and weight in bread wheat. *Functional & Integrative Genomics*, *14*(2), 341–349.

Horiguchi, G., Kim, G. T., & Tsukaya, H. (2005). The transcription factor AtGRF5 and the transcription coactivator AN3 regulate cell proliferation in leaf primordia of *Arabidopsis thaliana. Plant Journal, 43*(1), 68–78.

Howells, R. M., Craze, M., Bowden, S., & Wallington, E. J. (2018). Efficient generation of stable, heritable gene edits in wheat using CRISPR/Cas9. *BMC Plant Biology, 18(1),* 215.

Hu, J., Wang, Y., Fang, Y., Zeng, L., Xu, J., Yu, H., Shi, Z., Pan, J., Zhang, D., Kang, S., Zhu, L., Dong, G., Guo, L., Zeng, D., Zhang, G., Xie, L., Xiong, G., Li, J., & Qian, Q. (2015). A Rare Allele of GS2 Enhances Grain Size and Grain Yield in Rice. *Molecular Plant, 8*(10), 1455–1465.

Hu, L., Li, Y., Xu, W., Zhang, Q., Zhang, L., Qi, X., & Dong, H. (2012). Improvement of the photosynthetic characteristics of transgenic wheat plants by transformation with the maize C4 phosphoenolpyruvate carboxylase gene. *Plant Breeding*, *131*(3), 385–391.

Hu, M., Zhao, X., Liu, Q., Hong, X., Zhang, W., Zhang, Y., Sun, L., Li, H., & Tong, Y. (2018). Transgenic expression of plastidic glutamine synthetase increases nitrogen uptake and yield in wheat. *Plant Biotechnology Journal*, *16*.

Hu, J., Zheng, Q., Dong, C., Liang, Z., Tian, Z., & Dai, T. (2023a). Enhanced Stomatal Conductance Supports Photosynthesis in Wheat to Improved NH4+ Tolerance. *Plants*, *13*(1), 86.

Hu, Q., Jiang, B., Wang, L., Song, Y., Tang, X., Zhao, Y., Fan, X., Gu, Y., Zheng, Q., Cheng, J., & Zhang, H. (2023b). Genome-wide analysis of growth-regulating factor genes in grape (Vitis vinifera L.): identification, characterization and their responsive expression to osmotic stress. *Plant Cell Reports*, *42*(1), 107–121.

Hubbart, S., Peng, S., Horton, P., Chen, Y., & Murchie, E. H. (2007). Trends in leaf photosynthesis in historical rice varieties developed in the Philippines since 1966. *Journal of Experimental Botany*, *58*(12), 3429–3438.

Hughes, J., Hepworth, C., Dutton, C., Dunn, J. A., Hunt, L., Stephens, J., Waugh, R., Cameron, D. D., & Gray, J. E. (2017). Reducing Stomatal Density in Barley Improves Drought Tolerance without Impacting on Yield. *Plant Physiology*, *174*(2), 776–787.

Hutzler, P., Fischbach, R., Heller, W., Jungblut, T. P., Reuber, S., Schmitz, R., Veit, M., Weissenböck, G., & Schnitzler, J.-P. (1998). Tissue localization of phenolic compounds in plants by confocal laser scanning microscopy. *Journal of Experimental Botany*, *49*(323), 953–965.

Ihsan, M. Z., El-Nakhlawy, F. S., Ismail, S. M., Fahad, S., & Daur, I. (2016). Wheat Phenological Development and Growth Studies As Affected by Drought and Late Season High Temperature Stress under Arid Environment. *Front. Plant Sci*, *7*(795).

Isidro, J., Álvaro, F., Royo, C., Villegas, D., Miralles, D. J., & García del Moral, L. F. (2011). Changes in duration of developmental phases of durum wheat caused by breeding in Spain and Italy during the 20th century and its impact on yield. *Annals of Botany*, *107*(8), 1355–1366.

Iuchi, S., Kobayashi, M., Taji, T., Naramoto, M., Seki, M., Kato, T., Tabata, S., Kakubari, Y., Yamaguchi-Shinozaki, K., & Shinozaki, K. (2001). Regulation of drought tolerance by gene manipulation of 9-cis-epoxycarotenoid dioxygenase, a key enzyme in abscisic acid biosynthesis in Arabidopsis. *The Plant Journal*, *27*(4), 325–333.

Ivanova, L. A., & P'yankov, V. I. (2002). Structural Adaptation of the Leaf Mesophyll to Shading. *Russian Journal of Plant Physiology*, *49*(3), 419–431.

Jahan, E., Amthor, J. S., Farquhar, G. D., Trethowan, R., & Barbour, M. M. (2014). Variation in mesophyll conductance among Australian wheat genotypes. *Functional Plant Biology*, *41*(6), 568.

Jellings, A., & Leech, R. (1984). Anatomical Variation in First Leaves of Nine Tritucum Genotypes and Its Relationship To Photosynthetic Capacity. *New Phytologist*, *96*, 371–382.

Jinek, M., Chylinski, K., Fonfara, I., Hauer, M., Doudna, J. A., & Charpentier, E. (2012). A Programmable Dual-RNA–Guided DNA Endonuclease in Adaptive Bacterial Immunity. *Science, 337(6096),* 816–821.

Johnson, G., & Murchie, E. (2011). Gas Exchange Measurements for the Determination of Photosynthetic Efficiency in Arabidopsis Leaves. *Methods in Molecular Biology (Clifton, N.J.)*, *775*, 311–326.

Jones, M., Turner, N., & Osmond, C. (1981). Mechanisms of drought resistance. The Physiology and Biochemistry of Drought Resistance in Plants, 1, 15–37.

Jung, G., & Wernicke, W. (1990). Cell shaping and microtubules in developing mesophyll of wheat (*Triticum aestivum* L.). *Protoplasma*, *153*, 141–148.

Kaldenhoff, R. (2012). Mechanisms underlying CO_2 diffusion in leaves. *Current Opinion in Plant Biology*, *15*(3), 276–281.

Kalve, S., de Vos, D., & Beemster, G. T. S. (2014). Leaf development: a cellular perspective. *Frontiers in Plant Science*, *5*.

Karaba, A., Dixit, S., Greco, R., Aharoni, A., Trijatmiko, K., Marsch-Martinez, N., Krishnan, A., Nataraja, K., Udayakumar, M., & Pereira, A. (2007). Improvement of water use efficiency in rice by expression of HARDY, an Arabidopsis drought and salt tolerance gene. *Proceedings of the National Academy of Sciences of the United States of America*, *104*, 15270–15275.

Kardiman, R., & Ræbild, A. (2018). Relationship between stomatal density, size and speed of opening in Sumatran rainforest species. *Tree Physiology*, *38*(5), 696–705.

Katagiri, Y., Hasegawa, J., Fujikura, U., Hoshino, R., Matsunaga, S., & Tsukaya, H. (2016). The coordination of ploidy and cell size differs between cell layers in leaves. *Development, 143*(7), 1120–1125.

Khazaei, H., Monneveux, P., Hongbo, S., & Mohammady, S. (2010). Variation for stomatal characteristics and water use efficiency among diploid, tetraploid and hexaploid Iranian wheat landraces. *Genetic Resources and Crop Evolution*, *57*(2), 307–314.

Kilian, B., Özkan, H., Deusch, O., Effgen, S., Brandolini, A., Kohl, J., Martin, W., & Salamini, F. (2007). Independent Wheat B and G Genome Origins in Outcrossing Aegilops Progenitor Haplotypes. *Molecular Biology and Evolution*, *24*(1), 217–227.

Kilian, B., Özkan, H., Pozzi, C., & Salamini, F. (2009). Domestication of the Triticeae in the Fertile Crescent. In *Genetics and Genomics of the Triticeae* (pp. 81–119). Springer US.

Kim, J. H. (2019). Biological roles and an evolutionary sketch of the GRF-GIF transcriptional complex in plants. *BMB Reports*, *52*(4), 227–238.

Kim, J. H., Choi, D., & Kende, H. (2003). The AtGRF family of putative transcription factors is involved in leaf and cotyledon growth in Arabidopsis. *Plant Journal, 36*(1), 94–104.

Kim, J. H., & Kende, H. (2004). A transcriptional coactivator, AtGIF1, is involved in regulating leaf growth and morphology in Arabidopsis. *Proceedings of the National Academy of Sciences, 101*(36), 13374–13379.

Kim, J. H., & Lee, B. H. (2006). GROWTH-REGULATING FACTOR4 of *Arabidopsis thaliana* is required for development of leaves, cotyledons, and shoot apical meristem. *Journal of Plant Biology, 49*(6), 463–468.

Kim, J. H., & Tsukaya, H. (2015). Regulation of plant growth and development by the GROWTH-REGULATING FACTOR and GRF-INTERACTING FACTOR duo. *Journal of Experimental Botany*, *66*(20), 6093–6107.

Kislev, M. E., Nadel, D., & Carmi, I. (1992). Epipalaeolithic (19,000 BP) cereal and fruit diet at Ohalo II, Sea of Galilee, Israel. *Review of Palaeobotany and Palynology*, *73*(1), 161–166.

Klein, M., Perfus-Barbeoch, L., Frelet, A., Gaedeke, N., Reinhardt, D., Mueller-Roeber, B., Martinoia, E., & Forestier, C. (2003). The plant multidrug resistance ABC transporter AtMRP5 is involved in guard cell hormonal signalling and water use. *The Plant Journal*, *33*(1), 119–129.

Kondo, T., Kajita, R., Miyazaki, A., Hokoyama, M., Nakamura-Miura, T., Mizuno, S., Masuda, Y., Irie, K., Tanaka, Y., Takada, S., & et al. (2010). Stomatal density is controlled by a mesophyll-derived signaling molecule. *Plant and Cell Physiology*, *51*, 1–8.

Kondorosi, E., Roudier, F., & Gendreau, E. (2000). Plant cell-size control: growing by ploidy? *Current Opinion in Plant Biology, 3(*6), 488–492.

Lawson, T., & Blatt, M. R. (2014). Stomatal Size, Speed, and Responsiveness Impact on Photosynthesis and Water Use Efficiency. *Plant Physiology*, *164*(4), 1556–1570.

Lawson, T., & Vialet-Chabrand, S. (2019). Speedy stomata, photosynthesis and plant water use efficiency. *New Phytologist*, *221*(1), 93–98.

Leakey, A. D. B., Ferguson, J. N., Pignon, C. P., Wu, A., Jin, Z., Hammer, G. L., & Lobell, D. B. (2019). Water Use Efficiency as a Constraint and Target for Improving the Resilience and Productivity of C3 and C4 Crops. In *Annual Review of Plant Biology* (Vol. 70, pp. 781–808). Annual Reviews Inc.

Lee, B. H., Ko, J.-H., Lee, S., Lee, Y., Pak, J.-H., & Kim, J. H. (2009). The Arabidopsis GRF-INTERACTING FACTOR Gene Family Performs an Overlapping Function in Determining Organ Size as Well as Multiple Developmental Properties. *Plant Physiology, 151*(2), 655–668.

Lee, G.-H., Lee, B. H., Jung, J.-H., Lee, S.-J., Mai, T.-T., & Kim, J. H. (2022). Systematic Assessment of the Positive Role of Arabidopsis thaliana GROWTH-REGULATING FACTORs in Regulation of Cell Proliferation During Leaf Growth. *Journal of Plant Biology*, *65*(5), 413–422.

Lee, J., Hnilova, M., Maes, M., Lin, Y.-C., Putarjunan, A., Han, S.-K., Avila, J., & Torii, K. (2015). Competitive binding of antagonistic peptides fine-tunes stomatal patterning. *Nature*, *522*, 439–443.

Lee, W. S., Hammond-Kosack, K. E., & Kanyuka, K. (2012). Barley Stripe Mosaic Virus-Mediated Tools for Investigating Gene Function in Cereal Plants and Their Pathogens: Virus-Induced Gene Silencing, Host-Mediated Gene Silencing, and Virus-Mediated Overexpression of Heterologous Protein. *Plant Physiology*, *160*(2), 582–590.

Lehmann, P., & Or, D. (2015). Effects of stomata clustering on leaf gas exchange. *New Phytologist*, *207*(4), 1015–1025.

Lehmeier, C., Pajor, R., Lundgren, M. R., Mathers, A., Sloan, J., Bauch, M., Mitchell, A., Bellasio, C., Green, A., Bouyer, D., Schnittger, A., Sturrock, C., Osborne, C. P., Rolfe, S., Mooney, S., & Fleming, A. J. (2017). Cell density and airspace patterning in the leaf can be manipulated to increase leaf photosynthetic capacity. *Plant Journal*, *92*(6), 981–994.

Levesque, M. P., Vernoux, T., Busch, W., Cui, H., Wang, J. Y., Blilou, I., Hassan, H., Nakajima, K., Matsumoto, N., Lohmann, J. U., Scheres, B., & Benfey, P. N. (2006). Whole-Genome Analysis of the SHORT-ROOT Developmental Pathway in Arabidopsis. *PLOS Biology*, *4*(5), e143-.

Levitt, J. (1980). Responses of plants to environmental stresses. Volume II. Water, Radiation, Salt, and Other Stresses. (Academic Press).

Li, C., Zong, Y., Wang, Y., Jin, S., Zhang, D., Song, Q., Zhang, R., & Gao, C. (2018b). Expanded base editing in rice and wheat using a Cas9-adenosine deaminase fusion. *Genome Biology*, *19*(1), 59.

Li, J. R., Zhao, W., Li, Q. Z., Ye, X. G., An, B. Y., Li, X., & Zhang, X. S. (2005). RNA silencing of Waxy gene results in low levels of amylose in the seeds of transgenic wheat (Triticum aestivum L.). *Yi chuan xue bao = Acta genetica Sinica*, *32*(8), 846–854.

Li, Y., Song, G., Gao, J., Zhang, S., Zhang, R., Li, W., Chen, M., Liu, M., Xia, X., Risacher, T., & Li, G. (2018a). Enhancement of grain number per spike by RNA interference of cytokinin oxidase 2 gene in bread wheat. *Hereditas*, *155*(1), 33.

Li, Y., Wang, Q., Li, X., Xiao, X., Sun, F., Wang, C., Hu, W., Feng, Z., Chang, J., Chen, M., Wang, Y., Li, K., Yang, G., & He, G. (2012). Coexpression of the High Molecular Weight Glutenin Subunit 1Ax1 and Puroindoline Improves Dough Mixing Properties in Durum Wheat (Triticum turgidum L. ssp. durum). *PLOS ONE*, *7*(11), e50057.

Liang, Z., Chen, K., Li, T., Zhang, Y., Wang, Y., Zhao, Q., Liu, J., Zhang, H., Liu, C., Ran, Y., & Gao, C. (2017). Efficient DNA-free genome editing of bread wheat using CRISPR/Cas9 ribonucleoprotein complexes. *Nature Communications*, *8*(1), 14261.

Liang, Z., Chen, K., Yan, Y., Zhang, Y., & Gao, C. (2018). Genotyping genome-edited mutations in plants using CRISPR ribonucleoprotein complexes. *Plant Biotechnology Journal*, *16*(12), 2053–2062.

Liu, G., Wu, Y., Xu, M., Gao, T., Wang, P., Wang, L., Guo, T., & Kang, G. (2016). Virus-Induced Gene Silencing Identifies an Important Role of the TaRSR1 Transcription Factor in Starch Synthesis in Bread Wheat. *International Journal of Molecular Sciences*, *17*, 1557.

Liu, T., Ohashi-Ito, K., & Bergmann, D. C. (2009). Orthologs of Arabidopsis thaliana stomatal bHLH genes and regulation of stomatal development in grasses. *Development (Cambridge, England)*, *136*(13), 2265–2276.

Liu, W., Zhou, Y., Li, X., Wang, X., Dong, Y., Wang, N., Liu, X., Chen, H., Yao, N., Cui, X., Jameel, A., Wang, F., & Li, H. (2017). Tissue-Specific Regulation of Gma-miR396 Family on Coordinating Development and Low Water Availability Responses. *Frontiers in Plant Science*, *8*.

Lobell, D. B., Schlenker, W., & Costa-Roberts, J. (2011). Climate Trends and Global Crop Production Since 1980. *Science*, *333*(6042), 616–620.

Long, S. P., & Bernacchi, C. J. (2003). Gas exchange measurements, what can they tell us about the underlying limitations to photosynthesis? Procedures and sources of error. *Journal of Experimental Botany*, *54*(392), 2393–2401.

Lucrecia-Alvarez, M., Gómez, M., María Carrillo, J., & Vallejos, R. H. (2001). Analysis of dough functionality of flours from transgenic wheat. *Molecular Breeding*, *8*(1), 103–108.

Lundgren, M., & Fleming, A. (2020). Cellular perspectives for improving mesophyll conductance. *The Plant Journal*, *101*, 845–857.

Lundgren, M. R., Mathers, A., Baillie, A. L., Dunn, J., Wilson, M. J., Hunt, L., Pajor, R., Fradera-Soler, M., Rolfe, S., Osborne, C. P., Sturrock, C. J., Gray, J. E., Mooney, S. J., & Fleming, A. J. (2019). Mesophyll porosity is modulated by the presence of functional stomata. *Nature Communications*, *10*(1), 2825.

Lundgren, M. R., Osborne, C. P., & Christin, P.-A. (2014). Deconstructing Kranz anatomy to understand C4 evolution. *Journal of Experimental Botany, 65*(13), 3357–3369.

Maccaferri, M., Harris, N. S., Twardziok, S. O., Pasam, R. K., Gundlach, H., Spannagl, M., Ormanbekova, D., Lux, T., Prade, V. M., Milner, S. G., Himmelbach, A., Mascher, M., Bagnaresi, P., Faccioli, P., Cozzi, P., Lauria, M., Lazzari, B., Stella, A., Manconi, A., … Cattivelli, L. (2019).

Durum wheat genome highlights past domestication signatures and future improvement targets. *Nature Genetics*, *51*(5), 885–895.

Males, J. (2016). Think tank: water relations of Bromeliaceae in their evolutionary context. *Botanical Journal of the Linnean Society*, *181*(3), 415–440.

Mali, P., Esvelt, K. M., & Church, G. M. (2013). Cas9 as a versatile tool for engineering biology. *Nature Methods, 10(10),* 957–963.

Maosong, L., Chunyan, W., Jiqing, S., Yonggang, C., Xiufen, W., & Yongfeng, W. (2008). Evolutional trends of leaf stomatal and photosynthetic characteristics in wheat evolutions. *Acta Ecologica Sinica*, *28*(11), 5385–5391.

Masle, J., Gilmore, S., & Farquhar, G. (2005). The ERECTA gene regulates plant transpiration efficiency in Arabidopsis. *Nature*, *436*, 866–870.

Mathers, A., Hepworth, C., Baillie, A., Sloan, J., Jones, H., Lundgren, M., Fleming, A., Mooney, S., & Sturrock, C. (2018). Investigating the microstructure of plant leaves in 3D with lab-based X-ray computed tomography. *Plant Methods*, *14*, 99.

Matthews, J. S. A., Vialet-Chabrand, S., & Lawson, T. (2018). Acclimation to Fluctuating Light Impacts the Rapidity of Response and Diurnal Rhythm of Stomatal Conductance. *Plant Physiology*, *176*(3), 1939–1951.

McAusland, L., Vialet-Chabrand, S., Davey, P., Baker, N. R., Brendel, O., & Lawson, T. (2016). Effects of kinetics of light-induced stomatal responses on photosynthesis and water-use efficiency. *New Phytologist*, *211*(4), 1209–1220.

McAusland, L., Smith, K. E., Williams, A., Molero, G., & Murchie, E. H. (2021). Nocturnal stomatal conductance in wheat is growth-stage specific and shows genotypic variation. *New Phytologist*, *232*(1), 162–175.

McElwain, J. C., Yiotis, C., & Lawson, T. (2015). Using modern plant trait relationships between observed and theoretical maximum stomatal conductance and vein density to examine patterns of plant macroevolution. *New Phytologist*, *209*(1), 94–103.

McCann, M. C., & Carpita, N. C. (2008). Designing the deconstruction of plant cell walls. *Current Opinion in Plant Biology*, *11*(3), 314–320.

Miner, G. L., Bauerle, W. L., & Baldocchi, D. D. (2017). Estimating the sensitivity of stomatal conductance to photosynthesis: a review. *Plant, Cell & Environment*, *40*(7), 1214–1238.

Mitchell-Olds, T., & Schmitt, J. (2006). Genetic mechanisms and evolutionary significance of natural variation in Arabidopsis. *Nature*, *441*(7096), 947–952.

Mohammed, U., Caine, R. S., Atkinson, J. A., Harrison, E. L., Wells, D., Chater, C. C., Gray, J. E., Swarup, R., & Murchie, E. H. (2019). Rice plants overexpressing OsEPF1 show reduced stomatal density and increased root cortical aerenchyma formation. *Scientific Reports*, *9*(1).

Momayyezi, M., Borsuk, A. M., Brodersen, C. R., Gilbert, M. E., Théroux-Rancourt, G., Kluepfel, D. A., & McElrone, A. J. (2022). Desiccation of the leaf mesophyll and its implications for CO_2 diffusion and light processing. *Plant, Cell & Environment*, *45*(5), 1362–1381.

Morison, J.I.L. & Lawson, T. (2007). Does lateral gas diffusion in leaves matter? *Plant, Cell & Environment*, *30*(9), 1072–1085.

Morison, J. I. L., Lawson, T., & Cornic, G. (2007). Lateral CO_2 Diffusion inside Dicotyledonous Leaves Can Be Substantial: Quantification in Different Light Intensities. *Plant Physiology*, *145*(3), 680–690.

Morton, A. G. & Watson, D. J. (1948). A Physiological Study of Leaf Growth. *Annals of Botany*, *12*(47), 281–310.

Muszynski, M. G., Moss-Taylor, L., Chudalayandi, S., Cahill, J., del Valle-Echevarria, A. R., Alvarez-Castro, I., Petefish, A., Sakakibara, H., Krivosheev, D. M., Lomin, S. N., Romanov, G. A., Thamotharan, S., Dam, T., Li, B., & Brugière, N. (2020). The Maize Hairy Sheath Frayed1 (Hsf1) Mutation Alters Leaf Patterning through Increased Cytokinin Signalling. *The Plant Cell*, *32*(5), 1501–1518.

Nalam, V. J., Alam, S., Keereetaweep, J., Venables, B., Burdan, D., Lee, H., Trick, H. N., Sarowar, S., Makandar, R., & Shah, J. (2015). Facilitation of Fusarium graminearum Infection by 9-Lipoxygenases in Arabidopsis and Wheat. *Molecular Plant-Microbe Interactions®*, *28*(10), 1142–1152.

Nalam, V. J., Vales, M. I., Watson, C. J. W., Kianian, S. F., & Riera-Lizarazu, O. (2006). Map-based analysis of genes affecting the brittle rachis character in tetraploid wheat (Triticum turgidum L.). *Theoretical and Applied Genetics*, *112*(2), 373–381.

Nelson, E. A., Sage, T. L., & Sage, R. F. (2005). Functional leaf anatomy of plants with crassulacean acid metabolism. *Functional Plant Biology*, *32*(5), 409–419.

Nesbitt, M., & Samuel, D. (1998). Wheat Domestication: Archaeobotanical Evidence. *Science*, *279*(5356), 1431.

Nicotra, A. B., Leigh, A., Boyce, C. K., Jones, C. S., Niklas, K. J., Royer, D. L., & Tsukaya, H. (2011). The evolution and functional significance of leaf shape in the angiosperms. *Functional Plant Biology*, *38*(7), 535–552.

Nobel, P. (1999). *Physicochemical & environmental plant physiology* (2nd ed.). Academic Press.

Nowara, D., Gay, A., Lacomme, C., Shaw, J., Ridout, C., Douchkov, D., Hensel, G., Kumlehn, J., & Schweizer, P. (2010). HIGS: Host-Induced Gene Silencing in the Obligate Biotrophic Fungal Pathogen Blumeria graminis . *The Plant Cell*, *22*(9), 3130–3141.

Nunes, T., Zhang, D., & Raissi, M. (2019). Form, development and function of grass stomata. *The Plant Journal*, *101*, 780–799.

Omasa, K., Konishi, A., Tamura, H., & Hosoi, F. (2009). 3D Confocal Laser Scanning Microscopy for the Analysis of Chlorophyll Fluorescence Parameters of Chloroplasts in Intact Leaf Tissues. *Plant and Cell Physiology*, *50*(1), 90–105.

Omidbakhshfard, M. A., Proost, S., Fujikura, U., & Mueller-Roeber, B. (2015). Growth-Regulating Factors (GRFs): A Small Transcription Factor Family with Important Functions in Plant Biology. *Molecular Plant, 8*(7), 998–1010.

Omidbakhshfard, M. A., Fujikura, U., Olas, J. J., Xue, G.-P., Balazadeh, S., & Mueller-Roeber, B. (2018). GROWTH-REGULATING FACTOR 9 negatively regulates arabidopsis leaf growth by controlling ORG3 and restricting cell proliferation in leaf primordia. *PLOS Genetics*, *14*(7), e1007484-.

Ouyang, W., Struik, P. C., Yin, X., & Yang, J. (2017). Stomatal conductance, mesophyll conductance, and transpiration efficiency in relation to leaf anatomy in rice and wheat genotypes under drought. *Journal of Experimental Botany*, *68*(18), 5191–5205.

Ozeki, K., Miyazawa, Y., & Sugiura, D. (2022). Rapid stomatal closure contributes to higher water use efficiency in major C4 compared to C3 Poaceae crops. *Plant Physiology*, *189*(1)

Özkan, H., Tuna, M., Kilian, B., Mori, N., & Ohta, S. (2010). Genome size variation in diploid and tetraploid wild wheats. *AoB PLANTS*, *2010*.

Paddock, S. W. (2000). Principles and practices of laser scanning confocal microscopy. *Molecular Biotechnology*, *16*(2), 127–149.

Pajor, R., Fleming, A., Osborne, C. P., Rolfe, S. A., Sturrock, C. J., & Mooney, S. J. (2013). Seeing space: visualization and quantification of plant leaf structure using X-ray micro-computed tomography: View Point. *Journal of Experimental Botany*, *64*(2), 385–390.

Palevitz, B. A., & Mullinax, J. B. (1989). Developmental changes in the arrangement of cortical microtubules in stomatal cells of oat (*Avena sativa* L.). *Cell Motility, 13*(3), 170–180.

Pallardy, S. G. (2008). Transpiration and Plant Water Balance. In Physiology of Woody Plants (pp. 325–366). Elsevier.

Panteris, E., Apostolakos, P., & Galatis, B. (1993a). Microtubule organization and cell morphogenesis in two semi-lobed cell types of *Adiantum capillus-veneris* L. leaflets. *New Phytologist, 125*(3), 509–520.

Panteris, E., Apostolakos, P., & Galatis, B. (1993b). Microtubules and morphogenesis in ordinary pavement cells of *Vigna sinensis* leaves. *Protoplasma, 174*(3), 91–100.

Panteris, E., & Galatis, B. (2005). The morphogenesis of lobed plant cells in the mesophyll and epidermis: organization and distinct roles of cortical microtubules and actin filaments. *New Phytologist*, *167*(3), 721–732.

Parker, M., & Ford, MA. (1982). The structure of the mesophyll of flag leaves in three Triticum species. *Annals of Botany*, *49*, 65–176.

Parkhurst, D. F. (1994). Diffusion of CO_2 and other gases inside leaves. *New Phytologist*, *126*(3), 449–479.

Parkhurst, D. F., & Mott, K. A. (1990). Intercellular Diffusion Limits to CO_2 Uptake in Leaves 1: Studies in Air and Helox. *Plant Physiology*, *94*(3), 1024–1032.

Partier, A., Gay, G., Tassy, C., Beckert, M., Feuillet, C., & Barret, P. (2017). Molecular and FISH analyses of a 53-kbp intact DNA fragment inserted by biolistics in wheat (Triticum aestivum L.) genome. *Plant Cell Reports*, *36*(10), 1547–1559.

Peguero-Pina, J. J., Flexas, J., Galmés, J., Niinemets, Ü. L. O., Sancho-Knapik, D., Barredo, G., Villarroya, D. & Gil-Pelegrín, E, (2012). Leaf anatomical properties in relation to differences in mesophyll conductance to CO_2 and photosynthesis in two related Mediterranean Abies species. *Plant, Cell & Environment*, *35*(12), 2121–2129.

Pemadasa, M. A. (1979). Movements of abaxial and adaxial stomata. *New Phytologist*, *82*(1), 69–80.

Peña, P. A., Quach, T., Sato, S., Ge, Z., Nersesian, N., Changa, T., Dweikat, I., Soundararajan, M., & Clemente, T. E. (2017). Expression of the Maize Dof1 Transcription Factor in Wheat and Sorghum. *Frontiers in Plant Science*, *8*.

Peng, J. H., Sun, D., & Nevo, E. (2011). Domestication evolution, genetics and genomics in wheat. *Molecular Breeding*, *28*(3), 281–301.

Pieruschka, R., Chavarría-Krauser, A., Cloos, K., Scharr, H., Schurr, U., & Jahnke, S. (2008). Photosynthesis can be enhanced by lateral CO_2 diffusion inside leaves over distances of several millimeters. *New Phytologist*, *178*(2), 335–347.

Pieruschka, R., Schurr, U., & Jahnke, S. (2005). Lateral gas diffusion inside leaves. *Journal of Experimental Botany*, *56*(413), 857–864.

Pieruschka, R., Schurr, U., Jensen, M., Wolff, W. F., & Jahnke, S. (2006). Lateral diffusion of CO_2 from shaded to illuminated leaf parts affects photosynthesis inside homobaric leaves. *New Phytologist*, *169*(4), 779–788.

Pillitteri, L. J., & Torii, K. U. (2012). Mechanisms of Stomatal Development. *Annual Review of Plant Biology*, *63*(Volume 63, 2012), 591–614.

Pillitteri, L., Sloan, D., Bogenschutz, N., & Torii, K. (2007). Termination of asymmetric cell division and differentiation of stomata. *Nature*, *455*, 501–505.

Preece, C., Livarda, A., Christin, P. A., Wallace, M., Martin, G., Charles, M., Jones, G., Rees, M., & Osborne, C. P. (2017). How did the domestication of Fertile Crescent grain crops increase their yields? *Functional Ecology*, *31*(2), 387–397.

Puchta, H., & Fauser, F. (2013). Gene targeting in plants: 25 years later. *The International Journal of Developmental Biology, 57(6-7–8),* 629–637.

Qin, N., Xu, W., Hu, L., Li, Y., Wang, H., Qi, X., Fang, Y., & Hua, X. (2016). Drought tolerance and proteomics studies of transgenic wheat containing the maize C4 phosphoenolpyruvate carboxylase (PEPC) gene. *Protoplasma*, *253*(6), 1503–1512.

Qu, B., He, X., Wang, J., Zhao, Y., Teng, W., Shao, A., Zhao, X., Ma, W., Wang, J., Li, B., Li, Z., & Tong, Y. (2015). A Wheat CCAAT Box-Binding Transcription Factor Increases the Grain Yield of Wheat with Less Fertilizer Input. *Plant Physiology*, *167*(2), 411–423.

Raissig, M., Matos, J., Anleu Gil, M., Kornfeld, A., Bettadapur, A., Abrash, E., Allison, H., Badgley, G., & et al. (2017). Mobile MUTE specifies subsidiary cells to build physiologically improved grass stomata. *Science*, *335*, 1215–1218.

Raissig, M. T., Abrash, E., Bettadapur, A., Vogel, J. P., & Bergmann, D. C. (2016). Grasses use an alternatively wired bHLH transcription factor network to establish stomatal identity. *Proceedings of the National Academy of Sciences*, *113*(29), 8326–8331.

Ray, D. K., Mueller, N. D., West, P. C., & Foley, J. A. (2013). Yield Trends Are Insufficient to Double Global Crop Production by 2050. *PLOS ONE*, *8*(6), e66428.

Ray, D. K., Ramankutty, N., Mueller, N. D., West, P. C., & Foley, J. A. (2012). Recent patterns of crop yield growth and stagnation. *Nature Communications*, *3*(1), 1293.

Razzaq, A., Hafiz, I. A., Mahmood, I. and Hussain, A. (2011) *Development of in planta transformation protocol for wheat.* African Journal of Biotechnology, *10*(5), 740-750

Rebetzke, G. J., Condon, A. G., Richards, R. A., & Read, J. J. (2001). Phenotypic variation and sampling for leaf conductance in wheat (Triticum aestivum L.) breeding populations. *Euphytica*, *121*(3), 335–341.

Regina, A., Bird, A., Topping, D., Bowden, S., Freeman, J., Barsby, T., Kosar-Hashemi, B., Li, Z., Rahman, S., & Morell, M. (2006). High-amylose wheat generated by RNA interference improves indices of large-bowel health in rats. *Proceedings of the National Academy of Sciences*, *103*(10), 3546–3551.

Ren, T., Weraduwage, S. M., & Sharkey, T. D. (2019). Prospects for enhancing leaf photosynthetic capacity by manipulating mesophyll cell morphology. *Journal of Experimental Botany, 70*(4), 1153-1165.

Richard, R. A. (2006). Physiological traits used in the breeding of new cultivars for water-scarce environments. *Agricultural Water Management*, *80*, 197–211.

Richards, R. A., Rebetzke, G. J., Condon, A. G., & van Herwaarden, A. F. (2002). Breeding opportunities for increasing the efficiency of water use and crop yield in temperate cereals presented at the 1999 CSSA symposium on water use efficiency, organized by Div. C-2 char, Dr. Tom Gerik. *Crop Sci.*, *42*, 111–121.

Roche, D. (2015). Stomatal conductance is essential for higher yield potential of C3 crops. *Critical Reviews in Plant Sciences*, *34*, 429–435.

Roddy, A., Théroux-Rancourt, G., Abbo, T., Benedetti, J., Brodersen, C., Castro, M., Castro, S., Gilbride, A., Jensen, B., Jiang, G., & Al., E. (2020). The scaling of genome size and cell size limits maximum rates of photosynthesis with implications for ecological strategies. *International Journal of Plant Sciences*, *181*, 75–87.

Rodriguez, R. E., Mecchia, M. A., Debernardi, J. M., Schommer, C., Weigel, D., & Palatnik, J. F. (2010). Control of cell proliferation in *Arabidopsis thaliana* by microRNA miR396. *Development, 137*(1), 103–112.

Rooke, L., Békés, F., Fido, R., Barro, F., Gras, P., Tatham, A. S., Barcelo, P., Lazzeri, P., & Shewry, P. R. (1999). Overexpression of a Gluten Protein in Transgenic Wheat Results in Greatly Increased Dough Strength. *Journal of Cereal Science*, *30*(2), 115–120.

Rudall, P. J., Chen, E. D., & Cullen, E. (2017). Evolution and development of monocot stomata. American Journal of Botany, 104(8), 1122–1141.

Rudall, P. J., Hilton, J., & Bateman, R. M. (2013). Several developmental and morphogenetic factors govern the evolution of stomatal patterning in land plants. *The New Phytologist*, *200*(3), 598–614.

Sadras, V. O., Lawson, C., & Montoro, A. (2012). Photosynthetic traits in Australian wheat varieties released between 1958 and 2007. *Field Crops Research*, *134*, 19–29.

Salamini, F., Özkan, H., Brandolini, A., Schäfer-Pregl, R., & Martin, W. (2002). Genetics and geography of wild cereal domestication in the near east. *Nature Reviews Genetics*, *3*(6), 429–441.

Schindelin, J., Arganda-Carreras, I., Frise, E., Kaynig, V., Longair, M., Pietzsch, T., Preibisch, S., Rueden, C., Saalfeld, S., Schmid, B., Tinevez, J.-Y., White, D. J., Hartenstein, V., Eliceiri, K., Tomancak, P., & Cardona, A. (2012). Fiji: an open-source platform for biological-image analysis. *Nature Methods*, *9*(7), 676–682.

Schuler, M., Sedelnikova, O., Walker, B., Westhoff, P., & Langdale, J. (2018). SHORTROOT-mediated increase in stomatal density has no impact on photosynthetic efficiency. *Plant Physiology*, *176*, 757–772.

Seleiman, M. F., Al-Suhaibani, N., Ali, N., Akmal, M., Alotaibi, M., Refay, Y., Dindaroglu, T., Abdul-Wajid, H. H., & Battaglia, M. L. (2021). Drought Stress Impacts on Plants and Different Approaches to Alleviate Its Adverse Effects. *Plants*, *10*(2).

Serna, L. (2015). Development: Early events in asymmetric division. *Nature Plants*, *1*(2), 15008.

Shan, Q., Wang, Y., Li, J., & Gao, C. (2014). Genome editing in rice and wheat using the CRISPR/Cas system. *Nat Protoc*, *9*, 2395–3410.

Shan, Q., Wang, Y., Li, J., Zhang, Y., Chen, K., Liang, Z., Zhang, K., Liu, J., Xi, J. J., Qiu, J.-L., & Gao, C. (2013). Targeted genome modification of crop plants using a CRISPR-Cas system. *Nature Biotechnology*, *31*(8), 686–688.

Sharkey, T. D. (2016). What gas exchange data can tell us about photosynthesis. *Plant, Cell & Environment*, *39*(6), 1161–1163.

Shewry, P. R. (2009). Wheat. *Journal of Experimental Botany*, *60*(6), 1537–1553.

Shimano, S., Hibara, K. I., Furuya, T., Arimura, S. I., Tsukaya, H., & Itoh, J. I. (2018). Conserved functional control, but distinct regulation, of cell proliferation in rice and Arabidopsis leaves revealed by comparative analysis of GRF-INTERACTING FACTOR 1 orthologs. *Development (Cambridge), 145*(7).

Shindo, C., Bernasconi, G., & Hardtke, C. S. (2007). Natural Genetic Variation in Arabidopsis: Tools, Traits and Prospects for Evolutionary Ecology. *Annals of Botany*, *99*(6), 1043–1054.

Shrawat, A. K., & Armstrong, C. L. (2018). Development and Application of Genetic Engineering for Wheat Improvement. *Critical Reviews in Plant Sciences*, *37*(5), 335–421.

Singh, M., Kumar, M., Albertsen, M. C., Young, J. K., & Cigan, A. M. (2018). Concurrent modifications in the three homeologs of Ms45 gene with CRISPR-Cas9 lead to rapid generation of male sterile bread wheat (*Triticum aestivum* L.). *Plant Molecular Biology, 97(4)*, 371–383.

Sloan, J., Im-Chai, S., Qi, Y. N., Xiao, Y., Armand, J., Wilson, M. J., Zhu, X.-G., & Fleming, A. J. (2022). Stomatal density affects rice mesophyll cell size and shape and modulates a conserved pattern of cells through the leaf. *BioRxiv Plant Biology*.

Smidansky, E. D., Meyer, F. D., Blakeslee, B., Weglarz, T. E., Greene, T. W., & Giroux, M. J. (2007). Expression of a modified ADP-glucose pyrophosphorylase large subunit in wheat seeds stimulates photosynthesis and carbon metabolism. *Planta*, *225*(4), 965–976.

Smith, W. K., Vogelmann, T. C., DeLucia, E. H., Bell, D. T., & Shepherd, K. A. (1997). Leaf Form and Photosynthesis. *BioScience*, *47*(11), 785–793.

SOFI. (2018). The state of food security and nutrition in the world. Building Climate Resilience for Food Security and Nutrition. http://www.fao.org/ state-of-food-security-nutrition/en.

Sun, P., Zhang, W., Wang, Y., He, Q., Shu, F., Liu, H., Wang, J., Wang, J., Yuan, L., & Deng, H. (2016). OsGRF4 controls grain shape, panicle length and seed shattering in rice. *Journal of Integrative Plant Biology, 58*(10), 836–847.

Supartana, P., Shimizu, T., Nogawa, M., Shioiri, H., Nakajima, T., Haramoto, N., Nozue, M., & Kojima, M. (2006). Development of simple and efficient in Planta transformation method for wheat

(Triticum aestivum L.) using Agrobacterium tumefaciens. *Journal of Bioscience and Bioengineering*, *102*(3), 162–170.

Takeda, S., & Matsuoka, M. (2008). Genetic approaches to crop improvement: responding to environmental and population changes. *Nature Reviews Genetics*, *9*(6), 444–457.

Tanaka, Y., Sugano, S. S., Shimada, T., & Hara-Nishimura, I. (2013). Enhancement of leaf photosynthetic capacity through increased stomatal density in Arabidopsis. *New Phytologist*, *198*(3), 757–764.

Terashima, I., Hanba, Y. T., Tholen, D., & Niinemets, Ü. (2011). Leaf functional anatomy in relation to photosynthesis. *Plant Physiology*, *155*(1), 108–116.

Théroux-Rancourt, G., Earles, J. M., Gilbert, M. E., Zwieniecki, M. A., Boyce, C. K., McElrone, A. J., & Brodersen, C. R. (2017). The bias of a two-dimensional view: comparing two-dimensional and three-dimensional mesophyll surface area estimates using noninvasive imaging. *The New Phytologist*, *215*(4), 1609–1622.

Théroux-Rancourt, G., Roddy, A. B., Earles, J. M., Gilbert, M. E., Zwieniecki, M. A., Boyce, C. K., Tholen, D., McElrone, A. J., Simonin, K. A., & Brodersen, C. R. (2021). Maximum CO_2 diffusion inside leaves is limited by the scaling of cell size and genome size. *Proceedings. Biological Sciences*, *288*(1945), 20203145.

Tholen, D., Boom, C., & Zhu, X.-G. (2012). Opinion: Prospects for improving photosynthesis by altering leaf anatomy. *Plant Science*, *197*, 92–101.

Thompson, A. J., Andrews, J., Mulholland, B. J., McKee, J. M. T., Hilton, H. W., Horridge, J. S., Farquhar, G. D., Smeeton, R. C., Smillie, I. R. A., Black, C. R., & Taylor, I. B. (2007). Overproduction of Abscisic Acid in Tomato Increases Transpiration Efficiency and Root Hydraulic Conductivity and Influences Leaf Expansion. *Plant Physiology*, *143*(4), 1905–1917.

Tian, B., Talukder, S. K., Fu, J., Fritz, A. K., & Trick, H. N. (2018). Expression of a rice soluble starch synthase gene in transgenic wheat improves the grain yield under heat stress conditions. *In Vitro Cellular & Developmental Biology - Plant*, *54*(3), 216–227.

Tian, T., Ma, L., Liu, Y., Xu, D., Chen, Q., & Li, G. (2020). Arabidopsis FAR-RED ELONGATED HYPOCOTYL3 Integrates Age and Light Signals to Negatively Regulate Leaf Senescence. *The Plant Cell*, *32*(5), 1574–1588.

Truernit, E., Bauby, H., Dubreucq, B., Grandjean, O., Runions, J., Barthélémy, J., & Palauqui, J.-C. (2008). High-Resolution Whole-Mount Imaging of Three-Dimensional Tissue Organization and Gene Expression Enables the Study of Phloem Development and Structure in Arabidopsis. *The Plant Cell*, *20*(6), 1494–1503.

Uauy, C. (2017). Plant Genomics: Unlocking the Genome of Wheat's Progenitor. *Current Biology*, *27*(20), R1122–R1124.

Uauy, C., Distelfeld, A., Fahima, T., Blechl, A., & Dubcovsky, J. (2006). A NAC Gene Regulating Senescence Improves Grain Protein, Zinc, and Iron Content in Wheat. *Science*, *314*(5803), 1298–1301.

Upadhyay, S. K., Kumar, J., Alok, A., & Tuli, R. (2013). RNA-Guided Genome Editing for Target Gene Mutations in Wheat. *G3 Genes|Genomes|Genetics*, *3*(12), 2233–2238.

Urban, J., Ingwers, M., McGuire, M. A., & Teskey, R. O. (2017). Stomatal conductance increases with rising temperature. *Plant Signaling & Behavior,* 12(8), e1356534.

USDA (2024). *Production Trends - Wheat*. fas.usda.gov/data/production/commodity/0410000.

Vasil, V., Castillo, A. M., Fromm, M. E., & Vasil, I. K. (1992). Herbicide Resistant Fertile Transgenic Wheat Plants Obtained by Microprojectile Bombardment of Regenerable Embryogenic Callus. *Bio/Technology*, *10*(6), 667–674.

Vatén, A., & Bergmann, D. C. (2012). Mechanisms of stomatal development: an evolutionary view. *EvoDevo*, *3*(1), 11.

Vercruyssen, L., Verkest, A., Gonzalez, N., Heyndrickx, K. S., Eeckhout, D., Han, S.-K., Jégu, T., Archacki, R., van Leene, J., Andriankaja, M., de Bodt, S., Abeel, T., Coppens, F., Dhondt, S., de Milde, L., Vermeersch, M., Maleux, K., Gevaert, K., Jerzmanowski, A., … Inzé, D. (2014). ANGUSTIFOLIA3 Binds to SWI/SNF Chromatin Remodeling Complexes to Regulate Transcription during Arabidopsis Leaf Development. *The Plant Cell, 26*(1), 210–229.

Verma, K. K., Song, X.-P., Zeng, Y., Li, D.-M., Guo, D.-J., Rajput, V. D., Chen, G.-L., Barakhov, A., Minkina, T. M., & Li, Y.-R. (2020). Characteristics of Leaf Stomata and Their Relationship with Photosynthesis in *Saccharum officinarum* Under Drought and Silicon Application. *ACS Omega*, *5*(37), 24145–24153.

Vialet-Chabrand, S. R. M., Matthews, J. S., McAusland, L., Blatt, M. R., Griffiths, H., & Lawson, T. (2017). Temporal Dynamics of Stomatal Behavior: Modeling and Implications for Photosynthesis and Water Use. *Plant Physiology*, *174*(2), 603–613.

Vijayan, A., Tofanelli, R., Strauss, S., Cerrone, L., Wolny, A., Strohmeier, J., Kreshuk, A., Hamprecht, F. A., Smith, R. S., & Schneitz, K. (2021). A digital 3D reference atlas reveals cellular growth patterns shaping the Arabidopsis ovule. *ELife*, *10*, e63262.

Vogelmann, T. C. & Martin, G. (1993). The functional significance of palisade tissue: penetration of directional versus diffuse light. *Plant, Cell & Environment*, *16*(1), 65–72.

Wall, S., Cockram, J., Vialet-Chabrand, S., van Rie, J., Gallé, A., & Lawson, T. (2023). The impact of growth at elevated [CO_2] on stomatal anatomy and behavior differs between wheat species and cultivars. *Journal of Experimental Botany*, *74*(9), 2860–2874.

Wall, S., Vialet-Chabrand, S., Davey, P., van Rie, J., Galle, A., Cockram, J., & Lawson, T. (2022). Stomata on the abaxial and adaxial leaf surface contribute differently to leaf gas exchange and photosynthesis in wheat. *New Phytologist*.

Wang, H., & Clarke, J. M. (1993). Genotypic, intraplant, and environmental variation in stomatal frequency and size in wheat. *Canadian Journal of Plant Science*, *73*(3), 671–678.

Wang, H., Kong, F., & Zhou, C. (2021). From genes to networks: The genetic control of leaf development. *Journal of Integrative Plant Biology*, *63*(7), 1181–1196.

Wang, S. G., Jia, S. S., Sun, D. Z., Wang, H. Y., Dong, F. F., Ma, H. X., Jing, R. L., & Ma, G. (2015). Genetic basis of traits related to stomatal conductance in wheat cultivars in response to drought stress. *Photosynthetica*, *53*(2), 299–305.

Wang, J., Zhou, H., Zhao, Y., Sun, P., Tang, F., Song, X., & Lu, M.-Z. (2020). Characterization of poplar growth-regulating factors and analysis of their function in leaf size control. *BMC Plant Biology, 20*(1), 509.

Wang, W., Simmonds, J., Pan, Q., Davidson, D., He, F., Battal, A., Akhunova, A., Trick, H. N., Uauy, C., & Akhunov, E. (2018). Gene editing and mutagenesis reveal inter-cultivar differences and additivity in the contribution of TaGW2 homoeologues to grain size and weight in wheat. *Theoretical and Applied Genetics*, *131*(11), 2463–2475.

Wang, Y., Cheng, X., Shan, Q., Zhang, Y., Liu, J., Gao, C., & Qiu, J. L. (2014). Simultaneous editing of three homoeoalleles in hexaploid bread wheat confers heritable resistance to powdery mildew. *Nat Biotechnol*, *32*, 947–951.

Weichert, N., Saalbach, I., Weichert, H., Kohl, S., Erban, A., Kopka, J., Hause, B., Varshney, A., Sreenivasulu, N., Strickert, M., Kumlehn, J., Weschke, W., & Weber, H. (2010). Increasing Sucrose Uptake Capacity of Wheat Grains Stimulates Storage Protein Synthesis, *Plant Physiology*, *152*(2), 698–710.

Wernicke, W., Günther, P., & Jung, G. (1993). Microtubules and cell shaping in the mesophyll of *Nigella damascena* L. *Protoplasma, 173*(1), 8–12.

Wernicke, W., & Jung, G. (1992). Role of cytoskeleton in cell shaping of developing mesophyll of wheat (Triticum aestivum L.). *European Journal of Cell Biology*, *57*(1), 88–94.

Wheeler, T., & von Braun, J. (2013). Climate Change Impacts on Global Food Security. *Science*, *341*(6145), 508–513.

Willmer, C., & Fricker, M. (1996). The distribution of stomata. In C. Willmer & M. Fricker (Eds.), *Stomata* (pp. 12–35). Springer Netherlands.

Wilson, M. J., Fradera-Soler, M., Summers, R., Sturrock, C. J., & Fleming, A. J. (2021). Ploidy influences wheat mesophyll cell geometry, packing and leaf function. *Plant Direct*, *5*(4), e00314.

Wong, S. C., Canny, M. J., Holloway-Phillips, M., Stuart-Williams, H., Cernusak, L. A., Márquez, D. A., & Farquhar, G. D. (2022). Humidity gradients in the air spaces of leaves. *Nature Plants*.

Woodward, F. L., & Kelly, C. K. (1995). The influence of CO_2 concentration on stomatal density. *New Phytologist*, *131*, 311–327.

Wu, K., Wang, S., Song, W., Zhang, J., Wang, Y., Liu, Q., Yu, J., Ye, Y., Li, S., Chen, J., Zhao, Y., Wang, J., Wu, X., Wang, M., Zhang, Y., Liu, B., Wu, Y., Harberd, N. P., & Fu, X. (2020). Enhanced sustainable green revolution yield via nitrogen-responsive chromatin modulation in rice. *Science*, *367*(6478), eaaz2046.

Wu, W., Li, J., Wang, Q., Lv, K., Du, K., Zhang, W., Li, Q., Kang, X., & Wei, H. (2021). Growth-regulating factor 5 (GRF5)-mediated gene regulatory network promotes leaf growth and expansion in poplar. *New Phytologist, 230*(2), 612–628.

Wu, Z., Chen, L., Yu, Q., Zhou, W., Gou, X., Li, J., & Hou, S. (2019). Multiple transcriptional factors control stomata development in rice. *New Phytologist*, *223*(1), 220–232.

Wuyts, N., Palauqui, J. C., Conejero, G., Verdeil, J. L., Granier, C., & Massonnet, C. (2010). High-contrast three-dimensional imaging of the Arabidopsis leaf enables the analysis of cell dimensions in the epidermis and mesophyll. *Plant Methods*, *6*(1), 1–14.

Xiao, Y., Sloan, J., Hepworth, C., Fradera-Soler, M., Mathers, A., Thorley, R., Baillie, A., Jones, H., Chang, T., Chen, X., Yaapar, N., Osborne, C. P., Sturrock, C., Mooney, S. J., Fleming, A. J., & Zhu, X.-G. (2022). Defining the scope for altering rice leaf anatomy to improve photosynthesis: A modelling approach. *New Phytologist*

Xiong, Y., & Jiao, Y. (2019). The Diverse Roles of Auxin in Regulating Leaf Development. *Plants*, *8*(7).

Xu, Z., Jiang, Y., Jia, B., & Zhou, G. (2016). Elevated-CO_2 Response of Stomata and Its Dependence on Environmental Factors. *Frontiers in Plant Science*, *7*, 657.

Xynias, I. N., Mylonas, I., Korpetis, E. G., Ninou, E., Tsaballa, A., Avdikos, I. D., & Mavromatis, A. G. (2020). Durum Wheat Breeding in the Mediterranean Region: Current Status and Future Prospects. *Agronomy*, *10*(3), 432.

Yadav, D., Shavrukov, Y., Bazanova, N., Chirkova, L., Borisjuk, N., Kovalchuk, N., Ismagul, A., Parent, B., Langridge, P., Hrmova, M., & Lopato, S. (2015). Constitutive overexpression of the TaNF-YB4 gene in transgenic wheat significantly improves grain yield. *Journal of Experimental Botany*, *66*(21), 6635–6650.

Yan, L., Loukoianov, A., Blechl, A., Tranquilli, G., Ramakrishna, W., SanMiguel, P., Bennetzen, J. L., Echenique, V., & Dubcovsky, J. (2004). The Wheat VRN2 Gene Is a Flowering Repressor Down-Regulated by Vernalization. *Science*, *303*(5664), 1640–1644.

Yan, S., Yan, C., & Gu, M. (2008). Molecular mechanism of leaf development. *Hereditas (Beijing)*, *30*(9), 1127–1135.

Yin, X., Struik, P. C., Romero, P., Harbinson, J., Evers, J. B., van der Putten, P. E. L., & Vol, J. A. N. (2009). Using combined measurements of gas exchange and chlorophyll fluorescence to estimate parameters of a biochemical C3 photosynthesis model: a critical appraisal and a new integrated approach applied to leaves in a wheat (Triticum aestivum) canopy. *Plant, Cell & Environment*, *32*(5), 448–464.

Yoo, C. Y., Jin, J. B., Miura, K., Gosney, M., Jin, Y., Mickelbart, M.V., and Hasegawa, P. M. (2008). AtGTL1 transcription factor regulates water use efficiency and drought adaptation through Ca2+/Calmodulin signalling. *19th International Conference on Arabidopsis Research. Montreal, Canada July 23–27.*

Yoo, C. Y., Pence, H., Hasegawa, P., & Mickelbart, M. (2009). Regulation of transpiration to improve crop water use. *Critical Reviews in Plant Sciences*, *28*, 410–431.

Yoshida, S., Barbier de Reuille, P., Lane, B., Bassel, G. W., Prusinkiewicz, P., Smith, R. S., & Weijers, D. (2014). Genetic Control of Plant Development by Overriding a Geometric Division Rule. *Developmental Cell*, *29*(1), 75–87.

Yu, H., Chen, X., Hong, Y.-Y., Wang, Y., Xu, P., Ke, S.-D., Liu, H.-Y., Zhu, J.-K., Oliver, D. J., & Xiang, C.-B. (2008). Activated Expression of an Arabidopsis HD-START Protein Confers Drought Tolerance with Improved Root System and Reduced Stomatal Density. *The Plant Cell*, *20*(4), 1134–1151.

Yue, S. J., Li, H., Li, Y., Zhu, Y. J., Guo, J., Liu, Y. J., Chen, Y. J., & Jia, X. (2008). Generation of transgenic wheat lines with altered expression levels of 1Dx5 high-molecular weight glutenin subunit by RNA interference. *Journal of Cereal Science*, *47*, 153–161.

Zhang, B., Tong, Y., Luo, K., Zhai, Z., Liu, X., Shi, Z., Zhang, D., & Li, D. (2021a). Identification of GROWTH-REGULATING FACTOR transcription factors in lettuce (Lactuca sativa) genome and functional analysis of LsaGRF5 in leaf size regulation. *BMC Plant Biology*, *21*(1), 485.

Zhang, D., Sun, W., Singh, R., Zheng, Y., Cao, Z., Li, M., Lunde, C., Hake, S., & Zhang, Z. (2018). GRF-interacting factor1 Regulates Shoot Architecture and Meristem Determinacy in Maize. *The Plant Cell, 30*(2), 360–374.

Zhang, H., Xu, W., Wang, H., Hu, L., Li, Y., Qi, X., Zhang, L., Li, C., & Hua, X. (2014). Pyramiding expression of maize genes encoding phosphoenolpyruvate carboxylase (PEPC) and pyruvate orthophosphate dikinase (PPDK) synergistically improve the photosynthetic characteristics of transgenic wheat. *Protoplasma*, *251*(5), 1163–1173.

Zhang, Q., Peng, S., & Li, Y. (2019). Increase rate of light-induced stomatal conductance is related to stomatal size in the genus Oryza. *Journal of Experimental Botany*, *70*(19), 5259–5269.

Zhang, S., Zhu, L., Shen, C., Ji, Z., Zhang, H., Zhang, T., Li, Y., Yu, J., Yang, N., He, Y., Tian, Y., Wu, K., Wu, J., Harberd, N. P., Zhao, Y., Fu, X., Wang, S., & Li, S. (2021b). Natural allelic variation in a modulator of auxin homeostasis improves grain yield and nitrogen use efficiency in rice. *The Plant Cell*, *33*(3), 566–580.

Zhang, X., Chen, S., Sun, H., Wang, Y., & Shao, L. (2010). Water use efficiency and associated traits in winter wheat cultivars in the north China Plain. *Agricultural Water Management*, *97*, 1117–1125.

Zhang, X., Wollenweber, B., Jiang, D., Liu, F., & Zhao, J. (2008). Water deficits and heat shock effects on photosynthesis of a transgenic Arabidopsis thaliana constitutively expressing ABP9, a bZIP transcription factor. *Journal of Experimental Botany*, *59*(4), 839–848.

Zhang, Y., Bai, Y., Wu, G., Zou, S., Chen, Y., Gao, C., & Tang, D. (2017). Simultaneous modification of three homoeologs of Ta1 by genome editing enhances powdery mildew resistance in wheat. *The Plant Journal*, *91*(4), 714–724.

Zhang, Y., Liang, Z., Zong, Y., Wang, Y., Liu, J., Chen, K., Qiu, J.-L., & Gao, C. (2016). Efficient and transgene-free genome editing in wheat through transient expression of CRISPR/Cas9 DNA or RNA. *Nature Communications*, *7*(1), 12617.

Zhao, D., Derkx, A., Liu, D., Buchner, P., & Hawkesford, M. (2021). *Overexpression of a NAC transcription factor delays leaf senescence and increases grain nitrogen concentration in wheat*.

Zhao, Y.-Y., Lyu, M. A., Miao, F., Chen, G., & Zhu, X.-G. (2022). The evolution of stomatal traits along the trajectory toward C4 photosynthesis. *Plant Physiology, 190*(1), 441–458.

Zhao, T.J., Zhao, S.-Y., Chen, H.-M., Zhao, Q.-Z., Hu, Z.-M., Hou, B.-K., & Xia, G.-M. (2006). Transgenic wheat progeny resistant to powdery mildew generated by Agrobacterium inoculum to the basal portion of wheat seedling. *Plant Cell Reports*, *25*(11), 1199–1204.

Zhao, X. Y., Hong, P., Wu, J. Y., Chen, X. bin, Ye, X. G., Pan, Y. Y., Wang, J., & Zhang, X. S. (2016). The tae-miR408-Mediated Control of TaTOC1 Genes Transcription Is Required for the Regulation of Heading Time in Wheat. *Plant Physiology*, *170*(3), 1578–1594.

Zhao, X. Q., Nie, X.-L., & Xiao, X.-G. (2013). Over-Expression of a Tobacco Nitrate Reductase Gene in Wheat (Triticum aestivum L.) Increases Seed Protein Content and Weight without Augmenting Nitrogen Supplying. *PLOS ONE*, *8*(9), e74678-.

Zhou, H., Song, X., Wei, K., Zhao, Y., Jiang, C., Wang, J., Tang, F., & Lu, M. (2019). Growth-regulating factor 15 is required for leaf size control in Populus. *Tree Physiology*, *39*(3), 381–390.

Zong, Y., Song, Q., Li, C., Jin, S., Zhang, D., Wang, Y., Qiu, J.-L., & Gao, C. (2018). Efficient C-to-T base editing in plants using a fusion of nCas9 and human APOBEC3A. *Nature Biotechnology*, *36*(10), 950–953.

Zong, Y., Wang, Y., Li, C., Zhang, R., Chen, K., Ran, Y., Qiu, J.-L., Wang, D., & Gao, C. (2017). Precise base editing in rice, wheat and maize with a Cas9-cytidine deaminase fusion. *Nature Biotechnology*, *35*(5), 438–440.

Zoulias, N., Harrison, E., Casson, S., & Gray, J. (2018). Molecular control of stomatal development. *The Biochemical Journal*, *475*, 441–454.

Zhu, T., Wang, L., Rodriguez, J. C., Deal, K. R., Avni, R., Distelfeld, A., McGuire, P. E., Dvorak, J., & Luo, M.-C. (2019). Improved Genome Sequence of Wild Emmer Wheat Zavitan with the Aid of Optical Maps. *G3 Genes|Genomes|Genetics*, *9*(3), 619–624.

Zhuo, L., Zhao, W., Kong, S., Li, L., & Lin, S. (2023). Overview of molecular mechanisms of plant leaf development: a systematic review. *Frontiers in Plant Science*, *14*.

Appendices

The following are ANOVA significance table for Chapter 3 of this thesis. A summary of lines used is available in Table 3.1. P values for lines which would be significantly distinguished from each other at p<0.005 are shown, and level of significance is indicted by asterisks (p<0.05*, p<0.005**, p<0.0005***, P<0.0001****). Cultivation status is indicated by colour, with wild in black, Emmer in blue and Durum in red.

Appendix 1.1. Significance table for Figure 3.2a

	TRI18530	TRI18505	TRI16599	TRI18513	TRI16877	TRI28049	TRI14734	VOILUR	AVENTADUR	ANVERGUR
TRI18530		ns	ns	ns	ns	<0.0001(****)	<0.0001(****)	<0.0001(****)	<0.0001(****)	<0.0001(****)
TRI18505			ns	ns	0.0035(**)	<0.0001(****)	<0.0001(****)	<0.0001(****)	<0.0001(****)	<0.0001(****)
TRI16599				ns	0.0005(***)	<0.0001(****)	<0.0001(****)	<0.0001(****)	<0.0001(****)	<0.0001(****)
TRI18513					0.0216(*)	<0.0001(****)	<0.0001(****)	<0.0001(****)	<0.0001(****)	<0.0001(****)
TRI16877						0.038(*)	0.012(*)	0.0019(**)	<0.0001(****)	0.0005(***)
TRI28049							ns	ns	ns	ns
TRI14734								ns	ns	ns
VOILUR									ns	ns
AVENTADUR										ns
ANVERGUR										

Appendix 1.2. Significance table for Figure 3.2b

	TRI18530	TRI18505	TRI16599	TRI18513	TRI16877	TRI28049	TRI14734	VOILUR	AVENTADUR	ANVERGUR
TRI18530		ns	0.0324(*)	ns	ns	ns	ns	ns	ns	ns
TRI18505			0.0001(***)	ns	ns	ns	ns	ns	ns	ns
TRI16599				ns	0.0002(***)	<0.0001(****)	<0.0001(****)	ns	ns	ns
TRI18513					ns	ns	0.0364(*)	ns	ns	ns
TRI16877						ns	ns	ns	ns	ns
TRI28049							ns	ns	ns	0.0263(*)
TRI14734								ns	0.0473(*)	0.0182(*)
VOILUR									ns	ns
AVENTADUR										ns
ANVERGUR										

Appendix 1.3. Significance Table for Figure 3.2c (at 28-day timepoint)

	TRI18530	TRI18505	TRI16599	TRI18513	TRI16877	TRI28049	TRI14734	VOILUR	AVENTADUR	ANVERGUR
TRI18530		0.0189(*)	ns	ns	<0.0001(****)	<0.0001(****)	<0.0001(****)	ns	ns	0.0264(*)
TRI18505			0.0007(***)	0.0102(*)	ns	0.0012(**)	<0.0001(****)	ns	ns	ns
TRI16599				ns	<0.0001(****)	<0.0001(****)	<0.0001(****)	0.0184(*)	0.0052(**)	0.001(***)
TRI18513					<0.0001(****)	<0.0001(****)	<0.0001(****)	ns	ns	0.0142(*)
TRI16877						ns	0.0209(*)	ns	ns	ns
TRI28049							ns	<0.0001(****)	0.0002(***)	0.0008(***)
TRI14734								<0.0001(****)	<0.0001(****)	<0.0001(****)
VOILUR									ns	ns
AVENTADUR										ns
ANVERGUR										

Appendix 1.4. Significance Table for Figure 3.2d (at 28-day timepoint)

	TRI18530	TRI18505	TRI16599	TRI18513	TRI16877	TRI28049	TRI14734	VOILUR	AVENTADUR	ANVERGUR
TRI18530		ns	ns	ns	0.0255(*)	ns	ns	ns	ns	ns
TRI18505			ns	ns	ns	ns	ns	ns	ns	ns
TRI16599				ns	0.02(*)	ns	ns	ns	ns	ns
TRI18513					0.0088(**)	ns	ns	ns	ns	ns
TRI16877						ns	ns	ns	ns	ns
TRI28049							ns	ns	ns	ns
TRI14734								ns	ns	ns
VOILUR									ns	ns
AVENTADUR										ns
ANVERGUR										

Appendix 1.5. Significance Table for Figure 3.3a

	TRI18530	TRI18505	TRI16599	TRI18513	TRI16877	TRI14734	VOILUR	AVENTADUR	ANVERGUR
TRI18530		ns	ns	ns	ns	ns	ns	ns	ns
TRI18505			ns	ns	ns	ns	ns	ns	ns
TRI16599				ns	ns	0.0469(*)	ns	0.0344(*)	ns
TRI18513					ns	ns	ns	ns	ns
TRI16877						ns	ns	ns	ns
TRI14734							ns	ns	ns
VOILUR								ns	ns
AVENTADUR									ns
ANVERGUR									

Appendix 1.6. Significance Table for Figure 3.3b

	TRI18530	TRI18505	TRI16599	TRI18513	TRI16877	TRI28049	TRI14734	VOILUR	AVENTADUR	ANVERGUR
TRI18530		ns	ns	ns	ns	0.0418(*)	ns	0.0005(***)	0.0022(**)	0.0494(*)
TRI18505			ns	ns	ns	ns	ns	0.0007(***)	0.0031(**)	ns
TRI16599				ns	ns	ns	ns	ns	ns	ns
TRI18513					ns	ns	ns	0.0395(*)	ns	ns
TRI16877						ns	ns	0.0065(*)	0.0251(*)	ns
TRI28049							ns	ns	ns	ns
TRI14734								ns	ns	ns
VOILUR									ns	ns
AVENTADUR										ns
ANVERGUR										

Appendix 1.7. Significance Table for Figure 3.3c

	TRI18530	TRI18505	TRI16599	TRI18513	TRI16877	TRI28049	TRI14734	VOILUR	AVENTADUR	ANVERGUR
TRI18530		ns	ns	ns	ns	0.0362(*)	0.0248(*)	0.0038(**)	0.0091(**)	0.0151(*)
TRI18505			ns	ns	ns	ns	ns	ns	ns	ns
TRI16599				ns	ns	ns	ns	ns	ns	ns
TRI18513					ns	ns	ns	ns	ns	ns
TRI16877						ns	ns	ns	ns	ns
TRI28049							ns	ns	ns	ns
TRI14734								ns	ns	ns
VOILUR									ns	ns
AVENTADUR										ns
ANVERGUR										

Appendix 1.8. Significance Table for Figure 3.3d

	TRI18530	TRI18505	TRI16599	TRI18513	TRI16877	TRI28049	TRI14734	VOILUR	AVENTADUR	ANVERGUR
TRI18530		ns	ns	ns	ns	ns	ns	ns	ns	ns
TRI18505			ns	ns	ns	ns	ns	ns	ns	ns
TRI16599				ns	ns	ns	ns	ns	ns	ns
TRI18513					ns	ns	ns	ns	ns	ns
TRI16877						ns	ns	0.0445(*)	0.0335(*)	ns
TRI28049							ns	ns	ns	ns
TRI14734								ns	0.0394(*)	ns
VOILUR									ns	ns
AVENTADUR										ns
ANVERGUR										

Appendix 1.9. Significance Table for Figure 3.4a

	TRI18530	TRI18505	TRI16599	TRI18513	TRI16877	TRI28049	TRI14734	VOILUR	AVENTADUR	ANVERGUR
TRI18530		0.0176(*)	ns	ns	0.0408(*)	0.0007(***)	0.0007(***)	0.0046(**)	<0.0001(****)	<0.0001(****)
TRI18505			ns	ns	ns	ns	ns	ns	0.0008(***)	0.0083(**)
TRI16599				ns	ns	0.0265(*)	0.0414(*)	ns	<0.0001(****)	<0.0001(****)
TRI18513					ns	ns	ns	ns	<0.0001(****)	<0.0001****
TRI16877						ns	ns	ns	0.0003(***)	0.0033(**)
TRI28049							ns	ns	ns	ns
TRI14734								ns	0.0195(*)	ns
VOILUR									0.0032(**)	0.0303(*)
AVENTADUR										ns
ANVERGUR										

Appendix 1.10. Significance Table for Figure 3.4b

	TRI18530	TRI18505	TRI16599	TRI18513	TRI16877	TRI28049	TRI14734	VOILUR	AVENTADUR	ANVERGUR
TRI18530		0.0112(*)	ns	ns	<0.0001(***	ns	0.0077(**)	ns	0.0204(*)	0.0015(**)
TRI18505			ns	ns	ns	ns	ns	ns	ns	ns
TRI16599				ns	0.0493(*)	ns	ns	ns	ns	ns
TRI18513					0.0031(**)	ns	ns	ns	ns	ns
TRI16877						0.0014(**)	ns	0.0101(*)	ns	ns
TRI28049							ns	ns	ns	ns
TRI14734								ns	ns	ns
VOILUR									ns	ns
AVENTADUR										ns
ANVERGUR										

Appendix 1.11. Significance Table for Figure 3.4c

	TRI18530	TRI18505	TRI16599	TRI18513	TRI16877	TRI28049	TRI14734	VOILUR	AVENTADUR	ANVERGUR
TRI18530		ns	ns	ns	ns	ns	0.0322(*)	<0.0001(****)	<0.0001(****)	<0.0001(****)
TRI18505			ns	ns	ns	ns	ns	<0.0001(****)	0.0063(**)	0.0013(**)
TRI16599				ns	ns	ns	ns	<0.0001(****)	0.0209(*)	0.0047(**)
TRI18513					ns	ns	ns	<0.0001(****)	0.0006(***)	0.0001(***)
TRI16877						ns	ns	<0.0001(****)	<0.0001(****)	<0.0001(****)
TRI28049							ns	<0.0001(****)	<0.0001(****)	<0.0001(****)
TRI14734								0.0002(***)	ns	ns
VOILUR									ns	ns
AVENTADUR										ns
ANVERGUR										

Appendix 1.12. Significance Table for Figure 3.4d

	TRI18530	TRI18505	TRI16599	TRI18513	TRI16877	TRI28049	TRI14734	VOILUR	AVENTADUR	ANVERGUR
TRI18530		0.0365(*)	ns	ns	ns	ns	0.0016(**)	<0.0001(****)	<0.0001(****)	<0.0001(****)
TRI18505			ns	ns	ns	ns	ns	0.0244(*)	ns	0.0184(*)
TRI16599				ns	ns	ns	ns	0.0096(**)	ns	0.0071(**)
TRI18513					ns	ns	ns	0.0002(***)	0.0021(**)	0.0001(***)
TRI16877						ns	ns	0.0157(*)	ns	0.0117(*)
TRI28049							0.0218(*)	<0.0001(****)	0.0002(***)	<0.0001(****)
TRI14734								ns	ns	ns
VOILUR									ns	ns
AVENTADUR										ns
ANVERGUR										

Appendix 1.13. Significance Table for Figure 3.5a

	TRI18530	TRI18505	TRI16599	TRI18513	TRI16877	TRI28049	TRI14734	VOILUR	AVENTADUR	ANVERGUR
TRI18530		0.0051(*)	ns	ns	ns	<0.0001(****)	ns	ns	ns	ns
TRI18505			0.0237(*)	ns	ns	ns	ns	ns	ns	ns
TRI16599				ns	ns	0.0003(***)	ns	ns	ns	ns
TRI18513					ns	0.0071(*)	ns	ns	ns	ns
TRI16877						ns	ns	ns	ns	ns
TRI28049							0.0216(*)	0.0014(**)	ns	ns
TRI14734								ns	ns	ns
VOILUR									ns	ns
AVENTADUR										ns
ANVERGUR										

Appendix 1.14. Significance Table for Figure 3.5b

	TRI18530	TRI18505	TRI16599	TRI18513	TRI16877	TRI28049	TRI14734	VOILUR	AVENTADUR	ANVERGUR
TRI18530		ns	0.0137(*)	ns	ns	ns	ns	ns	ns	ns
TRI18505			0.0004(***)	ns	0.0055(*)	ns	ns	ns	ns	ns
TRI16599				0.003(**)	ns	ns	ns	0.0035(**)	<0.0001(****)	<0.0001(****)
TRI18513					0.0369(*)	ns	ns	ns	ns	ns
TRI16877						ns	ns	0.0422(*)	0.0008(**)	<0.0001(****)
TRI28049							ns	ns	ns	0.0111(*)
TRI14734								ns	0.0137(*)	0.0021(**)
VOILUR									ns	ns
AVENTADUR										ns
ANVERGUR										

Appendix 1.15. Significance Table for Figure 3.5c

	TRI18530	TRI18505	TRI16599	TRI18513	TRI16877	TRI28049	TRI14734	VOILUR	AVENTADUR	ANVERGUR
TRI18530		ns	0.0078(*)	ns	0.0004(***)	ns	0.0039(**)	ns	ns	ns
TRI18505			ns	ns	ns	ns	ns	ns	ns	ns
TRI16599				ns	ns	ns	ns	0.0371(*)	0.0398(*)	0.0019(**)
TRI18513					0.0103(*)	ns	ns	ns	ns	ns
TRI16877						ns	ns	0.0023(**)	0.0025(**)	<0.0001(****)
TRI28049							ns	ns	ns	ns
TRI14734								0.0196(*)	0.0211(*)	0.0009(**)
VOILUR									ns	ns
AVENTADUR										ns
ANVERGUR										

Appendix 1.16. Significance Table for Figure 3.5d

	TRI18530	TRI18505	TRI16599	TRI18513	TRI16877	TRI28049	TRI14734	VOILUR	AVENTADUR	ANVERGUR
TRI18530		0.0121(*)	ns	ns	ns	0.0166(*)	ns	ns	ns	0.0184(*)
TRI18505			<0.0001(****)	ns	0.0004(***)	ns	0.0011(**)	ns	ns	ns
TRI16599				0.0084(*)	ns	<0.0001(****)	ns	0.021(*)	<0.0001(****)	<0.0001(****)
TRI18513					ns	ns	ns	ns	ns	ns
TRI16877						0.0005(***)	ns	ns	0.0041(**)	0.0006(**)
TRI28049							0.0015(**)	ns	ns	ns
TRI14734								ns	0.0104(*)	0.0017(**)
VOILUR									ns	ns
AVENTADUR										ns
ANVERGUR										

Appendix 1.17. Significance Table for Figure 3.6a

	TRI18530	TRI18505	TRI16599	TRI18513	TRI16877	TRI28049	TRI14734	VOILUR	AVENTADUR	ANVERGUR
TRI18530		ns	ns	ns	ns	ns	ns	0.0063(*)	<0.0001(****)	0.0003(***)
TRI18505			ns	ns	ns	ns	ns	ns	0.0002(***)	0.0143(*)
TRI16599				ns	ns	ns	ns	0.0203(*)	<0.0001(****)	0.0013(**)
TRI18513					ns	ns	ns	0.0338(*)	<0.0001(****)	0.0023(**)
TRI16877						ns	ns	0.0012(**)	<0.0001(****)	<0.0001(****)
TRI28049							ns	ns	0.0106(*)	ns
TRI14734								ns	0.0139(*)	ns
VOILUR									ns	ns
AVENTADUR										ns
ANVERGUR										

Appendix 1.18. Significance Table for Figure 3.6b

	TRI18530	TRI18505	TRI16599	TRI18513	TRI16877	TRI28049	TRI14734	VOILUR	AVENTADUR	ANVERGUR
TRI18530		ns	ns	ns	ns	ns	ns	ns	0.0451(*)	ns
TRI18505			ns	ns	ns	ns	ns	ns	ns	ns
TRI16599				ns	ns	ns	ns	ns	0.0097(*)	ns
TRI18513					ns	ns	ns	ns	0.0284(*)	ns
TRI16877						ns	ns	ns	0.0012(**)	0.0442(*)
TRI28049							ns	ns	ns	ns
TRI14734								ns	ns	ns
VOILUR									0.0293(*)	ns
AVENTADUR										ns
ANVERGUR										

Appendix 1.19. Significance Table for Figure 3.7a

	TRI18530	TRI18505	TRI16599	TRI18513	TRI16877	TRI28049	TRI14734	VOILUR	AVENTADUR	ANVERGUR
TRI18530		ns	ns	ns	ns	ns	ns	0.0052(*)	ns	0.0052(*)
TRI18505			ns	ns	ns	ns	ns	ns	ns	ns
TRI16599				ns	ns	ns	ns	0.0075(*)	ns	0.0071(*)
TRI18513					ns	ns	ns	ns	ns	ns
TRI16877						ns	ns	ns	ns	ns
TRI28049							ns	<0.0001(****)	ns	<0.0001(****)
TRI14734								<0.0001(****)	ns	<0.0001(****)
VOILUR									0.0052(*)	ns
AVENTADUR										0.0052(*)
ANVERGUR										

Appendix 1.20. Significance Table for Figure 3.7b

	TRI18530	TRI18505	TRI16599	TRI18513	TRI16877	TRI28049	TRI14734	VOILUR	AVENTADUR	ANVERGUR
TRI18530		ns	ns	ns	ns	ns	ns	ns	ns	ns
TRI18505			ns	ns	ns	ns	ns	ns	ns	ns
TRI16599				ns	ns	ns	ns	ns	ns	ns
TRI18513					ns	ns	ns	ns	ns	ns
TRI16877						ns	ns	ns	ns	ns
TRI28049							ns	ns	ns	ns
TRI14734								ns	ns	ns
VOILUR									ns	ns
AVENTADUR										ns
ANVERGUR										

Appendix 1.21. Significance Table for Figure 3.7c

	TRI18530	TRI18505	TRI16599	TRI18513	TRI16877	TRI28049	TRI14734	VOILUR	AVENTADUR	ANVERGUR
TRI18530		ns	ns	ns	ns	ns	ns	ns	ns	ns
TRI18505			ns	ns	ns	0.0452(*)	ns	ns	ns	ns
TRI16599				ns	ns	0.0206(*)	ns	ns	ns	ns
TRI18513					0.0474(*)	0.0105(*)	ns	ns	ns	ns
TRI16877						ns	ns	0.0009(**)	ns	0.0314(*)
TRI28049							ns	0.0003(***)	0.0152(*)	0.0071(*)
TRI14734								ns	ns	ns
VOILUR									ns	ns
AVENTADUR										ns
ANVERGUR										

Appendix 1.22. Significance Table for Figure 3.7d

	TRI18530	TRI18505	TRI16599	TRI18513	TRI16877	TRI28049	TRI14734	VOILUR	AVENTADUR	ANVERGUR
TRI18530		ns	ns	ns	ns	ns	0.0001(***)	ns	ns	ns
TRI18505			ns	ns	ns	ns	0.012(*)	ns	ns	ns
TRI16599				ns	ns	ns	0.0175(*)	ns	ns	ns
TRI18513					ns	ns	0.0306(*)	ns	ns	ns
TRI16877						ns	ns	ns	ns	ns
TRI28049							ns	ns	ns	ns
TRI14734								ns	0.0076(**)	0.0004(***)
VOILUR									ns	ns
AVENTADUR										ns
ANVERGUR										

Appendix 1.23. Significance Table for Figure 3.9a

	TRI18530	TRI18505	TRI16599	TRI18513	TRI16877	TRI28049	TRI14734	VOILUR	AVENTADUR	ANVERGUR
TRI18530		ns	ns	ns	ns	ns	ns	0.0332(*)	0.0017(**)	0.0002(***)
TRI18505			ns	ns	ns	ns	ns	ns	0.0033(**)	0.0003(***)
TRI16599				ns	ns	ns	ns	0.0274(*)	0.0016(**)	0.0002(***)
TRI18513					ns	0.0069(*)	ns	ns	0.0274(*)	0.0026(**)
TRI16877						ns	ns	0.0025(**)	<0.0001(****)	<0.0001(****)
TRI28049							ns	<0.0001(****)	<0.0001(****)	<0.0001(****)
TRI14734								0.04(*)	0.0002(***)	<0.0001(****)
VOILUR									ns	ns
AVENTADUR										ns
ANVERGUR										

Appendix 1.24. Significance Table for Figure 3.9b

	TRI18530	TRI18505	TRI16599	TRI18513	TRI16877	TRI28049	TRI14734	VOILUR	AVENTADUR	ANVERGUR
TRI18530		ns	ns	ns	0.0091(*)	<0.0001(****)	<0.0001(****)	0.0069(*)	0.0006(**)	ns
TRI18505			ns	ns	ns	0.0002(***)	<0.0001(****)	ns	ns	ns
TRI16599				ns	ns	<0.0001(****)	<0.0001(****)	ns	ns	ns
TRI18513					0.0028(**)	<0.0001(****)	<0.0001(****)	0.0021(**)	0.0002(***)	ns
TRI16877						0.0094(*)	0.0021(**)	ns	ns	ns
TRI28049							ns	0.0125(*)	ns	0.0015(**)
TRI14734								0.0028(**)	ns	0.0004(***)
VOILUR									ns	ns
AVENTADUR										ns
ANVERGUR										

Appendix 1.25. Significance Table for Figure 3.9c

	TRI18530	TRI18505	TRI16599	TRI18513	TRI16877	TRI28049	TRI14734	VOILUR	AVENTADUR	ANVERGUR
TRI18530		ns	ns	ns	0.0214(*)	<0.0001(****)	<0.0001(****)	0.0149(8)	ns	ns
TRI18505			ns	ns	ns	0.0002(***)	<0.0001(****)	ns	ns	ns
TRI16599				ns	ns	0.0002(***)	<0.0001(****)	ns	ns	ns
TRI18513					0.0074(*)	<0.0001(****)	<0.0001(****)	0.0049(**)	0.0309(*)	ns
TRI16877						0.0132(*)	0.0034(**)	ns	ns	ns
TRI28049							ns	0.0193(*)	0.0086(*)	<0.0001(****)
TRI14734								0.0051(*)	0.0023(**)	<0.0001(****)
VOILUR									ns	ns
AVENTADUR										ns
ANVERGUR										